

**Thiol-redox proteomics
of *Mycobacterium smegmatis* in response
to ROS, RNS and antibiotics**

I n a u g u r a l d i s s e r t a t i o n

zur

Erlangung des akademischen Grades

doctor rerum naturalium (Dr. rer. nat.)

an der Mathematisch-Naturwissenschaftlichen Fakultät

der

Ernst-Moritz-Arndt-Universität Greifswald

vorgelegt von

Marcel Imber

geboren am 25.02.1988

in Ribnitz-Damgarten, Deutschland

Greifswald, den 9.Juli 2018

Dekan: Prof. Dr. Werner Weitschies

1. Gutachter: Prof. Dr. Haike Antelmann

2. Gutachter: Prof. Bruce Morgan

Tag der Promotion: 22.10.2018

Content

Zusammenfassung der Dissertation	4
Summary of the dissertation	8
Introduction and general conclusion	11
1. Adaptation of <i>Staphylococcus aureus</i> to infection conditions.....	11
2. Redox stress responses in bacterial systems	12
2.1 Sources and chemistry of reactive oxygen, nitrogen, chlorine and electrophilic species (ROS, RNS, RCS, RES)	12
2.1.1 Sources and chemistry of ROS	12
2.1.2 Sources and chemistry of RCS	14
2.1.3 Sources and chemistry of RNS and RES.....	14
2.2 Defense mechanisms and repair systems against ROS, RNS, RCS and RES	17
2.2.1 Detoxification of ROS and RCS.....	17
2.2.1 Detoxification of RNS and RES.....	18
2.3 The glyoxalase system: cellular adaption to methylglyoxal stress.....	19
3. Redox regulation by protein S-thiolation and its reversal in bacteria	20
3.1 The biosynthesis and functions of mycothiol in <i>Actinomycetes</i>	20
3.1.1 The functions of S-mycothiolated proteins in <i>M. smegmatis</i>	22
3.1.2 The functions of S-mycothiolated proteins in <i>C. diphtheriae</i>	24
3.2 The biosynthesis and functions of bacillithiol in <i>Firmicutes</i>	25
3.3 The role of protein S-bacillithiolation in Gram-positive <i>Firmicutes</i>	26
4. Redox regulation of protein S-thiolation by mycoredoxins and bacilliredoxins.....	28
4.1 Redox regulation of protein S-mycothiolation by mycoredoxin-1 (Mrx1)	28
4.2 Redox regulation of protein S-bacillithiolation by bacilliredoxin (Brx)	29
5. Redox regulation of the metabolic enzymes GapDH and AldA.....	31
5.1 The glyceraldehyde-3-phosphate dehydrogenase (GapDH) protein family	31
5.1.1 Structure and catalytic mechanism of GapDH	31

5.1.2 Functions and metabolic adaptation of GapDH under oxidative stress stress.....	33
5.2 The aldehyde dehydrogenase (ALDH) protein family.....	35
5.2.1 Structure and catalytic mechanism of ALDH enzymes	35
5.2.2 Functions and metabolic adaptation of ALDH under oxidative stress.....	36
6. Conclusion and future perspectives	38
7. References	39

Chapter 1: The glyceraldehyde-3-phosphate dehydrogenase GapDH of *Corynebacterium diphtheriae* is redox-controlled by protein S-mycothiolation under oxidative stress

Chapter 2: Protein S-bacillithiolation functions in thiol-protection and redox regulation of the glyceraldehyde-3-phosphate dehydrogenase Gap in *Staphylococcus aureus* under hypochlorite stress

Chapter 3: The aldehyde dehydrogenase AldA contributes to the hypochlorite defense and is redox-controlled by protein S-bacillithiolation in *Staphylococcus aureus*

Chapter 4: Redox regulation by reversible protein S-thiolation in Gram-positive bacteria

Curriculum vitae

Acknowledgements

Declaration

Zusammenfassung der Dissertation

Zum Thema:

**„Thiol-Redox Proteomik von *Mycobacterium smegmatis*
als Antwort auf ROS, RNS und Antibiotika“**

vorgelegt von

Marcel Imber

Zusammenfassung der Dissertation

Reaktive Sauerstoffspezies (ROS) verursachen oxidativen Stress in Bakterien und entstehen durch stufenweise Ein-Elektronen-Übertragungen auf molekularem Sauerstoff in der Atmungskette. Pathogene Bakterien sind oxidativen Stress durch die Immunabwehr des Wirts ausgesetzt, wobei ROS durch den oxidativen Burst in Makrophagen und Neutrophilen produziert werden. Neben ROS müssen sich Bakterien auch mit reaktiven Chlor-Spezies (RCS), reaktiven elektrophilen Spezies (RES) und reaktiven Stickstoffspezies (RNS) auseinandersetzen. Um sich gegen reaktive Spezies zu verteidigen, haben Bakterien verschiedene Schutzmechanismen und Reparatursysteme entwickelt. Sie nutzen niedermolekulare Thiolverbindungen um den reduzierten Zustand des Zytoplasmas aufrechtzuerhalten. Niedermolekulare Thiolverbindungen sind an post-translationalen Thiolmodifikationen von Proteinen durch S-Thiolierungen beteiligt. S-Thiolierungen dienen dem Schutz der Thiolgruppen von Cysteinen vor irreversibler Oxidation und regulieren Proteinaktivitäten nach oxidativem Stress.

Die niedermolekulare Thiolverbindung Glutathion (GSH) ist ein Tripeptid und kommt in millimolaren Konzentrationen im Zytoplasma von Eukaryoten und Gram-negativen Bakterien vor. Gram-positive Bakterien sind nicht in der Lage, GSH zu synthetisieren und produzieren stattdessen alternative niedermolekulare Thiolverbindungen. Mycothiol (MSH) fungiert als niedermolekulare Thiolverbindung in *Actinomyceten*, wie z.B. in Mykobakterien und Corynebakterien. In *Firmicuten*, wie z.B. in *Bacillus* und *Staphylococcus*-Spezies, wurde Bacillithiol (BSH) als niedermolekulare Thiolverbindung charakterisiert. Neben der Schutzfunktion von Thiolgruppen vor irreversibler Oxidation zu Sulfin- und Sulfonsäuren, sind Bacillithiol und Mycothiol auch an der Virulenz und dem Überleben von pathogenen Bakterien beteiligt. Weiterhin spielen sie eine wichtige Rolle in der Homöostase von Metall-Ionen und als Kofaktor von Enzymen für die Entgiftung von Xenobiotika, Toxinen und Antibiotika.

In der vorliegenden Arbeit sollte die Rolle von MSH und BSH in der Redoxregulation und beim Schutz von NaOCl-sensitiven metabolischen Enzymen unter oxidativem Stress in *Corynebacterium diphtheriae* und *Staphylococcus aureus* untersucht werden. Quantitative Redoxproteom-Analysen in *C. diphtheriae* und *S. aureus* hatten die Glycerinaldehyd-3-Phosphat Dehydrogenase GapDH und die Aldehyd-Dehydrogenase AldA als S-thioliert und stark oxidiert identifiziert. Deshalb habe ich in der Promotionsarbeit die Redoxregulation des metabolischen Enzyms GapDH aus *C. diphtheriae* durch S-Mycothiolierung als Antwort auf NaOCl und H₂O₂ Stress in **Kapitel 1** biochemisch untersucht. Die Redoxregulation von GapDH aus *C. diphtheriae* durch Thioredoxin (Trx) und Mycoredoxin1 (Mrx1) wurde weiterhin in dieser Doktorarbeit untersucht.

Es wurden im Redoxproteom von *C. diphtheriae* 26 S-mycothiolierte Proteine nach NaOCl-Stress mittels Shotgun-Proteomics identifiziert. Diese Proteine sind beteiligt am

Energiestoffwechsel (Ndh, GlpD), der Biosynthese von Aminosäuren (ThrA, LeuB), Purinen (PurA) und von Zellwandbausteinen (GlmS). Die glykolytische Glycerinaldehyd-3-Phosphat Dehydrogenase (GapDH) konnte als konserviertes Target für S-Thiolierungen in *C. diphtheriae* und *S. aureus* identifiziert werden. GapDH war mit einem Anteil von 0.75 % das am häufigsten vorkommende Protein im Cystein-Proteom von *C. diphtheriae*. GapDH ist in Prokaryoten und Eukaryoten ein konserviertes Target für die Redoxregulation durch S-Glutathionylierung nach oxidativem Stress. Die Oxidation von GapDH mittels NaOCl und H₂O₂-Stress ohne MSH *in vitro* führte zur Überoxidation und irreversiblen Inaktivierung von GapDH. In Gegenwart von MSH kam es nach H₂O₂ und NaOCl-Stress zur reversiblen Inaktivierung von GapDH durch S-Mycothiolierung *in vitro*. Weiterhin konnte gezeigt werden, dass die S-Mycothiolierung schneller ablief im Vergleich zur Überoxidation. Detaillierte Enzym-Kinetiken zeigten, dass die S-Mycothiolierung das Cys153 im aktiven Zentrum von GapDH effektiv vor der Überoxidation schützt. Die glykolytische Aktivität von GapDH konnte durch die Reduktion von S-mycothioliertem GapDH durch Mrx1 und Trx *in vitro* regeneriert werden. Wir konnten weiterhin zeigen, dass die Reduktion von S-mycothioliertem GapDH durch Mrx1 sehr viel schneller erfolgte als durch Trx. Diese Ergebnisse bestätigten frühere Publikationen zur Reaktivierung von S-mycothioliertem Mpx und MrsA durch Mrx1, welche um 2 Größenordnungen schneller ablief im Vergleich zur Reaktivierung durch das Trx-System.

Wir waren weiterhin an der Redoxregulation von Gap aus *S. aureus* nach NaOCl und H₂O₂-Stress interessiert, was in **Kapitel 2** beschrieben wird. Mittels der Redox-Proteomics-Analyse OxICAT wurden 58 NaOCl-sensitive Proteine identifiziert und quantifiziert, die im Vergleich zur Kontrolle einen erhöhte Thiol-Oxidation nach NaOCl-Stress aufwiesen. Dabei zeigten die Aldehyd-Dehydrogenasen Gap und AldA eine 29 % erhöhte Oxidation nach NaOCl-Stress in den Cysteinen im katalytischen aktiven Zentrum. Weiterhin konnten die fünf S-bacillithiolierten Proteine Gap, AldA, GuaB, RpmJ und PpaC mittels Shotgun Proteomik in *S. aureus* identifiziert werden. Dabei ist wiederum Gap das mit 4% am häufigsten vorkommende Protein im Cystein-Proteom von *S. aureus*. Wir konnten durch biochemische Aktivitätsmessungen zeigen, dass Gap aus *S. aureus* sehr sensitiv gegenüber Oxidationen durch H₂O₂ und NaOCl-Stress ist. Die Oxidation von Gap durch H₂O₂ und NaOCl-Stress ohne BSH führte zur irreversiblen Inaktivierung durch Überoxidation des Cys151 zur Sulfonsäure. In Gegenwart von BSH kam es zur reversiblen Inhibierung der glykolytischen Aktivität von GapDH durch S-Bacillithiolierung, welche schneller ablief im Vergleich zur Überoxidation ohne BSH. Enzymatische Aktivitätsmessungen zeigten, das Cys151 durch S-Bacillithiolierung effektiv vor der Überoxidation geschützt werden kann. Weiterhin konnten wir zeigen, dass das Baciliredoxin Brx eine Reduktion und Reaktivierung von S-bacillithioliertem Gap *in vitro* katalysieren kann. Durch Kooperation mit Frauke Gräter (Universität Heidelberg) wurde ein molekulares Docking von BSH in das aktive Zentrum von Gap *in silico* durchgeführt. Das

Docking von BSH zeigte, dass die S-Bacillithiolierung von Gap keine großen Strukturänderungen erforderte.

Neben dem glykolytischen Enzym Gap wurde die Aldehyd-Dehydrogenase AldA am Cys279 nach NaOCl-Stress im aktiven Zentrum in *S. aureus* als S-bacillithioliert identifiziert. Deshalb wurde die Expression, Redoxregulation und die strukturellen Änderungen von AldA aus *S. aureus* nach S-Bacillithiolierung untersucht, was in **Kapitel 3** dieser Arbeit beschrieben ist. BSH-spezifische Western-Blots zeigten die S-Bacillithiolierung von AldA nach Oxidation durch H₂O₂-Stress und BSH *in vitro*. Das *aldA*-Gen wird durch den alternativen Sigmafaktor SigmaB in *S. aureus* reguliert, was bereits früher publiziert worden ist. In Northernblot-Experimenten konnte eine SigmaB-unabhängige Induktion der *aldA*-Transkription in *S. aureus* nach Formaldehyd, NaOCl und Diamid-Stress gezeigt werden. Mittels einer *aldA*-Deletionsmutante konnte demonstriert werden, dass AldA für das Wachstum und Überleben von *S. aureus* nach NaOCl-Stress wichtig ist. Aktivitätsmessungen von AldA zur Aldehyd-Oxidation konnten die NAD⁺-abhängige Oxidation von Formaldehyd, Methylglyoxal, Glycolaldehyd und Acetaldehyd *in vitro* nachweisen. Dies zeigte, dass AldA ein breites Substratspektrum aufweist, wobei das natürliche Aldehyd-Substrat von AldA bisher unbekannt ist.

Es wurde weiterhin eine C279S-Mutante erzeugt, um die Funktion des konservierten Cys279 im aktiven Zentrum für die Aktivität von AldA nachzuweisen. Das gereinigte AldAC279S-Protein war katalytisch inaktiv *in vitro*. Die *aldAC279S*-Mutante war ebenfalls sensitiv gegenüber NaOCl-Stress *in vivo*, was durch Komplementation bestätigt werden konnte. In Aktivitätsassays konnte gezeigt werden, dass das gereinigte AldA-Protein sensitiv gegenüber einer Überoxidation durch H₂O₂ ist und in Gegenwart von BSH S-bacillithioliert wird. Mittels molekularen Dockings und molekular-dynamischen Simulationen wurde durch Kooperation mit Agnieszka Bronowska (University of Newcastle) bestätigt, dass die S-Bacillithiolierung von AldA am Cys279 keine Strukturveränderungen erfordert, was die Ergebnisse zu Gap bestätigte. Es konnte weiterhin gezeigt werden, dass BSH in zwei verschiedenen Positionen im aktiven Zentrum von AldA lokalisiert ist, was vom NAD⁺ Kofaktor abhängt. Im Apoenzym ist BSH am Cys279 im „ruhenden“ Zustand lokalisiert, während BSH im Holoenzym die Disulfidbindung mit Cys279 im „aktivierten“ Zustand eingeht. Ähnliche Positionen von BSH im aktiven Zentrum von Cys151 von Gap im ruhenden oder aktivierten Zustand konnten auch in der früheren Docking Analyse bestätigt werden.

Zusammenfassend konnte mit AldA ein weiterer Schutzmechanismus von *S. aureus* gegenüber oxidativem Stress identifiziert werden. Es wird vermutet, dass AldA eine Funktion bei der Entgiftung von toxischem Methylglyoxal oder anderen Aldehyden unter NaOCl-Stress besitzen könnte, was in Folgeanalysen weiter untersucht werden sollte.

Summary of the dissertation

On the subject:

**„Thiol-redox proteomics of *Mycobacterium smegmatis*
in response to ROS, RNS and Antibiotics “**

submitted by

Marcel Imber

Summary of the dissertation

Bacteria are exposed to oxidative stress as an unavoidable consequence of their aerobic lifestyle. Reactive oxygen species (ROS) are generated in the stepwise one-electron reduction of molecular oxygen during the respiration. Pathogens encounter ROS during the oxidative burst of macrophages as part of the host immune defense. Besides ROS, bacteria also have to cope with reactive chlorine, electrophilic and nitrogen species (RCS, RES, RNS). To cope with these reactive species, bacteria have evolved different defense and repair mechanisms. To maintain the reduced state of the cytoplasm, they utilize low molecular weight (LMW) thiols. LMW thiols are small thiol-containing compounds that can undergo post-translational thiol-modifications with protein thiols, termed as S-thiolations. S-thiolations function as major redox regulatory and thiol-protection mechanism under oxidative stress conditions.

In eukaryotes and Gram-negative bacteria, the tripeptide glutathione (GSH) functions as major LMW thiol, which is present in millimolar concentrations. The *Actinomycetes*, such as *Mycobacterium* and *Corynebacterium* species do not produce GSH and utilize instead mycothiol (MSH) as their alternative LMW thiol. In *Firmicutes*, including *Bacillus* and *Staphylococcus* species, bacillithiol (BSH) functions as the major LMW thiol. LMW thiols protect protein thiols against the irreversible overoxidation of cysteine residues to sulfinic and sulfonic acids. In addition, LMW thiols contribute to the virulence and survival of pathogens, function in metal homeostasis and serve as enzyme cofactors for detoxification of xenobiotics and antibiotics.

In this doctoral thesis, we aimed to investigate the roles of MSH and BSH in redox regulation of main metabolic enzymes under oxidative stress in the pathogens *Corynebacterium diphtheriae* and *Staphylococcus aureus*. Previous redox proteomics studies identified the glyceraldehyde-3-phosphate dehydrogenase GapDH and the aldehyde dehydrogenase AldA as S-thiolated in *S. aureus* and *C. diphtheriae*. Thus, we aimed to study the redox regulation of the metabolic enzyme GapDH in *C. diphtheriae* in response to NaOCl and H₂O₂ stress by S-mycothiolation, which is described in **chapter 1**. Moreover, we studied the involvement of the mycoredoxin-1 (Mrx1) and thioredoxin (Trx) pathways in reactivation of S-mycothiolated GapDH *in vitro*.

Using shotgun proteomics, 26 S-mycothiolated proteins were identified under NaOCl stress in *C. diphtheriae*. These are involved in energy metabolism (Ndh, GlpD) and in the biosynthesis of amino acids (ThrA, LeuB), purines (PurA) and cell wall metabolites (GlmS). The glycolytic GapDH was identified as conserved target for S-thiolation across Gram-positive bacteria. GapDH was the most abundant protein, contributing with 0.75 % to the total cysteine proteome. Moreover, GapDH is a conserved target for redox regulation and S-glutathionylation in response to oxidative stress in several prokaryotic and eukaryotic organisms. Treatment of GapDH with NaOCl and H₂O₂ in the absence of MSH resulted in irreversible enzyme

inactivation due to overoxidation. Pretreatment of GapDH with MSH prior to H₂O₂ or NaOCl exposure resulted in reversible inactivation due to S-mycothiolation of the active site Cys153. Since S-mycothiolation is faster compared to overoxidation, S-mycothiolation efficiently protects the GapDH active site against overoxidation. The activity of S-mycothiolated GapDH could be restored by both, the Mrx1 and Trx pathway *in vitro*. Interestingly, the recovery of S-mycothiolated GapDH by Mrx1 was faster compared to its reduction by the Trx pathway. In previous studies, the reactivation of S-mycothiolated Mpx and MrsA by the mycoredoxin pathway occurred also faster compared to the Trx pathway, which is consistent with our results.

We were further interested to analyze the redox regulation of the glyceraldehyde-3-phosphate dehydrogenase Gap of *S. aureus* under NaOCl and H₂O₂ stress, which is described in **chapter 2**. Using the quantitative redox proteomic approach OxICAT, 58 NaOCl-sensitive cystein residues with >10% thiol oxidation under NaOCl stress were identified. Gap and AldA showed the highest oxidation increase of 29% under NaOCl stress at their active site cystein residues. Using shotgun proteomics, five S-bacillithiolated proteins were identified, including Gap, AldA, GuaB, RpmJ and PpaC. Gap contributed with 4 % as most abundant cystein protein to the total cystein proteome. Our activity assays demonstrated that Gap of *S. aureus* is highly sensitive to overoxidation by H₂O₂ and NaOCl *in vitro* in the absence of BSH. The active site Cys151 of Gap was oxidized to the BSH mixed disulfide under H₂O₂ and NaOCl stress in the presence of BSH *in vitro*, which resulted in the reversible Gap inactivation. Moreover, inactivation of Gap by NaOCl and H₂O₂ due to S-bacillithiolation was faster compared to overoxidation, indicating that S-bacillithiolation protects the Gap active site against overoxidation *in vitro*. We further showed that the bacilliredoxin Brx catalyzes the reduction of S-bacillithiolated Gap *in vitro*. Molecular docking of BSH into the Gap active site revealed that S-bacillithiolation does not require major structural changes.

Apart from Gap, the aldehyde dehydrogenase AldA was identified as S-bacillithiolated at its active site Cys279 under NaOCl stress in *S. aureus* previously. Thus, the expression, function, redox regulation and structural changes of AldA were analysed under NaOCl and aldehyde stress in *S. aureus* as summarized in **chapter 3**. AldA was S-bacillithiolated in the presence of H₂O₂ and BSH as demonstrated in BSH-specific Western blots *in vitro*. The expression of *aldA* was previously shown to be regulated by the alternative sigma factor SigmaB in *S. aureus*. Transcription of *aldA* was strongly increased in a SigmaB-independent manner under formaldehyde, NaOCl and diamide stress in *S. aureus*. Using an *aldA* deletion mutant, we demonstrated that *aldA* is required for growth and survival under NaOCl stress in *S. aureus*. The purified AldA enzyme was shown to catalyze the oxidation of various aldehyde substrates, including formaldehyde, methylglyoxal, glycolaldehyde and acetaldehyde *in vitro*. In addition, the function of the conserved Cys279 for AldA activity was investigated *in vivo* and *in vitro*. The purified AldAC279S mutant was shown to be inactive for aldehyde oxidation *in*

vitro. Moreover, the *aldAC279S* mutant was very sensitive under NaOCl stress *in vivo*, and this phenotype could be reversed using the *aldA* complemented strain. These experiments demonstrate the function of Cys279 for AldA activity both *in vitro* and *in vivo*. AldA activity assays showed that AldA is sensitive to overoxidation and irreversible inactivation by H₂O₂ alone *in vitro*. In the presence of BSH, AldA is protected against overoxidation by reversible S-bacillithiolation *in vitro*. Molecular docking and molecular dynamics simulations revealed that BSH occupies two different positions in the Cys279 active site, which depend on the NAD⁺ cofactor. In the apoenzyme, BSH forms the disulfide with Cys279 in the “resting” state position, while Cys279 is S-bacillithiolated in the “attacking” state position in the holoenzyme in the presence of the NAD⁺ cofactor.

Introduction and general conclusion

1. Adaptation of *Staphylococcus aureus* to infection conditions

Staphylococcus aureus is a common commensal bacterium, but also a major human and animal pathogen. *S. aureus* colonizes the anterior nares of one quarter of the human population [1]. However, in immune comprised persons or under the hospital settings, *S. aureus* is often a leading cause of infectious diseases, such as bacteremia, infective endocarditis, skin and soft tissue infections and pneumonia [2]. The high diversity of virulence factors determines the high pathogenicity of *S. aureus* during host invasion. These virulence factors include toxins, proteases, lipases, nucleases, metalloproteases, superantigens as well as factors for attachment, evasion and penetration of host tissues during infections (**Figure 1**) [1].

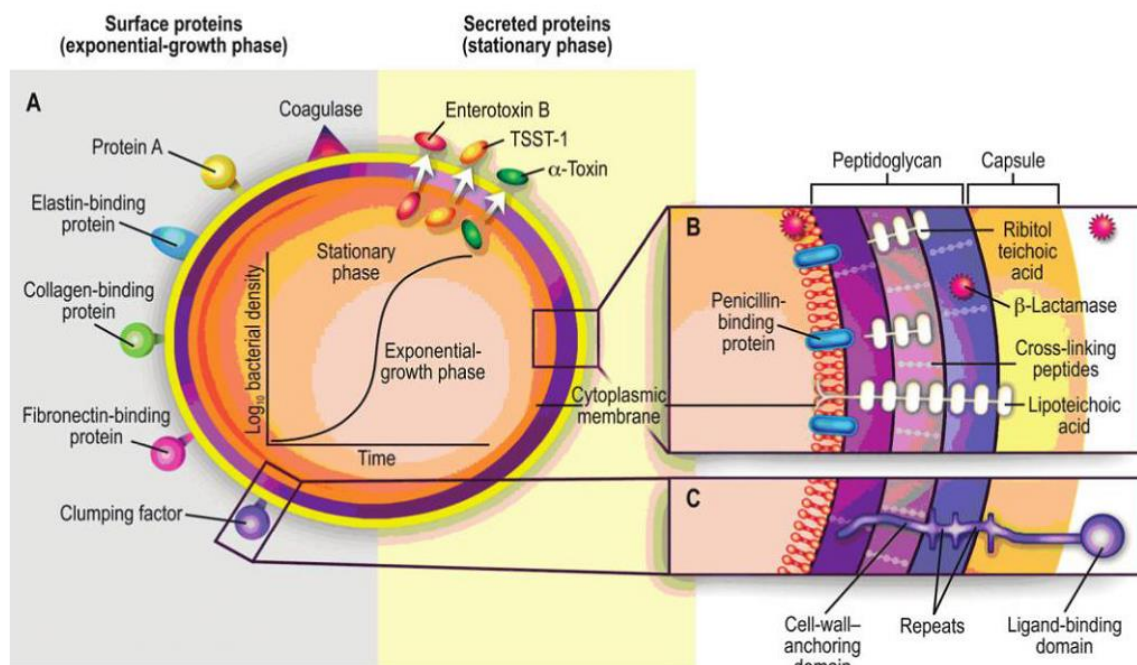


Figure 1: Pathogenic factors of *Staphylococcus aureus* that play a role in virulence. Surface proteins are involved in the attachment to the host and secreted toxins mediate sepsis (**A**). Cross sections of the cell envelope of *S. aureus* (**B, C**). TSST-1; toxic shock syndrome toxin 1. The figure is from reference [1].

The adherence to host tissue under infections is mediated by numerous surface proteins, called “microbial surface components recognizing adhesive matrix molecules” in *S. aureus* [3]. *S. aureus* is able to evade host defenses, antimicrobials and antibiotics by formation of biofilms and small-colony variants (SVCs) [4, 5]. The production of antiphagocytic microcapsules and leucocidins as well as the secretion of chemotaxis inhibitory proteins help *S. aureus* to evade the host immune system during infection [6-8]. The expression of numerous enzymes, such as

proteases, lipases and elastases enable *S. aureus* to invade and destroy the host tissue. Furthermore, the activation of the host immune system, coagulation pathways and superantigens result in septic shock or sepsis-like syndromes [9, 10]. During *S. aureus* infection, activated neutrophils produce hypochlorous acid (HOCl) to destroy the invading pathogen. Production of HOCl is catalyzed by the myeloperoxidase (MPO) [11]. *S. aureus* is able to detoxify HOCl and other reactive species. In addition, the low molecular weight (LMW) thiol bacillithiol (BSH) protects cellular biomolecules from oxidative damage [12, 13]. It is therefore of utmost importance to study the adaptation of *S. aureus* to the host immune defense under infection conditions to identify new drug targets to effectively combat *S. aureus* infections.

2. Redox stress responses in bacterial systems

2.1 Sources and chemistry of reactive oxygen, nitrogen, chlorine and electrophilic species (ROS, RNS, RCS, RES)

The bacterial cytoplasm is a strongly reducing environment under physiological conditions with a redox potential (E°) of approximately -260 to -280 mV as determined in *Escherichia coli* [14]. The reduced state of the cytoplasm is maintained by abundant LMW thiols as well as thiol-disulfide reducing systems. Alterations in the cellular redox state are caused by different reactive species, such as reactive oxygen, nitrogen, chlorine and electrophilic species (ROS, RNS, RCS, RES) [15]. Bacteria are exposed to different reactive species during respiration, autoxidation of enzymes, by exogenous antibiotics or xenobiotics, by microbial communities or during host-pathogen interactions [15-17].

2.1.1 Sources and chemistry of ROS

ROS are constantly generated from the sequential one-electron reduction of molecular oxygen (O_2), that produces superoxide anions ($O_2^{\bullet-}$), hydrogen peroxide (H_2O_2) and highly reactive hydroxyl radicals (OH^{\bullet}) (**Figure 2**). The generation of $O_2^{\bullet-}$ and H_2O_2 also occurs during the autoxidation of non-respiratory flavoproteins. Therefore, electrons are transferred from molecular oxygen to dihydroflavin, resulting in the formation of $O_2^{\bullet-}$ and a flavosemiquinone anion, which leads to H_2O_2 production [18]. The oxidative burst of macrophages leads to the release of $O_2^{\bullet-}$, H_2O_2 , nitric oxide (NO) and hypochlorous acid (HOCl) to kill invading pathogenic bacteria. The pathogens are first engulfed by activated macrophages into phagosomes. The phagocytic NADPH oxidase (NOX) pumps electrons into the phagosomal lumen to reduce molecular oxygen to $O_2^{\bullet-}$. The superoxide dismutase (SOD) converts $O_2^{\bullet-}$ to H_2O_2 [11, 19]. Degranulation releases millimolar amounts of myeloperoxidase (MPO). MPO dismutates $O_2^{\bullet-}$ to H_2O_2 and provides chlorine for an efficient conversion of H_2O_2 to HOCl [11].

The highly reactive $\text{OH}\cdot$ is generated by the reaction of H_2O_2 with Fe^{2+} in the Fenton reaction which can damage all cellular biomolecules (**Figure 2**) [20, 21].

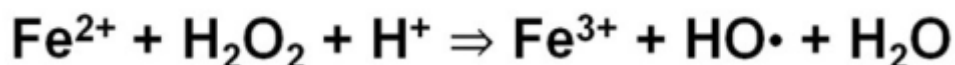
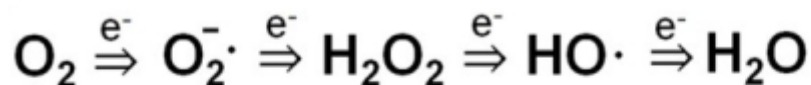


Figure 2: Sources of reactive oxygen species (ROS) in bacteria. ROS, including superoxide anions ($\text{O}_2^{\cdot-}$), hydrogen peroxide (H_2O_2) and hydroxyl radicals ($\text{OH}\cdot$) are generated during the incomplete one-electron reduction of molecular oxygen. The highly reactive hydroxyl radical is produced in the Fenton reaction by reaction of H_2O_2 and Fe^{2+} . The figure is from reference [22].

ROS can oxidize several amino acids in proteins, including cysteine, methionine and tryptophane as well as LMW thiols. The thiol group of cysteine is the main target for post-translational thiol modifications by ROS due to its nucleophilic character. Protein thiols can either be reversibly oxidized to protein disulfides or irreversibly overoxidized to sulfinic or sulfonic acids [15, 16]. The ROS-induced oxidation of protein thiols is initiated by the formation of the cysteine sulfenic acid intermediate (R-SOH). The unstable cysteine sulfenic acid rapidly reacts with other protein thiols to form intramolecular and intermolecular protein disulfides. Cysteine sulfenic acids can also react with LMW thiols to form mixed disulfides, termed as S-thiolations. S-thiolations protect protein thiols against the irreversible overoxidation to cysteine sulfinic ($\text{R-SO}_2\text{H}$) and sulfonic acid ($\text{R-SO}_3\text{H}$) [16]. Sulfiredoxins are able to reduce cysteine sulfinic acid intermediates in 2-Cys peroxiredoxins, but they are only present in eukaryotes [23]. Superoxide can also react with NO, which generates peroxynitrite (ONOO^-) in a diffusion-controlled process [24]. The oxidation of FeS clusters by $\text{O}_2^{\cdot-}$ and H_2O_2 releases non-protein bound iron inside the cell, that can undergo Fenton reactions, increasing the level of $\text{OH}\cdot$. Hydroxyl radicals can induce DNA strand breaks and oxidation of DNA bases, leading to an increase in mismatches and mutations [25-27].

2.1.2 Sources and chemistry of RCS

Reactive chlorine species (RCS) include hypochlorous acid (HOCl) and chloramines (RNHCl) as byproducts of the oxidation of primary and secondary amines. HOCl is generated during the oxidative burst in neutrophils, catalyzed by MPO. RCS react with almost all cellular components, including amino acids, LMW thiols, DNA, metal centers and lipids. The resulted unfolding of proteins by aggregation or degradation can lead to cell death. HOCl reacts with protein thiols to generate an unstable sulfenylchloride (R-SCI) intermediate that can further react with water to generate cysteine sulfenic acid (**Figure 3**). These reactive intermediates can either be overoxidized to cysteine sulfinic and sulfonic acids or further react with other protein thiols to form disulfides. Moreover, disulfides are oxidized by HOCl to thiosulfates [R-S(O)-S-R] or thiosulfonates [R-S(O₂)-S-R] [17, 28].

Methionine residues are oxidized to reversible methionine sulfoxides and irreversible dehydromethionines [29]. HOCl also reacts with primary and secondary amines, leading to the formation of chloramines. Chloramines rapidly decompose to their respective aldehydes or react with iron and copper ions to generate RNS (**Figure 3**) [30]. HOCl and chloramines can lead to DNA and RNA damage by chlorination of primary and secondary nucleotide bases [31].

2.1.3 Sources and chemistry of RNS and RES

RNS include nitric oxide (NO), peroxynitrite (ONOO⁻), S-nitrosothiol (RS-NO), S-nitrothiol (RS-NO₂) and other nitrogen oxides. Neutrophils generate NO in an enzyme-catalyzed oxidation of L-arginine to L-citrulline by the inducible nitric oxide synthase (iNOS). Peroxynitrite is produced by the rapid reaction of NO with O₂^{•-} [16, 32, 33]. RNS cause the reversible S-nitrosylation of protein thiols and LMW thiols. The generation of S-nitrosothiols occurs by reaction of a thiolate with a nitrosonium cation (NO⁺) or by reaction of a thiyl intermediate with nitrogen dioxide radicals (NO₂[•]) [34]. At high concentrations, tyrosine can undergo RNS-catalyzed nitration of tyrosine to 3-nitrotyrosine. RNS also have an impact on the iron metabolism through disruption of FeS clusters and the formation of metal-nitrosyl complexes [24]. In eukaryotes, NO or its one-electron reduced protonated form nitroxyl (HNO) plays a role in signal transduction [35].

Reactive electrophilic species (RES) are small molecules with electron-deficient carbon centers that undergo covalent reactions by accepting an electron pair from a nucleophilic molecule. Electrophilic species that alter the cellular redox state include quinones, aldehydes, α,β-unsaturated dicarbonyl compounds, epoxides and diamide [16, 22, 36].

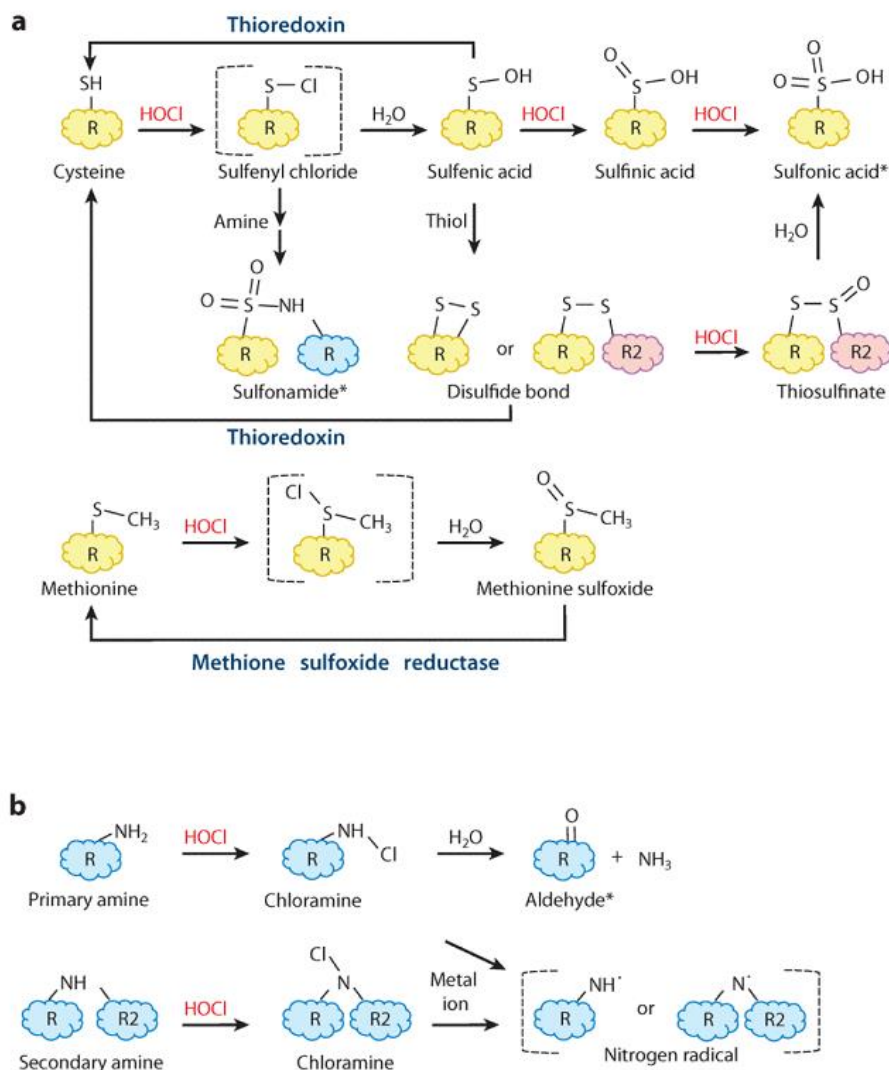


Figure 3: Chemistry of hypochlorous acid (HOCl) with biomolecules. HOCl reacts with the sulfur-containing amino acids cysteine and methionine in proteins. Reactions of HOCl with cysteine generate an unstable sulfenylchloride intermediate, that can undergo further oxidations to sulfinic and sulfonic acids, inter- or intramolecular disulfides and sulfonamides. Sulfenic acids and disulfides are reversible intermediates, reduced by thioredoxins, while sulfonic acids and sulfonamides represent dead-end products. Methionine is oxidized to methionine sulfoxide, reversed by the methionine sulfoxide reductase (**a**). The reaction of HOCl with primary and secondary amines leads to the formation of chloramines, that can undergo reactions to generate aldehyde or nitrogen radicals (**b**). The figure is from reference [17].

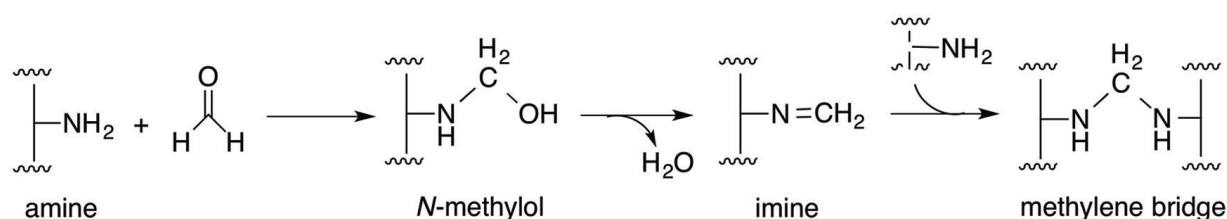
RES can be generated during normal cellular metabolism or often as secondary reactive metabolites from oxidation products of amino acids, lipids, carbohydrates and nucleic acids. The α,β -unsaturated dicarbonyl compound methylglyoxal is generated as a byproduct of the glycolysis or as a consequence of HOCl stress at the host-pathogen interface [15, 37, 38]. RES can also be produced by biotransformation of xenobiotic compounds [39]. Quinones are

other electrophiles that are present in the soil in humic substances. Ubiquinone and menaquinone are lipid-electron carriers of the respiratory chain [40, 41].

RES are able to react with cysteine, histidine, lysine and arginine residues as well as DNA bases. Proteins with nucleophilic cysteine thiols are preferred targets for RES due to their low pK_a [15]. Formaldehyde can undergo 1,2-addition reactions with amines and further dehydration to imines (Schiff base formation). These labile Schiff bases can form cross-links with several amino acid residues, including cysteine, arginine and tyrosine. Formaldehyde can also induce direct modifications of cysteine thiols to hydroxymethylthiols in proteins (**Figure 4**). Formaldehyde also reacts with the N² nitrogen of desoxyguanosine [42, 43].

Methylglyoxal is an α,β -unsaturated dicarbonyl compound that reacts with nucleophilic DNA bases and cysteine thiols via Michael addition. Furthermore, methylglyoxal conjugates the amino acids cysteine, arginine and lysine, leading to the formation of advanced glycation end-products [43, 44]. Electrophilic quinones can form irreversible thiol-S-alkylations with cysteine residues and LMW thiols by Michael addition. The redox reaction of quinones generates highly reactive semiquinone radicals that lead to the formation of $O_2^{\bullet-}$ (**Figure 4**) [39, 45].

A Reaction with amines



B Reaction with thiols

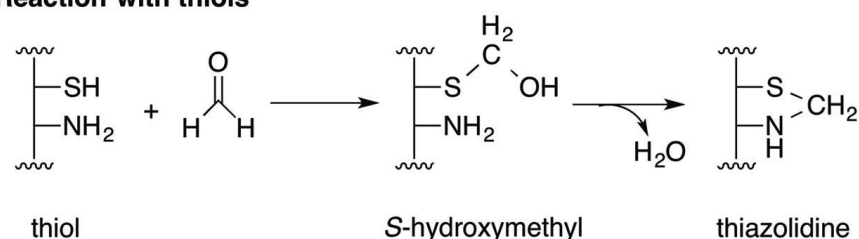


Figure 4: Chemistry of formaldehyde with biomolecules. Formaldehyde can react with amine groups in biomolecules to form imine adducts via the formation of an N-methylol intermediate. Imines can react with other amines in biomolecules to form cross-linking methylene bridges between proteins and DNA molecules (**A**). Reactions of formaldehyde with thiol groups generate S-hydroxymethyl and thiazolidine adducts (**B**).

2.2 Defense mechanisms and repair systems against ROS, RNS, RCS and RES

2.2.1 Detoxification of ROS and RCS

Bacteria evolved many enzymatic and non-enzymatic protection and repair mechanisms to cope with ROS, RNS, RCS and RES. The high reaction rates of $O_2^{\bullet-}$ and H_2O_2 with biomolecules require the synthesis of ROS scavenging enzymes, including superoxide dismutase (SOD), catalase and peroxidases (**Figure 5**). Superoxide dismutases are the first line of defense against oxidative damage, catalyzing the dismutation of $O_2^{\bullet-}$ to H_2O_2 . Due to the limited membrane permeability of $O_2^{\bullet-}$, SODs are present in all cellular compartments [46]. *E. coli* contains three distinct SODs, a cytoplasmic iron- and manganese-containing SOD (FeSOD and MnSOD) and a periplasmic copper-zinc SOD (CuZnSOD). The two cytoplasmic SODs are expressed under iron starvation and controlled by the Fur repressor. Some anaerobic organisms scavenge $O_2^{\bullet-}$ by superoxide reductases due to their lack of SOD [46, 47].

Catalases and peroxidases effectively scavenge endogenous H_2O_2 , keeping the cellular concentration at almost 20 nM in *E. coli* [21]. Catalases catalyze the disproportion of H_2O_2 to water and molecular oxygen [48]. Based on their structure, catalases are classified into monofunctional catalases, catalase-peroxidases and Mn-catalases (pseudo-catalases) [49]. The monofunctional catalases and catalase-peroxidases contain heme as active site that can generate the reactive ferryl/radical species during the reduction of H_2O_2 . The ferryl/radical intermediate is potentially dangerous for the cell. Thus, catalases are only active at high concentrations of H_2O_2 . Under low H_2O_2 levels, peroxidases are favored, because they do not form a reactive intermediate in their catalytic H_2O_2 reduction cycle [18, 21].

Peroxidases are widely distributed in mammals, plants, yeasts and bacteria, catalyzing the reduction of H_2O_2 to water at the expense of various electron donors [50]. In *E. coli*, the thiol-based AhpCF peroxiredoxin system uses electrons from NADPH to reduce H_2O_2 to water [18]. The selenium-containing glutathione peroxidase (Gpx) reduces H_2O_2 to water as well as lipid peroxides to lipid alcohols. In the Gpx reaction, GSH is oxidized to GSSG, which is recycled by the glutathione reductase with NADPH as electron donor (**Figure 5**) [51, 52].

The bacterial responses to RCS and ROS are connected due to their high reactivity with cysteine thiols. Catalases and peroxidases are considered as H_2O_2 -detoxifying enzymes, but also play a role in RCS scavenging [17]. Global transcriptome profiling in response to RCS stress in *E. coli*, *Bacillus subtilis* and *Pseudomonas aeruginosa* reveals the upregulation of catalases, peroxidases and methionine sulfoxide reductases (Msr) [53-57].

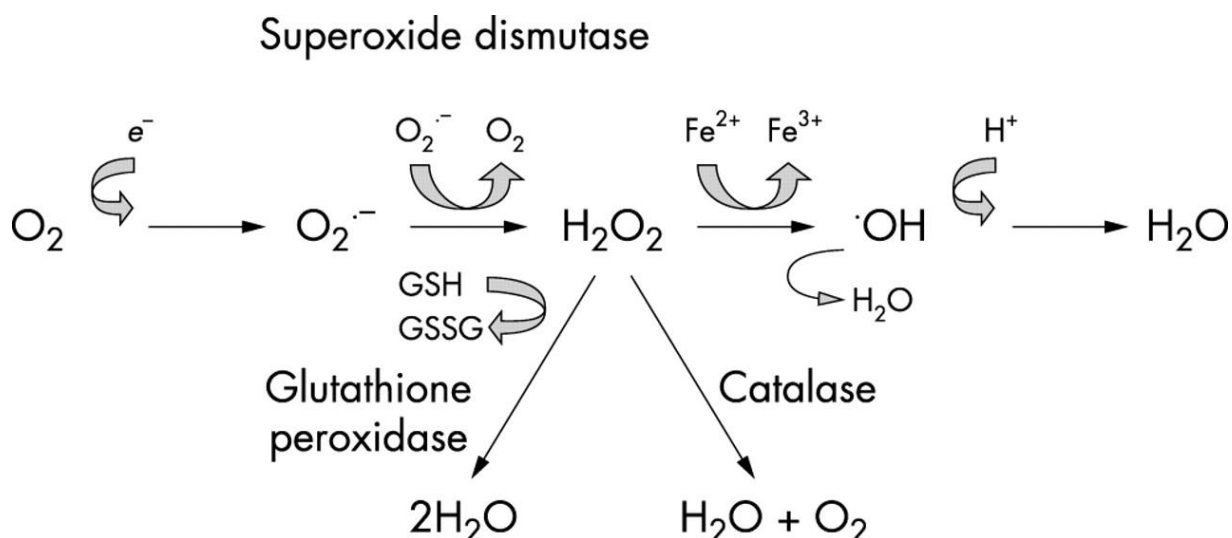


Figure 5: Scavenging enzymes for ROS. Superoxide dismutases, catalases and peroxidases are the main detoxification enzymes in bacteria. Superoxide dismutases catalyze the dismutation of $O_2^{\cdot-}$ to H_2O_2 . Catalases catalyze the disproportion of H_2O_2 to H_2O and O_2 . Peroxidases, such as the glutathione peroxidase Gpx, reduce H_2O_2 to water and thereby oxidize glutathione (GSH) to glutathione disulfide (GSSG). The figure is from reference [58].

The high reaction rate of RCS with GSH provides effective protection and reduces the damage of other essential cellular components [59, 60]. In *B. subtilis*, the methionine synthase (MetE) catalyzes the final step in the methionine synthesis, and is protected at its catalytic cysteine residue by S-bacillithiolation under HOCl-treatment [55]. A major defense mechanism against RCS-induced protein unfolding and aggregation is the upregulation of molecular chaperones and proteases. The redox-regulated chaperone Hsp33 is activated under HOCl stress conditions that leads to protein unfolding [61, 62]. Furthermore, increased levels of $OH\cdot$ under HOCl stress require the control of cellular metal pools. Mutants of *E. coli* lacking *fur* are more sensitive to HOCl compared to wild-type cells [63, 64]. Bacteria can also respond to RCS stress by changing the permeability and hydrophobicity of the outer membrane. In *E. coli*, the *ycfR* gene is strongly induced by RCS, leading to a reduced permeability and increased hydrophobicity of the outer membrane [65, 66].

2.2.1 Detoxification of RNS and RES

RNS, such as $ONOO^-$ react with LMW thiols by the formation of S-nitrosoglutathione as major defense mechanism [67, 68]. Reactions of $ONOO^-$ with haemoglobin and diffusion across the red blood cell membrane provide an alternative protection mechanism in eukaryotes [69-71]. The rapid reduction of $ONOO^-$ to nitrite by the selenocysteine containing glutathione peroxidase protects the cell from the formation of 3-nitrotyrosine [72].

RES include aldehydes, diamide and quinones that are detoxified by specific enzymes. The two-electron reduction of quinones to hydroquinones is catalyzed by the NADPH-

dependent quinone oxidoreductase 1 (NQO1), by-passing the formation of the highly reactive semiquinone [73]. Some quinones and the azo-compound diamide can be detoxified by reduction or ring-cleavage through azoreductases, nitroreductases and thiol-dependent dioxygenases [16].

The toxic aldehydes formaldehyde and methylglyoxal are degraded by specific aldehyde dehydrogenases and thiol-dependent glyoxalases [74]. Bacteria also assimilate formaldehyde by the ribulose monophosphate (RuMP)-dependent pathway leading to fructose-6-phosphate formation, which is further directed into the glycolytic pathway [75]. The detoxification of methylglyoxal in bacteria requires GSH- or BSH-dependent glyoxalase systems as well as thiol-independent oxidation pathways that require NAD⁺ [76].

2.3 The glyoxalase system: cellular adaptation to methylglyoxal stress

Methylglyoxal is a natural metabolite that is produced as a byproduct of glycolysis, lipid peroxidation, acetone metabolism, L-threonine degradation and DNA oxidation [76]. The methylglyoxal synthase (MgsA) catalyzes methylglyoxal formation from the glycolytic intermediate dihydroxyacetone phosphate (DHAP) [76, 77]. In the fatty acid/acetone metabolism, methylglyoxal is produced from acetone by enzymes of the cytochrome P450 gene subfamily. The NADPH-dependent conversion of acetone to methylglyoxal is controlled by formation of an acetol intermediate [78]. In the threonine and glycine metabolism, the metabolic intermediate aminoacetone is converted to methylglyoxal by the amine oxidase, which is termed as aminoacetone oxidase [77].

Methylglyoxal causes a variety of cytotoxic effects, including DNA damage, modification of amino acids and formation of glycation end-products. Thus, bacteria evolved different detoxification pathways for methylglyoxal removal [37, 79, 80]. The glyoxalase system is the major enzymatic pathway for degradation of methylglyoxal, which is ubiquitously distributed in all domains of life (**Figure 6**). Glyoxalases are classified into GSH-dependent and GSH-independent glyoxalases in *E. coli* [76, 81]. The GSH-dependent glyoxalase system of *E. coli* consists of the glyoxalase-I (GlxI; S-lactoylglutathione methylglyoxal lyase) and the glyoxalase-II (GlxII; S-hydroxyacylglutathione hydrolase) [77].

In the glyoxalase pathway, methylglyoxal reacts spontaneously with GSH to form a GSH-hemithioacetal intermediate. Glyoxalase I catalyzes the isomerization of GSH-hemithioacetal to S-lactoyl-GSH. Glyoxalase II hydrolyzes the thioester S-lactoyl-GSH into D-lactate to regenerate GSH [77, 79]. The S-lactoyl-GSH intermediate is required for activation of the KefBC- potassium/proton antiporter, leading to potassium efflux and proton import. Proton influx causes cytoplasmic acidification to prevent the interaction of methylglyoxal with DNA bases as protection mechanism against methylglyoxal (**Figure 6**) [82]. S-lactoyl-GSH also induces metabolic responses by generation of S-lactoylcysteinylglycine via the γ -

glutamyltranspeptidase, GTP-promoted assembly of microtubules, neutrophil movement and secretion of granules [81].

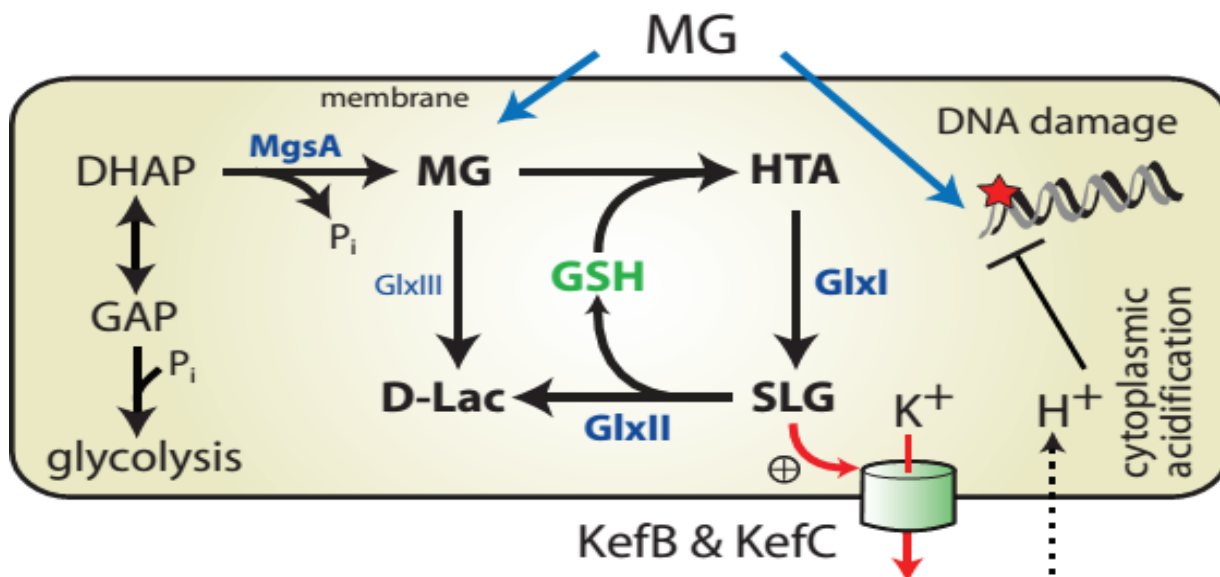


Figure 6: Methylglyoxal detoxification by glyoxalases in *E. coli*. Methylglyoxal (MG) is generated as a byproduct of the glycolysis or derived from exogenous sources. MG leads to the damage of cellular macromolecules, including DNA bases. In *E. coli*, the GSH-dependent and GSH-independent glyoxalase systems detoxify MG to D-lactate. The GSH-dependent glyoxalase system consists of glyoxalase-I (GlxI) and glyoxalase-II (GlxII) and provides the main route for MG detoxification. The intermediate S-lactoylglutathione activates the KefBC potassium/proton antiporter, leading to cytoplasmic acidification. The GSH-independent glyoxalase III (GlxIII) directly converts MG to D-Lactate. The figure is from [83].

The GSH-independent glyoxalase system requires the glyoxalase-III, originally identified as heat shock protein HchA in *E. coli*. Glyoxalase-III catalyzes the direct conversion of methylglyoxal to D-lactate without GSH [37, 76]. In the Gram-positive bacterium *B. subtilis*, related BSH-dependent glyoxalases GlxA and GlxB as well as BSH-independent systems (GlxC) could have been characterized recently [82].

3. Redox regulation by protein S-thiolation and its reversal in bacteria

3.1 The biosynthesis and functions of mycothiol in *Actinomycetes*

The cysteinyl pseudo-disaccharide mycothiol (MSH; AcCys-GlcN-Ins) is the major LMW thiol in *Actinomycetes*, including *Streptomyces*, *Mycobacteria* and *Corynebacteria* [84, 85]. The biosynthesis of MSH is catalyzed in five enzymatic steps, which involve MshA, MshA2, MshB, MshC and MshD (**Figure 7**). The first step of the MSH biosynthesis is catalyzed by the glycosyltransferase MshA which conjugates *myo*-inositol-1-P to UDP-GlcNAc, leading to the formation of the pseudodisaccharide phosphate GlcNAc-Ins-P. In the second step, the phosphatase MshA2 catalyzes dephosphorylation of GlcNAc-Ins-P to GlcNAc-Ins. The third

step involves the metal-dependent deacetylase MshB for deacetylation of GlcNAc-Ins, leading to the formation of GlcN-Ins [84, 86]. The MshB enzyme is a homolog of the MS-conjugate amidase Mca that catalyzes the hydrolysis of MS-conjugates. In the fourth step of the MSH biosynthesis, the ATP-dependent ligase MshC ligates cysteine to GlcN-Ins leading to Cys-GlcN-Ins. The Cys ligase MshC is a homolog of the Cys-tRNA synthetase. The acetyltransferase MshD catalyzes the acetylation of the cysteine amino group by acetyl-CoA as final step of the MSH biosynthesis [84, 85, 87].

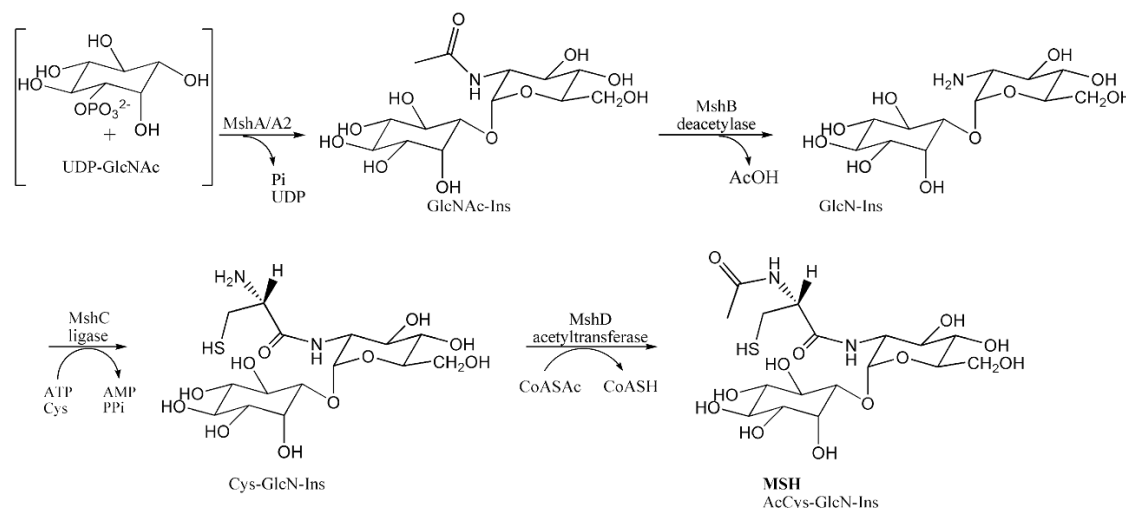


Figure 7: The MSH biosynthesis pathway in *Mycobacterium tuberculosis*. The MSH biosynthesis requires the precursor UDP-N-acetyl glucosamine, inositol-1-phosphate and cysteine. The stepwise MSH synthesis involves the glycosyltransferase MshA, the phosphatase MshA2, the deacetylase MshB, the ATP-dependent cysteine ligase MshC and the acetyltransferase MshD. The figure is from [88].

MSH serves as a thiol-cofactor for many detoxification enzymes that are involved in the detoxification of antibiotics, xenobiotics, ROS, RCS, RES, RNS and other reactive species [84]. Under oxidative stress, MSH is oxidized to mycothiol disulfide (MSSM) which requires the NADPH-dependent mycothiol disulfide reductase (Mtr) for NADPH-dependent reduction of MSSM to maintain a high MSH:MSSM redox ratio [85].

MSH conjugates xenobiotics and antibiotics either spontaneously or enzyme-catalyzed by MSH S-transferases (Mst), which belong to the DinB superfamily [89]. These MSH-S-conjugates are hydrolyzed by the mycothiol-S-conjugate amidase (Mca), releasing mercapturic acid derivatives (AcCysSR) and GlcN-Ins. GlcN-Ins is recycled to MSH and the toxic mercapturic acid derivatives are exported from the cell. Mca was shown to be involved in detoxification of MSH-S-conjugates with the antibiotics cerulenin and rifamycin in *Mycobacteria* [85]. MSH was also identified as sulfur donor for incorporation of the methylmercapto group into lincomycin in *Streptomyces lincolnensis* through unusual S-glycosylation reactions. This indicates a direct function of MSH in the biosynthesis of the sulfur-containing antibiotic lincomycin [90].

MSH serves as a cofactor for the MSH-dependent peroxidase Mpx that is involved in the detoxification of peroxides. Mpx was identified as S-mycothiolated Gpx-homolog under oxidative stress in *C. glutamicum* [91]. The MSH-dependent detoxification enzyme MscR is a dual function enzyme with S-nitrosylmycothiol (MSNO) reductase and formaldehyde dehydrogenase activity. Formaldehyde is conjugated to MSH, leading to S-hydroxymethyl-MSH, which is further oxidized to an S-formyl thioester and formate. MSNO is converted to MSH sulfonamide (MSONH₂) by MscR [84, 85]. The maleylpyruvate isomerase of *Corynebacterium glutamicum* uses MSH as a cofactor for the enzymatic isomerization of maleylpyruvate to fumarylpyruvate [92]. MSH also functions as cofactor of the MSH-dependent arsenate reductases ArsC1/C2 in the detoxification of arsenate [91, 93]. Moreover, MSH serves as reservoir for cysteine and is much less susceptible to autoxidation when compared to cysteine [85]. MSH also has an important function in the virulence and survival of the pathogen *M. tuberculosis* under infection conditions. MSH is essential for growth and viability in *M. tuberculosis* since the *mshC* mutant could only be generated in the presence of a second copy of *mshC* [94].

3.1.1 The functions of S-mycothiolated proteins in *M. smegmatis*

Protein S-mycothiolation is a widespread redox modification under NaOCl stress in *Actinomycetes* and involved in many cellular processes, including energy metabolism, fatty acid biosynthesis, nucleotide biosynthesis, amino acid biosynthesis, translation and in the oxidative stress response. In total, 58 S-mycothiolated proteins could be identified under NaOCl stress in *Mycobacterium smegmatis* (**Figure 8**) [95]. The peroxiredoxins Tpx, AhpC and OsmC are S-mycothiolated at their active and/or resolving cysteine residues, which are involved in redox regulation and detoxification processes in *M. smegmatis*. The global transcriptional regulator for iron uptake of the DtxR-family (IdeR) was S-mycothiolated at Cys102 in its primary iron-binding site [95].

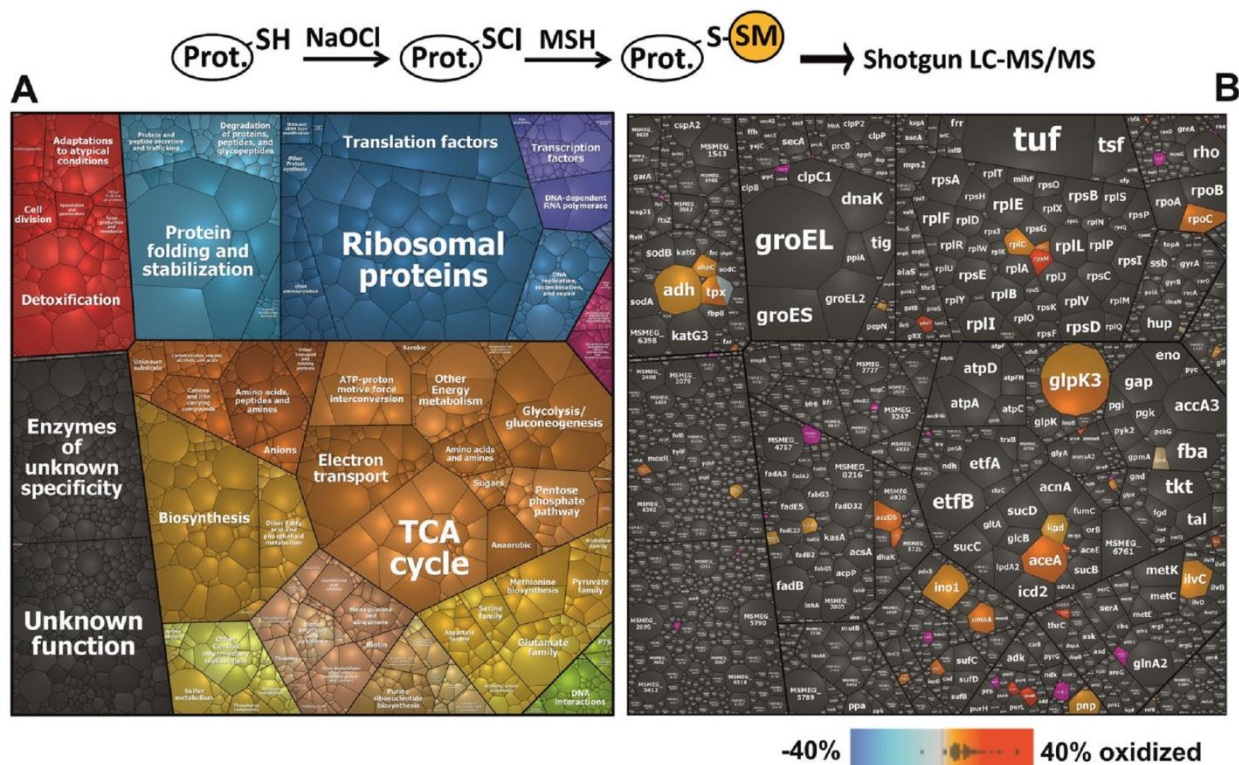


Figure 8: In total, 58 S-mycothiolated proteins of *M. smegmatis* were identified under NaOCl stress by proteomics, which are shown in comparison to their protein abundances in Voronoi treemaps. **(A)** Functional classification of the *M. smegmatis* proteome according to TIGRfam annotations, which served as legend for the Voronoi treemap in **(B)**. **(B)** The treemap includes the 58 identified S-mycothiolated proteins shown by an orange-red color gradient based on their cysteine oxidation level as quantified by the OxICAT [95]. Non-modified proteins are colored in grey and S-mycothiolated proteins, that were not identified using the OxICAT approach, are shown in pink. The cell size of the identified proteins is determined by the total spectral counts as protein abundance. The figure is from [95].

Many abundant enzymes of the energy metabolism were identified as S-mycothiolated in *M. smegmatis*, that are involved in the glycerol catabolism, glycolysis, the glyoxalate shunt and gluconeogenesis. The glycerol kinase GlpK3 and the glycerol dehydrogenase Adh2 are abundant S-mycothiolated proteins since glycerol is used as sole source of carbon and energy in *M. smegmatis*. The generation of dihydroxyacetone phosphate (DHAP) involves GlpK3 and Adh2. Thus, S-mycothiolation could prevent glycerol degradation under NaOCl stress to save the carbon and energy source. The isocitrate lyase AceA and the *myo*-inositol-1-phosphate synthase Ino1 were further identified as abundant S-mycothiolated proteins in *M. smegmatis*. AceA is the key enzyme of the glyoxalate bypass. Thus, S-mycothiolation of AceA could contribute to the survival of *M. smegmatis* under oxidative stress [95]. Furthermore, abundant enzymes involved in the biosynthesis of fatty acids as precursors for mycolic acids were S-mycothiolated in *M. smegmatis*, including acetyl-CoA carboxylases (AccD5 and AccD6), the enoyl-CoA hydratase (EchA6), the methoxy mycolic acid synthase (UmaA), the acyl-CoA

metabolites (GlmS). Interestingly, the glycolytic GapDH was identified as most abundant S-mycothiolated protein, contributing with 0.75 % to the total cysteine proteome in *C. diphtheriae*. In this doctoral thesis, GapDH was further analyzed for its redox regulation by S-mycothiolation under NaOCl and H₂O₂ stress and its reversal by the Mrx1 and Trx pathways *in vitro*.

3.2 The biosynthesis and functions of bacillithiol in *Firmicutes*

Bacillithiol (BSH, Cys-GlcN-malate) is the α -anomeric glycoside of L-cysteiny-D-glucosamine with L-malic acid which functions as the major LMW thiol in many Firmicutes bacteria, including *Bacillus* and *Staphylococcus* species [96]. The biosynthesis of BSH occurs in three steps by the enzymes BshA, BshB and BshC. The glycosyltransferase BshA catalyzes the conjugation of UDP-N-acetylglucosamine (UDP-GlcNAc) to L-malate, leading to GlcNAc-Mal (**Figure 10**). GlcNAc-Mal is further deacetylated by the deacetylase BshB to GlcN-Mal. The cysteine ligase BshC adds cysteine to GlcN-Mal as final step in the BSH biosynthesis.

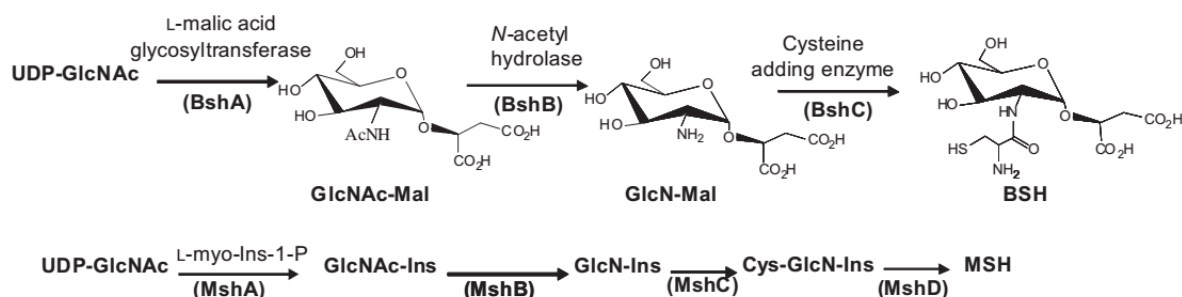


Figure 9: The BSH biosynthesis pathway in comparison to the MSH biosynthesis. The BSH biosynthesis requires the precursor UDP-N-acetyl glucosamine, L-malate and cysteine and is catalyzed in three steps by the glycosyltransferase BshA, N-acetyl hydrolase BshB and the cysteine-adding enzyme BshC to generate BSH. The MSH biosynthesis shows similarities to the BSH biosynthesis pathway including the homologous enzymes MshA, MshB and MshC. The figure is from reference [97].

BSH functions in the detoxification of thiol-reactive compounds, electrophiles, alkylating agents and antibiotics. BSH-deficient mutants in *B. subtilis* showed increased sensitivity towards hypochlorite, diamide, methylglyoxal, ROS, osmotic and acidic stress, alkylating agents and fosfomycin in phenotype studies. Thus, BSH is involved in the detoxification of various reactive species and toxic compounds. The NADPH-dependent flavin oxidoreductase YpdA was suggested to function as bacillithiol disulfide (BSSB) reductase to maintain BSH in its reduced state [55, 97].

The BSH-dependent thiol-S-transferase FosB is involved in the detoxification of the antibiotic fosfomycin and cleaves the ring structure of the BSH-fosfomycin-conjugate [98]. The *fosB* and *bsh* mutants showed equal sensitivities towards fosfomycin treatment in *B. subtilis* and *S. aureus*, indicating that FosB is a BSH-dependent S-transferase for fosfomycin detoxification. Co-crystallization of the *S. aureus* FosB with BSH resulted in the formation of a BSH-mixed disulfide at the active site Cys9 of FosB of *S. aureus* *in vitro* [97, 99]. Apart from

FosB, the BSH S-transferase BstA catalyzes the conjugation of BSH to reactive electrophiles, such as chlorinated hydrocarbons and monobromobimane *in vitro*. The resulting mercapturic acids are exported from the cell by potential efflux pumps that are encoded by the *yfiS* and *yfiU* genes [89].

BSH functions in detoxification of methylglyoxal as cofactor for the BSH-dependent glyoxalases GlxA and GlxB in *B. subtilis*. Methylglyoxal reacts spontaneously with BSH to form BSH-hemithioacetal that is converted to S-lactoyl-BSH by GlxA. GlxB catalyzes the hydrolysis of S-lactoyl-BSH to lactate as end product, which is secreted from the cell [82]. In addition, phenotype studies in *B. subtilis* indicated the involvement of BSH in the detoxification of heavy metals, such as tellurite and selenite [100]. BSH also binds and stores Zn^{2+} and functions as an intracellular Zn^{2+} buffer in metal ion homeostasis. The thiolate, amine and carboxylate groups of BSH serve as ideal ligands for metal coordination, binding Zn^{2+} as $(\text{BSH})_2:\text{Zn}^{2+}$ complex under Zn^{2+} stress [101]. Treatment of the BSH-deficient mutant with Zn^{2+} resulted in a decreased accumulation of Zn^{2+} , due to an increased expression of the CadA and CzcD efflux systems. BSH also protects against Zn^{2+} toxicity in cells lacking Zn^{2+} efflux pumps [101].

BSH also plays an important role in the virulence and survival of *S. aureus* under infection conditions as revealed by phenotype analysis of *bshA* mutants in clinical methicillin-resistant *S. aureus* (MRSA) isolates. The survival of *S. aureus* COL and USA300 *bshA* mutants as well as the natural *bshC* mutant of strain SH1000 were decreased in phagocytosis infection assays, using murine macrophages and human whole-blood assays [102] [103]. These results suggest a role of BSH in the defense against the host-immune system and in the survival of *S. aureus* under infection conditions.

3.3 The role of protein S-bacillithiolation in Gram-positive *Firmicutes*

BSH plays an important role in post-translational modifications of proteins under oxidative stress in *B. subtilis* and *S. aureus*. In response to HOCl stress, protein thiols are oxidized to mixed disulfides with BSH, termed as protein S-bacillithiolation [104-106]. In total, eight common and 29 unique S-bacillithiolated proteins were identified in *Bacillus* and *Staphylococcus species* previously [106]. Many of the identified S-bacillithiolated proteins control important cellular processes, such as the biosynthesis of amino acids, cofactors and nucleotides as well as protein translation. The methionine synthase MetE was identified as the most abundant S-bacillithiolated protein in *B. subtilis*, which was S-bacillithiolated at the active site Cys730 and at the non-conserved Cys719 [105]. The MarR-type repressor OhrR was S-bacillithiolated at its redox-sensing Cys15. S-bacillithiolation of OhrR at its lone cysteine residue leads to inactivation of its repressor function and derepression of transcription of the *ohrA* gene, encoding the peroxiredoxin OhrA [104, 105]. The translation elongation factor EF-Tu (TufA) and the IMP dehydrogenase GuaB were also identified as abundant and essential

S-bacillithiolated proteins under NaOCl stress [55, 91, 106]. The bacilliredoxins BrxA, BrxB and BrxC were identified as S-bacillithiolated in *B. subtilis* and *S. carnosus*, which could represent snapshots of intermediates in the bacilliredoxin pathway [106, 107].

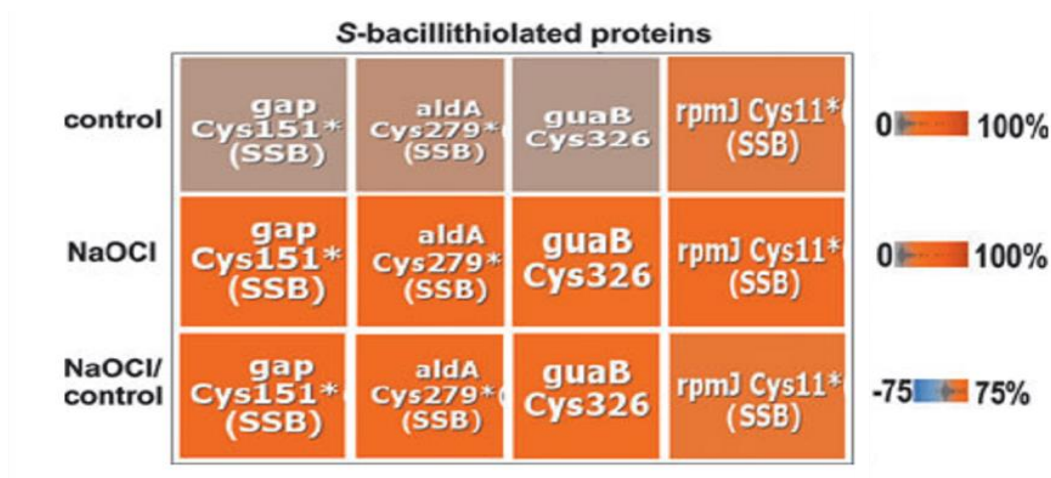


Figure 10: Close-up of the redox treemap of *S. aureus* showing S-bacillithiolated proteins identified under NaOCl stress *in vivo*. Enlarged section of the redox treemap is shown that include the identified S-bacillithiolated proteins (Gap, AldA, GuaB, RpmJ). The close-up shows the percentage of thiol oxidation under control, NaOCl stress, and the percentage of oxidation increase under NaOCl stress versus control by a color gradient. The asterisks denote conserved cysteine residues. The figure is from reference [108].

In *S. aureus*, five S-bacillithiolated proteins could have been identified using shotgun LC-MS/MS analysis under NaOCl stress, including Gap, AldA, GuaB, RpmJ and PpaC [108] (**Figure 11**). GuaB, Gap and AldA were S-bacillithiolated at their conserved catalytic active site Cys307, Cys151 and Cys279 residues, respectively.

The glycolytic Gap is the most abundant S-bacillithiolated protein contributing with 4 % to the total cysteine proteome of *S. aureus* [108]. As part of this doctoral thesis, the redox regulation of Gap of *S. aureus* by S-bacillithiolation and bacilliredoxin under NaOCl and H₂O₂ stress was studied in detail in comparison to GapDH of *C. diphtheriae*. In addition, the aldehyde dehydrogenase AldA was identified as another target for S-bacillithiolation in *S. aureus*. Thus, we studied the redox regulation, expression, function and structural changes of AldA in *S. aureus* more in detail. AldA was identified as an important enzyme that contributes to the HOCl defense in *S. aureus* [109].

4. Redox regulation of protein S-thiolation by mycoredoxins and bacilliredoxins

4.1 Redox regulation of protein S-mycothiolation by mycoredoxin-1 (Mrx1)

The redox regulation of protein S-mycothiolations requires specific thiol-disulfide reducing pathways to restore the protein activity. The Mrx1/MSH/Mtr system is specific for the demycothiolation of MSH-mixed protein disulfides (**Figure 12**). Mycoredoxin-1 (Mrx1) was characterized as a glutaredoxin-homolog in *Actinomyces* [110]. Mrx1 has a typical Trx-like fold with a CGYC catalytic active site, composed of a four-stranded antiparallel β -sheet and surrounded by three α -helices. The CGYC motif is located at the N-terminus of the first α -helix. The conserved proline residue (Pro57) is located in *cis*-conformation opposite to the active site. The active site Cys14 is solvent exposed in the oxidized and reduced form of Mrx1, while the C-terminal resolving Cys17 is buried inside the protein [110]. Mrx1 has a negative redox potential of -218 mV that is in the same range as for glutaredoxin. Thus, Mrx1 functions as effective thiol disulfide reducing enzyme in *Actinomyces* [111]. Mrx1 catalyzes the demycothiolation of MSH-mixed protein disulfides in a bimolecular nucleophilic substitution reaction analogous to the monothiol reaction mechanism of glutaredoxins. During demycothiolation of the substrate, Mrx1 is S-mycothiolated at its active site Cys14. Oxidized Mrx1 is regenerated by MSH leading to the formation of MSSM, which is recycled back to MSH by Mtr with NADPH as electron donor. The electron transfer from the Mrx1/MSH/Mtr electron pathway to the MSH-mixed disulfide substrate was shown in a hydroxyethyl disulfide (HED) assay [110].

The thiol peroxidase Tpx was identified as S-mycothiolated at its active and resolving Cys60 and Cys94 residues under HOCl stress *in vivo*. Mrx1 was shown to catalyze the demycothiolation of Tpx-SSM as the first substrate *in vitro* [91]. The membrane-associated peroxidase AhpE of *M. tuberculosis* was S-mycothiolated at its active site Cys45 *in vitro* and also shown to be reduced by Mrx1 as another substrate [112].

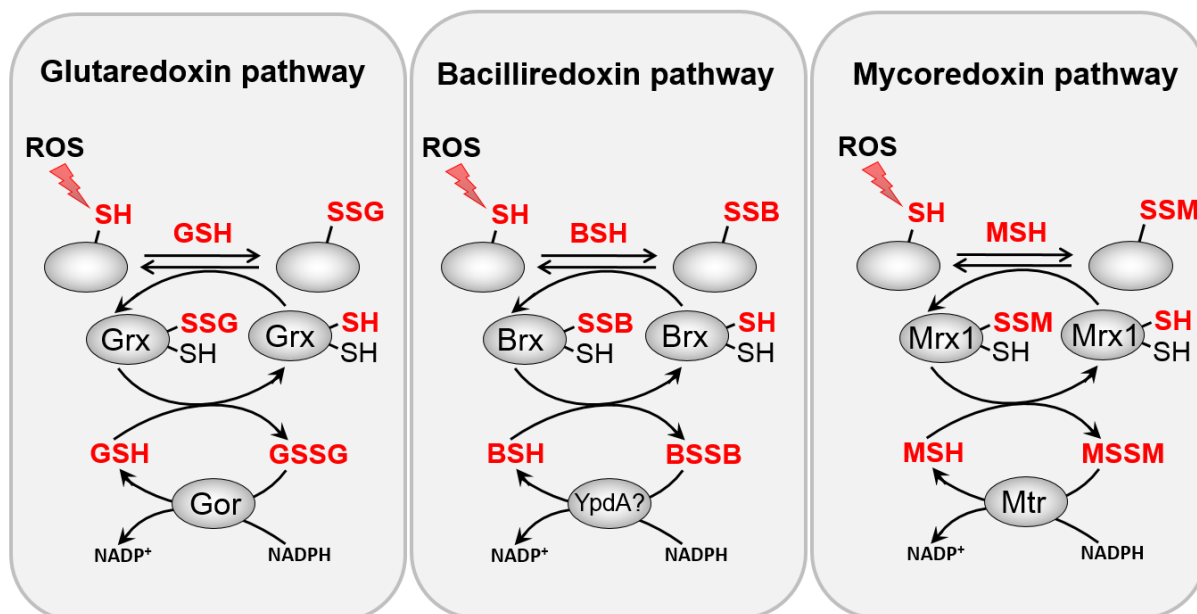


Figure 11: Reduction of protein S-glutathionylations, S-bacillithiolations and S-mycothiolations by glutaredoxin, bacilliredoxin and mycoredoxin pathways. The S-glutathionylated proteins are reduced by glutaredoxins (Grx) leading to a Grx-SSG intermediate that is reduced by GSH, leading to GSSG which is recycled back to GSH by the NADPH-dependent GSSG reductase (Gor). Analogous bacilliredoxin and mycoredoxin pathways have been characterized in BSH- and MSH-utilising Gram-positive bacteria. The S-bacillithiolated proteins are reduced by bacilliredoxins (Brx) leading to Brx-SSB formation. Brx-SSB is reduced by BSH with the generation of BSSB that likely requires the NADPH-dependent BSSB reductase YpdA for regeneration of BSH. In *Actinomycetes*, mycoredoxin1 catalyzes the reduction of S-mycothiolated proteins, leading to Mrx1-SSM generation that is recycled by MSH and the NADPH-dependent MSSM reductase Mtr.

4.2 Redox regulation of protein S-bacillithiolation by bacilliredoxin (Brx)

The reduction of S-bacillithiolated proteins in *Firmicutes* is catalyzed by the bacilliredoxin redox pathway (**Figure 12**). The bacilliredoxins BrxA and BrxB were identified as paralogs of the DUF1094 family in *B. subtilis*, which shared 53 % sequence identity. Phylogenomic profiling identifies BrxA and BrxB as Trx-like proteins with unusual CGC active sites [113, 114]. The crystal structure of BrxA reveals overall structural similarities to thioredoxins. However, the redox potential was determined as -130 mV, which is much more positive compared to that of thioredoxin proteins [115]. Furthermore, BrxC was identified as candidate for a monothiol Brx which has a TCPIS active site motif and is similar to monothiol Grxs. However, the function of BrxC in de-bacillithiolation remains to be elucidated [116]. The flavin disulfide reductase YpdA was suggested as putative BSSB reductase in the STRING search due to its phylogenetic co-occurrence together with the BSH biosynthesis enzymes. However, the catalytic activity of YpdA in BSSB reduction could not be demonstrated [97]. Bacilliredoxins function analogous to glutaredoxins by the attack of the active site cysteine on BSH-mixed protein disulfides,

resulting in the transfer of BSH to the active site cysteine of Brx [113]. In *B. subtilis*, the S-bacillithiolated OhrR repressor and the methionine synthase MetE were identified as natural substrates for BrxA and BrxB *in vitro*. While de-bacillithiolation of OhrR-SSB is catalyzed mainly by BrxB, reduction of MetE-SSB can be catalyzed by both BrxA and BrxB [113].

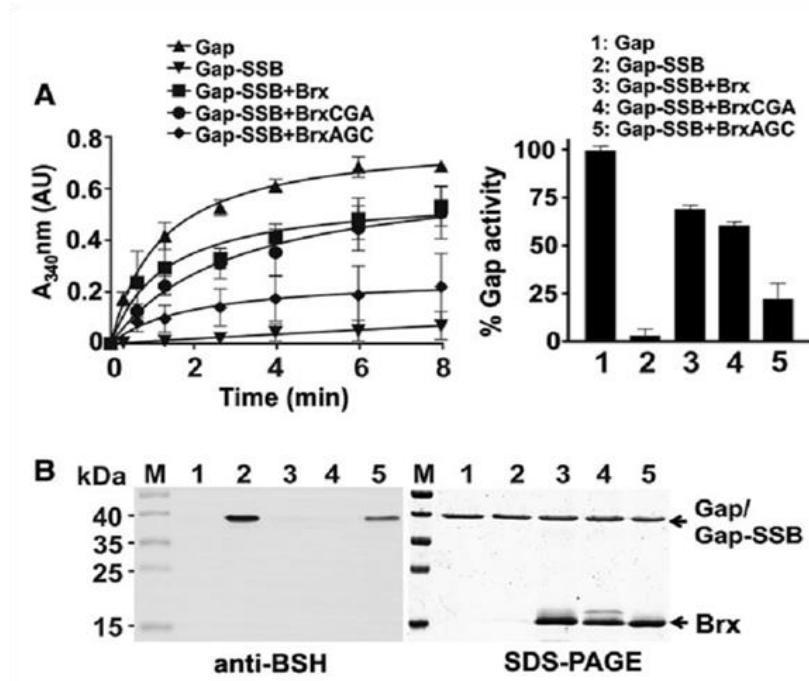


Figure 13: Recycling of S-bacillithiolated Gap requires the bacilliredoxin Brx *in vitro*. (A) Gap activity is reversibly inhibited by S-bacillithiolation *in vitro* and can be restored by reduction using the bacilliredoxin Brx (SAUSA300_1321). De-bacillithiolation required the Brx active site Cys. The BrxAGC mutant showed weak activity to reduce Gap-SSB, while the BrxCGA mutant could restore Gap activity similar to the wild-type Brx protein. S-bacillithiolated Gap was generated *in vitro* by treatment of Gap with H₂O₂ in the presence of BSH. (B) De-bacillithiolation of Gap-SSB by Brx and its cysteine mutant proteins *in vitro* was monitored using nonreducing BSH-specific Western blot analysis. The SDS-PAGE is shown as loading control (right). The numbers 1–5 shown in the BSH Western blot and in the SDS-PAGE refer to the legend shown in (A).

In this doctoral thesis, we studied the function of Brx of *S. aureus* in reduction of S-bacillithiolated Gap *in vitro* (Figure 13). Gap activity could be restored by de-bacillithiolation with the Brx wild type and BrxCGA resolving cysteine mutant proteins, but not with the BrxAGC active site mutant protein. The reduction of Gap-SSB by Brx wild type and the BrxCGA mutant was confirmed in BSH-specific Western blots. Our results indicate that S-bacillithiolation of Gap functions in protection and redox regulation of the Gap active site cysteine and can be reversed by the bacilliredoxin Brx *in vitro*.

5. Redox regulation of the metabolic enzymes GapDH and AldA

5.1 The glyceraldehyde-3-phosphate dehydrogenase (GapDH) protein family

5.1.1 Structure and catalytic mechanism of GapDH

The glyceraldehyde-3-phosphate dehydrogenase (GapDH) is highly conserved across all kingdoms of life [117]. Many bacteria contain a single GapDH, while others possess multiple GapDH homologs. In *E. coli*, *gapA*, *gapB* and *gapC* encode for three GapDH homologs [118]. In *B. subtilis* and *S. aureus*, two GapDH homologs are encoded by *gapA* and *gapB*. GapA functions in the glycolysis using NAD^+ as cofactor, while GapB participates in the gluconeogenesis with NADP^+ as cofactor [119, 120]. The phosphorylating glyceraldehyde-3-phosphate dehydrogenase (GapDH, EC 1.2.1.12) is a member of the GapDH protein family, while the non-phosphorylating glyceraldehyde-3-phosphate dehydrogenase (GapDN, EC 1.2.1.9) belongs to the aldehyde dehydrogenase (ALDH) superfamily [121, 122]. GapDN is present in plants, algae and bacteria, catalyzing the NADP^+ -dependent oxidation of glyceraldehyde-3-phosphate (G3P) to 3-phosphoglycerate (3-PG) [123]. The homotetrameric GapDH is the key enzyme of the glycolysis and catalyzes the oxidative phosphorylation of G3P to 1,3-bis-phosphoglycerate (1,3-BPG) (**Figure 14**). All GapDH structures share a common conserved fold composed of a NAD(P)^+ -binding domain and a catalytic domain [124-126].

The catalytic mechanism of the phosphorylating GapDH is initiated by the nucleophilic attack of the active site cysteine on the aldehyde carbon of the G3P substrate, forming a covalently enzyme-bound hemithioacetal intermediate. The transfer of a reactive hydride ion to a tightly bound NAD^+ oxidizes the thiol-bond of the hemithioacetal to an energy rich thioester bond, releasing NADH . The hydride ion transfer is stabilized by an adjacent histidine residue in the active site of the enzyme. The binding of a second NAD^+ molecule to the acyl-enzyme intermediate stabilizes the negatively charged carbonyl group of the thioester and makes the carbonyl vulnerable to a nucleophilic attack by the inorganic phosphate. The phosphorolysis reaction of inorganic phosphate and the acyl-enzyme intermediate releases the product 1,3-BPG [127-129].

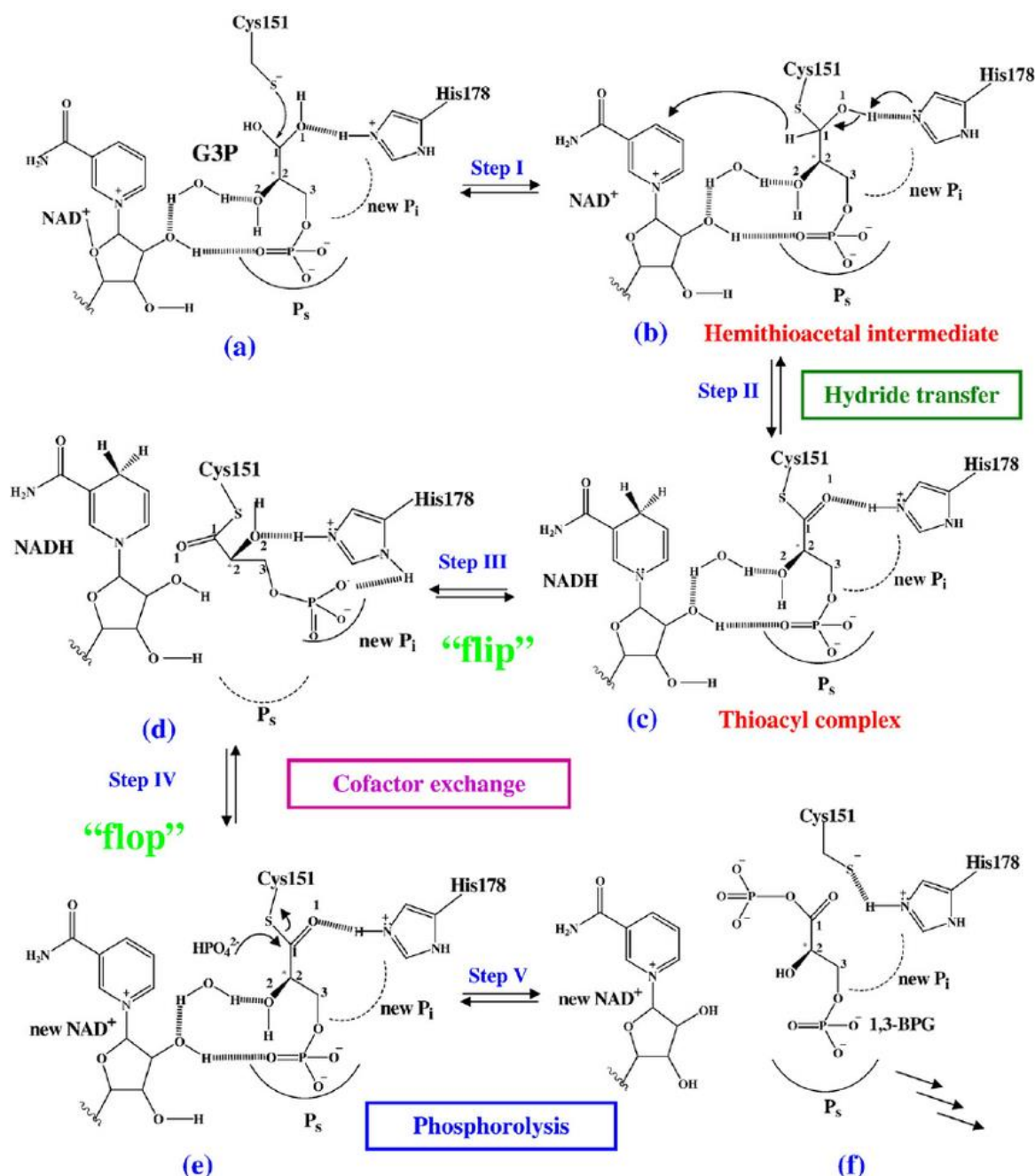


Figure 14: The catalytic mechanism of the phosphorylating glyceraldehyde-3-phosphate dehydrogenase 1 (GapDH1) of *S. aureus* MRSA252. In the first step, D-glyceraldehyde-3-phosphate (G3P) binds to the active site of GapDH (a). The nucleophilic attack of the catalytic active site Cys151 at the aldehyde carbon of G3P leads to the formation of a tetrahedral hemithioacetal intermediate (b). The second step involves a hydride transfer from the hemithioacetal intermediate to NAD⁺, leading to a thioacyl complex (c). In the third step, the G3P phosphate group is repositioned ("flip") (d). In the fourth step, the NAD⁺ cofactor is released and a new NAD⁺ enters the active site. The phosphate group of G3P relocates again ("flop") to restore hydrogen-bonding with NAD⁺ (e). In the fifth step, the phosphorolysis releases the 1,3-bisphosphoglycerate (1,3-BPG) from the active site of Gap. The figure is from reference [130].

5.1.2 Functions and metabolic adaptation of GapDH under oxidative stress

GapDH is a multifunctional enzyme that is involved in numerous cellular processes, including transcriptional and post-transcriptional regulation, chromatin structure, intracellular trafficking, DNA replication and DNA repair [131-133]. Other functions of bacterial GapDHs are mainly associated with their extracellular localization. GapDH of pathogenic bacteria was shown to be secreted and localized at the bacterial surface, enabling the colonization and manipulation of host cells [134]. In pathogenic *E. coli*, GapDH contributes to the host infection by interaction with human plasminogen and fibrinogen [135]. Secreted GapDH can catalyze its own post-translational modification by ADP-ribosylation to protect bacteria against oxidative stress [136]. The interaction of secreted GapDH with mucin was shown for probiotic strains, contributing to intestinal colonization [137, 138]. In *Mycoplasma pneumoniae*, GapDH is located at the surface and contributes to the colonization of the respiratory tract by interaction with extracellular matrix proteins of human host cells [139].

In *E. coli*, GapDH has also intracellular functions that are not related to its glycolytic function. GapDH was shown to interact with the phosphoglycolate phosphatase (Gph). Gph is involved in the DNA repair of 3'-phosphoglycolate ends that are generated by the antibiotic bleomycin [140, 141]. GapDH also interacts with proteins of the base-excision repair (BER) pathway, including Endo IV, uracil DNA glycosylase (UDG) and the single-stranded DNA binding protein (SSB) [134].

The GapDH active site cysteine is highly sensitive to oxidation by H_2O_2 and subject to numerous post-translational thiol-modifications. The redox sensitivity of the GapDH active site depends on a highly conserved proton relay mechanism that enhances its reactivity towards H_2O_2 [142]. The H_2O_2 -dependent oxidation of GapDH leads to its inactivation and re-direction of the glycolytic flux into the pentose phosphate shunt for NADPH generation. NADPH is required as cofactor for thiol-disulfide reductases. The reactivation of S-thiolated GapDH itself requires NADPH-dependent reducing systems. Therefore, GapDH is kept inactive by S-thiolation until NADPH levels are restored, allowing a reactivation of GapDH activity [17, 142, 143]. Our results showed a high sensitivity of GapDH of *C. diphtheriae* and *S. aureus* towards H_2O_2 and NaOCl-induced overoxidation *in vitro*. GapDH was identified as S-mycothiolated under NaOCl stress in *C. diphtheriae* *in vivo*. Thus, we investigated the kinetics of GapDH inactivation under H_2O_2 and NaOCl-stress in the overoxidation and S-mycothiolation pathways in comparison (**Figure 15**).

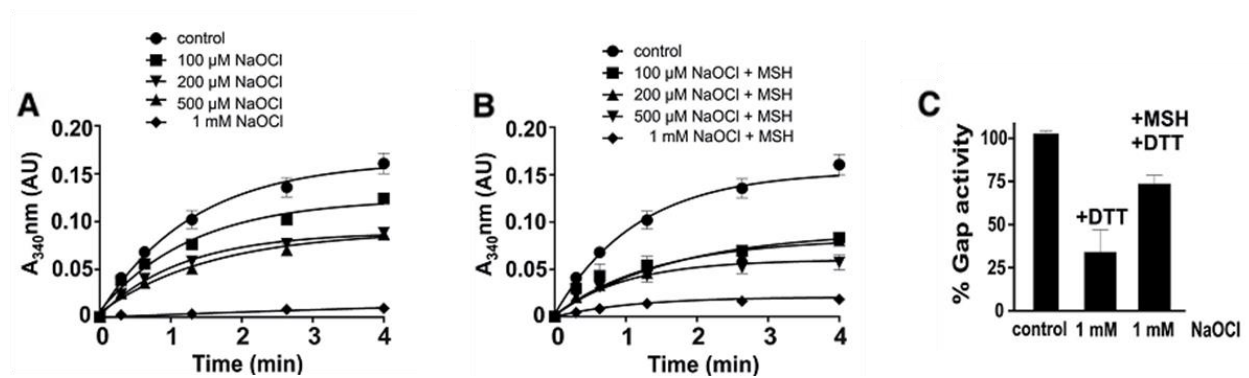


Figure 15: Protein S-mycothiolation protects GapDH of *C. diphtheriae* against overoxidation under NaOCl stress *in vitro*. GapDH was inactivated by NaOCl alone (A) or in the presence of NaOCl and MSH (B), followed by reduction with 10 mM DTT (C). The inhibition of GapDH activity is due to overoxidation and intramolecular disulfide formation with NaOCl alone. However, GapDH activity is reversibly inhibited by NaOCl and MSH due to S-mycothiolation of the active site Cys153.

In *S. aureus*, the glycolytic GapDH was identified as most abundant target for S-bacillithiolation under NaOCl stress *in vivo*. Thus, we further analyzed the inactivation of Gap of *S. aureus* by H_2O_2 and NaOCl-induced oxidation in the absence and presence of BSH (Figure 16). The results showed that GapDH of *S. aureus* is faster inactivated by H_2O_2 and NaOCl stress due to S-bacillithiolation compared to the overoxidation. These results indicate that S-bacillithiolation of the GapDH active site can effectively protect the enzyme against the irreversible overoxidation under H_2O_2 and NaOCl stress.

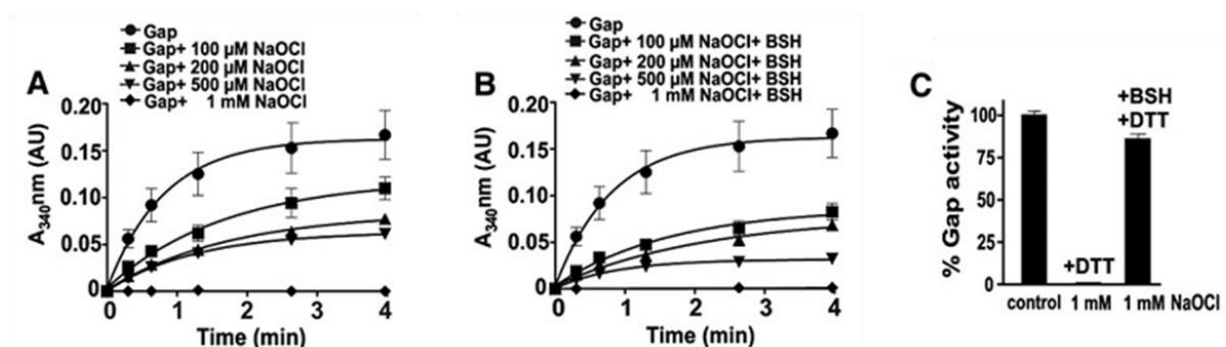


Figure 16: Protein S-bacillithiolation protects Gap of *S. aureus* against overoxidation under NaOCl stress *in vitro*. Gap was inactivated by NaOCl alone (A) or in the presence of NaOCl and BSH (B), followed by reduction with 10 mM DTT (C). The inhibition of Gap activity is due to overoxidation with NaOCl alone, while Gap activity was reversibly inhibited with NaOCl and BSH due to S-bacillithiolation of the active site Cys151.

The kinetic comparison of both GapDH enzymes further suggests that the *S. aureus* Gap enzyme is more sensitive to oxidative inactivation compared to GapDH of *C. diphtheriae* since lower NaOCl doses effectively inhibited *S. aureus* Gap activity. This higher sensitivity of *S.*

aureus Gap may be due to the absence of the second cysteine in the otherwise highly conserved C₁₅₃TTNC₁₅₇ motif, which is present in GapDH of *C. diphtheriae*.

5.2 The aldehyde dehydrogenase (ALDH) protein family

5.2.1 Structure and catalytic mechanism of the ALDH enzymes

The aldehyde dehydrogenase (ALDH) family is a unique class of enzymes that includes NAD⁺-dependent aldehyde dehydrogenases (ALDH, EC 1.2.1.3) and some NADP⁺-dependent aldehyde dehydrogenases (ALDH, EC 1.2.1.4) [144]. These enzymes are different compared to other classes of aldehyde dehydrogenases, such as haemoprotein/quinoprotein ALDHs, molybdoprotein ALDHs and tungsten-containing aldehyde ferredoxin oxidoreductases. Haemoprotein/quinoprotein ALDHs contain a pyroloquinoline, quinone or quinoxaline as prosthetic group and a quinoprotein-specific super barrel domain [145]. Molybdoprotein ALDHs contain an FeS cluster in their active site and need molybdopterin-cytosine-dinucleotide, FAD⁺ and an acid-labile sulfide as cofactors [146]. Tungsten-containing aldehyde ferredoxin oxidoreductases utilize tungsten, FeS clusters and molybdopterin to oxidize aldehyde substrates [147]. Enzymes of the ALDH family contain NAD⁺ or in some exceptions NADP⁺ as cofactor and do not require molybdopterin-based cofactors and FeS clusters.

The ALDH proteins are tetramers or dimers. Each subunit contains a catalytic domain, an 'arm-like' bridging domain and the Rossmann-fold domain [148]. ALDHs have a β - α , β NAD⁺-binding mode at their Rossmann-fold domain. This is different from the classical β - α , β NAD⁺-binding mode observed in all other aldehyde dehydrogenases with Rossmann-folds [148]. A funnel passage is located at the interface of all three domains that leads to the catalytic pocket. The lower portion of the funnel is composed of highly conserved residues of the nucleotide-binding and catalytic domains that form the catalytic active site. The hydride transfer from the cofactor to the substrate is catalyzed in the active site [149]. ALDHs catalyze the NAD⁺-dependent oxidation of aldehydes to their carboxylic acids in four steps (**Figure 17**) [150]. In the first step, a tetrahedral hemithioacetal-enzyme complex is formed. NAD⁺ binding repositions the catalytic cysteine, allowing the nucleophilic attack on the carbonyl carbon of an aldehyde substrate. The nucleophilicity of the catalytic cysteine is achieved by deprotonation through an adjacent conserved glutamate residue. In the second step, hydride transfer from the hemithioacetal intermediate to NAD⁺ generates a covalent thioester intermediate. In the third step, NADH is released from the enzyme allowing hydrolysis of the thioester intermediate. Therefore, nucleophilic water attacks the thioester intermediate to generate a second tetrahedral intermediate. In the final step, hydrolysis of the thioacyl enzyme complex releases a carboxylic acid product [150].

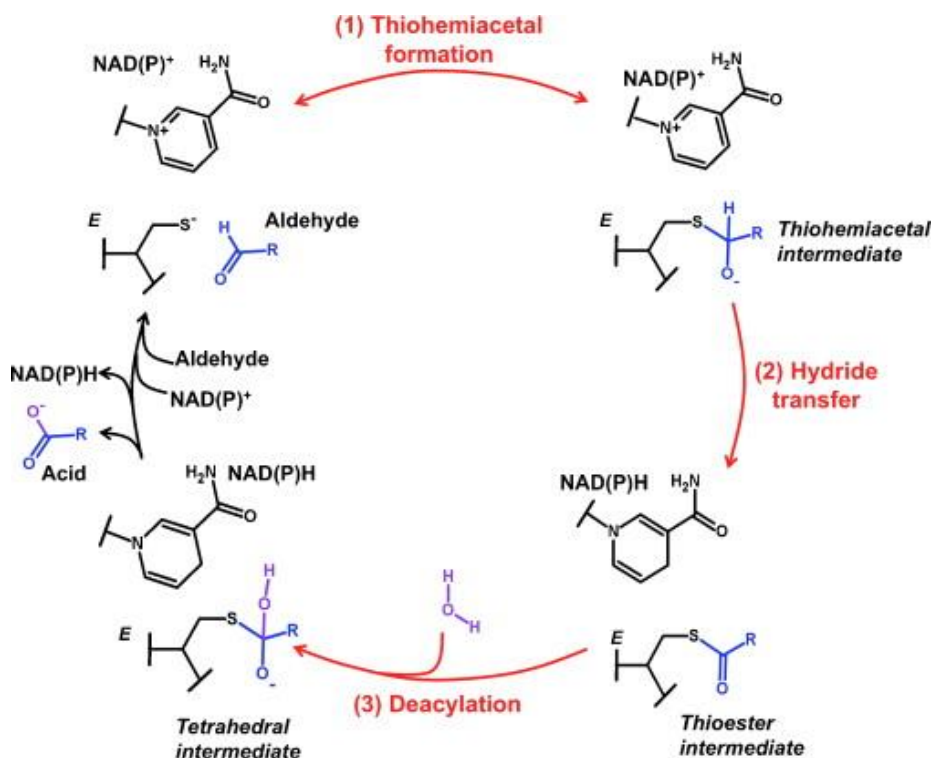


Figure 17: Catalytic mechanism of the NAD(P)⁺-dependent aldehyde dehydrogenases. NAD(P)⁺ binds tightly to the active site and repositions the catalytic active site cysteine. Nucleophilic attack of the catalytic cysteine at the aldehyde carbon leads to formation of a thiohemiacetal intermediate **(1)**. Hydride transfer to NAD(P)⁺ results in a thioester intermediate **(2)**. Deacylation is catalyzed by attack of a nucleophilic water molecule, generating a tetrahedral intermediate. In the final hydrolysis, a carboxylic acid product is released **(3)**. The figure is from reference [151].

5.2.2 Functions and metabolic adaptation of ALDHs under oxidative stress

The main function of ALDHs is the oxidation of metabolic and biogenic amine-derived aldehydes to their corresponding carboxylic acids [144]. The substrate specificity of ALDHs depends on the amino acid residues at the upper portion of the funnel at the interface of all three domains. The betaine aldehyde dehydrogenase of *S. aureus* uses betaine aldehyde as substrate, which is oxidized to the osmoprotectant glycine betaine [150]. The human succinic semialdehyde dehydrogenase from the brain uses succinic semialdehyde as substrate [152]. The rat liver formaldehyde dehydrogenase specifically catalyzes the oxidation of S-hydroxymethyl glutathione [153]. The salicylaldehyde dehydrogenase (NahF) from *Pseudomonas putida* is an example for an ALDH with a broad substrate spectrum. This enzyme catalyzes the oxidation of salicylaldehyde and several other aliphatic and aromatic aldehydes [154].

In this doctoral thesis, we characterized the NAD⁺-dependent aldehyde dehydrogenase AldA of *S. aureus*. AldA showed a broad substrate specificity for the oxidation of formaldehyde, methylglyoxal, glycolaldehyde and acetaldehyde as potential substrates (**Figure 18**). Transcription of *aldA* is induced under NaOCl, diamide and formaldehyde stress in a SigmaB-

independent manner. In phenotype survival assays, the *aldA* mutant was very sensitive to NaOCl stress, indicating that AldA could be involved in detoxification of aldehydes that are elevated under NaOCl stress. Thus, AldA could function in the detoxification of methylglyoxal that is produced under NaOCl stress in *S. aureus*. The increased production of methylglyoxal under HOCl stress was previously shown in *E. coli* [38].

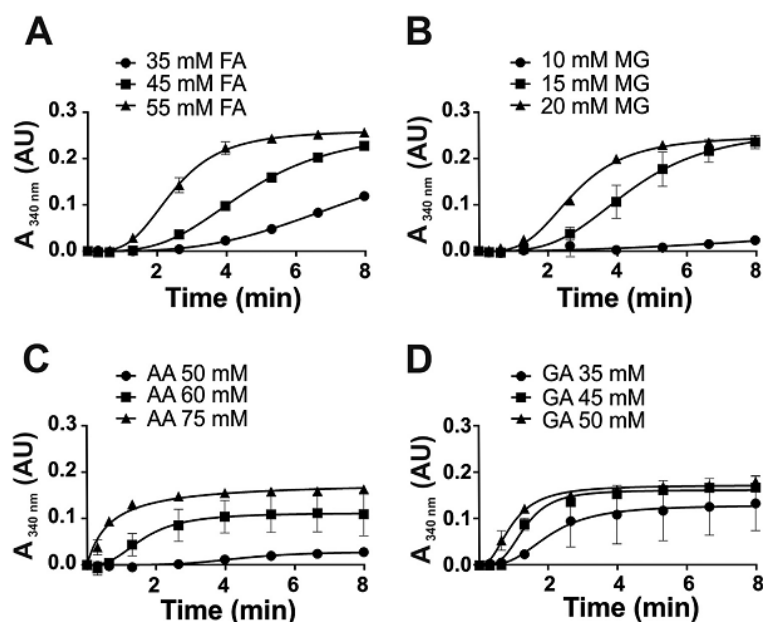


Figure 18: Purified AldA shows broad substrate specificity towards various aldehydes *in vitro*.

The catalytic activity of the aldehyde dehydrogenase AldA was analyzed with increasing concentrations of different aldehyde substrates ranging from 10-100 μ M, including **(A)** formaldehyde (FA), **(B)** methylglyoxal (MG), **(C)** acetaldehyde (AA) and **(D)** glycolaldehyde (GA). The oxidation of aldehydes was measured in the presence of NAD⁺ as coenzyme and NADH generation was monitored at 340 nm using a spectrophotometer.

Apart from their role in aldehyde detoxification, ALDHs have other catalytic and non-catalytic functions. Some ALDHs have an additional esterase activity to catalyze ester hydrolysis [155]. Some ALDHs were shown to bind androgen, cholesterol, thyroid hormone and exogenously derived xenobiotics [156]. In addition, these enzymes can function as antioxidants by contributing to the production of NAD(P)H or by scavenging hydroxyl radicals *via* cysteine sulfhydryl groups [157, 158]. ALDHs were shown to play a role in pheromone metabolism and developmental processes [148].

We could show that AldA of *S. aureus* is protected by S-bacillithiolation against the irreversible inactivation to overoxidation under oxidative stress *in vitro*. This could be a new mechanism for the metabolic adaptation of *S. aureus* under infection conditions **(Figure 19)**. Thus, AldA represents a novel thiol-switch mechanism required for the defense of *S. aureus* under HOCl stress.

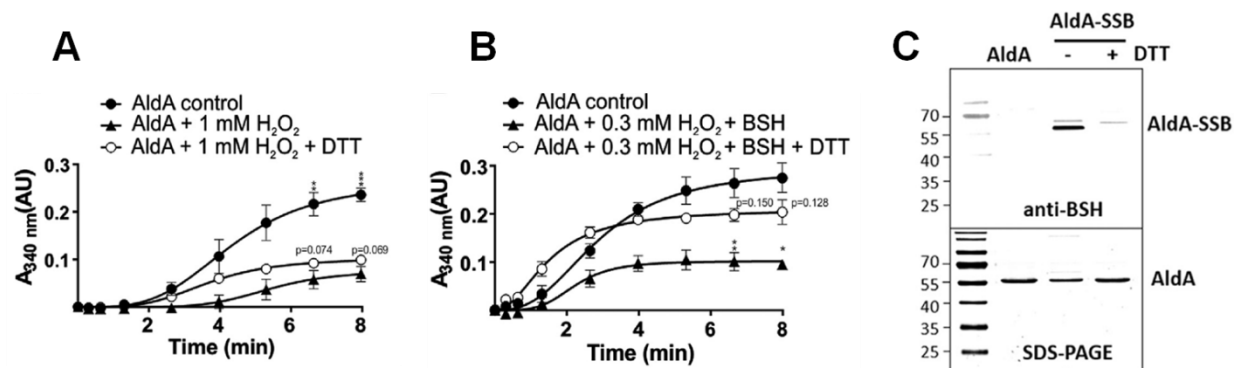


Figure 19: Protein S-bacillithiolation protects AldA of *S. aureus* against overoxidation under H₂O₂ stress *in vitro*. AldA is irreversibly inactivated by H₂O₂ alone due to overoxidation (**A**). In the presence of H₂O₂ and BSH, AldA is reversibly inactivated due to S-bacillithiolation (**B,C**) as revealed by DTT reduction (**A, B**) and BSH-specific Western blots (**C**). Thus, S-bacillithiolation protects the AldA active site against overoxidation under H₂O₂ stress. AldA activity was measured with methylglyoxal as substrate.

6. Conclusion and future perspectives

Bacteria have evolved specific strategies to resist oxidative stress and to survive in an aerobic environment. LMW thiols are important defense mechanisms in bacteria that mediate protection against various reactive species, including ROS, RCS, RES and RNS. Under oxidative stress, LMW thiols can form mixed disulfides with proteins that are termed as S-thiolations. Protein S-thiolation functions in redox regulation of protein activities and in thiol-protection against overoxidation under oxidative stress. In this doctoral thesis, we have studied the redox regulation of main metabolic enzymes that are highly sensitive to oxidation under HOCl stress, including the glycolytic GapDH and the aldehyde dehydrogenase AldA of *C. diphtheriae* and *S. aureus*. We could confirm that GapDH and AldA are protected by S-bacillithiolation or S-mycothiolation against overoxidation to sulfonic acids under NaOCl and H₂O₂ stress. In addition, the reversible inactivation of GapDH and AldA by S-thiolation was shown to occur faster compared to the overoxidation. We further analyzed the roles of the bacilliredoxin and mycoredoxin pathways for reactivation of the S-thiolated enzymes in *S. aureus* and *C. diphtheriae*. Thus, our studied not only identified new S-thiolated proteins in human pathogens, but also new substrates for bacilliredoxins and mycoredoxins in pathogenic bacteria. Thus, the detailed biochemical results of this doctoral thesis provide new insights into the protective roles of BSH and MSH of main metabolic enzymes under infection-like conditions in *S. aureus* and *C. diphtheriae*. Since BSH is important for virulence in *S. aureus*, these S-bacillithiolated enzymes could be new drug targets that could be used in drug design to combat multi-resistant *S. aureus* infections.

7. References

- [1] Gordon, R. J.; Lowy, F. D. Pathogenesis of methicillin-resistant *Staphylococcus aureus* infection. *Clin Infect Dis : an official publication of the Infectious Diseases Society of America* **46 Suppl 5**:S350-359; 2008.
- [2] Tong, S. Y.; Davis, J. S.; Eichenberger, E.; Holland, T. L.; Fowler, V. G., Jr. *Staphylococcus aureus* infections: epidemiology, pathophysiology, clinical manifestations, and management. *Clin Microbiol Rev* **28**:603-661; 2015.
- [3] Patti, J. M.; Allen, B. L.; McGavin, M. J.; Hook, M. MSCRAMM-mediated adherence of microorganisms to host tissues. *Ann Rev Microbiol.* **48**:585-617; 1994.
- [4] Donlan, R. M.; Costerton, J. W. Biofilms: survival mechanisms of clinically relevant microorganisms. *Clin Microbiol Rev* **15**:167-193; 2002.
- [5] Kahl, B.; Herrmann, M.; Everding, A. S.; Koch, H. G.; Becker, K.; Harms, E.; Proctor, R. A.; Peters, G. Persistent infection with small colony variant strains of *Staphylococcus aureus* in patients with cystic fibrosis. *J Infect Dis.* **177**:1023-1029; 1998.
- [6] O'Riordan, K.; Lee, J. C. *Staphylococcus aureus* capsular polysaccharides. *Clin Microbiol Rev* **17**:218-234; 2004.
- [7] Foster, T. J. Immune evasion by staphylococci. *Nat Rev Microbiol.* **3**:948-958; 2005.
- [8] Gladstone, G. P.; Van Heyningen, W. E. Staphylococcal leucocidins. *Br J Exp Pathol.* **38**:123-137; 1957.
- [9] Lowy, F. D. *Staphylococcus aureus* infections. *N Engl J Med.* **339**:520-532; 1998.
- [10] McCormick, J. K.; Yarwood, J. M.; Schlievert, P. M. Toxic shock syndrome and bacterial superantigens: an update. *Annu Rev Microbiol.* **55**:77-104; 2001.
- [11] Winterbourn, C. C.; Kettle, A. J. Redox reactions and microbial killing in the neutrophil phagosome. *Antioxid Redox Signal.* **18**:642-660; 2013.
- [12] Chandrangu, P.; Loi, V. V.; Antelmann, H.; Helmann, J. D. The Role of Bacillithiol in Gram-Positive *Firmicutes*. *Antioxid Redox Signal.* **28**:445-462; 2018.
- [13] Posada, A. C.; Kolar, S. L.; Dusi, R. G.; Francois, P.; Roberts, A. A.; Hamilton, C. J.; Liu, G. Y.; Cheung, A. Importance of bacillithiol in the oxidative stress response of *Staphylococcus aureus*. *Infect Immun.* **82**:316-332; 2014.
- [14] Hwang, C.; Sinskey, A. J.; Lodish, H. F. Oxidized redox state of glutathione in the endoplasmic reticulum. *Science (New York, N.Y.)* **257**:1496-1502; 1992.
- [15] Luebke, J. L.; Giedroc, D. P. Cysteine sulfur chemistry in transcriptional regulators at the host-bacterial pathogen interface. *Biochemistry* **54**:3235-3249; 2015.
- [16] Antelmann, H.; Helmann, J. D. Thiol-based redox switches and gene regulation. *Antioxid Redox Signal.* **14**:1049-1063; 2011.
- [17] Gray, M. J.; Wholey, W. Y.; Jakob, U. Bacterial responses to reactive chlorine species. *Ann Rev Microbiol.* **67**:141-160; 2013.
- [18] Imlay, J. A. The molecular mechanisms and physiological consequences of oxidative stress: lessons from a model bacterium. *Nat Rev Microbiol.* **11**:443-454; 2013.
- [19] Slauch, J. M. How does the oxidative burst of macrophages kill bacteria? Still an open question. *Mol Microbiol.* **80**:580-583; 2011.

- [20] Imlay, J. A. Pathways of oxidative damage. *Ann Rev Microbiol.* **57**:395-418; 2003.
- [21] Mishra, S.; Imlay, J. Why do bacteria use so many enzymes to scavenge hydrogen peroxide? *Arch Biochem Biophys.* **525**:145-160; 2012.
- [22] Loi, V. V.; Rossius, M.; Antelmann, H. Redox regulation by reversible protein S-thiolation in bacteria. *Front Microbiol.* **6**:187; 2015.
- [23] Lowther, W. T.; Haynes, A. C. Reduction of cysteine sulfinic acid in eukaryotic, typical 2-Cys peroxiredoxins by sulfiredoxin. *Antioxid Redox Signal.* **15**:99-109; 2011.
- [24] Toledo, J. C., Jr.; Augusto, O. Connecting the chemical and biological properties of nitric oxide. *Chem Res Toxicol.* **25**:975-989; 2012.
- [25] Gardner, P. R.; Fridovich, I. Superoxide sensitivity of the Escherichia coli aconitase. *J Biol Chem.* **266**:19328-19333; 1991.
- [26] Keyer, K.; Imlay, J. A. Superoxide accelerates DNA damage by elevating free-iron levels. *Proc Natl Acad Sci U S A.* **93**:13635-13640; 1996.
- [27] Balasubramanian, B.; Pogozelski, W. K.; Tullius, T. D. DNA strand breaking by the hydroxyl radical is governed by the accessible surface areas of the hydrogen atoms of the DNA backbone. *Proc Natl Acad Sci U S A.* **95**:9738-9743; 1998.
- [28] Hawkins, C. L.; Pattison, D. I.; Davies, M. J. Hypochlorite-induced oxidation of amino acids, peptides and proteins. *Amino acids.* **25**:259-274; 2003.
- [29] Peskin, A. V.; Turner, R.; Maghzal, G. J.; Winterbourn, C. C.; Kettle, A. J. Oxidation of methionine to dehydromethionine by reactive halogen species generated by neutrophils. *Biochemistry* **48**:10175-10182; 2009.
- [30] Hawkins, C. L.; Davies, M. J. Hypochlorite-induced damage to DNA, RNA, and polynucleotides: formation of chloramines and nitrogen-centered radicals. *Chem Res Toxicol.* **15**:83-92; 2002.
- [31] Prutz, W. A. Hypochlorous acid interactions with thiols, nucleotides, DNA, and other biological substrates. *Arch Biochem Biophys.* **332**:110-120; 1996.
- [32] Martinez, M. C.; Andriantsitohaina, R. Reactive nitrogen species: molecular mechanisms and potential significance in health and disease. *Antioxid Redox Signal.* **11**:669-702; 2009.
- [33] Stuehr, D. J. Enzymes of the L-arginine to nitric oxide pathway. *J Nutr.* **134**:2748S-2751S; discussion 2765S-2767S; 2004.
- [34] Vazquez-Torres, A. Redox active thiol sensors of oxidative and nitrosative stress. *Antioxid Redox Signal.* **17**:1201-1214; 2012.
- [35] Ignarro, L. J.; Buga, G. M.; Wood, K. S.; Byrns, R. E.; Chaudhuri, G. Endothelium-derived relaxing factor produced and released from artery and vein is nitric oxide. *Proc Natl Acad Sci U S A.* **84**:9265-9269; 1987.
- [36] Farmer, E. E.; Davoine, C. Reactive electrophile species. *Curr Opin Plant Biol.* **10**:380-386; 2007.
- [37] Ferguson, G. P.; Totemeyer, S.; MacLean, M. J.; Booth, I. R. Methylglyoxal production in bacteria: suicide or survival? *Arch Microbiol.* **170**:209-218; 1998.
- [38] Gray, M. J.; Wholey, W. Y.; Parker, B. W.; Kim, M.; Jakob, U. NemR is a bleach-sensing transcription factor. *J Biol Chem.* **288**:13789-13798; 2013.
- [39] Marnett, L. J.; Riggins, J. N.; West, J. D. Endogenous generation of reactive oxidants and electrophiles and their reactions with DNA and protein. *J Clin Invest.* **111**:583-593; 2003.

- [40] Ratasuk, N.; Nanny, M. A. Characterization and quantification of reversible redox sites in humic substances. *Environ Sci Technol.* **41**:7844-7850; 2007.
- [41] Nohl, H.; Jordan, W.; Youngman, R. J. Quinones in Biology: Functions in electron transfer and oxygen activation. *Free Radic Biol Med.* **2**:211-279; 1986.
- [42] Metz, B.; Kersten, G. F.; Hoogerhout, P.; Brugghe, H. F.; Timmermans, H. A.; de Jong, A.; Meiring, H.; ten Hove, J.; Hennink, W. E.; Crommelin, D. J.; Jiskoot, W. Identification of formaldehyde-induced modifications in proteins: reactions with model peptides. *J Biol Chem.* **279**:6235-6243; 2004.
- [43] LoPachin, R. M.; Gavin, T. Molecular mechanisms of aldehyde toxicity: a chemical perspective. *Chem Res Toxicol.* **27**:1081-1091; 2014.
- [44] Bourajjaj, M.; Stehouwer, C. D.; van Hinsbergh, V. W.; Schalkwijk, C. G. Role of methylglyoxal adducts in the development of vascular complications in diabetes mellitus. *Biochem Soc Trans* **31**:1400-1402; 2003.
- [45] Cadenas, E.; Hochstein, P.; Ernster, L. Pro- and antioxidant functions of quinones and quinone reductases in mammalian cells. *Adv Enzymol Relat Areas Mol Biol.* **65**:97-146; 1992.
- [46] Roos, G.; Messens, J. Protein sulfenic acid formation: from cellular damage to redox regulation. *Free Radic Biol Med.* **51**:314-326; 2011.
- [47] Imlay, J. A. Cellular defenses against superoxide and hydrogen peroxide. *Annu Rev Biochem.* **77**:755-776; 2008.
- [48] Kehler, J. P.; Robertson, J. D.; Smith, C. V. 1.14 - Free Radicals and Reactive Oxygen Species A2 - McQueen, Charlene A. *Comprehensive Toxicology (Second Edition)*. Oxford: Elsevier; 2010: 277-307.
- [49] Liu, X.; Kokare, C. Chapter 11 - Microbial Enzymes of Use in Industry A2 - Brahmachari, Goutam. *Biotechnology of Microbial Enzymes*: Academic Press; 2017: 267-298.
- [50] Djordjevic, V. B. Free radicals in cell biology. *Int Rev Cytol.* **237**:57-89; 2004.
- [51] Tabet, F.; Touyz, R. M. Chapter 30 - Reactive Oxygen Species, Oxidative Stress, and Vascular Biology in Hypertension A2 - Lip, Gregory Y.H. In: Hall, J. E., ed. *Comprehensive Hypertension*. Philadelphia: Mosby; 2007: 337-347.
- [52] Weydert, C. J.; Cullen, J. J. Measurement of superoxide dismutase, catalase and glutathione peroxidase in cultured cells and tissue. *Nat Protoc.* **5**:51-66; 2010.
- [53] Wang, S.; Deng, K.; Zaremba, S.; Deng, X.; Lin, C.; Wang, Q.; Tortorello, M. L.; Zhang, W. Transcriptomic response of *Escherichia coli* O157:H7 to oxidative stress. *Appl Environ Microbiol.* **75**:6110-6123; 2009.
- [54] Dukan, S.; Turlin, E.; Biville, F.; Bolbach, G.; Touati, D.; Tabet, J. C.; Blais, J. C. Coupling 2D SDS-PAGE with CNBr cleavage and MALDI-TOFMS: a strategy applied to the identification of proteins induced by a hypochlorous acid stress in *Escherichia coli*. *Anal Chem.* **70**:4433-4440; 1998.
- [55] Chi, B. K.; Gronau, K.; Mäder, U.; Hessling, B.; Becher, D.; Antelmann, H. S-bacillithiolation protects against hypochlorite stress in *Bacillus subtilis* as revealed by transcriptomics and redox proteomics. *Mol Cell Proteomics.* : MCP **10**:M111.009506; 2011.
- [56] Small, D. A.; Chang, W.; Toghrol, F.; Bentley, W. E. Toxicogenomic analysis of sodium hypochlorite antimicrobial mechanisms in *Pseudomonas aeruginosa*. *Appl Microbiol Biotechnol.* **74**:176-185; 2007.
- [57] Ceragioli, M.; Mols, M.; Moezelaar, R.; Ghelardi, E.; Senesi, S.; Abee, T. Comparative transcriptomic and phenotypic analysis of the responses of *Bacillus cereus* to various disinfectant treatments. *Appl Environ Microbiol.* **76**:3352-3360; 2010.

- [58] Nedeljkovic, Z. S.; Gokce, N.; Loscalzo, J. Mechanisms of oxidative stress and vascular dysfunction. *Postgrad Med J.* **79**:195-199; quiz 198-200; 2003.
- [59] Chesney, J. A.; Eaton, J. W.; Mahoney, J. R., Jr. Bacterial glutathione: a sacrificial defense against chlorine compounds. *J Bacteriol.* **178**:2131-2135; 1996.
- [60] Dukan, S.; Belkin, S.; Touati, D. Reactive oxygen species are partially involved in the bacteriocidal action of hypochlorous acid. *Arch Biochem Biophys.* **367**:311-316; 1999.
- [61] Jakob, U.; Eser, M.; Bardwell, J. C. Redox switch of hsp33 has a novel zinc-binding motif. *J Biol Chem.* **275**:38302-38310; 2000.
- [62] Jakob, U.; Muse, W.; Eser, M.; Bardwell, J. C. Chaperone activity with a redox switch. *Cell* **96**:341-352; 1999.
- [63] Candeias, L. P.; Stratford, M. R.; Wardman, P. Formation of hydroxyl radicals on reaction of hypochlorous acid with ferrocyanide, a model iron(II) complex. *Free Radic Res.* **20**:241-249; 1994.
- [64] Dukan, S.; Touati, D. Hypochlorous acid stress in *Escherichia coli*: resistance, DNA damage, and comparison with hydrogen peroxide stress. *J Bacteriol.* **178**:6145-6150; 1996.
- [65] Deng, K.; Wang, S.; Rui, X.; Zhang, W.; Tortorello, M. L. Functional analysis of ycfR and ycfQ in *Escherichia coli* O157:H7 linked to outbreaks of illness associated with fresh produce. *Appl Environ Microbiol.* **77**:3952-3959; 2011.
- [66] Mermod, M.; Magnani, D.; Solioz, M.; Stoyanov, J. V. The copper-inducible ComR (YcfQ) repressor regulates expression of ComC (YcfR), which affects copper permeability of the outer membrane of *Escherichia coli*. *Biometals.* **25**:33-43; 2012.
- [67] Karoui, H.; Hogg, N.; Frejaville, C.; Tordo, P.; Kalyanaraman, B. Characterization of sulfur-centered radical intermediates formed during the oxidation of thiols and sulfite by peroxynitrite. ESR-spin trapping and oxygen uptake studies. *J Biol Chem.* **271**:6000-6009; 1996.
- [68] Radi, R.; Beckman, J. S.; Bush, K. M.; Freeman, B. A. Peroxynitrite oxidation of sulfhydryls. The cytotoxic potential of superoxide and nitric oxide. *J Biol Chem.* **266**:4244-4250; 1991.
- [69] Denicola, A.; Souza, J. M.; Radi, R. Diffusion of peroxynitrite across erythrocyte membranes. *Proc Natl Acad Sci U S A.* **95**:3566-3571; 1998.
- [70] Marla, S. S.; Lee, J.; Groves, J. T. Peroxynitrite rapidly permeates phospholipid membranes. *Proc Natl Acad Sci U S A.* **94**:14243-14248; 1997.
- [71] Hunt, J. A.; Lee, J.; Groves, J. T. Amphiphilic peroxynitrite decomposition catalysts in liposomal assemblies. *Chem Biol.* **4**:845-858; 1997.
- [72] Sies, H.; Sharov, V. S.; Klotz, L. O.; Briviba, K. Glutathione peroxidase protects against peroxynitrite-mediated oxidations. A new function for selenoproteins as peroxynitrite reductase. *J Biol Chem.* **272**:27812-27817; 1997.
- [73] Siegel, D.; Yan, C.; Ross, D. NAD(P)H:quinone oxidoreductase 1 (NQO1) in the sensitivity and resistance to antitumor quinones. *Biochem Pharmacol.* **83**:1033-1040; 2012.
- [74] Nguyen, T. T.; Eiamphungporn, W.; Mäder, U.; Liebeke, M.; Lalk, M.; Hecker, M.; Helmann, J. D.; Antelmann, H. Genome-wide responses to carbonyl electrophiles in *Bacillus subtilis*: control of the thiol-dependent formaldehyde dehydrogenase AdhA and cysteine proteinase YraA by the MerR-family regulator YraB (AdhR). *Mol Microbiol.* **71**:876-894; 2009.
- [75] Chen, N. H.; Djoko, K. Y.; Veyrier, F. J.; McEwan, A. G. Formaldehyde Stress Responses in Bacterial Pathogens. *Front Microbiol.* **7**:257; 2016.

- [76] Lee, C.; Park, C. Bacterial Responses to Glyoxal and Methylglyoxal: Reactive Electrophilic Species. *Int J Mo Sci.* **18**; 2017.
- [77] Kalapos, M. P. Methylglyoxal in living organisms: chemistry, biochemistry, toxicology and biological implications. *Toxicol Lett.* **110**:145-175; 1999.
- [78] Casazza, J. P.; Felver, M. E.; Veech, R. L. The metabolism of acetone in rat. *J Biol Chem.* **259**:231-236; 1984.
- [79] Chakraborty, S.; Karmakar, K.; Chakravorty, D. Cells producing their own nemesis: understanding methylglyoxal metabolism. *IUBMB life* **66**:667-678; 2014.
- [80] Edagwa, B.; Wang, Y.; Narayanasamy, P. Synthesis of azide derivative and discovery of glyoxalase pathway inhibitor against pathogenic bacteria. *Bioorg Med Chem Lett.* **23**:6138-6140; 2013.
- [81] Thornalley, P. J. The glyoxalase system: new developments towards functional characterization of a metabolic pathway fundamental to biological life. *Biochem J.* **269**:1-11; 1990.
- [82] Chandrangu, P.; Dusi, R.; Hamilton, C. J.; Helmann, J. D. Methylglyoxal resistance in *Bacillus subtilis*: contributions of bacillithiol-dependent and independent pathways. *Mol Microbiol.* **91**:706-715; 2014.
- [83] Ozyamak, E.; de Almeida, C.; de Moura, A. P.; Miller, S.; Booth, I. R. Integrated stress response of *Escherichia coli* to methylglyoxal: transcriptional readthrough from the nemRA operon enhances protection through increased expression of glyoxalase I. *Mol Microbiol.* **88**:936-950; 2013.
- [84] Newton, G. L.; Buchmeier, N.; Fahey, R. C. Biosynthesis and functions of mycothiol, the unique protective thiol of Actinobacteria. *Microbiol Mol Biol Rev.* : *MMBR* **72**:471-494; 2008.
- [85] Jothivasan, V. K.; Hamilton, C. J. Mycothiol: synthesis, biosynthesis and biological functions of the major low molecular weight thiol in *actinomycetes*. *Nat Prod Rep.* **25**:1091-1117; 2008.
- [86] Buchmeier, N. A.; Newton, G. L.; Koledin, T.; Fahey, R. C. Association of mycothiol with protection of *Mycobacterium tuberculosis* from toxic oxidants and antibiotics. *Mol Microbiol.* **47**:1723-1732; 2003.
- [87] Newton, G. L.; Av-Gay, Y.; Fahey, R. C. A novel mycothiol-dependent detoxification pathway in mycobacteria involving mycothiol S-conjugate amidase. *Biochemistry* **39**:10739-10746; 2000.
- [88] Vilcheze, C.; Av-Gay, Y.; Attarian, R.; Liu, Z.; Hazbon, M. H.; Colangeli, R.; Chen, B.; Liu, W.; Alland, D.; Sacchettini, J. C.; Jacobs, W. R., Jr. Mycothiol biosynthesis is essential for ethionamide susceptibility in *Mycobacterium tuberculosis*. *Mol Microbiol.* **69**:1316-1329; 2008.
- [89] Newton, G. L.; Leung, S. S.; Wakabayashi, J. I.; Rawat, M.; Fahey, R. C. The DinB superfamily includes novel mycothiol, bacillithiol, and glutathione S-transferases. *Biochemistry* **50**:10751-10760; 2011.
- [90] Zhao, Q.; Wang, M.; Xu, D.; Zhang, Q.; Liu, W. Metabolic coupling of two small-molecule thiols programs the biosynthesis of lincomycin A. *Nature* **518**:115-119; 2015.
- [91] Chi, B. K.; Busche, T.; Van Laer, K.; Basell, K.; Becher, D.; Clermont, L.; Seibold, G. M.; Persicke, M.; Kalinowski, J.; Messens, J.; Antelmann, H. Protein S-mycothiolation functions as redox-switch and thiol protection mechanism in *Corynebacterium glutamicum* under hypochlorite stress. *Antioxid Redox Signal.* **20**:589-605; 2014.
- [92] Feng, J.; Che, Y.; Milse, J.; Yin, Y. J.; Liu, L.; Ruckert, C.; Shen, X. H.; Qi, S. W.; Kalinowski, J.; Liu, S. J. The gene ncgl2918 encodes a novel maleylpyruvate isomerase that needs mycothiol as cofactor and links mycothiol biosynthesis and gentisate assimilation in *Corynebacterium glutamicum*. *J Biol Chem.* **281**:10778-10785; 2006.

- [93] Ordóñez, E.; Van Belle, K.; Roos, G.; De Galan, S.; Letek, M.; Gil, J. A.; Wyns, L.; Mateos, L. M.; Messens, J. Arsenate reductase, mycothiol, and mycoredoxin concert thiol/disulfide exchange. *J Biol Chem.* **284**:15107-15116; 2009.
- [94] Sareen, D.; Newton, G. L.; Fahey, R. C.; Buchmeier, N. A. Mycothiol is essential for growth of *Mycobacterium tuberculosis* Erdman. *J Bacteriol.* **185**:6736-6740; 2003.
- [95] Hillion, M.; Bernhardt, J.; Busche, T.; Rossius, M.; Maass, S.; Becher, D.; Rawat, M.; Wirtz, M.; Hell, R.; Ruckert, C.; Kalinowski, J.; Antelmann, H. Monitoring global protein thiol-oxidation and protein S-mycothiolation in *Mycobacterium smegmatis* under hypochlorite stress. *Sci Rep.* **7**:1195; 2017.
- [96] Newton, G. L.; Rawat, M.; La Clair, J. J.; Jothivasan, V. K.; Budiarto, T.; Hamilton, C. J.; Claiborne, A.; Helmann, J. D.; Fahey, R. C. Bacillithiol is an antioxidant thiol produced in Bacilli. *Nat Chem Biol.* **5**:625-627; 2009.
- [97] Gaballa, A.; Newton, G. L.; Antelmann, H.; Parsonage, D.; Upton, H.; Rawat, M.; Claiborne, A.; Fahey, R. C.; Helmann, J. D. Biosynthesis and functions of bacillithiol, a major low-molecular-weight thiol in Bacilli. *Proc Natl Acad Sci U S A.* **107**:6482-6486; 2010.
- [98] Lamers, A. P.; Keithly, M. E.; Kim, K.; Cook, P. D.; Stec, D. F.; Hines, K. M.; Sulikowski, G. A.; Armstrong, R. N. Synthesis of bacillithiol and the catalytic selectivity of FosB-type fosfomycin resistance proteins. *Org Lett.* **14**:5207-5209; 2012.
- [99] Thompson, M. K.; Keithly, M. E.; Goodman, M. C.; Hammer, N. D.; Cook, P. D.; Jagessar, K. L.; Harp, J.; Skaar, E. P.; Armstrong, R. N. Structure and function of the genomically encoded fosfomycin resistance enzyme, FosB, from *Staphylococcus aureus*. *Biochemistry* **53**:755-765; 2014.
- [100] Helmann, J. D. Bacillithiol, a new player in bacterial redox homeostasis. *Antioxid Redox Signal.* **15**:123-133; 2011.
- [101] Ma, Z.; Chandrangsu, P.; Helmann, T. C.; Romsang, A.; Gaballa, A.; Helmann, J. D. Bacillithiol is a major buffer of the labile zinc pool in *Bacillus subtilis*. *Mol Microbiol.* **94**:756-770; 2014.
- [102] Pöther, D. C.; Gierok, P.; Harms, M.; Mostertz, J.; Hochgräfe, F.; Antelmann, H.; Hamilton, C. J.; Borovok, I.; Lalk, M.; Aharonowitz, Y.; Hecker, M. Distribution and infection-related functions of bacillithiol in *Staphylococcus aureus*. *Int J Med Microbiol. : IJMM* **303**:114-123; 2013.
- [103] Rajkarnikar, A.; Strankman, A.; Duran, S.; Vargas, D.; Roberts, A. A.; Barretto, K.; Upton, H.; Hamilton, C. J.; Rawat, M. Analysis of mutants disrupted in bacillithiol metabolism in *Staphylococcus aureus*. *Biochem Biophys Res Commun.* **436**:128-133; 2013.
- [104] Lee, J. W.; Soonsanga, S.; Helmann, J. D. A complex thiolate switch regulates the *Bacillus subtilis* organic peroxide sensor OhrR. *Proc Natl Acad Sci U S A.* **104**:8743-8748; 2007.
- [105] Chi, B. K.; Gronau, K.; Mäder, U.; Hessling, B.; Becher, D.; Antelmann, H. S-bacillithiolation protects against hypochlorite stress in *Bacillus subtilis* as revealed by transcriptomics and redox proteomics. *Mol Cell Proteomics.: MCP* **10**:M111 009506; 2011.
- [106] Chi, B. K.; Roberts, A. A.; Huyen, T. T.; Basell, K.; Becher, D.; Albrecht, D.; Hamilton, C. J.; Antelmann, H. S-bacillithiolation protects conserved and essential proteins against hypochlorite stress in *firmicutes* bacteria. *Antioxid Redox Signal.* **18**:1273-1295; 2013.
- [107] Ayala-Castro, C.; Saini, A.; Outten, F. W. Fe-S cluster assembly pathways in bacteria. *Microbiol Mol Biol Rev. : MMBR* **72**:110-125, table of contents; 2008.
- [108] Imber, M.; Huyen, N. T. T.; Pietrzyk-Brzezinska, A. J.; Loi, V. V.; Hillion, M.; Bernhardt, J.; Thärichen, L.; Kolsek, K.; Saleh, M.; Hamilton, C. J.; Adrian, L.; Gräter, F.; Wahl, M. C.; Antelmann, H. Protein S-Bacillithiolation Functions in Thiol Protection and Redox Regulation of the Glyceraldehyde-3-Phosphate Dehydrogenase Gap in *Staphylococcus aureus* Under Hypochlorite Stress. *Antioxid Redox Signal.* **28**:410-430; 2018.

- [109] Imber, M.; Loi, V. V.; Reznikov, S.; Fritsch, V. N.; Pietrzyk-Brzezinska, A. J.; Prehn, J.; Hamilton, C.; Wahl, M. C.; Bronowska, A. K.; Antelmann, H. The aldehyde dehydrogenase AldA contributes to the hypochlorite defense and is redox-controlled by protein S-bacillithiolation in *Staphylococcus aureus*. *Redox Biol.* **15**:557-568; 2018.
- [110] Van Laer, K.; Buts, L.; Foloppe, N.; Vertommen, D.; Van Belle, K.; Wahni, K.; Roos, G.; Nilsson, L.; Mateos, L. M.; Rawat, M.; van Nuland, N. A.; Messens, J. Mycoredoxin-1 is one of the missing links in the oxidative stress defence mechanism of Mycobacteria. *Mol Microbiol.* **86**:787-804; 2012.
- [111] Aslund, F.; Berndt, K. D.; Holmgren, A. Redox potentials of glutaredoxins and other thiol-disulfide oxidoreductases of the thioredoxin superfamily determined by direct protein-protein redox equilibria. *J Biol Chem.* **272**:30780-30786; 1997.
- [112] Hugo, M.; Van Laer, K.; Reyes, A. M.; Vertommen, D.; Messens, J.; Radi, R.; Trujillo, M. Mycothiol/mycoredoxin 1-dependent reduction of the peroxiredoxin AhpE from *Mycobacterium tuberculosis*. *J Biol Chem.* **289**:5228-5239; 2014.
- [113] Gaballa, A.; Chi, B. K.; Roberts, A. A.; Becher, D.; Hamilton, C. J.; Antelmann, H.; Helmann, J. D. Redox regulation in *Bacillus subtilis*: The bacilliredoxins BrxA(YphP) and BrxB(YqiW) function in de-bacillithiolation of S-bacillithiolated OhrR and MetE. *Antioxid Redox Signal.* **21**:357-367; 2014.
- [114] Hochgräfe, F.; Mostertz, J.; Albrecht, D.; Hecker, M. Fluorescence thiol modification assay: oxidatively modified proteins in *Bacillus subtilis*. *Mol Microbiol.* **58**:409-425; 2005.
- [115] Derewenda, U.; Boczek, T.; Gorres, K. L.; Yu, M.; Hung, L. W.; Cooper, D.; Joachimiak, A.; Raines, R. T.; Derewenda, Z. S. Structure and function of *Bacillus subtilis* YphP, a prokaryotic disulfide isomerase with a CXC catalytic motif. *Biochemistry* **48**:8664-8671; 2009.
- [116] Petersohn, A.; Brigulla, M.; Haas, S.; Hoheisel, J. D.; Volker, U.; Hecker, M. Global analysis of the general stress response of *Bacillus subtilis*. *J Bacteriol.* **183**:5617-5631; 2001.
- [117] Stone, E. M.; Rothblum, K. N.; Alevy, M. C.; Kuo, T. M.; Schwartz, R. J. Complete sequence of the chicken glyceraldehyde-3-phosphate dehydrogenase gene. *Proc Natl Acad Sci U S A.* **82**:1628-1632; 1985.
- [118] Boschi-Muller, S.; Azza, S.; Pollastro, D.; Corbier, C.; Branlant, G. Comparative enzymatic properties of GapB-encoded erythrose-4-phosphate dehydrogenase of *Escherichia coli* and phosphorylating glyceraldehyde-3-phosphate dehydrogenase. *J Biol Chem.* **272**:15106-15112; 1997.
- [119] Fillinger, S.; Boschi-Muller, S.; Azza, S.; Dervyn, E.; Branlant, G.; Aymerich, S. Two glyceraldehyde-3-phosphate dehydrogenases with opposite physiological roles in a nonphotosynthetic bacterium. *J Biol Chem.* **275**:14031-14037; 2000.
- [120] Purves, J.; Cockayne, A.; Moody, P. C.; Morrissey, J. A. Comparison of the regulation, metabolic functions, and roles in virulence of the glyceraldehyde-3-phosphate dehydrogenase homologues gapA and gapB in *Staphylococcus aureus*. *Infect Immun.* **78**:5223-5232; 2010.
- [121] Rosenberg, L. L.; Arnon, D. I. The preparation and properties of a new glyceraldehyde-3-phosphate dehydrogenase from photosynthetic tissues. *J Biol Chem.* **217**:361-371; 1955.
- [122] Habenicht, A.; Hellman, U.; Cerff, R. Non-phosphorylating GAPDH of higher plants is a member of the aldehyde dehydrogenase superfamily with no sequence homology to phosphorylating GAPDH. *J Mol Biol.* **237**:165-171; 1994.
- [123] Boyd, D. A.; Cvitkovitch, D. G.; Hamilton, I. R. Sequence, expression, and function of the gene for the nonphosphorylating, NADP-dependent glyceraldehyde-3-phosphate dehydrogenase of *Streptococcus mutans*. *J Bacteriol.* **177**:2622-2627; 1995.
- [124] Nicholls, C.; Li, H.; Liu, J. P. GAPDH: a common enzyme with uncommon functions. *Clin Exp Pharmacol Physiol.* **39**:674-679; 2012.

- [125] Frayne, J.; Taylor, A.; Cameron, G.; Hadfield, A. T. Structure of insoluble rat sperm glyceraldehyde-3-phosphate dehydrogenase (GAPDH) via heterotetramer formation with *Escherichia coli* GAPDH reveals target for contraceptive design. *J Biol Chem.* **284**:22703-22712; 2009.
- [126] Didierjean, C.; Corbier, C.; Fatih, M.; Favier, F.; Boschi-Muller, S.; Branlant, G.; Aubry, A. Crystal structure of two ternary complexes of phosphorylating glyceraldehyde-3-phosphate dehydrogenase from *Bacillus stearothermophilus* with NAD and D-glyceraldehyde 3-phosphate. *J Biol Chem.* **278**:12968-12976; 2003.
- [127] Segal, H. L.; Boyer, P. D. The role of sulfhydryl groups in the activity of D-glyceraldehyde 3-phosphate dehydrogenase. *J Biol Chem.* **204**:265-281; 1953.
- [128] Nagradova, N. K. Study of the properties of phosphorylating D-glyceraldehyde-3-phosphate dehydrogenase. *Biochemistry. Biokhimiia* **66**:1067-1076; 2001.
- [129] Martin, W. F.; Cerff, R. Physiology, phylogeny, early evolution, and GAPDH. *Protoplasma* **254**:1823-1834; 2017.
- [130] Mukherjee, S.; Dutta, D.; Saha, B.; Das, A. K. Crystal structure of glyceraldehyde-3-phosphate dehydrogenase 1 from methicillin-resistant *Staphylococcus aureus* MRSA252 provides novel insights into substrate binding and catalytic mechanism. *J Mol Biol.* **401**:949-968; 2010.
- [131] Sirover, M. A. New nuclear functions of the glycolytic protein, glyceraldehyde-3-phosphate dehydrogenase, in mammalian cells. *J Cell Biochem.* **95**:45-52; 2005.
- [132] Sirover, M. A. On the functional diversity of glyceraldehyde-3-phosphate dehydrogenase: biochemical mechanisms and regulatory control. *Biochim Biophys Acta.* **1810**:741-751; 2011.
- [133] Sirover, M. A. New insights into an old protein: the functional diversity of mammalian glyceraldehyde-3-phosphate dehydrogenase. *Biochim Biophys Acta.* **1432**:159-184; 1999.
- [134] Ferreira, E.; Gimenez, R.; Canas, M. A.; Aguilera, L.; Aguilar, J.; Badia, J.; Baldoma, L. Glyceraldehyde-3-phosphate dehydrogenase is required for efficient repair of cytotoxic DNA lesions in *Escherichia coli*. *Int J Biochem Cell Biol.* **60**:202-212; 2015.
- [135] Egea, L.; Aguilera, L.; Gimenez, R.; Sorolla, M. A.; Aguilar, J.; Badia, J.; Baldoma, L. Role of secreted glyceraldehyde-3-phosphate dehydrogenase in the infection mechanism of enterohemorrhagic and enteropathogenic *Escherichia coli*: interaction of the extracellular enzyme with human plasminogen and fibrinogen. *Int J Biochem Cell Biol.* **39**:1190-1203; 2007.
- [136] Aguilera, L.; Gimenez, R.; Badia, J.; Aguilar, J.; Baldoma, L. NAD⁺-dependent post-translational modification of *Escherichia coli* glyceraldehyde-3-phosphate dehydrogenase. *Int Microbiol. : the official journal of the Spanish Society for Microbiology* **12**:187-192; 2009.
- [137] Kinoshita, H.; Uchida, H.; Kawai, Y.; Kawasaki, T.; Wakahara, N.; Matsuo, H.; Watanabe, M.; Kitazawa, H.; Ohnuma, S.; Miura, K.; Horii, A.; Saito, T. Cell surface *Lactobacillus plantarum* LA 318 glyceraldehyde-3-phosphate dehydrogenase (GAPDH) adheres to human colonic mucin. *J Appl Microbiol.* **104**:1667-1674; 2008.
- [138] Sanchez, B.; Schmitter, J. M.; Urdaci, M. C. Identification of novel proteins secreted by *Lactobacillus plantarum* that bind to mucin and fibronectin. *J Mol Microbiol Biotechnol.* **17**:158-162; 2009.
- [139] Dumke, R.; Hausner, M.; Jacobs, E. Role of *Mycoplasma pneumoniae* glyceraldehyde-3-phosphate dehydrogenase (GAPDH) in mediating interactions with the human extracellular matrix. *Microbiology (Reading, England)* **157**:2328-2338; 2011.
- [140] Ferreira, E.; Gimenez, R.; Aguilera, L.; Guzman, K.; Aguilar, J.; Badia, J.; Baldoma, L. Protein interaction studies point to new functions for *Escherichia coli* glyceraldehyde-3-phosphate dehydrogenase. *Res Microbiol.* **164**:145-154; 2013.

- [141] Teresa Pellicer, M.; Felisa Nunez, M.; Aguilar, J.; Badia, J.; Baldoma, L. Role of 2-phosphoglycolate phosphatase of *Escherichia coli* in metabolism of the 2-phosphoglycolate formed in DNA repair. *J Bacteriol.* **185**:5815-5821; 2003.
- [142] Peralta, D.; Bronowska, A. K.; Morgan, B.; Doka, E.; Van Laer, K.; Nagy, P.; Grater, F.; Dick, T. P. A proton relay enhances H₂O₂ sensitivity of GAPDH to facilitate metabolic adaptation. *Nat Chem Biol.* **11**:156-163; 2015.
- [143] Hildebrandt, T.; Knuesting, J.; Berndt, C.; Morgan, B.; Scheibe, R. Cytosolic thiol switches regulating basic cellular functions: GAPDH as an information hub? *Biol Chem.* **396**:523-537; 2015.
- [144] Hempel, J.; Nicholas, H.; Lindahl, R. Aldehyde dehydrogenases: widespread structural and functional diversity within a shared framework. *Prot Sci* **2**:1890-1900; 1993.
- [145] Toyama, H.; Mathews, F. S.; Adachi, O.; Matsushita, K. Quinohemoprotein alcohol dehydrogenases: structure, function, and physiology. *Arch Biochem Biophys.* **428**:10-21; 2004.
- [146] Kim, S. W.; Luykx, D. M.; de Vries, S.; Duine, J. A. A second molybdoprotein aldehyde dehydrogenase from *Amycolatopsis methanolica* NCIB 11946. *Arch Biochem Biophys.* **325**:1-7; 1996.
- [147] Heider, J.; Ma, K.; Adams, M. W. Purification, characterization, and metabolic function of tungsten-containing aldehyde ferredoxin oxidoreductase from the hyperthermophilic and proteolytic archaeon *Thermococcus* strain ES-1. *J Bacteriol.* **177**:4757-4764; 1995.
- [148] Liu, Z. J.; Sun, Y. J.; Rose, J.; Chung, Y. J.; Hsiao, C. D.; Chang, W. R.; Kuo, I.; Perozich, J.; Lindahl, R.; Hempel, J.; Wang, B. C. The first structure of an aldehyde dehydrogenase reveals novel interactions between NAD and the Rossmann fold. *Nat Struct Biol.* **4**:317-326; 1997.
- [149] Marchitti, S. A.; Brocker, C.; Stagos, D.; Vasiliou, V. Non-P450 aldehyde oxidizing enzymes: the aldehyde dehydrogenase superfamily. *Expert Opin Drug Metab Toxicol.* **4**:697-720; 2008.
- [150] Halavaty, A. S.; Rich, R. L.; Chen, C.; Joo, J. C.; Minasov, G.; Dubrovskaya, I.; Winsor, J. R.; Myszka, D. G.; Duban, M.; Shuvalova, L.; Yakunin, A. F.; Anderson, W. F. Structural and functional analysis of betaine aldehyde dehydrogenase from *Staphylococcus aureus*. *Acta Crystallogr D Biol Crystallogr.* **71**:1159-1175; 2015.
- [151] Munoz-Clares, R. A.; Gonzalez-Segura, L.; Diaz-Sanchez, A. G. Crystallographic evidence for active-site dynamics in the hydrolytic aldehyde dehydrogenases. Implications for the deacylation step of the catalyzed reaction. *Chem Biol Interact.* **191**:137-146; 2011.
- [152] Ryzlak, M. T.; Pietruszko, R. Human brain "high Km" aldehyde dehydrogenase: purification, characterization, and identification as NAD⁺-dependent succinic semialdehyde dehydrogenase. *Arch Biochem Biophys.* **266**:386-396; 1988.
- [153] Koivusalo, M.; Baumann, M.; Uotila, L. Evidence for the identity of glutathione-dependent formaldehyde dehydrogenase and class III alcohol dehydrogenase. *FEBS Letters* **257**:105-109; 1989.
- [154] Coitinho, J. B.; Pereira, M. S.; Costa, D. M.; Guimaraes, S. L.; Araujo, S. S.; Hengge, A. C.; Brandao, T. A.; Nagem, R. A. Structural and Kinetic Properties of the Aldehyde Dehydrogenase NahF, a Broad Substrate Specificity Enzyme for Aldehyde Oxidation. *Biochemistry* **55**:5453-5463; 2016.
- [155] Sydow, K.; Daiber, A.; Oelze, M.; Chen, Z.; August, M.; Wendt, M.; Ullrich, V.; Mulsch, A.; Schulz, E.; Keaney, J. F., Jr.; Stamler, J. S.; Munzel, T. Central role of mitochondrial aldehyde dehydrogenase and reactive oxygen species in nitroglycerin tolerance and cross-tolerance. *J Clin Invest.* **113**:482-489; 2004.
- [156] Vasiliou, V.; Pappa, A.; Estey, T. Role of human aldehyde dehydrogenases in endobiotic and xenobiotic metabolism. *Drug Metab Rev.* **36**:279-299; 2004.
- [157] Lassen, N.; Pappa, A.; Black, W. J.; Jester, J. V.; Day, B. J.; Min, E.; Vasiliou, V. Antioxidant function of corneal ALDH3A1 in cultured stromal fibroblasts. *Free Radic Biol Med.* **41**:1459-1469; 2006.

[158] Uma, L.; Hariharan, J.; Sharma, Y.; Balasubramanian, D. Corneal aldehyde dehydrogenase displays antioxidant properties. *Exp Eye Res.* **63**:117-120; 1996.

Marcel Imber's contributions to the published and submitted manuscripts:

(1) Hillion M, **Imber M**, Pedre B, Bernhardt J, Saleh M, Loi VV, Maaß S, Becher D, Astolfi Rosado L, Adrian L, Weise C, Hell R, Wirtz M, Messens J, Antelmann H. The glyceraldehyde-3-phosphate dehydrogenase GapDH of *Corynebacterium diphtheriae* is redox-controlled by protein S-mycothiolation under oxidative stress. *Sci Rep* 7: 5020. (2017)

Marcel Imber was involved in purification of GapDH from *C. diphtheriae* and in the biochemical enzyme kinetics of GapDH inactivation due to overoxidation and S-mycothiolation. Marcel Imber also performed the MSH-specific Western blot analysis. Together with all other authors, he prepared the figures for publication and contributed to writing of the manuscript.

(2) **Imber M***, Huyen NT*, Pietrzyk-Brzezinska AJ*, Loi VV*, Hillion M, Bernhardt J, Thärichen L, Kolšek K, Saleh M, Hamilton CJ, Adrian L, Gräter F, Wahl MC, Antelmann H. Protein S-bacillithiolation functions in thiol protection and redox regulation of the glyceraldehyde-3-phosphate dehydrogenase Gap in *Staphylococcus aureus* under hypochlorite stress. *Antioxid Redox Signal* 28: 410-430. (2018)

Marcel Imber contributed to the identification of S-bacillithiolated proteins by mass spectrometry. He was involved in purification of Gap from *S. aureus* and in the biochemical enzyme kinetics of Gap inactivation due to overoxidation and S-bacillithiolation. Marcel Imber performed the BSH-specific Western blot analysis. Together with all other authors, he prepared the figures for publication and contributed to writing of the manuscript.

(3) **Imber M***, Loi VV*, Reznikov S, Fritsch VN, Pietrzyk-Brzezinska AJ, Prehn J, Hamilton CJ, Wahl MC, Bronowska AK, Antelmann H. The aldehyde dehydrogenase AldA contributes to the hypochlorite defense and is redox-controlled by protein S-bacillithiolation in *Staphylococcus aureus*. *Redox Biol.* 15: 557-568. (2018).

Marcel Imber was involved in the biochemical experiments for AldA and AldAC279S protein purification, AldA enzyme activity assays and Western blot analysis for AldA S-bacillithiolation. Together with all other authors, he prepared the figures for publication and contributed to writing of the manuscript.

*Shared first authorships.

(4) **Imber M**, Pietrzyk-Brzezinska AJ and Antelmann H. Redox-regulation by reversible protein S-thiolation in Gram-positive bacteria. Review. *Redox Biol.*, Submitted on 03rd July 2018.

Marcel Imber contributed with writing of the review and prepared some figures of the manuscript.

Date:

04.07.2018

04.07.2018

Signatures:

Marcel Imber

Prof. Haike Antelmann

Freie Universität Berlin
FB Bio/Chem/Pharm - Mikrobiologie

Königin-Luise-Str. 12-16
14195 Berlin

Chapter 1

The glyceraldehyde-3-phosphate dehydrogenase GapDH of *Corynebacterium diphtheriae* is redox-controlled by protein S-mycothiolation under oxidative stress

Melanie Hillion^{1*}, **Marcel Imber**^{1*}, Brandán Pedre^{2,3,4*}, Jörg Bernhardt^{5*}, Malek Saleh¹, Vu Van Loi¹, Sandra Maaß⁵, Dörte Becher⁵, Leonardo Astolfi Rosado^{2,3,4}, Lorenz Adrian⁶, Chris Weise⁷, Markus Wirtz⁸, Rüdiger Hell⁸, Joris Messens^{2,3,4} and Haike Antelmann^{1#}

¹*Institute for Biology-Microbiology, Freie Universität Berlin, D-14195 Berlin, Germany*

²*Center for Structural Biology, VIB, B-1050 Brussels, Belgium*

³*Brussels Center for Redox Biology, B-1050 Brussels, Belgium*

⁴*Structural Biology Brussels, Vrije Universiteit Brussel, B-1050 Brussels, Belgium*

⁵*Institute for Microbiology, Ernst-Moritz-Arndt-University of Greifswald, D-17487 Greifswald, Germany*

⁶*Department Isotope Biogeochemistry, Helmholtz Centre for Environmental Research-UFZ, Leipzig, Germany*

⁷*Institute for Chemistry and Biochemistry, Freie Universität Berlin, D-14195 Berlin, Germany*

⁸*Plant Molecular Biology, Centre for Organismal Studies Heidelberg, University of Heidelberg, Heidelberg, Germany*

Published in: *Scientific Reports* 7: 5020. (2017)

#Corresponding author: haike.antelmann@fu-berlin.de

Authors contributions:



Marcel Imber was involved in purification of GapDH and in the biochemical enzyme kinetics of GapDH inactivation due to overoxidation and S-mycothiolation. Marcel Imber also performed the MSH-specific Western blot analysis. All other authors conceived the ideas and hypotheses, designed and performed the proteomics and Mrx1 experiments. All authors prepared the figures and contributed to writing of the manuscript.

* Shared first authorships

SCIENTIFIC REPORTS

OPEN

The glyceraldehyde-3-phosphate dehydrogenase GapDH of *Corynebacterium diphtheriae* is redox-controlled by protein S-mycothiolation under oxidative stress

Melanie Hillion¹ , Marcel Imber¹, Brandán Pedre^{2,3,4}, Jörg Bernhardt⁵, Malek Saleh¹, Vu Van Loi¹, Sandra Maaß⁵, Dörte Becher⁵, Leonardo Astolfi Rosado^{2,3,4}, Lorenz Adrian⁶, Christoph Weise⁷, Rüdiger Hell⁸, Markus Wirtz¹ , Joris Messens^{2,3,4} & Haïke Antelmann¹

Mycothiol (MSH) is the major low molecular weight (LMW) thiol in Actinomycetes and functions in post-translational thiol-modification by protein S-mycothiolation as emerging thiol-protection and redox-regulatory mechanism. Here, we have used shotgun-proteomics to identify 26 S-mycothiolated proteins in the pathogen *Corynebacterium diphtheriae* DSM43989 under hypochlorite stress that are involved in energy metabolism, amino acid and nucleotide biosynthesis, antioxidant functions and translation. The glyceraldehyde-3-phosphate dehydrogenase (GapDH) represents the most abundant S-mycothiolated protein that was modified at its active site Cys153 *in vivo*. Exposure of purified GapDH to H₂O₂ and NaOCl resulted in irreversible inactivation due to overoxidation of the active site *in vitro*. Treatment of GapDH with H₂O₂ or NaOCl in the presence of MSH resulted in S-mycothiolation and reversible GapDH inactivation *in vitro* which was faster compared to the overoxidation pathway. Reactivation of S-mycothiolated GapDH could be catalyzed by both, the Trx and the Mrx1 pathways *in vitro*, but demycothiolation by Mrx1 was faster compared to Trx. In summary, we show here that S-mycothiolation can function in redox-regulation and protection of the GapDH active site against overoxidation in *C. diphtheriae* which can be reversed by both, the Mrx1 and Trx pathways.

Bacteria are exposed to various redox-active compounds, such as reactive oxygen species (ROS) in their natural habitat or during infections and are equipped with specific protection mechanisms¹. To cope with ROS, bacteria use different antioxidant enzymes, such as catalases, peroxiredoxins, superoxide dismutase and low molecular weight (LMW) thiols to maintain the reduced state of the cytoplasm and to survive oxidative stress^{2–4}. Gram-negative bacteria utilize glutathione (GSH) as their major LMW thiol, but GSH is absent in most Gram-positive bacteria. Instead, the Actinomycetes that include streptomycetes, corynebacteria and mycobacteria produce mycothiol (MSH) as their major LMW thiol⁵. MSH functions in detoxification of various redox-active compounds, including ROS, electrophiles and antibiotics in all Actinomycetes^{6–8}. Apart from its

¹Institute for Biology-Microbiology, Freie Universität Berlin, D-14195, Berlin, Germany. ²Center for Structural Biology, VIB, B-1050, Brussels, Belgium. ³Brussels Center for Redox Biology, B-1050, Brussels, Belgium. ⁴Structural Biology Brussels, Vrije Universiteit Brussel, B-1050, Brussels, Belgium. ⁵Institute for Microbiology, Ernst-Moritz-Arndt-University of Greifswald, D-17487, Greifswald, Germany. ⁶Department Isotope Biogeochemistry, Helmholtz Centre for Environmental Research-UFZ, Leipzig, Germany. ⁷Institute for Chemistry and Biochemistry, Freie Universität Berlin, D-14195, Berlin, Germany. ⁸Plant Molecular Biology, Centre for Organismal Studies Heidelberg, University of Heidelberg, Heidelberg, Germany. Melanie Hillion, Marcel Imber, Brandán Pedre and Jörg Bernhardt contributed equally to this work. Correspondence and requests for materials should be addressed to H.A. (email: haïke.antelmann@fu-berlin.de)

detoxification functions, MSH is also involved in post-translational thiol-modification and forms mixed disulfides with protein thiols under hypochlorite stress^{9,10}. Protein S-mycothiolation is an emerging thiol-protection and redox-regulatory mechanism in Actinomycetes. In *Corynebacterium glutamicum*, we identified 25 S-mycothiolated proteins using shotgun LC-MS/MS analysis¹⁰. These include conserved targets for S-thiolation across different Gram-positive bacteria, such as the thiol-peroxidase Tpx, the inosine monophosphate (IMP) dehydrogenase GuaB and ribosomal proteins^{10,11}. In *Mycobacterium smegmatis*, protein S-mycothiolation was more abundant with 58 identified proteins, which correlates with the 20-fold higher MSH content in mycobacteria compared to corynebacteria⁹.

The redox-regulatory mechanisms of S-mycothiolated proteins have been studied thus far for several antioxidant enzymes, such as thiol peroxidases (Tpx, Mpx, AhpE) and methionine sulfoxide reductases (MsrA)^{10,12–15}. Moreover, Tpx has been shown to function as a peroxidase and as oligomeric chaperone in response to different levels of H₂O₂¹⁵. Regeneration of peroxidase and methionine sulfoxide reductase activities requires both the mycoredoxin (Mrx1) and thioredoxin pathways *in vitro*^{10,12,13,16,17}. Apart from its redox-regulatory role for antioxidant enzymes, MSH also functions in thiol-protection of the methionine synthase MetE by protein S-mycothiolation under acid stress conditions¹⁸.

In this work, we have used shotgun proteomics to identify 26 S-mycothiolated proteins in the pathogen *Corynebacterium diphtheriae*. As major redox-controlled metabolic enzyme, the glycolytic glyceraldehyde-3-phosphate dehydrogenase DIP1310 (GapDH) was S-mycothiolated under NaOCl stress at the active site Cys in *C. diphtheriae* *in vivo*. GapDH is a conserved target for redox-regulation and post-translational thiol-modifications including S-glutathionylations across all domains of life^{19,20}. In *Staphylococcus aureus*, the glycolytic GapDH was recently shown as major target for S-bacillithiolation which contributes with 4% to the total Cys proteome²¹. GapDH uses the active site Cys for the nucleophilic attack at the aldehyde group of glyceraldehyde-3-phosphate (G3P) to catalyze its phosphorylation to 1,3-bisphosphoglycerate, generating NADH in this process²⁰. The relatively high reactivity of the active site thiolate towards H₂O₂ depends on the stabilization of the transition state and a dedicated proton relay mechanism that promotes leaving group departure^{20,22}. S-glutathionylation of GapDH from the plant *Arabidopsis thaliana* resulted in enzyme inactivation which could be faster regenerated by glutaredoxins compared to thioredoxins²³. Here, we studied the redox-regulation of GapDH of *C. diphtheriae* in response to oxidative stress by protein S-mycothiolation *in vitro*. We show that S-mycothiolation functions in redox regulation and efficiently protects the active site against overoxidation by H₂O₂ and NaOCl which can be reversed by both, the Mrx1 and Trx pathways. Thus, striking similarities exist in the redox-control mechanisms of GapDH homologs from prokaryotic and eukaryotic organisms that involve protein S-thiolations using different thiol-redox systems for recycling, and as such for controlling central glycolytic activities.

Results

Identification of 26 S-mycothiolated proteins in *C. diphtheriae* under NaOCl stress using shotgun LC-MS/MS analysis. The role of protein S-mycothiolation in thiol-protection and redox regulation has been studied previously in *C. glutamicum*¹⁰ and *M. smegmatis*⁹. In this study, we were interested to identify the targets for protein S-mycothiolation in the pathogen *C. diphtheriae* under NaOCl stress. Cells of *C. diphtheriae* DSM43989 were grown in heart-infusion broth (HIB) and transferred at an OD₅₈₀ of 0.8 into a minimal medium (BMM) for NaOCl stress exposure to avoid the quenching of NaOCl by the rich HIB medium. Treatment of cells with 300 μM and 400 μM NaOCl resulted in a delay of growth with slow recovery after overnight growth (Fig. 1A). Using MSH-specific non-reducing Western blots, a strongly increased protein S-mycothiolation pattern could be detected after 30 min of 300–400 μM NaOCl stress (Fig. 1B). We further analysed the MSH level in *C. diphtheriae* under NaOCl stress using thiol-metabolomics. The MSH level was determined as 0.3 ± 0.03 μmol/g raw dry weight (rdw) under control conditions which decreased 4-fold after 30 min of NaOCl treatment (Fig. 1C). Thus, the depletion of MSH correlates with increased protein S-mycothiolation under NaOCl stress. This confirms our previous results in *M. smegmatis* where strong MSH depletion was also observed under NaOCl stress⁹.

Using LTQ-Orbitrap LC-MS/MS analysis, we identified 26 S-mycothiolated proteins in *C. diphtheriae* in NaOCl-treated cells based on the 484 Da mass increase of MSH at cysteine residues (Tables 1, S1 and S2). These S-mycothiolated proteins are displayed in a Voronoi treemap where the spectral protein abundance determines the cell size of each protein that is present in the proteome and the S-mycothiolated proteins are marked in red (Fig. 2). The 26 S-mycothiolated proteins of *C. diphtheriae* include only 5 conserved targets for S-thiolation, such as the peroxiredoxin AhpC, the ribosomal proteins RplC and RpsM, the glycolytic enzyme glyceraldehyde-3-phosphate dehydrogenase (GapDH) and the IMP dehydrogenase GuaB (Tables 1, S1 and S2). The ribose 5-phosphate isomerase DIP1796 was identified as S-mycothiolated in *C. diphtheriae* which functions in the pentose phosphate pathway and was previously found S-glutathionylated in the photosynthetic organism *Chlamydomonas reinhardtii*²⁴. In *Leishmania*, this enzyme is essential for replication of the intracellular form of the parasite, and in *Trypanosoma brucei* the knockout mutant has a reduced infectivity in mice²⁵. Other S-mycothiolated proteins are involved in energy metabolism (Ndh, GlpD, DIP1726), amino acid biosynthesis pathways (ThrA, LeuB, DapA, GlnA), purine biosynthesis (PurA), iron sulfur cluster biosynthesis (DIP1631) and cell wall biosynthesis (GlmS). The NADH dehydrogenase (Ndh) is an abundant enzyme that plays a role in the respiratory chain. S-mycothiolation of Ndh was found at the non-conserved Cys159. Some S-mycothiolated proteins are Cys-rich proteins including the glutamine synthetase GlnA1, the 4- α -glucanotransferase MalQ (DIP1726), and PurA, which possess 4 to 8 Cys residues. GlnA1 catalyzes the condensation of glutamate and ammonia to form glutamine and plays a major role in the survival of *Mycobacterium tuberculosis* under infection inside macrophages²⁶. In conclusion, the identified S-mycothiolated proteins are mainly involved in cellular metabolism, and share as main and conserved targets for S-thiolations: GapDH, GuaB, AhpC and the ribosomal proteins RplC and RpsM.

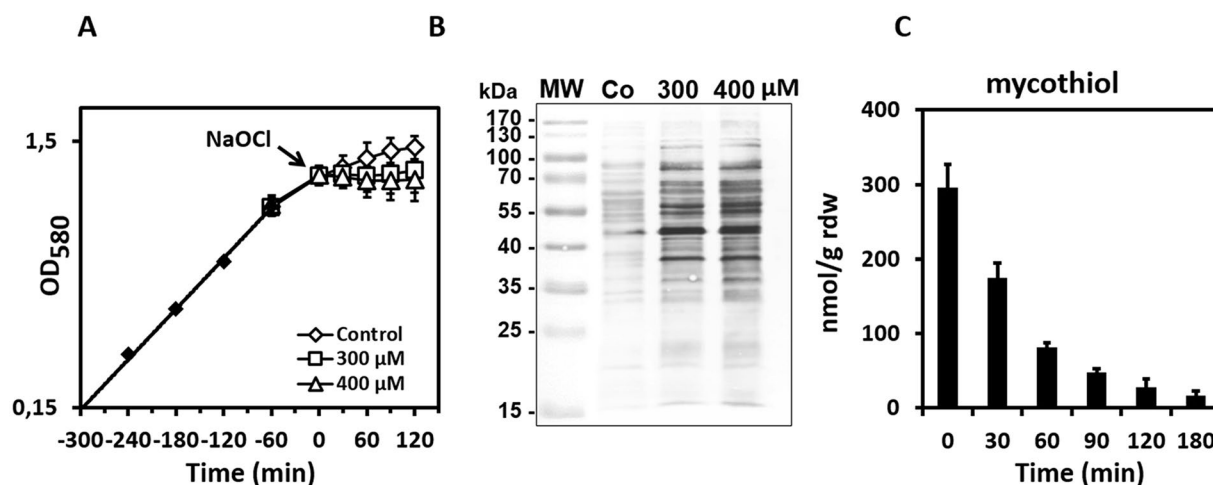


Figure 1. Protein S-mycothiolation pattern and MSH depletion in *C. diphtheriae* under NaOCl stress. *C. diphtheriae* was grown in HIB medium to an OD₅₈₀ of 0.75–0.8, transferred to BMM and treated with 300 and 400 μM NaOCl which resulted in growth delay (A) and strongly increased protein S-mycothiolation as revealed by non-reducing MSH-specific Western blots (B). The level of reduced MSH was 0.3 μmol/g rdw in the control and strongly depleted under NaOCl stress in the thiol-metabolome indicating that MSH is used for protein S-mycothiolation (C). All data represent mean values of three independent biological replicates and the error bars given were calculated as standard error of the mean (SEM).

Contribution of S-mycothiolated proteins to the total Cys proteome. It was interesting to note that GapDH was S-mycothiolated at the active site Cys153 in *C. diphtheriae*. Previously, we found that GapDH is the major target for S-bacillithiolation in *S. aureus* contributing with 4% Cys abundance to the total Cys proteome²¹. Thus, we calculated the percentages of Cys contributions of GapDH and other S-mycothiolated proteins to the total Cys proteome in *C. diphtheriae* (Figs 3 and S1, Table S4). In total, 2266 proteins are encoded in the genome of *C. diphtheriae* DSM43989 that include 1847 Cys proteins with 6156 Cys residues. The theoretical Cys content in the proteome of *C. diphtheriae* is 0.85% confirming that Cys is the rarest amino acid in the *C. diphtheriae* proteome (Figure S1). Next, we calculated the percentages of Cys abundances of all Cys proteins expressed in the proteome based on their spectral counts that are multiplied by the numbers of Cys residues. The spectral counts of the 1030 expressed proteins are visualized in a Cys proteome treemap including 805 Cys proteins (Fig. 3, Tables S3 and S4). The cell size indicates the spectral protein abundance and the color-code denotes the Cys content. About 395 Cys proteins contain only 1–2 Cys residues while the remaining 410 proteins have 3 or more Cys residues. These include 11 proteins with more than 10 Cys residues and the FeS-cluster oxidoreductase DIP2133 was identified as the most Cys-rich protein with 18 Cys residues. Of note, 83 Cys proteins were found to contribute to 60% of the total Cys abundances in the proteome including 55 Cys-rich proteins with more than 3 Cys residues (Figure S1). The RNA polymerase subunit beta' (RpoC) and two translation elongation factors (Tuf and FusaA) account for 2.5–4.5% of the total Cys abundance in the proteome. Furthermore, the Cys abundance treemap also visualizes that many ribosomal proteins and abundant chaperones and proteases (GroES, GroL1, GroL2, DnaK and ClpB) are devoid of Cys residues (Fig. 3).

Of the 26 S-mycothiolated proteins, 24 proteins were quantified based on their total spectral counts (Tables S3 and S4). Eleven S-mycothiolated proteins were found to contribute with 0.2–0.75% to the total Cys abundance, including the glycolytic GapDH on the top with 0.75%. Thus, in *C. diphtheriae*, GapDH is also the most abundant target for S-mycothiolation in comparison to all other identified S-mycothiolated proteins. Apart from GapDH, the AhpC homolog DirA, the IMP dehydrogenase GuaB, the glucanotransferase MalQ (DIP1726) and the glutamine synthetase GlnA1 contributed with 0.4–0.6% to the total Cys abundance in the proteome (Fig. 3; Table S4). As noted already, many S-mycothiolated proteins are Cys-rich proteins with more than 4 Cys residues which might explain why they are susceptible to S-mycothiolation under NaOCl stress. In conclusion, the comparison of the S-mycothiolated proteins with their Cys abundances in the total Cys proteome indicates that GapDH makes a major contribution to the S-mycothiolome in *C. diphtheriae* under NaOCl stress.

GapDH is reversibly inhibited and protected against overoxidation by S-mycothiolation under H₂O₂ and NaOCl stress *in vitro*. GapDH was identified as S-mycothiolated at its active site Cys153 that is highly sensitive to oxidation by H₂O₂ and located in a conserved C₁₅₃TTNC₁₅₇ motif present in prokaryotic and eukaryotic GapDH homologs (Figure S2). Under peroxide stress, the active site Cys is initially oxidized to a sulfenic acid that reacts further with LMW thiols, such as GSH, leading to S-glutathionylation^{22,27}. In the absence of thiol-redox systems or adjacent thiols, Cys-SOH can react further to irreversible oxidation forms, such as sulfinic or sulfonic acids^{1,28}. S-glutathionylation functions in redox control and protects catalytic and vulnerable Cys residues against overoxidation^{22,29–31}.

We were interested to investigate if S-mycothiolation controls GapDH activity and functions in thiol-protection against overoxidation *in vitro*. The His-tagged enzyme was cloned in *Escherichia coli*, purified

Protein	Locus Tag	Function	Cys-SSM	Cys-SSM peptide sequence	Ortholog and conservation* of Cys with -SSM in <i>Mtb</i>
Antioxidant enzymes					
DirA (AhpC)	DIP1420	2-Cys peroxiredoxin	Cys61** active site	(K)DFTFVC ₆₁ PTEIAAFGK(L)	Rv2428*
Protein synthesis					
RplC	DIP0473	50S ribosomal protein L3	Cys154**	(R)VGGIGAC ₁₅₄ ATPGR(V)	Rv0701*
RpsM	DIP0546	30S ribosomal protein S13	Cys86**	(K)IEIGC ₈₆ YQGLR(H)	Rv3460c*
Pth	DIP0897	Peptidyl-tRNA hydrolase	Cys49	(K)ASGAVIEVGGC ₄₉ R(V)	Rv1014c
DIP1398	DIP1398	RNA methyltransferase	Cys376* nucleophile	(R)AIAQSGPQAAIHIGC ₃₇₆ DPATFAR(D)	Rv2689c*
Energy metabolism					
DIP1726	DIP1726	Putative glucanotransferase	Cys45	(R)SLGVC ₄₅ FGNEDEPATDHEPLTGPMPSEDQIR(Y)	Rv1781c
Gap	DIP1310	Glyceraldehyde 3-phosphate DH	Cys153** active site	(K)HNIISNASC ₁₅₃ TTNCLAPMAK(V)	Rv1436*
DIP1796	DIP1796	Putative ribose/galactose isomerase	Cys143	(R)RIDILC ₁₄₃ EYER(T)	Rv2465c
DIP0655	DIP0655	Putative ribokinase	Cys171	(R)GTVVVNLAPVIDVDRDC ₁₇₁ LLR(A)	—
GlpD	DIP2237	Putative glycerol-3-phosphate DH	Cys10	(K)SHC ₁₀ TFNPDIYQDVWQR(F)	Rv2249c
Ndh	DIP1217	NADH dehydrogenase	Cys159	(R)AEmC ₁₅₉ EDPKER(E)	Rv1854c
Biosynthesis of amino acids					
ThrA	DIP1036	Homoserine dehydrogenase	Cys243	(R)VTYADVYC ₂₄₃ EGISK(I)	Rv1294
DIP0511	DIP0511	4-hydroxy-tetrahydrodipicolinate synthase	Cys141	(R)AVAAATSLPVIAYDIPVC ₁₄₁ VHTK(L)	—
DapA	DIP1464	4-hydroxy-tetrahydrodipicolinate synthase	Cys161	(R)SVVPIAPDTLC ₁₆₁ R(L)	Rv2753c
DIP0974	DIP0974	Putative aminotransferase	Cys138	(R)C ₁₃₈ DAPHELPNDIDLVFINSPTSPTGR(V)	Rv1178
GlnA1	DIP1644	Glutamine synthetase	Cys220	(R)QHPEC ₂₂₀ GTGSQEQINR(F)	—
LeuB	DIP1105	3-isopropylmalate dehydrogenase	Cys130	(R)EGTEGLYC ₁₃₀ GNGGTLR(E)	Rv2995c
Biosynthesis of nucleotides					
DIP1631	DIP1631	Uncharacterized protein	Cys43*	(R)IAVQPGGC ₄₃ SGLR(Y)	Rv2204c*
GuaB	DIP0580	Inosine-5'-monophosphate DH	Cys317** active site	(K)VGIGPGSIC ₃₁₇ TTR(V)	Rv3410c*
PurA	DIP2063	Adenylosuccinate synthetase	Cys423	(R)DQTIVC ₄₂₃ HDVMEA(-)	Rv0357c
Other functions					
DIP0913	DIP0913	Uncharacterized protein	Cys22	(K)ERPTAGPQLYPVTC ₂₂ EAVVSAIR(A)	—
DIP1026	DIP1026	Conserved ATP-binding protein	Cys75	(R)IC ₇₅ LEADLGPVR(F)	Rv1278
DIP1102	DIP1102	Putative uncharacterized protein	Cys441	(R)LLSAC ₄₄₁ PESGLYK(G)	—
DIP1250	DIP1250	M18 family aminopeptidase	Cys401*	(K)AGSSHQVFGNNSVPC ₄₀₁ GSTIGPITATR(L)	Rv0800*
DIP1287	DIP1287	UPF0210 protein DIP1287	Cys324	(K)GGMMAC ₃₂₄ SR(V)	—
GlmS	DIP1700	Glutamine-fructose-6-P aminotransferase	Cys74	(K)VQALEQELETSPMPQSC ₇₄ LGIGHTR(W)	Rv3436c

Table 1. Identification of 26 S-mycothiolated proteins in *C. diphtheriae* DSM43989 using shotgun LC-MS/MS analysis after exposure to 400 μ M NaOCl for 30 min. The S-mycothiolated proteins were identified using shotgun LC-MS/MS analysis and the Scaffold proteome software based on the mass increase of 484 Da (for -SSM) at Cys peptides. The table lists the Uniprot-accession number, protein name, conservation of the protein and the S-mycothiolated Cys residue in *M. tuberculosis* (*Mtb*) and the Cys-SSM peptide sequence. Conserved Cys residues are indicated with (*) and are shown in bold-face. Cys residues that were previously identified S-mycothiolated or S-bacillithiolated in *C. glutamicum*, *M. smegmatis* or *S. aureus* are indicated with (#).

and subjected to GapDH activity assays after exposure to H₂O₂ and NaOCl in the absence and presence of MSH *in vitro*. The inhibition of glycolytic GapDH activity by H₂O₂ and NaOCl was measured spectrophotometrically with G3P as substrate in the presence of NAD⁺ as coenzyme. NADH production was monitored in function of time as an absorbance increase at 340 nm¹⁰. The remaining GapDH activity was calculated from the slope in the kinetic curves as described previously²². Treatment with 200 μ M H₂O₂ alone did not affect GapDH activity, but 500 μ M H₂O₂ resulted in a 60% GapDH activity decrease. The enzyme was fully inactivated with 1 mM H₂O₂ (Fig. 4A). GapDH inactivation with 1 mM H₂O₂ was 65% irreversible while 35% activity could be recovered with 10 mM DTT (Fig. 4C). This suggests that the GapDH active site was rapidly overoxidized to Cys sulfonic acid by H₂O₂, but part of the enzyme was also reversibly inactivated perhaps due to an intramolecular disulfide between Cys153 and Cys157 (Fig. 4D). This intramolecular disulfide has been detected also in other GapDH homologs of *E. coli* and *Bacillus subtilis* under oxidative stress^{32, 33}. Using Orbitrap mass spectrometry, we could confirm the formation of the Cys153-sulfonic acid and of the intramolecular disulfide between Cys153 and Cys157 after exposure to 1 mM H₂O₂ (Figure S3A). In agreement with the activity assays, the overoxidized Cys153-peptide was detected at higher abundance compared to the intramolecular disulfide peptide.

Next, we analyzed whether S-mycothiolation can prevent overoxidation of the GapDH active site. Thus, the inhibition of GapDH activity and its reversibility was analyzed in the presence of H₂O₂ and MSH. GapDH was

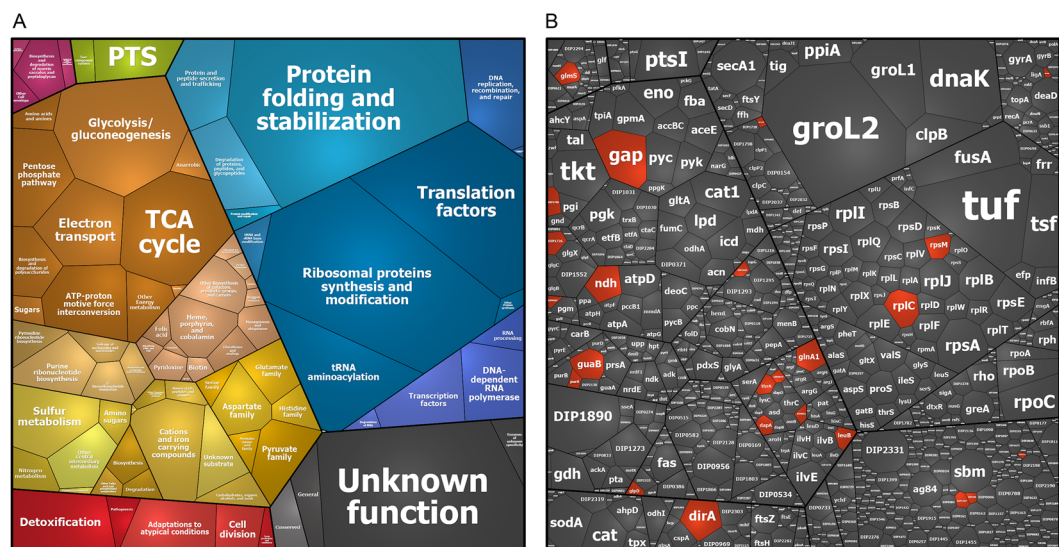


Figure 2. Voronoi treemaps show total protein abundance and 26 S-mycothiolated proteins identified in *C. diphtheriae* under NaOCl stress using shotgun LC-MS/MS analysis. **(A)** The treemap legend shows the classification of the *C. diphtheriae* proteome into functional categories as revealed by TIGRfam annotations. **(B)** The spectral protein abundance determines the cell size of each protein identified in the total proteome (Table S3). The 26 identified S-mycothiolated proteins under NaOCl stress are red-colored in the proteome treemap. The protein abundance treemap indicates that Gap, DirA (AhpC), Ndh and GuaB belong to the most abundant S-mycothiolated proteins in the total proteome.

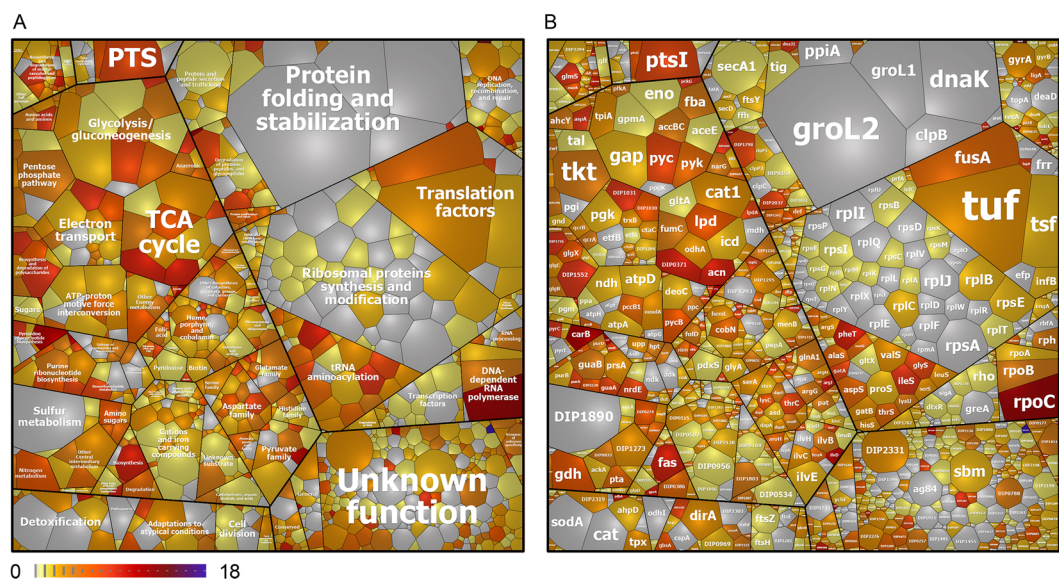


Figure 3. The total Cys abundance treemap of *C. diphtheriae* with proteins color-coded according to their number of Cys residues. **(A)** The treemap legend shows the functional classification of 1030 proteins detected in the proteome of *C. diphtheriae* as revealed by their TIGRfam annotations. **(B)** The spectral protein abundance determines the cell size of each protein identified in the total proteome (Table S3). The 805 Cys proteins were color-coded using a yellow-red color gradient based on their numbers of Cys residues. Non-Cys proteins are displayed in grey. The Cys abundance treemap visualizes that *C. diphtheriae* contains many Cys-rich proteins with >4 Cys residues in the proteome. The most abundant S-mycothiolated proteins Gap, DirA (AhpC), Ndh and GuaB contribute with 0.4–0.8% to the total Cys proteome. The values of calculated Cys abundances are shown in Table S4.

pre-treated with a 10-molar excess of MSH before it was subjected to 200 μ M, 500 μ M and 1 mM H_2O_2 . Of note, GapDH inactivation by H_2O_2 and MSH was faster compared to H_2O_2 alone since 200–500 μ M H_2O_2 resulted in a 40–75% GapDH activity decrease in the presence of MSH (Fig. 4B). The treatment with 1 mM H_2O_2 and MSH lead to a complete enzyme inactivation which was comparable to the inactivation by H_2O_2 alone. However,

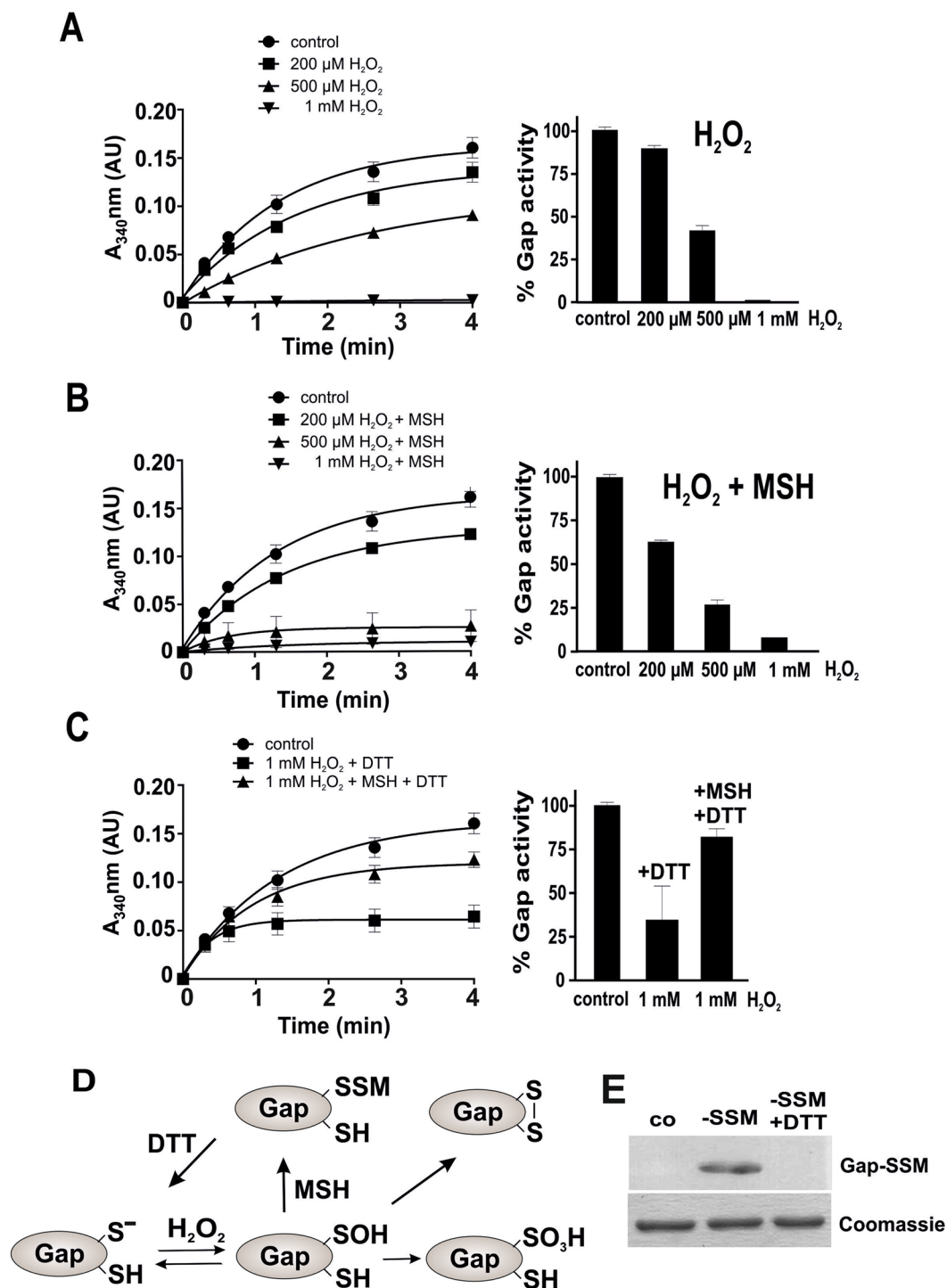


Figure 4. S-mycothiolation protects GapDH against overoxidation under H_2O_2 stress *in vitro*. (A,B) The NAD^+ -dependent GapDH activity was determined in a spectrophotometric assay by monitoring NADH generation during G3P oxidation at 340 nm. Inactivation of GapDH activity was performed using 200 μM , 500 μM and 1 mM H_2O_2 (A) in the absence and (B) in the presence of 1 mM MSH. (A,C) GapDH is 65% irreversibly inactivated with 1 mM H_2O_2 alone due to overoxidation of the active site Cys. (B,C) GapDH activity is reversibly inhibited due to S-mycothiolation with 1 mM H_2O_2 and MSH and could be reactivated by 10 mM DTT. (E) Non-reducing MSH specific Western blot analysis confirmed the S-mycothiolation of GapDH under H_2O_2 and MSH treatment and its reduction by DTT. (D) These results suggest that the GapDH active site Cys forms a sulfenic acid that reacts further to form Cys sulfonic acid and intramolecular disulfides in the presence of 1 mM H_2O_2 alone. GapDH is protected against this irreversible overoxidation by S-mycothiolation of the active site Cys in the presence of MSH and H_2O_2 . All data represent mean values of three independent replicate experiments and the error bars given were calculated as standard error of the mean (SEM).

GapDH inactivation by H_2O_2 and MSH was 80% reversible with 10 mM DTT, which indicates that Cys153 is S-mycothiolated in the presence of MSH and H_2O_2 . The S-mycothiolated Cys153 peptide could be verified by mass spectrometry and by non-reducing MSH-specific Western blot analysis (Figs 4E, S3B and S4A). In addition, the intramolecular Cys153-SS-Cys157 disulfide peptide was also detected by mass spectrometry (Figure S3B). These results provide evidence for the high reactivity of the nucleophilic active site Cys153 towards H_2O_2 , its vulnerability to overoxidation and the protection from overoxidation by S-mycothiolation (Fig. 4E). Moreover, our results support that GapDH inactivation by S-mycothiolation occurs faster compared to overoxidation by H_2O_2 alone which was observed in the activity assays with 200 and 500 μM H_2O_2 (Fig. 4A,B). Thus, S-mycothiolation can efficiently prevent the overoxidation of the GapDH active site.

However, S-mycothiolation of the GapDH active site Cys153 was observed *in vivo* under conditions of NaOCl stress. Thus, we analyzed GapDH inactivation with different NaOCl concentrations in the absence or presence of MSH. The incubation of GapDH with 100 μM NaOCl did not affect its activity and concentrations of 200–500 μM led to a 40% activity decrease (Fig. 5A). GapDH was fully inactivated with 1 mM NaOCl. Interestingly, the treatment of GapDH with 1 mM NaOCl was also partly (30%) reversible with 10 mM DTT (Figure 5C). This suggests that GapDH inactivation must be caused by both, irreversible overoxidation of Cys153 and reversible Cys153-SS-Cys157 intramolecular disulfide bond formation under NaOCl stress (Fig. 5D). Using Orbitrap mass spectrometry, we could confirm the overoxidation of GapDH as main modification which occurred in this case at Cys153 and Cys157. The intramolecular disulfide between Cys153 and Cys157 was also detected under NaOCl stress, but at lower abundance (Figure S3C). In conclusion, GapDH is subject to overoxidation and intramolecular disulfide formation under both, H_2O_2 and NaOCl treatment *in vitro*.

To investigate whether S-mycothiolation can prevent the overoxidation of the active site by NaOCl, we repeated the GapDH activity assays above and pretreated the enzyme with 10-fold molar excess of MSH prior to NaOCl exposure. Exposure of GapDH to 100 μM NaOCl resulted in 35% activity decrease while 200–500 μM NaOCl caused 50% enzyme inactivation (Fig. 5B). Treatment with 1 mM NaOCl in the presence of MSH led to 90% inactivation. Thus, it appears that GapDH inactivation with 100–500 μM NaOCl and MSH is faster compared to inactivation with NaOCl alone. GapDH inactivation by 1 mM NaOCl and MSH was almost completely reversible, since about 75% GapDH activity could be recovered with DTT. These results indicate that the GapDH active site should be protected against overoxidation by S-mycothiolation under NaOCl treatment in the presence of MSH. The S-mycothiolation of GapDH after NaOCl treatment was verified by MSH-specific Western blots and both S-mycothiolated Cys153 and Cys157 peptides were identified by mass spectrometry (Figures S3D and S4B). Apart from S-mycothiolation, we identified less abundant Cys153-SS-Cys157 intramolecular disulfides under NaOCl stress in the presence of MSH. In conclusion, our activity assays provide evidence that the S-mycothiolation pathway occurs faster compared to the overoxidation under both, H_2O_2 and NaOCl treatment *in vitro*. Thus, S-mycothiolation can efficiently protect the active site against overoxidation and irreversible inactivation under H_2O_2 and NaOCl stress *in vitro* (Figs 4D and 5D). In addition, intramolecular disulfides were detected under both, H_2O_2 and NaOCl treatment in the presence and absence of MSH as an additional redox-regulatory mechanism of GapDH.

Reactivation of S-mycothiolated GapDH requires the Mrx1/MSH/Mtr and Trx/TrxR electron transfer pathways.

Previous studies have demonstrated that both, the Mrx1 and Trx electron transfer pathways can function in reduction of the S-mycothiolated peroxidase Mpx *in vitro*^{13,34}. Moreover, de-mycothiolation by Mrx1 was shown to operate faster via a monothiol reaction mechanism compared to the reduction via Trx using a dithiol mechanism. Thus, we were interested to see if the Mrx1 and/or Trx electron transfer pathways could function in the reduction of S-mycothiolated GapDH resulting in recovery of its glycolytic activity *in vitro*. Regeneration of GapDH activity using Mrx1 and/or Trx should work only with the S-mycothiolated protein, but not with the overoxidized GapDH protein. Thus, the GapDH activity assay was performed after treatment of S-mycothiolated and overoxidized GapDH with the Mrx1 and Trx pathways (Fig. 6A,B). The regeneration of GapDH activity after Mrx1 and Trx reduction was followed by monitoring the NADH production at 340 nm. The results showed that both, Mrx1 and Trx can catalyze the reduction of S-mycothiolated GAPDH to regenerate GapDH activity *in vitro* (Fig. 6A,B). In contrast, Mrx1 and Trx could not restore the activity of overoxidized GapDH that was irreversibly inactivated using 10 mM H_2O_2 alone (Fig. 6A,B). To verify the de-mycothiolation of S-mycothiolated GapDH by Mrx1 and Trx, we performed a MSH-specific Western blot analysis (Fig. 6D). The results showed that Mrx1 and the Mrx1 resolving Cys mutant (Mrx1C15S) could reduce the GapDH MSH-mixed disulfide in this de-mycothiolation assay as shown by a decreased intensity of the S-mycothiolated GapDH band. Similarly, the reduction of GapDH-SSM by Trx and the Trx resolving Cys mutant (TrxC35S) are shown using the MSH-specific Western blot analysis. Here, the transfer of MSH to the Trx active site was clearly visible (Fig. 6D).

Next, we analyzed whether there is a catalytically relevant reduction mechanism of GapDH by the Mrx1 and Trx electron pathways which can be monitored by NADPH consumption. The Mrx1/MSH/Mtr/NADPH and Trx/TrxR/NADPH pathways were reconstituted *in vitro* using S-mycothiolated GapDH as substrate and NADPH consumption was followed over time in progress curves. First, we analyzed reduction of S-mycothiolated GapDH with the Mrx1/MSH/Mtr pathway at 340 nm. However, we failed to see any higher NADPH consumption rate using the Mrx1 electron transfer pathway. We concluded that reduction of S-mycothiolated GapDH with the Mrx1 pathway might be too fast and already finished before we started the measurement. Therefore, we decided to shift to a stopped flow device with a 2 ms mixing time. Under the same conditions, we found that most NADPH was already consumed within 5 seconds (Fig. 6E). In contrast, de-mycothiolation of S-mycothiolated GapDH could be measured in the Trx-coupled assay using a spectrophotometer. Here, NADPH is much slower consumed within 100 to 400 seconds. The NADPH consumption rate using Trx was higher for S-mycothiolated GapDH compared to the reduced GapDH control, indicating that Trx is able to reduce S-mycothiolated GapDH (Fig. 6F). In conclusion, our results demonstrate that both Mrx1 and Trx can provide electrons for GapDH

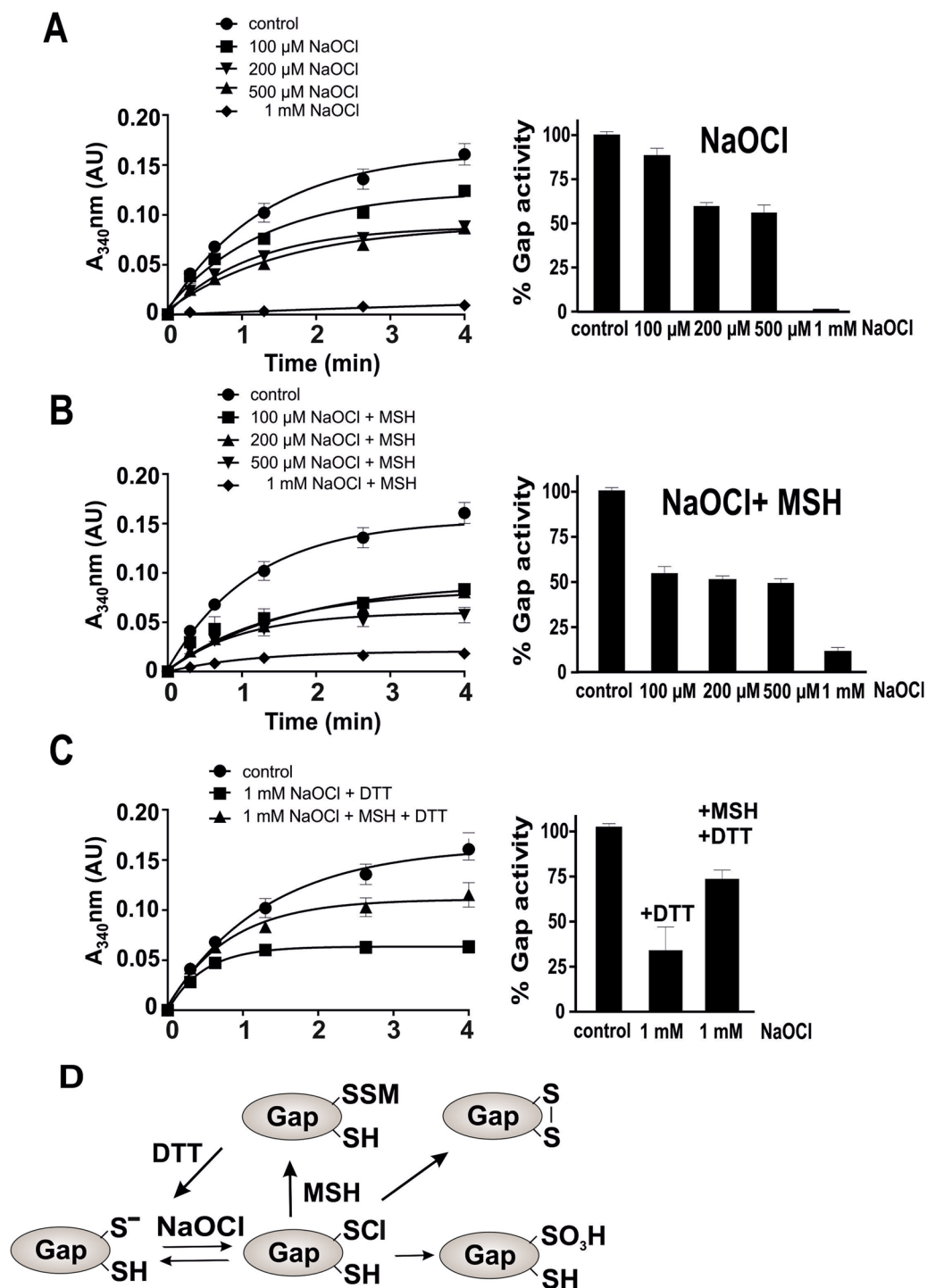


Figure 5. S-mycothiolation protects GapDH against overoxidation under NaOCl stress *in vitro*. (A,B) The NAD⁺-dependent GapDH activity was determined in a spectrophotometric assay by monitoring NADH generation during G3P oxidation at 340 nm. Inactivation of the GapDH activity was performed with 100, 200, 500 μ M and 1 mM NaOCl (A) without or (B) with MSH pre-treatment. (A,C) GapDH inactivation with 1 mM NaOCl alone is mostly irreversible due to the overoxidation of the active site to Cys sulfonic acid. (B,C) GapDH activity is reversibly inhibited due to S-mycothiolation with 1 mM NaOCl and MSH and could be reactivated by 10 mM DTT. The S-mycothiolation of Gap was confirmed by MSH-specific Western blots (Figure S4). (D) These results suggest that the GapDH active site Cys is chlorinated by NaOCl alone to form Cys-sulphenylchloride (-S \cdot Cl) that reacts further to form Cys sulfonic acid and intramolecular disulfides in the absence of MSH. GapDH is protected against overoxidation by S-mycothiolation of the active site Cys in the presence of MSH. All data represent mean values of three independent replicate experiments and the error bars given were calculated as standard error of the mean (SEM).

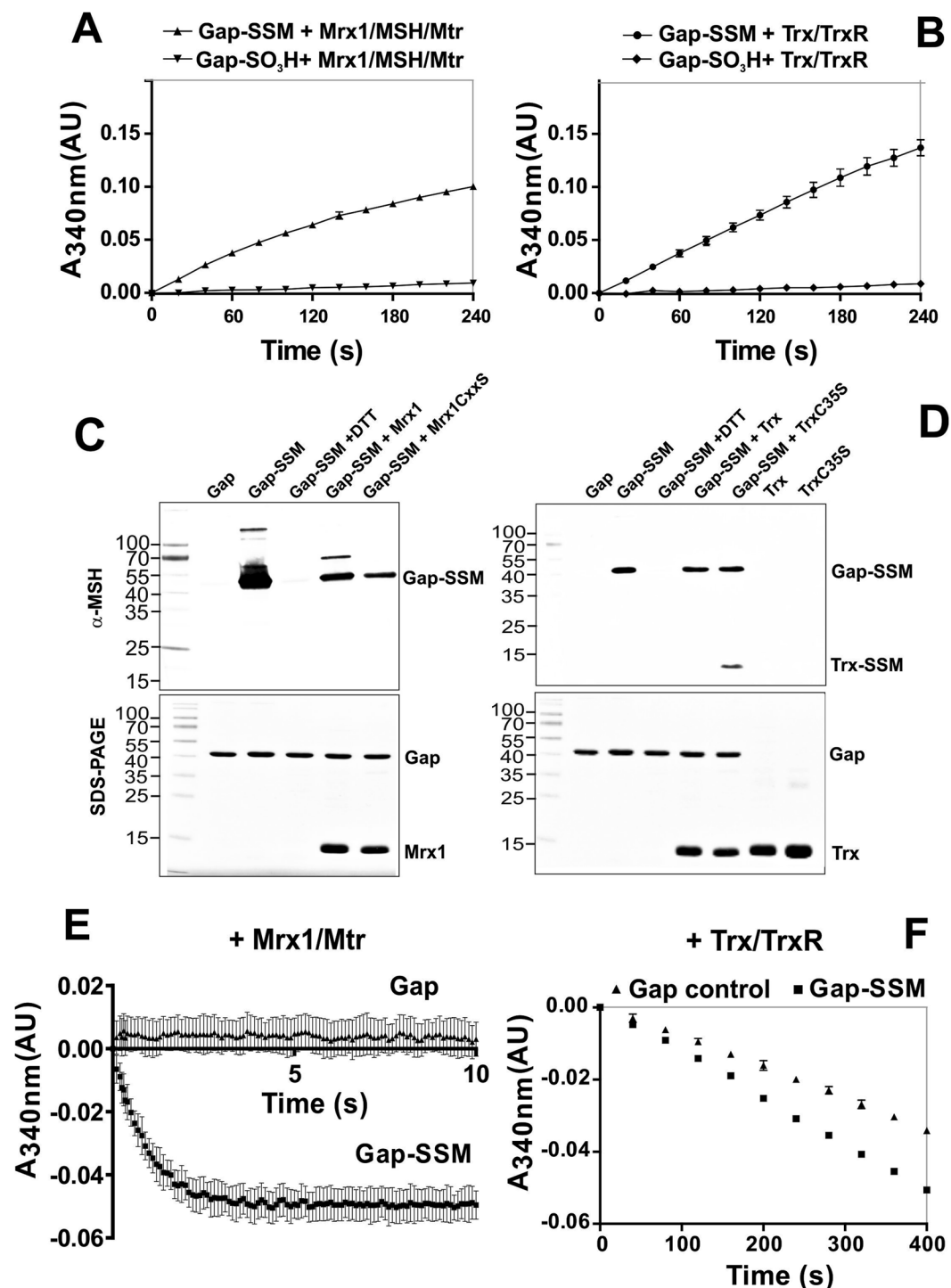


Figure 6. Re-activation of S-mycothiolated GapDH by the Trx/TrxR and Mrx/MSH/Mtr electron transfer pathways. (A,B) GapDH activity could be restored after demycothiolation of S-mycothiolated GapDH with Mrx1 and Trx as shown by NADH production in the G3P oxidation assay. In contrast, overoxidized GapDH that was treated with 10 mM H₂O₂ alone could not be reactivated by the Mrx1 and Trx pathways. (C,D) MSH-specific non-reducing Western blot analysis confirmed the S-mycothiolation of GapDH *in vitro* and its demycothiolation by the Mrx1 and Trx pathways. The transfer of MSH to the Trx resolving Cys mutant TrxC35S is shown. (E,F) The Mrx1/MSH/Mtr and Trx/TrxR electron transfer pathways both reduce S-mycothiolated GapDH with different reaction rates as revealed by progress curves of NADPH consumption. The demycothiolation of GapDH by the Mrx1-pathway was faster compared to the Trx-pathway. All data represent mean values of three independent replicate experiments and the error bars given were calculated as standard error of the mean (SEM).

de-mycothiolation. However, Mrx1 reduces the MSH mixed disulfide of GapDH much faster compared to Trx. Thus, our results show that S-mycothiolation of GapDH can efficiently function in protection of the active site against overoxidation and can be reversed using both, the Mrx1 and Trx pathways *in vitro*.

Discussion

Protein S-mycothiolation is a widespread and emerging redox modification in Actinomycetes and functions in redox regulation and thiol-protection against overoxidation to Cys sulfonic acids under conditions of NaOCl stress^{9, 10}. Hypochlorous acid (HOCl) is encountered by the pathogens *C. diphtheriae* and *M. tuberculosis* particularly during infections. HOCl is generated in neutrophils by the enzyme myeloperoxidase (MPO) with the aim to kill pathogenic bacteria^{35, 36}. HOCl is a strong thiol-oxidant and chlorinating agent that reacts with Cys residues to sulfinylchlorides (-S-Cl) and further to protein disulfides^{37, 38}, such as S-thiolations as we observed in Gram-positive bacteria⁴.

We identified 25 S-mycothiolated proteins in *C. glutamicum*¹⁰ and 26 proteins in *C. diphtheriae* while protein S-mycothiolation was more abundant in *M. smegmatis*⁹ with 58 identified proteins under NaOCl stress. The different numbers of S-mycothiolated proteins might be related to the different MSH contents between corynebacteria and mycobacteria³⁹. Mycobacteria produce high levels of up-to 20 mM MSH⁵ and we recently estimated 6 $\mu\text{mol/g}$ rdw MSH in *M. smegmatis*⁹. However, the MSH-levels determined in *C. diphtheriae* are 20-fold lower with 0.3 $\mu\text{mol/g}$ rdw according to this work and previous studies⁵. Due to the low MSH-content, the number of S-mycothiolated proteins might be lower in *C. diphtheriae* and *C. glutamicum* compared to mycobacteria. This indicates that in addition to MSH, unknown alternative LMW thiols might function in corynebacteria to maintain the thiol-redox homeostasis and to protect proteins by alternative S-thiolations. Recent studies further suggest that overexpression of the mycothiol disulfide reductase (Mtr) under oxidative stress conditions could play an important role in the maintenance of the redox homeostasis by increasing the levels of reduced MSH⁴⁰. In *M. tuberculosis*, MSH and the alternative LMW thiol ergothioneine (EGT) have been shown to be critical for redox homeostasis, energy metabolism and virulence and mutants deficient in MSH or EGT biosynthesis showed overlapping responses in the transcriptome^{41, 42}. The EGT levels were also elevated in a *M. smegmatis* *mshA* mutant⁴³. Thus, it remains to be elucidated whether EGT plays also a role as alternative LMW thiol in corynebacteria. In addition, it is also possible that the lower intracellular MSH level and the lower level of protein S-mycothiolation in corynebacteria is related to their 2–3-fold smaller genome size compared to mycobacteria.

The comparison of the functions and conservation of all identified S-mycothiolated proteins across Actinomycetes indicates that these are involved in a variety of cellular pathways. S-mycothiolated proteins participate in energy metabolism, fatty acid and mycolic acid biosynthesis, nucleotide, cofactor, mycothiol and amino acid biosynthesis, redox regulation, detoxification, transcription and translation. Some S-mycothiolated proteins are conserved and essential targets for S-thiolation across Gram-positive bacteria, such as thiol-peroxidases and peroxiredoxins (Tpx, AhpC), ribosomal proteins (RpsM, RplC), the IMP dehydrogenase (GuaB), the myo-inositol-1-phosphate synthase (Ino1), the methionine synthase (MetE), and the conserved glycolytic GapDH.

These conserved targets for S-mycothiolations overlap also with conserved S-bacillithiolated proteins in *Firmicutes*, such as *Bacillus* and *Staphylococcus* species^{11, 44}. Of note, the methionine synthase MetE is the most abundant S-bacillithiolated metabolic enzyme in *B. subtilis*, while GapDH represents the major S-bacillithiolated protein in *S. aureus*^{21, 33}. GapDH of *S. aureus* contributes with 4% Cys abundance to the total Cys proteome and is the most abundant Cys protein in the proteome. In *C. diphtheriae*, GapDH represents also the most abundant S-mycothiolated protein, but contributes only with 0.75% Cys abundance to the total Cys proteome. In *C. glutamicum*, the major targets for S-mycothiolation are the maltodextrin phosphorylase MalP and the thiol-peroxidase Tpx and it was shown that S-mycothiolation inhibited the activities of MalP and Tpx^{10, 15}. Thus, it seems that abundant redox-sensitive metabolic enzymes are the main targets for inactivation by S-thiolations in different bacteria. The different abundances of the S-mycothiolated MetE, MalP and GapDH in corynebacteria most likely depend on the different minimal growth media used for bacterial cultivations.

In addition, we found that many S-mycothiolated proteins of *C. diphtheriae* contain a high number of Cys residues explaining their susceptibility to oxidative inactivation. The glycolytic GapDH was S-mycothiolated at its active Cys153 residue that is known to be highly susceptible to oxidation by H_2O_2 ^{45–48}. GapDH is a well-known and conserved target for redox-regulation and S-glutathionylation in response to oxidative stress in several prokaryotic and eukaryotic organisms, including bacteria, malaria parasites, yeast, plants and human cell^{19, 20, 49}. GapDH inactivation in response to oxidative stress has been shown to reprogram central carbon metabolism and to re-direct the glycolytic flux into the pentose phosphate pathway (PPP) to increase NADPH production under conditions of high demands for reducing equivalents^{50, 51}. Thus, the goal of the GapDH inactivation by S-thiolation could be metabolic adaptation to provide more NADPH as reducing power in the cell under oxidative stress. In fact, a change of the global carbon flux was shown in *E. coli* under superoxide and H_2O_2 stress leading to an increased NADPH/NADH ratio^{52, 53}. Post-translational thiol-modifications play a key role in this metabolic adaptation to oxidative stress in different organisms and can change enzyme functions to re-configure central carbon metabolism which confers high metabolic plasticity^{50, 51}.

In this study, we have asked the question whether S-mycothiolation can function in thiol-protection and redox-regulation of GapDH activity in *C. diphtheriae* under H_2O_2 - and NaOCl stress. To address this question, GapDH was inactivated with H_2O_2 and NaOCl in the absence and presence of MSH to analyze the kinetics of the irreversible overoxidation and S-mycothiolation pathways *in vitro*. The kinetic curves of H_2O_2 and NaOCl-dependent GapDH inactivation showed that the majority (65%) of the glycolytic activity is rapidly irreversibly inhibited with 1 mM H_2O_2 and NaOCl without pre-exposure to MSH. The mass spectrometry data confirmed the overoxidation of the active site Cys153 with H_2O_2 and NaOCl alone. In addition, 35% of GapDH activity was reversibly inhibited by 1 mM H_2O_2 and NaOCl alone due to an intramolecular Cys153-SS-Cys157 disulfide that was identified using mass spectrometry. In presence of MSH, GapDH inactivation by H_2O_2 and NaOCl was faster due to S-mycothiolation which was fully reversible with DTT and confirmed also by MSH-specific Western blot analysis.

This indicates that the GapDH overoxidation can be prevented by the faster S-mycothiolation. These results are in agreement with kinetic measurements performed for the related GapDH homolog of *S. aureus*²¹. The *S. aureus* GapDH was highly susceptible to overoxidation in the presence of H₂O₂ and NaOCl which could be prevented by S-bacillithiolation²¹. Interestingly, the comparison of the kinetics for the dose-dependent inactivation suggests that the *S. aureus* GapDH enzyme is more sensitive to oxidative inactivation compared to GapDH of *C. diphtheriae* since lower H₂O₂ and NaOCl doses inhibited *S. aureus* GapDH activity. This higher sensitivity of *S. aureus* GapDH may be due to the fact that Cys157 is replaced by a serine in the otherwise highly conserved C₁₅₃TTNC₁₅₇ motif²¹, so there is no possibility of intramolecular disulfide formation to prevent overoxidation (Figure S2). The active site Cys in *Homo sapiens* GapDH was demonstrated to provide a proton relay mechanism that determines H₂O₂-sensitivity of GapDH for oxidation²². On the other hand, *S. aureus* GapDH contains a threonine in position 243 instead of the otherwise conserved valine, which compensates for the disappearance of the oxidation sensitivity in the C157S mutant. This was demonstrated with the *Homo sapiens* GapDH C156S mutant, where an additional V243T mutation restores the oxidation sensitivity²². Our results strongly suggest that the second conserved cysteine might play an important role for oxidation sensitivity of GapDH and prevents overoxidation through intramolecular disulfide formation. Further studies are required to confirm whether Cys157 or other structural features make a difference in the sensitivity of GapDH to overoxidation and S-mycothiolation.

The strong H₂O₂ reactivity of the GapDH active site thiolate was recently shown to depend on a specific H₂O₂ binding pocket, transition state stabilization, and a dedicated proton relay mechanism promoting hydroxyl leaving-group departure^{20,22}. This proton relay also determines the preferred modification by S-glutathionylation in eukaryotic organisms which requires the initial formation of a sulfenic acid at Cys153 followed by reaction with GSH to form the mixed disulfide. This proton relay explains why GapDH of *C. diphtheriae* is a preferred target for S-mycothiolation under H₂O₂ and NaOCl. Our results confirmed the reactivity of the GapDH active site Cys towards H₂O₂- and NaOCl-dependent oxidation and the preference for formation of S-thiolations as observed in other GapDH homologs.

The reduction of S-mycothiolated proteins was previously shown to require both, the Mrx1 and Trx pathways for the regeneration of the activities of Mpx and MsrA *in vitro*^{12,13,16,34,54}. Mpx and MsrA form intramolecular disulfides and S-mycothiolations under H₂O₂ treatment *in vitro* that are reduced by the Trx and Mrx1 pathways. Here, we have shown that reduction and re-activation of S-mycothiolated GapDH also requires both, the Mrx1 and the Trx pathway *in vitro*. We have further shown that Mrx1 is much faster than Trx in reduction of S-mycothiolated GapDH. Thus, Mrx1 can take over the role of Trx, especially when Trx, as a ubiquitous disulfide reductase, is busy with reducing other non-native disulfides upon recovery from oxidative stress. Mrx1 efficiently functions in regeneration of GapDH activity to restore cellular growth and survival. The overlapping roles of Mrx1 and Trx in demycothiolation at different reaction rates were recently shown for Mpx recycling¹³. In agreement with our GapDH results, Mpx de-mycothiolation was also about two orders of magnitude more efficient with the Mrx1 system. De-mycothiolation of Mpx by Mrx1 occurs via a monothiol mechanism, which generates MSSM, and de-mycothiolation by Trx occurs via a dithiol-mechanism, generating oxidized Trx and reduced MSH. Both results suggest Mrx1 is the primary de-mycothiolating enzyme in Actinomycetes, with Trx having only a residual contribution. Under these premises, Trx would only be able to take over the role of Mrx1 if the concentration of reduced MSH is limiting, or if Trx is present at a much higher concentration than Mrx1 inside the cell. In conclusion, de-mycothiolation using the Mrx1 and Trx pathways may be a common mechanism to recover after oxidative stress when the pentose pathway has again produced enough NADPH to ensure the regeneration of oxidized Cys residues.

Similar to our studies, the de-glutathionylating activity of Trx was shown for GapDH isoform 1 (AtGapC1) from *A. thaliana* that could be reactivated by glutaredoxin C and less efficiently by thioredoxin *in vitro*²³. De-glutathionylation using Trx1 and Grx1 was also demonstrated for other GapDH homologs and S-glutathionylated enzymes in the malaria parasite, *Plasmodium falciparum* and in yeast cells^{49,55,56}. In *C. glutamicum*, overexpression of the MSH disulfide reductase Mtr resulted in a higher reduced level of MSH and increased activities of several redox-enzymes, including Mpx, MsrA, Trx, and Mrx1⁴⁰. Thus, future research should be directed to explore the cross-talk of the Mrx1 and Trx systems in regenerating S-mycothiolated proteins and MSH itself to restore the redox balance during the recovery from oxidative stress.

Material and Methods

Bacterial strains and growth conditions. *C. diphtheriae* DSM43989 was grown under vigorous agitation in Heart Infusion broth (HIB) (Difco) at 37°C to an optical density at 580 nm (OD₅₈₀) of 0.75–0.8. For NaOCl stress exposure, the cells were harvested, washed and re-suspended into Belitsky Minimal Medium (BMM) and further cultivated until cells have reached an OD₅₀₀ of ~1. *E. coli* strains used were DH5α and BL21(DE3)plysS which were cultivated in Luria-Bertani (LB) medium at 37°C in the presence of the appropriate antibiotics, such as ampicillin (100 µg/ml) and chloramphenicol (25 µg/ml). Sodium hypochlorite (NaOCl, 15% stock solution) was purchased from Sigma Aldrich. For stress experiments, *C. diphtheriae* cells were treated with 400 µM NaOCl for 30 min.

Identification of S-mycothiolated peptides using LTQ-Orbitrap Velos mass spectrometry. N-ethylmaleimide (NEM)-alkylated protein extracts were prepared from *C. diphtheriae* cells exposed to 400 µM NaOCl for 30 min and separated by 15% non-reducing SDS-PAGE followed by tryptic in-gel digestion and LTQ-Orbitrap-Velos mass spectrometry as described¹⁰. Post-translational thiol-modifications of proteins were identified by searching all MS/MS spectra in “dta” format against the *C. diphtheriae* target-decoy protein sequence database extracted from UniprotKB release 12.7 (UniProt Consortium, Nucleic acids research 2007, 35, D193–197) using Sorcerer™-SEQUEST® (Sequest v. 2.7 rev. 11, Thermo Electron including Scaffold 4.0, Proteome Software Inc., Portland, OR). The SEQUEST search parameters and thiol-modifications were used as described¹⁰ using the following parameters: parent ion mass tolerance 10 ppm and fragment ion mass tolerance 1.00 Da. Two tryptic miscleavages were allowed. Methionine oxidation (+15.994915 Da), cysteine alkylation (+125.04767 Da for NEM), S-cysteinylations (+119.004099 Da for C3H7NO2S) and S-mycothiolations

(+484.13627 Da for MSH) were set as variable post-translational modifications in the Sequest search. Sequest identifications required ΔCn scores of >0.10 and XCorr scores of >2.2 , 3.3 and 3.75 for doubly, triply and quadruply charged peptides. Neutral loss precursor ions characteristic for the loss of myo-inositol (-180 Da) served for verification of the S-mycothiolated peptides. The mass spectrometry (MS) proteomics datasets (MS raw files and Scaffold files) are deposited into the ProteomeXchange database via the PRIDE partner repository with the dataset identifier PXD003321.

Mass spectrometry of the H_2O_2 -treated overoxidized GapDH was performed after in-gel tryptic digestion using nLC-MS/MS by an Orbitrap fusion as described previously⁵⁷.

Monobromobimane-labelling and HPLC-thiol metabolomics analysis. Cells were cultivated in HIB medium and transferred to BMM medium for the NaOCl stress experiments as described above. Thiol-labelling using monobromobimane (mBBR) was performed as described previously¹¹. The mBBR-labelled thiols were separated by reverse phase chromatography and quantified by fluorescence detection using the same HPLC system as described⁵⁸. The following gradient method was applied: 10 min 92% buffer A (10% methanol, 0.25% acetic acid, pH 3.9) supplemented with 8% buffer B (90% methanol, 0.25% acetic acid, pH 3.9), linear increase to 40% buffer B in 10 min, constant flow of 40% buffer B for 5 min, linear increase to 90% buffer B in 5 min, washing with 100% buffer B for 2 min followed by re-equilibration with 8% buffer B for 8 min. The flow rate was constantly set to 1.5 ml min^{-1} .

Expression, cloning and purification of recombinant His₆-tagged GapDH protein. The DIP1310 gene encoding GapDH was amplified by PCR using the primer pairs *Gap*-for (5'-GGAATTCCATATGGTGACGATTCGCGTAGGTATCA-3') and *Gap*-rev (5'-CTAGCTAGCTTAGTGATGGTGATGGTGATGGAGACGCTCACCGACGTATTC-3') with *C. diphtheriae* DSM43989 chromosomal DNA as template. The PCR product was digested with *Nhe*I and *Nde*I restriction enzymes and cloned into a similarly digested pET11b expression vector resulting in pET11b-*gapDH* that was transformed into *E. coli* BL21(DE3)*plysS*. The *gapDH* sequence was confirmed by DNA sequencing. For GapDH overproduction, the *E. coli* BL21(DE3)*plysS* strain with plasmid pET11b-*gap* was cultured in LB broth medium to an OD_{600} of 0.5 to 0.7 at 37 °C. Protein expression was induced with 1 mM IPTG (Isopropyl- β -D-1-thiogalactopyranoside) and cultivation was continued for 4 hours. Recombinant His₆-tagged GapDH was purified by affinity chromatography using His Trap™ HP Ni-NTA columns (5 ml; GE Healthcare, Chalfont St Giles, UK) and the ÄKTA purifier liquid chromatography system (GE Healthcare) according to the instructions of the manufacturers. Purified GapDH was dialyzed against 20 mM Tris-HCl, pH 8.0 and concentrated to 20 mg/ml using Vivaspın Ultra concentrators (Sartorius, Göttingen, Germany). The cloning and purifications of recombinant His₆-tagged proteins Mrx1, Mtr, Trx and TrxR were performed as described previously⁵⁹.

Production and purification of mycothiol. MSH was purified from *M. smegmatis* mc²155 that was grown to the late exponential phase in Middlebrook 7H9 broth with 0.05% Tween 80 and 10% oleic albumin dextrose catalase (OADC) at 37 °C as described¹³. The cells were harvested by centrifugation and disrupted using a French press (Constant Systems). The purified MSH was reduced with TCEP following several additional chromatographic steps. The concentration of MSH was determined by HPLC by correlating the MSH mBBR conjugate elution peak of an ACE 5 C18 column (Achrom) with a known standard. The sample purity was checked with Proton Nuclear Magnetic Resonance (¹H NMR).

Non-reducing Western blot analysis. MSH-specific Western blot analysis of the GapDH MSH-mixed disulfides were carried out using rabbit anti-MSH specific antiserum (1:1000-dilution) as described previously¹³.

Glycolytic GapDH activity assay. GapDH was reduced before the activity assays with 10 mM DTT for 30 minutes at room temperature. Excess of DTT was removed by desalting with Micro Biospin 6 columns (Biorad). Glycolytic GapDH activity was monitored spectrophotometric at 340 nm and 25 °C by the production of NADH. The oxidation of G3P to 1,3-bisphosphoglycerate (1,3 BPG) was measured in an assay mixture containing 1.25 mM NAD⁺ and 0.25 μ M GapDH in argon-flushed 20 mM Tris/HCl with 1.25 mM EDTA and 15 mM sodium arsenate as described previously²². After pre-incubation, the reaction was started by addition of 0.25 mM D,L-G3P. Sodium arsenate was used as a co-substrate to form unstable 1-arseno,3-phosphoglycerate. Degradation of the product allows a favorable equilibrium for measuring the rate of GapDH activity in the glycolytic forward reaction.

Inactivation of GapDH by H₂O₂ and NaOCl treatment. Pre-reduced GapDH (25 μ M) was incubated with different concentrations of H₂O₂ and NaOCl (100, 200, 500 μ M, 1 mM) in the absence or presence of 1 mM MSH for 5 min at 37 °C in an assay mixture containing 1.25 mM NAD⁺ and 0.25 μ M GapDH in argon-flushed 20 mM Tris-HCl with 1.25 mM EDTA and 15 mM sodium arsenate. After the removal of excess H₂O₂ and MSH, 0.25 mM D,L-G3P was added as substrate, GapDH activity was measured spectrophotometric by the production of NADH. The reversibility of the reaction was analyzed by measuring the GapDH activity after reduction with 10 mM DTT for 30 min.

De-mycothiolation of GapDH by the Mrx1/MSH/Mtr and Trx/TrxR pathways. GapDH, Mrx1 and Trx were reduced before the assays with 10 mM DTT for 30 minutes at room temperature. Excess of DTT was removed by desalting with Micro Biospin 6 columns. Pre-reduced GapDH (25 μ M) was pre-incubated with 10-molar excess of MSH at 37 °C for 5 min, then 100-fold molar excess of H₂O₂ was added and the mixture was incubated at 37 °C for 5 min. Excess of H₂O₂ and MSH were removed on a PD-10 desalting column (GE

Healthcare). The NADPH consumption during the de-mycothiolation reactions was monitored spectrophotometrically at 340 nm and 37 °C, using argon-flushed 50 mM Hepes/NaOH, pH 8, 500 mM NaCl, 1 mM EDTA. For the reduction of S-mycothiolated GapDH by the Trx pathway, we used 2 μ M Trx, 5 μ M Trx-reductase and 250 μ M NADPH in a Spectramax 340PC plate reader (Molecular Devices). For the reduction of S-mycothiolated GapDH by the Mrx1 pathway, we used 20 nM Mrx1, 5 μ M MSH, 5 μ M MSSM reductase and 250 μ M NADPH in SX-20 stopped flow (Applied PhotoPhysics). After 5 min pre-incubation of this mixture at 37 °C, 60 μ M mycithiolated GapDH was added to initiate the reaction. Three technical and experimental replicates were performed.

References

- Antelmann, H. & Helmman, J. D. Thiol-based redox switches and gene regulation. *Antioxid Redox Signal* **14**, 1049–63 (2011).
- Fahey, R. C. Glutathione analogs in prokaryotes. *Biochim Biophys Acta* **1830**, 3182–98 (2013).
- Van Laer, K., Hamilton, C. J. & Messens, J. Low-molecular-weight thiols in thiol-disulfide exchange. *Antioxid Redox Signal* **18**, 1642–53 (2013).
- Loi, V. V., Rossius, M. & Antelmann, H. Redox regulation by reversible protein S-thiolation in bacteria. *Front Microbiol* **6**, 187 (2015).
- Newton, G. L. *et al.* Distribution of thiols in microorganisms: mycithiol is a major thiol in most actinomycetes. *J Bacteriol* **178**, 1990–5 (1996).
- Liu, Y. B. *et al.* Physiological roles of mycithiol in detoxification and tolerance to multiple poisonous chemicals in *Corynebacterium glutamicum*. *Arch Microbiol* **195**, 419–29 (2013).
- Newton, G. L., Buchmeier, N. & Fahey, R. C. Biosynthesis and functions of mycithiol, the unique protective thiol of Actinobacteria. *Microbiol Mol Biol Rev* **72**, 471–94 (2008).
- Rawat, M. *et al.* Mycithiol-deficient *Mycobacterium smegmatis* mutants are hypersensitive to alkylating agents, free radicals, and antibiotics. *Antimicrobial Agents and Chemotherapy* **46**, 3348–3355 (2002).
- Hillion, M. *et al.* Monitoring global protein thiol-oxidation and protein S-mycithiolation in *Mycobacterium smegmatis* under hypochlorite stress. *Sci Rep* **7**, 1195 (2017).
- Chi, B. K. *et al.* Protein S-mycithiolation functions as redox-switch and thiol protection mechanism in *Corynebacterium glutamicum* under hypochlorite stress. *Antioxid Redox Signal* **20**, 589–605 (2014).
- Chi, B. K. *et al.* S-bacillithiolation protects conserved and essential proteins against hypochlorite stress in firmicutes bacteria. *Antioxid Redox Signal* **18**, 1273–95 (2013).
- Tossounian, M. A. *et al.* *Corynebacterium diphtheriae* methionine sulfoxide reductase A exploits a unique mycithiol redox relay mechanism. *J Biol Chem* **290**, 11365–11375 (2015).
- Pedre, B. *et al.* The *Corynebacterium glutamicum* mycithiol peroxidase is a reactive oxygen species-scavenging enzyme that shows promiscuity in thiol redox control. *Mol Microbiol* **96**, 1176–1191 (2015).
- Hugo, M. *et al.* Mycithiol/mycoredoxin 1-dependent reduction of the peroxiredoxin AhpE from *Mycobacterium tuberculosis*. *J Biol Chem* **289**, 5228–39 (2014).
- Si, M. *et al.* Graded response of the multifunctional 2-Cysteine peroxiredoxin, CgPrx, to increasing levels of hydrogen peroxide in *Corynebacterium glutamicum*. *Antioxid Redox Signal* **26**, 1–14 (2017).
- Si, M. R. *et al.* *Corynebacterium glutamicum* methionine sulfoxide reductase A uses both mycoredoxin and thioredoxin for regeneration and oxidative stress resistance. *Appl Environ Microbiol* **81**, 2781–2796 (2015).
- Si, M. R. *et al.* Functional characterization of a mycithiol peroxidase in *Corynebacterium glutamicum* that uses both mycoredoxin and thioredoxin reducing systems in the response to oxidative stress. *Biochem J* **469**, 45–57 (2015).
- Liu, Y. *et al.* Mycithiol protects *Corynebacterium glutamicum* against acid stress via maintaining intracellular pH homeostasis, scavenging ROS, and S-mycithiolating MetE. *J Gen Appl Microbiol* **62**, 144–53 (2016).
- Brandes, N., Schmitt, S. & Jakob, U. Thiol-based redox switches in eukaryotic proteins. *Antioxid Redox Signal* **11**, 997–1014 (2009).
- Hildebrandt, T., Knesting, J., Berndt, C., Morgan, B. & Scheibe, R. Cytosolic thiol switches regulating basic cellular functions: GAPDH as an information hub? *Biol Chem* **396**, 523–537 (2015).
- Imber, M. *et al.* Protein S-bacillithiolation functions in thiol protection and redox regulation of the glyceraldehyde-3-phosphate dehydrogenase Gap in *Staphylococcus aureus* under hypochlorite stress. *Antioxid Redox Signal* (2017).
- Peralta, D. *et al.* A proton relay enhances H₂O₂ sensitivity of GAPDH to facilitate metabolic adaptation. *Nat Chem Biol* **11**, 156–63 (2015).
- Bedhomme, M. *et al.* Glutathionylation of cytosolic glyceraldehyde-3-phosphate dehydrogenase from the model plant *Arabidopsis thaliana* is reversed by both glutaredoxins and thioredoxins *in vitro*. *Biochem J* **445**, 337–47 (2012).
- Zaffagnini, M. *et al.* Glutathionylation in the Photosynthetic Model Organism *Chlamydomonas reinhardtii*: A Proteomic Survey. *Mol Cell Proteomics* **11**, 15 (2012).
- Faria, J. *et al.* Disclosing the essentiality of ribose-5-phosphate isomerase B in *Trypanosomatids*. *Sci Rep* **6**, 26937 (2016).
- Tullius, M. V., Harth, G. & Horwitz, M. A. Glutamine synthetase GlnA1 is essential for growth of *Mycobacterium tuberculosis* in human THP-1 macrophages and guinea pigs. *Infection and Immunity* **71**, 3927–3936 (2003).
- Shenton, D. & Grant, C. M. Protein S-thiolation targets glycolysis and protein synthesis in response to oxidative stress in the yeast *Saccharomyces cerevisiae*. *Biochem J* **374**, 513–9 (2003).
- Hillion, M. & Antelmann, H. Thiol-based redox switches in prokaryotes. *Biol Chem* **396**, 415–44 (2015).
- Ghezzi, P. Protein glutathionylation in health and disease. *Biochim Biophys Acta* **1830**, 3165–72 (2013).
- Ghezzi, P. Regulation of protein function by glutathionylation. *Free Radic Res* **39**, 573–80 (2005).
- Dalle-Donne, I., Rossi, R., Colombo, G., Giustarini, D. & Milzani, A. Protein S-glutathionylation: a regulatory device from bacteria to humans. *Trends Biochem Sci* **34**, 85–96 (2009).
- Leichert, L. I. *et al.* Quantifying changes in the thiol redox proteome upon oxidative stress *in vivo*. *Proc Natl Acad Sci USA* **105**, 8197–202 (2008).
- Chi, B. K. *et al.* S-bacillithiolation protects against hypochlorite stress in *Bacillus subtilis* as revealed by transcriptomics and redox proteomics. *Mol Cell Proteomics* **10**(M11), 009506 (2011).
- Si, M. *et al.* Functional characterization of a mycithiol peroxidase in *Corynebacterium glutamicum* that uses both mycoredoxin and thioredoxin reducing systems in the response to oxidative stress. *The Biochem J* **469**, 45–57 (2015).
- Winterbourn, C. C. & Kettle, A. J. Redox reactions and microbial killing in the neutrophil phagosome. *Antioxid Redox Signal* **18**, 642–60 (2013).
- Winterbourn, C. C., Kettle, A. J. & Hampton, M. B. Reactive Oxygen Species and Neutrophil Function. *Annu Rev Biochem* **85**, 765–92 (2016).
- Davies, M. J. Myeloperoxidase-derived oxidation: mechanisms of biological damage and its prevention. *J Clin Biochem Nutr* **48**, 8–19 (2011).
- Hawkins, C. L., Pattison, D. I. & Davies, M. J. Hypochlorite-induced oxidation of amino acids, peptides and proteins. *Amino Acids* **25**, 259–74 (2003).

39. Newton, G. L. *et al.* Distribution of thiols in microorganisms: Mycothiol is a major thiol in most actinomycetes. *J Bacteriol* **178**, 1990–1995 (1996).
40. Si, M. *et al.* Overexpression of mycothiol disulfide reductase enhances *Corynebacterium glutamicum* robustness by modulating cellular redox homeostasis and antioxidant proteins under oxidative stress. *Sci Rep* **6**, 29491 (2016).
41. Saini, V. *et al.* Ergothioneine Maintains Redox and Bioenergetic Homeostasis Essential for Drug Susceptibility and Virulence of *Mycobacterium tuberculosis*. *Cell Rep* **14**, 572–85 (2016).
42. Sassetti, C. M. & Rubin, E. J. Genetic requirements for mycobacterial survival during infection. *Proc Natl Acad Sci USA* **100**, 12989–94 (2003).
43. Ta, P., Buchmeier, N., Newton, G. L., Rawat, M. & Fahey, R. C. Organic hydroperoxide resistance protein and ergothioneine compensate for loss of mycothiol in *Mycobacterium smegmatis* mutants. *J Bacteriol* **193**, 1981–90 (2011).
44. Chandrangu, P., Loi, V.V., Antelmann, H. & Helmmann, J.D. The role of bacillithiol in Gram-positive *Firmicutes*. *Antioxid Redox Signal* (2017).
45. Little, C. & O'Brien, P. J. Mechanism of peroxide-inactivation of the sulphhydryl enzyme glyceraldehyde-3-phosphate dehydrogenase. *Eur J Biochem* **10**, 533–8 (1969).
46. Zaffagnini, M. *et al.* Tuning cysteine reactivity and sulfenic acid stability by protein microenvironment in glyceraldehyde-3-phosphate dehydrogenases of *Arabidopsis thaliana*. *Antioxid Redox Signal* **24**, 502–17 (2016).
47. Winterbourn, C. C. & Hampton, M. B. Thiol chemistry and specificity in redox signaling. *Free Radic Biol Med* **45**, 549–61 (2008).
48. Baty, J. W., Hampton, M. B. & Winterbourn, C. C. Proteomic detection of hydrogen peroxide-sensitive thiol proteins in Jurkat cells. *Biochem J* **389**, 785–95 (2005).
49. Kehr, S. *et al.* Protein S-glutathionylation in malaria parasites. *Antioxid Redox Signal* **15**, 2855–65 (2011).
50. Ralser, M. *et al.* Dynamic rerouting of the carbohydrate flux is key to counteracting oxidative stress. *J Biol* **6**, 10 (2007).
51. Grant, C. M. Metabolic reconfiguration is a regulated response to oxidative stress. *J Biol* **7**, 1 (2008).
52. Rui, B. *et al.* A systematic investigation of *Escherichia coli* central carbon metabolism in response to superoxide stress. *BMC Systems Biology* **4**, 12 (2010).
53. Brumaghim, J. L., Li, Y., Henle, E. & Linn, S. Effects of hydrogen peroxide upon nicotinamide nucleotide metabolism in *Escherichia coli* - Changes in enzyme levels and nicotinamide nucleotide pools and studies of the oxidation of NAD(P)H by Fe(III). *J Biol Chem* **278**, 42495–42504 (2003).
54. Van Laer, K. *et al.* Mycoredoxin-1 is one of the missing links in the oxidative stress defence mechanism of mycobacteria. *Mol Microbiol* **86**, 787–804 (2012).
55. Greetham, D. *et al.* Thioredoxins function as deglutathionylase enzymes in the yeast *Saccharomyces cerevisiae*. *BMC Biochem* **11**, 3 (2010).
56. Tan, S. X. *et al.* The thioredoxin-thioredoxin reductase system can function *in vivo* as an alternative system to reduce oxidized glutathione in *Saccharomyces cerevisiae*. *J Biol Chem* **285**, 6118–26 (2010).
57. Kublik, A. *et al.* Identification of a multi-protein reductive dehalogenase complex in *Dehalococcoides mccartyi* strain CBDB1 suggests a protein-dependent respiratory electron transport chain obviating quinone involvement. *Environ Microbiol* **18**, 3044–56 (2016).
58. Wirtz, M., Droux, M. & Hell, R. O-acetylserine (thiol) lyase: an enigmatic enzyme of plant cysteine biosynthesis revisited in *Arabidopsis thaliana*. *J Exp Bot* **55**, 1785–98 (2004).
59. Ordóñez, E. *et al.* Arsenate reductase, mycothiol, and mycoredoxin concert thiol/disulfide exchange. *J Biol Chem* **284**, 15107–16 (2009).

Acknowledgements

This work was supported by an ERC Consolidator grant (GA 615585) MYCOTHILOME and the DFG Research Training Group GRK1947, project [C1] to H.A. We further acknowledge support from the DFG priority program SPP1710 on “Thiol-based redox switches”, project AN746/4-1 to H.A. and project WI 3560/2-1 and HE 1848/16-1 to M.W. and R.H. This work was further supported by the following institutions: (i) agentschap voor Innovatie door Wetenschap en Technologie (IWT), (ii) Vlaams Instituut voor Biotechnologie (VIB), (iii) the SPR34 project of the Vrije Universiteit Brussel (VUB), (iv) Research Foundation Flanders (FWO), and (v) Flanders Hercules Foundation (grant number HERC16) for the purification platform to J.M. Mass spectrometry of GapDH was performed at the Centre for Chemical Microscopy (ProVIS) at the Helmholtz Centre for Environmental Research, which is supported by European regional development funds (EFRE-Europe Funds Saxony) and the Helmholtz Association.

Author Contributions

M.H., B.P., M.S., M.I., V.V.L., L.A.R., J.M. and H.A. conceived the ideas and hypotheses, designed and performed the GapDH experiments and analyzed the data. M.H. performed the proteomics experiments, processed and analyzed the data. M.H. and J.B. performed the bioinformatics analysis and treemap constructions. S.M., D.B., L.A. and C.W. performed peptide measurements using mass spectrometry. M.W. and R.H. performed the thiol-metabolomics analysis. H.A., M.H., B.P. and J.M. wrote the manuscript and prepared the figures. All authors reviewed and approved the manuscript.

Additional Information

Supplementary information accompanies this paper at doi:10.1038/s41598-017-05206-2

Competing Interests: The authors declare that they have no competing interests.

Publisher's note: Springer Nature remains neutral with regard to jurisdictional claims in published maps and institutional affiliations.



Open Access This article is licensed under a Creative Commons Attribution 4.0 International License, which permits use, sharing, adaptation, distribution and reproduction in any medium or format, as long as you give appropriate credit to the original author(s) and the source, provide a link to the Creative Commons license, and indicate if changes were made. The images or other third party material in this article are included in the article's Creative Commons license, unless indicated otherwise in a credit line to the material. If material is not included in the article's Creative Commons license and your intended use is not permitted by statutory regulation or exceeds the permitted use, you will need to obtain permission directly from the copyright holder. To view a copy of this license, visit <http://creativecommons.org/licenses/by/4.0/>.

Chapter 2

Protein S-bacillithiolation functions in thiol-protection and redox regulation of the glyceraldehyde-3-phosphate dehydrogenase Gap in *Staphylococcus aureus* under hypochlorite stress

Marcel Imber^{1*}, Nguyen Thi Thu Huyen^{1*}, Agnieszka J. Pietrzyk-Brzezinska^{2*}, Vu Van Loi^{1*}, Melanie Hillion¹, Jörg Bernhardt³, Lena Thärichen^{4,5}, Katra Kolsek⁵, Malek Saleh¹, Chris J. Hamilton⁶, Lorenz Adrian⁷, Frauke Gräter^{4,5}, Markus C. Wahl, and Haike Antelmann^{1#}

¹*Institute for Biology-Microbiology and* ²*Laboratory of Structural Biochemistry, Freie Universität Berlin, Berlin, Germany.*

³*Institute for Microbiology, Ernst-Moritz-Arndt-Universität of Greifswald, Greifswald, Germany.*

⁴*Molecular Biomechanics, Interdisciplinary Center for Scientific Computing (IWR), Heidelberg University, Heidelberg, Germany.*

⁵*Heidelberg Institute of Theoretical Studies, Heidelberg, Germany.*

⁶*School of Pharmacy, University of East Anglia, Norwich Research Park, Norwich, United Kingdom.*

⁷*Department Isotope Biogeochemistry, Helmholtz Centre for Environmental Research-UFZ, Leipzig, Germany*

Published in: *Antioxidants & Redox Signaling* 28: 410-430. (2018)

#Corresponding author: haike.antelmann@fu-berlin.de

Authors contributions:

Marcel Imber contributed to the identification of S-bacillithiolated proteins by mass spectrometry. He was involved in purification of Gap from *S. aureus* and in the biochemical enzyme kinetics of Gap inactivation due to overoxidation and S-bacillithiolation. **Marcel Imber** performed the BSH-specific Western blot analysis. Vu Van Loi, Nguyen Thi Thu Huyen and Melanie Hillion contributed with the plasmid constructions and proteomics analysis. Pietrzyk-Brzezinska, Markus C. Wahl, Lena Thärichen and Frauke Gräter were involved in structural analysis. All authors prepared the figures for publications and contributed to writing of the manuscript.

* Shared first authorships



Protein *S*-Bacillithiolation Functions in Thiol Protection and Redox Regulation of the Glyceraldehyde-3-Phosphate Dehydrogenase Gap in *Staphylococcus aureus* Under Hypochlorite Stress

Marcel Imber,^{1,*} Nguyen Thi Thu Huyen,^{1,*} Agnieszka J. Pietrzyk-Brzezinska,^{2,*} Vu Van Loi,^{1,*} Melanie Hillion,¹ Jörg Bernhardt,³ Lena Thärichen,^{4,5} Katri Kolšek,⁵ Malek Saleh,¹ Chris J. Hamilton,⁶ Lorenz Adrian,⁷ Frauke Gräter,^{4,5} Markus C. Wahl,² and Haike Antelmann¹

Abstract

Aims: Bacillithiol (BSH) is the major low-molecular-weight thiol of the human pathogen *Staphylococcus aureus*. In this study, we used OxICAT and Voronoi redox treemaps to quantify hypochlorite-sensitive protein thiols in *S. aureus* USA300 and analyzed the role of BSH in protein *S*-bacillithiolation.

Results: The OxICAT analyses enabled the quantification of 228 Cys residues in the redox proteome of *S. aureus* USA300. Hypochlorite stress resulted in >10% increased oxidation of 58 Cys residues (25.4%) in the thiol redox proteome. Among the highly oxidized sodium hypochlorite (NaOCl)-sensitive proteins are five *S*-bacillithiolated proteins (Gap, AldA, GuaB, RpmJ, and PpaC). The glyceraldehyde-3-phosphate (G3P) dehydrogenase Gap represents the most abundant *S*-bacillithiolated protein contributing 4% to the total Cys proteome. The active site Cys151 of Gap was very sensitive to overoxidation and irreversible inactivation by hydrogen peroxide (H₂O₂) or NaOCl *in vitro*. Treatment with H₂O₂ or NaOCl in the presence of BSH resulted in reversible Gap inactivation due to *S*-bacillithiolation, which could be regenerated by the bacilliredoxin Brx (SAUSA300_1321) *in vitro*. Molecular docking was used to model the *S*-bacillithiolated Gap active site, suggesting that formation of the BSH mixed disulfide does not require major structural changes.

Conclusion and Innovation: Using OxICAT analyses, we identified 58 novel NaOCl-sensitive proteins in the pathogen *S. aureus* that could play protective roles against the host immune defense and include the glycolytic Gap as major target for *S*-bacillithiolation. *S*-bacillithiolation of Gap did not require structural changes, but efficiently functions in redox regulation and protection of the active site against irreversible overoxidation in *S. aureus*. *Antioxid. Redox Signal.* 28, 410–430.

Keywords: *Staphylococcus aureus*, *S*-bacillithiolation, thiol-redox proteomics, Gap, bacilliredoxin

¹Institute for Biology-Microbiology and ²Laboratory of Structural Biochemistry, Freie Universität Berlin, Berlin, Germany.

³Institute for Microbiology, Ernst-Moritz-Arndt-Universität of Greifswald, Greifswald, Germany.

⁴Molecular Biomechanics, Interdisciplinary Center for Scientific Computing (IWR), Heidelberg University, Heidelberg, Germany.

⁵Heidelberg Institute of Theoretical Studies, Heidelberg, Germany.

⁶School of Pharmacy, University of East Anglia, Norwich Research Park, Norwich, United Kingdom.

⁷Department Isotope Biogeochemistry, Helmholtz Centre for Environmental Research-UFZ, Leipzig, Germany.

*These authors contributed equally to this work.

Innovation

Using quantitative redox proteomics, 58 redox-sensitive protein thiols were identified in the methicillin-resistant *Staphylococcus aureus* strain USA300 that showed >10% increased oxidation under NaOCl stress. The glyceraldehyde-3-phosphate dehydrogenase Gap was identified as most abundant target for thiol oxidation and represents the major S-bacillithiolated protein in *S. aureus* cells. Molecular docking of bacillithiol (BSH) into the active site suggests that S-bacillithiolation does not require major structural changes. Finally, our biochemical assays confirm that S-bacillithiolation efficiently protects the Gap active site against overoxidation by H₂O₂ and NaOCl and inhibits Gap activity, which can be reversed by the bacilliredoxin Brx *in vitro*.

Introduction

STAPHYLOCOCCUS AUREUS IS a common commensal bacterium that colonizes the anterior nares and the skin of one quarter of the human population without causing symptoms of infections (22). However, *S. aureus* can also cause infections ranging from local skin or soft tissue infections to life-threatening diseases, such as septicemia, endocarditis, and necrotizing pneumonia, when the pathogen enters the bloodstream (2, 8, 53). Many nosocomial infections are caused by multiple antibiotic-resistant strains, such as methicillin-resistant *S. aureus* (MRSA) isolates (50). Moreover, new community-acquired MRSA strains are emerging quickly with other strains that are resistant to the last resort of antibiotics, such as vancomycin (22). Thus, to understand the adaptation of the pathogen to the host defense, it is of utmost importance to identify new drug targets for the treatment of MRSA infections.

The success of *S. aureus* as a leading pathogen is caused by high diversity of different virulence factors, such as toxins, proteases, lipases, and superantigens, as well as efficient protection mechanisms against the host immune defense during invasion. During infections, *S. aureus* has to cope with the oxidative burst of activated macrophages and neutrophils, including reactive oxygen and nitrogen species (ROS, RNS) and the strong oxidant hypochlorous acid (HOCl) (75, 76). HOCl is produced in neutrophils by the enzyme myeloperoxidase (MPO) from hydrogen peroxide (H₂O₂) and chloride (44). The involvement of HOCl as prime mechanism for oxidative killing of *S. aureus* by neutrophils has been shown using MPO inhibitors (29). Moreover, killing of many bacteria by isolated neutrophils is strongly inhibited in the absence of MPO (44).

S. aureus uses several redox-sensing virulence regulators, such as SarA and the MarR/OhrR-type regulators, MgrA and SarZ, for defense against oxidative stress. These control large regions of virulence factors, antibiotic resistance determinants, and ROS detoxification enzymes (11–13, 35). MgrA and SarZ are both single Cys MarR/OhrR-type repressors that sense and respond to ROS via thiol-based redox switches and by Cys phosphorylation (63, 70). In addition, *S. aureus* uses the low-molecular-weight (LMW) thiol bacillithiol (BSH, Cys-GlcNAc-Mal) to maintain the reduced state of the cytoplasm. BSH plays an important role in detoxification of redox-active compounds in *S. aureus* since *bshA* mutants displayed increased sensitivities to ROS, hypochlorite,

electrophiles, and the antibiotic fosfomycin (52, 64, 65). Moreover, BSH mediates protection under infection-like conditions as shown in phagocytosis assays using human macrophages (64, 65). Apart from BSH, also CoenzymeA (CoASH) and cysteine are found as abundant alternative LMW thiols in *S. aureus* cells (58).

Under hypochlorite stress, we have shown that BSH is also used for S-thiolation of redox-sensitive Cys residues and forms mixed disulfides with proteins that are termed as S-bacillithiolation. S-bacillithiolation protects protein thiols against overoxidation to sulfonic acids and is an important redox regulatory device in Firmicutes analogous to S-glutathionylation in eukaryotes (15, 16, 47, 52). The presence of CoASH and cysteine as LMW thiols suggests that alternative S-thiolations are also possible in *S. aureus*, such as S-cysteinylation or CoASH mixed disulfides. In support of this notion, *S. aureus* encodes a CoASH disulfide reductase (Cdr) that functions in reduction of CoASH mixed protein disulfides (55).

Using shotgun proteomics, we have previously identified 54 S-bacillithiolated proteins in different *Bacillus species* and *Staphylococcus carnosus* (16). Among these are eight conserved S-bacillithiolated proteins, such as the methionine synthase MetE, the inorganic pyrophosphatase PpaC, and the inosine-5'-monophosphate (IMP) dehydrogenase GuaB. The glutaredoxin-like YphP protein of the UPF0403 family was also S-bacillithiolated in *Bacillus subtilis* *in vivo* at its CGC active site motif (15). YphP and its paralog YqiW were renamed as BrxA and BrxB based on their function as bacilliredoxins in the reduction of S-bacillithiolated OhrR and MetE *in vitro* (24). Reduction of S-bacillithiolated proteins leads to Brx-SSB formation, which requires BSH and a still unknown BSSB reductase for recycling (24, 25, 31, 52). We have recently fused the YphP homolog (Brx) of *S. aureus* USA300 (SAUSA300_1321) to roGFP2 to construct a dynamic biosensor to monitor BSH redox potential changes *in vivo* (51). Brx-roGFP2 was highly specific to recognize BSSB, which confirms the role of Brx as bacilliredoxin also in *S. aureus*.

The physiological role of S-bacillithiolation in redox regulation has been demonstrated for the redox-sensing OhrR repressor and the methionine synthase MetE under hypochlorite stress in *B. subtilis*. S-bacillithiolation of MetE in its active site Zn center leads to its inactivation and subsequent methionine auxotrophy (15). The DNA-binding activity of the organic hydroperoxide repressor, OhrR, is inhibited by S-bacillithiolation under sodium hypochlorite (NaOCl) and cumene hydroperoxide stress, which results in the expression of the OhrA peroxiredoxin as ROS protection mechanism (15, 47).

However, the targets for S-bacillithiolation or reversible thiol oxidation under hypochlorite stress are unknown in the major pathogen *S. aureus*, which could provide leads in drug design to treat MRSA infections. In this study, we have combined the quantitative redox proteomic approach OxICAT (9, 48, 49) and shotgun proteomics to quantify NaOCl-sensitive proteins and to identify S-bacillithiolated proteins in *S. aureus* USA300. We found that 25% protein thiols showed >10% increased oxidation under NaOCl stress. The glycolytic Gap was identified as the most abundant S-bacillithiolated protein in *S. aureus*. Our results document that S-bacillithiolation protects the active site against overoxidation and inhibits Gap activity *in vitro*.

Results

Identification of 58 NaOCl-sensitive proteins using the quantitative redox proteomic approach OxICAT in *S. aureus* USA300

We were interested to study the role of BSH for *S.* bacillithiolation and the global thiol oxidation state under hypochlorite stress in the major pathogen *S. aureus*. Thus, we performed a quantitative thiol redox proteomic approach based on OxICAT (48, 49) and analyzed the percentages of thiol oxidation levels in *S. aureus* USA300 in response to 150 μ M NaOCl stress, as determined previously (51). OxICAT is based on the differential thiol labeling of reduced Cys residues with light isotope-coded affinity tag (12 C-ICAT), followed by reduction of reversible thiol oxidation (e.g., protein disulfides and *S*-thiolation) with Tris (2-carboxyethyl) phosphine (TCEP) and subsequent labeling of previously oxidized thiols with heavy 13 C-ICAT reagent (48). Light and heavy ICAT-labeled peptide pairs show a mass difference of 9 Da

after separation using mass spectrometry (MS). The quantification of the percentage of thiol oxidation for each Cys peptide is based on the calculation of the intensity of the heavy ICAT-labeled Cys peptide in relation to the total intensity of the light and heavy ICAT-labeled Cys peptides.

The OxICAT analysis enabled the quantification of the percentages of reversible thiol oxidation for 228 Cys peptides in the thiol redox proteome of *S. aureus* USA300 (Supplementary Table S1; Supplementary Data; Supplementary Data are available online at www.liebertpub.com/ars). The percentages of thiol oxidation were color coded and visualized in *Voronoi redox treemaps* according to the TIGRfam classification of *S. aureus* USA300 (Fig. 1).

In untreated *S. aureus* cells, we identified 193 Cys residues (84.6%) with a thiol oxidation level of <25%, including 107 Cys residues (46.9%) with <10% oxidation, indicating that the majority of thiols are in a reduced state (Tables 1 and 2; Supplementary Table S1). Only 35 Cys residues (15.3%) showed basal-level oxidation of >25% in the control. These

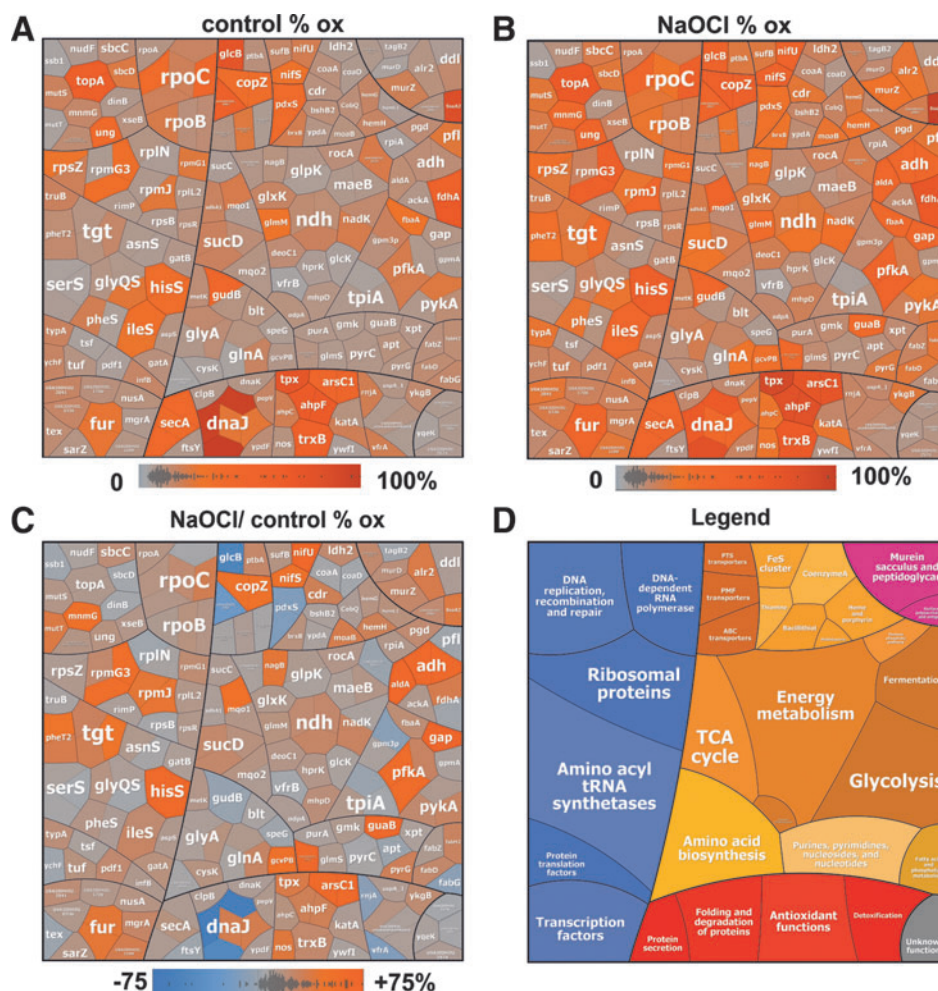


FIG. 1. Percentages of thiol oxidation for 228 Cys peptides that are identified in *Staphylococcus aureus* USA300 and visualized using *Voronoi redox treemaps*. The percentages of thiol oxidation of 228 Cys residues that are identified using OxICAT in *S. aureus* USA300 in the control (A) and 30 min after exposure to 150 μ M NaOCl stress (B) are visualized using *Voronoi redox treemaps*. The gray–red color gradient denotes 0–100% oxidation. The *Voronoi redox treemap* in (C) shows the percentages of oxidation changes under NaOCl stress using a blue–red color gradient ranging from –75% to +75% oxidation. The treemap in (D) serves as the legend showing the functional classifications of proteins. The treemaps are generated using the Paver software (Decodon) based on the OxICAT data presented in Supplementary Tables S1 and proteins were classified according to the *S. aureus* USA300 TIGRfam annotation. NaOCl, sodium hypochlorite.

TABLE 1. OVERVIEW OF % THIOL OXIDATION OF 228 CYS RESIDUES IN THE REDOX PROTEOME OF *STAPHYLOCOCCUS AUREUS*

228 Cys residues	<25% (<10%)	>25% (>40%)
% Thiol oxidation Control	193 (107) 84.6% (46.9%)	35 (15) 15.3% (6.6%)
% Thiol oxidation NaOCl	159 (35) 69.7% (15.3%)	69 (27) 30.2% (11.8%)
	<10%	>10% (20–30%)
% Thiol oxidation increase (NaOCl/Control)	170 74.6%	58 (19) 25.4% (8.3%)

Overview of % thiol oxidation of 228 Cys peptides identified in the redox proteome of the *S. aureus* USA300 under control and NaOCl stress, as revealed by OxICAT. All reduced Cys peptides have an oxidation degree of <25% that include those with <10% oxidation, shown in parenthesis. Oxidized Cys peptides have an oxidation degree of >25%. The % thiol oxidation increase includes Cys peptides with no significant increased oxidation (<10%) and those with >10% increased oxidation in response to NaOCl stress compared with the control. The % thiol-oxidation and % thiol-oxidation increase and related Cys numbers are shown in **bold-faced**. The percentage of Cys numbers in relation to all Cys residues is shown in *non-bold faced*.

NaOCl, sodium hypochlorite.

basal-level oxidized proteins include predicted redox-sensitive proteins (21), such as the thiol peroxidase Tpx, the alkyl hydroperoxide reductase large subunit AhpF, the arsenate reductase ArsC1, and the thioredoxin reductase TrxB1. Tpx and AhpCF were previously found as basal-level oxidized in the redox proteomes of *Escherichia coli* and *Bacillus* species (16, 48). Tpx was also S-mycothiolated in *Corynebacterium glutamicum* at the conserved active site Cys60 (14). In addition, the topoisomerase TopA and the DnaJ chaperone are basal-level oxidized at their Zn-binding Cys residues.

To discover novel NaOCl-sensitive proteins, we analyzed the percentages of thiol oxidation levels under NaOCl stress and its oxidation increase using OxICAT (Fig. 1 and Tables 2; Supplementary Table S1). The OxICAT approach enabled the identification of 58 NaOCl-sensitive Cys residues (25.4%) with >10% increased oxidation, including 19 Cys residues with 20–30% oxidation change under NaOCl stress (Tables 1 and 2 and Supplementary Table S1). Several NaOCl-sensitive proteins have antioxidant functions, such as the AhpCF peroxiredoxins, the thioredoxin reductase TrxB1, and the arsenate reductase ArsC. Furthermore, interesting proteins are the nitric oxide synthase (USA300HOU_1916) and the CoASH disulfide reductase Cdr (USA300HOU_0929), the latter is oxidized at the conserved Cys16. Apart from Cdr, the putative BSH disulfide reductase YpdA (USA300GOU_1417) was oxidized at the same conserved Cys14, but its oxidation is not increased under NaOCl stress (Supplementary Table S1). Moreover, we observed a slightly increased oxidation of the deacetylase BshB2 involved BSH biosynthesis and of the bacilliredoxin YqiW (BrxB) under NaOCl stress. The oxidation of Cdr, YpdA, BshB2, and BrxB could indicate increased S-bacillithiolation and CoASH mixed protein disulfides under NaOCl stress.

NaOCl-sensitive proteins are often oxidized in CxxC motifs and at conserved Zn-binding sites. Examples for Zn redox switches are the Zn-containing alcohol dehydrogenase Adh (USA300HOU_0610), the ribosomal proteins RpmG3

(USA300HOU_1553), and RpmJ (USA300HOU_2218). Zn-containing ribosomal proteins share three to four Cys residues that are suggested to serve as reservoir for Zn storage (54). As another Zn redox switch, we identified the ferric uptake repressor Fur that showed 16.6% increased oxidation at its Zn-binding site at Cys 140 and Cys143 under NaOCl stress (Tables 2; Supplementary Table S1; Figs. 1–2). Fur contains two CxxC motifs that form a structural Cys4:Zn site and are required for stability. In addition, two regulatory iron-binding sites are present in Fur (32). FurA of *Anabaena* was described as redox switch under oxidative stress and Cys101 in the CxxC motif is essential for iron-sensing and DNA-binding activity (7).

The copper chaperone CopZ was 19.8% oxidized in its CxxC motif that is required for Cu binding (67). The interaction of the *B. subtilis* CopZ homolog with BSH has been recently studied leading to the formation of S-bacillithiolated apo-CopZ and Cu(i)-bound forms of CopZ (42). In addition, NaOCl-sensitive Cys residues often coordinate FeS clusters or function in FeS cluster biogenesis. The FeS cluster scaffold protein NifU showed 26% increased oxidation at Cys41 that binds the FeS cluster during the assembly. The cysteine desulfurase NifS exhibits 20.6% higher oxidation levels at the catalytic Cys371 that forms the persulfide with the sulfur released during cysteine desulfuration (5). In addition, the FeS cluster assembly protein SufB is oxidized in its FeS cluster binding Cys302. It is interesting to note that the *nifS-nifU-sufB* genes are cotranscribed in an operon.

As NaOCl-sensing redox regulators, the MarR/OhrR family repressors, MgrA and SarZ (USA300HOU_0709 and USA300HOU_2368), were identified that showed 10.5% and 6.5% increased oxidation levels under NaOCl stress at their redox-sensing single Cys (Fig. 2). The DNA-binding activity of MgrA and SarZ was inhibited by S-thiolation using a synthetic thiol *in vitro* (11, 13, 35). In this study, increased oxidation of MgrA and SarZ was found in *S. aureus* under NaOCl stress, indicating that both could be redox controlled by S-bacillithiolation analogous to OhrR of *B. subtilis* (47). OhrR and SarZ both control a homologous *ohrA* peroxiredoxin gene that confers resistance to organic hydroperoxides and NaOCl in *B. subtilis* (13). Northern blot analyses revealed increased transcription of *ohrA* under NaOCl stress, indicating that SarZ oxidation leads to its inactivation and derepression of *ohrA* transcription (Fig. 3). We further noted the 15% increased oxidation of the virulence factor and secretory antigen SsaA2 at its conserved single Cys171 under NaOCl stress. The homologous SceB precursor (Sca_1790) of *S. carnosus* was previously S-bacillithiolated at the conserved Cys in NaOCl-treated cells (16). Thus, SsaA2 is most likely also S-bacillithiolated in *S. aureus*.

The NaOCl-sensitive proteins of *S. aureus* include many metabolic enzymes that function in energy metabolism and in different biosynthesis pathways for amino acids, fatty acids, nucleotides, and cofactors. NaOCl-sensitive enzymes involved in energy metabolism include the glycolytic glyceraldehyde-3-phosphate (G3P) dehydrogenase Gap and phosphofructokinase PfkA (USA300HOU_1685), the alcohol dehydrogenase Adh, the aldehyde dehydrogenase AldA (USA300HOU_2110), the formate dehydrogenase FdhA (USA300HOU_2291), and the malate dehydrogenase Mqo (USA300HOU_2348). Gap and AldA both showed the highest oxidation increase of 29% and 26% under NaOCl stress at their

TABLE 2. QUANTIFICATION OF 58 CYS PEPTIDES WITH REVERSIBLE THIOL OXIDATION THAT SHOWED >10% INCREASED OXIDATION IN *STAPHYLOCOCCUS AUREUS* USA300 UNDER NaOCl STRESS USING THE OxiCAT APPROACH

Locus tag	Gene name	Protein function	Cys	Buried/ Exposed	RSA (%)	% Diff NaOCl/Co	Mean % oxidation control	CV	Mean % oxidation NaOCl	CV
Cell envelope function										
USA300HOU_2065	alr2	Alanine racemase	Cys311 ^a	B	3.7	14.56	8.22	0.16	22.79	0.14
USA300HOU_2065	alr2	Alanine racemase	Cys304	B	8.7	13.89	9.86	0.11	23.75	0.08
USA300HOU_2112	murZ	UDP-N-acetylglucosamine 1-carboxyvinyltransferase	Cys110	B	7.7	10.03	16.57	0.10	26.60	0.16
USA300HOU_2112	murZ	UDP-N-acetylglucosamine 1-carboxyvinyltransferase	Cys118 ^a	E	56.2	10.03	16.57	0.10	26.60	0.16
USA300HOU_2280	SsaA2	Secretory antigen SsaA2	Cys171 ^a	B	1.3	14.94	71.35	0.14	86.29	0.02
Protein quality control (Chaperones and proteases)										
USA300HOU_1580	dnaJ	Chaperone DnaJ	Cys149 ^a	B	8.3	13.44	21.81	0.43	35.24	0.10
USA300HOU_1580	dnaJ	Chaperone DnaJ	Cys152 ^a	B	24.7	13.44	21.81	0.43	35.24	0.10
Detoxification and adaptation to atypical environments										
USA300HOU_1700	tpx [#]	Thiol peroxidase	Cys60 ^a	B	2.6	14.48	62.73	0.05	77.21	0.02
USA300HOU_0403	ahpF [#]	Peroxiredoxin subunit F	Cys335 ^a	B	3.3	12.54	56.65	0.08	69.19	0.05
USA300HOU_0403	ahpF [#]	Peroxiredoxin subunit F	Cys338 ^a	B	7.5	12.54	56.65	0.08	69.19	0.05
USA300HOU_0839	arsC1 [#]	Arsenate reductase	Cys10 ^a	B	10.1	24.59	38.55	0.11	63.14	0.12
USA300HOU_0839	arsC1 [#]	Arsenate reductase	Cys13 ^a	B	8.9	24.59	38.55	0.11	63.14	0.12
USA300HOU_1916	nos	Nitric oxide synthase	Cys131	B	10.9	15.52	9.34	0.03	24.85	0.53
DNA replication, recombination, and repair										
USA300HOU_2714	mmG	Glucose-inhibited division protein A	Cys274 ^a	B	13.4	20.86	13.36	0.41	34.22	0.18
USA300HOU_2481	mutT	Mutator protein mutT	Cys87	B	1.5	14.82	4.45	0.25	19.26	0.19
Transcription and transcriptional regulators										
USA300HOU_1499	fur	Fur repressor	Cys140 ^a	B	3.1	16.63	22.73	0.51	39.36	0.30
USA300HOU_1499	fur	Fur repressor	Cys143 ^a	B	7.5	16.63	22.73	0.51	39.36	0.30
USA300HOU_0709	mgrA	MarR/OhrR transcriptional regulator	Cys12	B	5.0	10.46	6.62	0.11	17.08	0.02
USA300HOU_2368	sarZ	MarR/OhrR transcriptional regulator	Cys13	B	4.2	6.31	8.43	0.29	14.73	0.07
USA300HOU_1199	USA300HOU_1199	Nucleic acid-binding, transcription termination	Cys11 ^a	B	2.8	13.33	8.21	0.35	21.54	0.38
USA300HOU_0537	rpoC	RNA polymerase subunit beta'	Cys75 ^a	B	4.3	13.00	37.68	0.11	50.69	0.08

(continued)

TABLE 2. (CONTINUED)

<i>Locus tag</i>	<i>Gene name</i>	<i>Protein function</i>	<i>Cys</i>	<i>Buried/ Exposed</i>	<i>RSA (%)</i>	<i>% Diff NaOCl/Co</i>	<i>Mean % oxidation control</i>	<i>CV</i>	<i>Mean % oxidation NaOCl</i>	<i>CV</i>
Translation (Aminacyl tRNA synthetases, translation factors, and ribosomal proteins)										
Amino acyl tRNA synthetases										
USA300HOU_1629	hisS	Histidine-tRNA ligase	Cys191	B	8.5	24.59	29.40	0.25	53.99	0.10
USA300HOU_1629	hisS	Histidine-tRNA ligase	Cys194	B	4.3	24.59	29.40	0.25	53.99	0.10
USA300HOU_1130	ileS	Isoleucine-tRNA ligase	Cys124 ^a	B	0.9	10.77	23.74	0.18	34.51	0.03
USA300HOU_1732	pheT2	Phenylalanine-tRNA ligase beta subunit	Cys126 ^a	B	4.0	18.48	11.13	0.74	29.61	0.01
USA300HOU_1732	pheT2	Phenylalanine-tRNA ligase beta subunit	Cys167 ^a	B	2.0	13.79	12.38	0.29	26.17	0.05
USA300HOU_1638	tgt	Queuine tRNA-ribosyltransferase	Cys12 ^a	B	15.2	12.73	9.32	0.07	22.04	0.42
USA300HOU_1638	tgt	Queuine tRNA-ribosyltransferase	Cys281 ^a	B	2.5	18.74	13.36	0.25	32.10	0.14
USA300HOU_1638	tgt	Queuine tRNA-ribosyltransferase	Cys174 ^a	B	1.5	11.40	8.79	0.00	20.19	0.34
Ribosomal proteins; synthesis and modification										
USA300HOU_1553	rpmG3	Ribosomal protein L33	Cys9 ^a	B	3.9	21.76	29.30	0.02	51.06	0.04
USA300HOU_1553	rpmG3	Ribosomal protein L33	Cys12 ^a	B	25.6	21.76	29.30	0.02	51.06	0.04
USA300HOU_1553	rpmG3	Ribosomal protein L33	Cys36 ^a	B	6.6	9.46	5.76	0.10	15.22	0.12
USA300HOU_2218	rpmJ	Ribosomal protein L36	Cys11 ^a (-SSB)	B	4.5	16.93	21.38	0.17	38.32	0.11
USA300HOU_2218	rpmJ	Ribosomal protein L36	Cys27 ^a	B	3.1	16.52	6.69	0.43	23.21	0.10
Transport and binding proteins										
USA300HOU_2553	copZ [#]	Copper chaperone	Cys13 ^a	B	6.2	19.85	30.60	0.28	50.45	0.13
USA300HOU_2553	copZ [#]	Copper chaperone	Cys16 ^a	B	3.3	19.85	30.60	0.28	50.45	0.13
Energy metabolism (ATP synthesis, central carbon metabolism)										
Glycolysis										
USA300HOU_0802	gap	Glyceraldehyde-3-phosphate DH	Cys151 ^a (-SSB)	B	10.5	29.46	8.28	0.13	37.74	0.04
USA300HOU_1685	pfkA	6-phosphofructokinase	Cys73 ^a	B	24.1	10.90	7.00	0.52	17.90	0.04
USA300HOU_1685	pfkA	6-phosphofructokinase	Cys226	B	17.4	23.24	18.46	0.11	41.70	0.18
USA300HOU_1685	pfkA	6-phosphofructokinase	Cys232	B	2.8	23.24	18.46	0.11	41.70	0.18
USA300HOU_1684	pykA	Pyruvate kinase	Cys266 ^a	B	1.7	10.52	11.24	0.31	21.76	0.11
Fermentation										
USA300HOU_0610	adh	Alcohol DH	Cys34	B	4.1	25.18	11.02	0.35	36.20	0.28
USA300HOU_0610	adh	Alcohol DH	Cys37 ^a	B	2.3	25.18	11.02	0.35	36.20	0.28
USA300HOU_2110	aldA	Aldehyde DH	Cys279 ^a (-SSB)	B	1.4	26.29	11.14	0.14	37.43	0.06
USA300HOU_2291	fdhA	Formate DH alpha subunit	Cys386 ^a	B	15.8	13.68	47.82	0.07	61.50	0.09
Tricarboxylic acid cycle										
USA300HOU_2348	mqo1	Malate:quinone oxidoreductase	Cys97	B	7.6	20.95	18.56	0.51	39.50	0.12

(continued)

TABLE 2. (CONTINUED)

Locus tag	Gene name	Protein function	Cys	Buried/ Exposed	RSA (%)	% Diff NaOCl/Co	Mean % oxidation control	CV	Mean % oxidation NaOCl	CV
Other energy metabolism										
USA300HOU_0964	nadK	NAD(+) kinase	Cys208 ^a	B	1.8	11.00	18.36	0.17	29.35	0.15
USA300HOU_0563	nagB	Glucosamine-6-phosphate deaminase	Cys239	B	3.9	16.40	9.49	0.07	25.89	0.11
USA300HOU_0902	ndh	NADH dehydrogenase	Cys199	B	2.6	10.23	15.39	0.19	25.62	0.08
Amino acid biosynthesis										
USA300HOU_1536	gcvPB	Glycine DH (decarboxylating) subunit 2	Cys80 ^a	B	4.0	20.24	7.86	0.81	28.10	0.48
USA300HOU_1240	glnA	Glutamate—ammonia ligase	Cys291	B	4.1	10.52	14.77	0.05	25.29	0.33
Fatty acid, phospholipid and sterol metabolism										
USA300HOU_0942	fabH2	3-oxoacyl-[acyl-carrier-protein] synthase	Cys220	B	7.2	11.15	11.09	0.35	22.24	0.06
Nucleotide biosynthesis										
USA300HOU_0413	guaB	Inosine-5'-monophosphate DH	Cys326	B	1.4	25.09	7.49	0.28	32.58	0.06
USA300HOU_2115	pyrG	CTP synthase	Cys439 ^a	B	2.1	12.29	8.25	0.47	20.54	0.09
USA300HOU_2265	USA300HOU_2265	Inosine-adenosine-guanosine-nucleoside hydrolase	Cys284	B	10.8	24.99	8.80	0.43	33.79	0.14
Biosynthesis of cofactors, prosthetic groups, and carriers										
USA300HOU_0929	cdh	Coenzyme A disulfide reductase	Cys16 ^a	B	2.1	12.44	9.59	0.26	22.03	0.79
USA300HOU_0561	bshB2	Bacillithiol biosynthesis deacetylase	Cys72 ^a	B	7.3	3.39	10.81	0.02	14.19	0.14
USA300HOU_1417	ypdA	Putative bacillithiol disulfide reductase	Cys14 ^a	B	5.9	3.20	8.39	0.58	11.59	0.08
USA300HOU_1365	brxB	Bacilliredoxin, YphP/YqiW family	Cys144 ^a	B	14.7	7.39	17.90	0.32	25.29	0.28
USA300HOU_1824	hemH	Ferrochelatase	Cys276	B	2.9	12.51	14.25	0.38	26.76	0.05
USA300HOU_0873	nifS	SufS subfamily cysteine desulfurase	Cys371 ^a	B	3.4	20.64	26.61	0.31	47.25	0.15
USA300HOU_0874	nifU	Iron-sulfur (Fe-S) cluster formation protein	Cys41 ^a	B	11.1	26.30	17.85	0.09	44.15	0.15
USA300HOU_0875	sufB	Iron-sulfur (Fe-S) cluster formation protein	Cys302	B	3.7	6.48	13.74	0.19	20.22	0.08
USA300HOU_2257	moaB	Molybdopterin cofactor biosynthesis protein	Cys34	B	20.8	13.81	9.42	0.06	23.23	0.13

Quantification of 58 Cys peptides with reversible thiol-oxidations in *S. aureus* USA300 that showed >10% increased oxidation under NaOCl stress using the OxICAT method. *S. aureus* USA300 was harvested before (control) and 30 min after exposure to 150 μ M NaOCl. Reduced and reversibly oxidized Cys residues were labeled with light and heavy ICAT reagents, respectively, using the OxICAT method. Quantification of % thiol oxidation was performed using the MaxQuant software (<http://141.61.102.17/maxquant.doku.php?id=start&#maxquant>). The table includes locus tags, protein names, functions, Cys peptide sequences, surface accessibilities, and % oxidation of the Cys residues under control and NaOCl stress conditions. Conserved Cys and their functions were marked with ^a and identified by searching the Conserved Domain Database (CDD) (www.ncbi.nlm.nih.gov/Structure/cdd/wrpsb.cgi). *S*-bacillithiolated Cys residues are marked with # that were identified listed in Supplementary Figure S1. Cys functions were identified from the CDD and UniprotKB database and predicted proteins with redox-sensitive Cys residues are marked with # that were identified using the THIOREDOXOME database (<http://gladyshlab.org/THIOREDOXOME/tdb.html>). The relative surface accessibility (RSA) for buried (B) or exposed (E) Cys residues was calculated using the NetSurfP ver. 1.1 (<http://www.cbs.dtu.dk/services/NetSurfP/>). The % thiol oxidation of each identified Cys peptide was calculated using the intensity values provided by MaxQuant software. Based on the % thiol oxidation of each Cys under control and NaOCl stress conditions, the % oxidation increase under NaOCl treatment was then calculated for each experiment. The CV is calculated as relative variability that equals the standard deviation divided by the mean of biological replicates for control and NaOCl stress samples, respectively. NaOCl-sensitive peptides with >10% increased thiol oxidation under NaOCl stress are highlighted using a gray shading gradient.

BSh, bacillithiol; CV, coefficient of variation; NADH, nicotinamide adenine dinucleotide; ICAT, isotope-coded affinity tag; RSA, relative surface accessibility; DH, dehydrogenase.

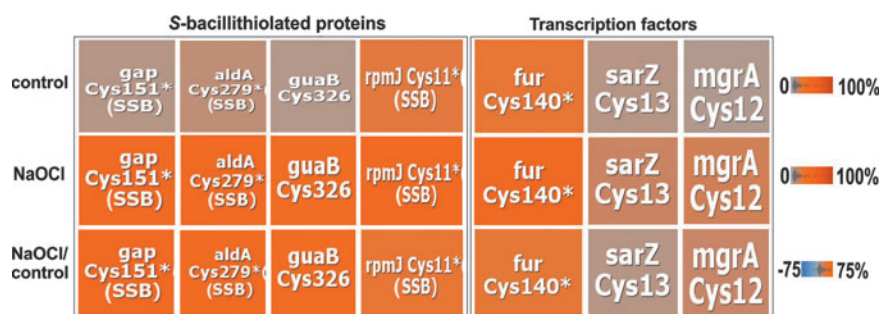


FIG. 2. Close-ups of the redox treemaps of *S. aureus* USA300 showing S-bacillithiolated enzymes and redox regulators (SarZ, MgrA, and Fur). Enlarged sections of the redox treemaps are shown that include the identified S-bacillithiolated proteins (Gap, AldA, GuaB, RpmJ) and NaOCl-sensitive redox-sensing regulators (MgrA, SarZ, and Fur). The close-ups show the percentages of thiol oxidation under control, NaOCl stress, and the percentage of oxidation change under NaOCl stress versus control as revealed in Figure 1 using the same color gradient. The symbol * denotes conserved Cys.

catalytic active sites at Cys151 and Cys279, respectively. Furthermore, the IMP dehydrogenase GuaB and the purine nucleosidase USA300HOU_2265 both displayed 25% increased oxidation under NaOCl stress (Tables 2; Supplementary Table S1).

Among the cell wall biosynthesis enzymes, the alanine racemase Alr2 (USA300HOU_2065) and the UDP-N-acetylglucosamine 1-carboxyvinyltransferase MurZ (USA300HOU_2112) were identified as NaOCl-sensitive proteins. The glucose-inhibited division protein MnmG showed 20.8% increased oxidation under NaOCl stress. Many aminoacyl-tRNA synthetases were strongly oxidized under NaOCl stress. We detected 18–24% higher oxidation levels for the histidine- and phenylalanine tRNA ligases (HisS and PheT2) and for the queuine tRNA ribosyltransferase (Tgt) under NaOCl stress.

Five S-bacillithiolated proteins were identified using shotgun proteomics in S. aureus, including the glycolytic Gap as major target

We used the previously applied shotgun proteomic approach for identification of S-bacillithiolated proteins under nonreducing conditions based on the 396 Da mass increase at Cys residues (16). Five S-bacillithiolated proteins were identified in NaOCl-treated cells of *S. aureus* USA300, including Gap, AldA, GuaB, RpmJ, and the manganese-dependent inorganic pyrophosphatase PpaC (Table 3; Supplementary Fig. S1). GuaB was S-bacillithiolated at its active

site Cys307, which forms the thioimide intermediate with the substrate and is S-thiolated also in other gram-positive bacteria (Table 3; Supplementary Fig. S1).

Gap and AldA were S-bacillithiolated at their catalytic active sites at Cys151 and Cys279, respectively (Fig. 2 and Table 3; Supplementary Fig. S1). The AldA homolog of *S. carnosus* was previously found S-bacillithiolated at Cys279 (16). The active site Cys of Gap is a conserved target for S-glutathionylation in eukaryotic Gap homologs. Cys151 of Gap showed 29.5% oxidation increase under NaOCl stress in the OxICAT analysis, which is reflected also by the mass spectra of the ICAT-labeled Cys151-peptides (Fig. 4A). Nonreducing BSH-specific Western blots further identified that Gap is the most abundant S-bacillithiolated protein under hypochlorite stress based on the size and supported by the MS results (Fig. 4B; Supplementary Fig. S1). Gap-SSB was detected in the *S. aureus* USA300 and COL strains, but is absent in the *bshA* mutant as expected.

Gap contributes as most abundant Cys protein with 4% to the total Cys proteome

We were further interested in the contribution of Gap and other S-bacillithiolated proteins to the total Cys proteome of *S. aureus*. *S. aureus* USA300 encodes for 2694 proteins. These include 1864 proteins with 4935 Cys residues, indicating that the Cys content is 0.64% in the theoretical proteome (Supplementary Fig. S2A, B). Using shotgun proteomics, the spectral protein abundance for 600 proteins,

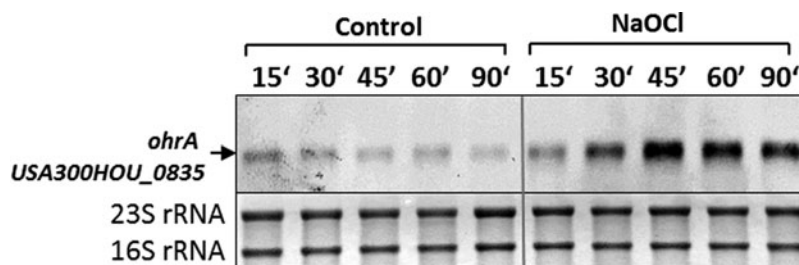


FIG. 3. Northern blot analysis showing transcriptional induction of the SarZ-regulated *ohrA* gene (USA300-HOU_0835) under NaOCl stress. RNA was isolated from *S. aureus* USA300 grown in Belitsky minimal medium under control and NaOCl stress conditions and subjected to Northern blot analysis for *ohrA* (USA300HOU_0835) transcription. Transcription of *ohrA* is upregulated due to SarZ thiol oxidation and inactivation under NaOCl stress as revealed by OxICAT analysis *in vivo*.

TABLE 3. IDENTIFICATION OF THE S-BACILLITHIOLATED GAP, ALDA, PPA, RpmJ, AND GUA IN STAPHYLOCOCCUS AUREUS USA300 USING SHOTGUN LC-MS/MS ANALYSIS

Protein	Accession	Function	Cys-SSB peptides	Prob (%)	SEQUEST XCorr	SEQUEST ΔCn	Cys-Mod.	Observed mass	Actual mass	Charge	ΔDa	ΔPPM
Gap	A8Z1A0_ STAAT	Glyceraldehyde-3-phosphate dehydrogenase	(K)TIVENTNHQELDG SETVVSAGASCI51 (+BSH)ITNSLAP VAK(V)	99	4.8813	0.7119	(+396)	1,262.92	3,785.73	3	0.00989	2.6
AldA	A8YY87_ STAAT	Aldehyde dehydrogenase	(K)VVNNITGQVC279 (+BSH)TAGTR(V)	99	2.9038	0.7827	(+396)	605.9328	1,814.78	3	-0.00041	-0.2
PpaC	PPAC_ STAAT	Mn-dependent inorganic pyrophosphatase	(R)JANFETAGPLC 110(+BSH)YR(A)	99	3.2907	0.6747	(+396)	925.9006	1,849.79	2	0.00081	0.4
RpmJ	RL36_ STAAT	50S ribosomal protein L36	(K)VRPSVKPIC11 (+BSH)EK(C)	99	2.0458	0.5926	(+396)	826.4047	1,650.79	2	-0.00051	-0.3
GuaB	A8Z0R0_ STAAT	Inosine-5'-monophosphate dehydrogenase	(K)VGIGPGSIC307 (+BSH)ITTR(V)	99	2.2835	0.6759	(+396)	778.8504	1,555.69	2	0.00077	0.5

Identification of S-bacillithiolated peptides in the *S. aureus* USA300 wild type using shotgun LC-MS/MS analysis and their Sequest Xcorr, ΔCn scores, and mass deviations. The *S. aureus* USA300 wild type was exposed to 150 μM NaOCl for 30 min and S-bacillithiolated proteins were identified using shotgun LC-MS/MS analysis and the Scaffold proteome software based on the mass increase of 396 Da (+BSH) at Cys peptides. The table lists the Uniprot accession number, protein name, function and molecular weight, the S-bacillithiolated Cys peptide sequence, and the quality control criteria for the peptide-SSB as obtained from the LC-MS/MS analysis and the Scaffold software (Xcorr, ΔCn scores, mass deviations Δppm, and ΔDa, observed and theoretical peptide masses, and charges of the modified peptide).

The S-bacillithiolated Cys is shown in *bold-faced*.

LC-MS/MS, liquid chromatography tandem mass spectrometry.

including 398 Cys-containing proteins, was determined in the proteome of *S. aureus* USA300 (Supplementary Table S2 and Supplementary Fig. S2C). The protein abundance in the proteome is visualized using Voronoi treemaps (Fig. 5). The cell size corresponds to the spectral protein abundance and the color code denotes the numbers of Cys residues. The majority of 226 Cys proteins identified in the proteome possess only 1–2 Cys residues. However, there are also six proteins with >10 Cys residues. The most Cys-rich protein was identified as the formate dehydrogenase FdhA that contains 26 Cys residues coordinating several FeS clusters. Based on their spectral abundance, we identified 50 abundant Cys-containing proteins that contribute to 60% of the total *S. aureus* Cys proteome (Supplementary Fig. S2C). The redox state for the majority of these Cys peptides was quantified using the OxICAT approach (Supplementary Table S1). The Cys abundance treemap also shows that many ribosomal proteins and the pyruvate dehydrogenase do not possess Cys residues (Fig. 5).

The S-bacillithiolated Gap was identified among the most abundant Cys-containing proteins and contributes with 4% of the total Cys proteome (Supplementary Fig. S2C). This indicates that Gap makes the major contribution to the S-bacillithiolome of *S. aureus* as visualized also by the BSH Western blots. The other S-bacillithiolated proteins, AldA, RpmJ, GuaB, and PpaC, are less abundant and make with 0.1–0.7% of Cys abundance only a minor contribution to the total Cys proteome (Supplementary Table S2).

H₂O₂ and NaOCl-induced inactivation pathways of Gap in *S. aureus* due to overoxidation and S-bacillithiolation in vitro

The active site of Gap is usually present in a highly conserved CTTNC motif in different organisms (Supplementary Fig. S3). However, in the *S. aureus* Gap, the second cysteine is replaced by a serine. The identification of S-bacillithiolated Gap under hypochlorite stress was intriguing since a previous proteomic study has shown that Gap of *S. aureus* is very sensitive to overoxidation to the sulfonic acid form in the presence of 100 mM *H₂O₂* *in vivo* (73). In another proteomic study, Gap was identified as reversibly oxidized by 10 mM *H₂O₂* in *S. aureus* (19). Thus, we were interested to study the inhibition of Gap activity *in vitro* due to overoxidation and S-bacillithiolation under both *H₂O₂* and NaOCl stresses.

Gap of *S. aureus* was purified as His-tagged protein from *E. coli*. The inhibition of Gap activity by increasing *H₂O₂* concentrations was monitored spectrophotometrically with G3P as substrate in the presence of NAD⁺. The remaining Gap activity was determined by nicotinamide adenine dinucleotide (NADH) generation as absorbance change at 340 nm during the slope in the reaction, as described previously (61). Treatment of Gap with 100 μM *H₂O₂* leads to a 50% decrease in Gap activity, while exposure to 1–10 mM *H₂O₂* resulted in complete enzyme inactivation (Fig. 6A). Inactivation of Gap with 1–10 mM *H₂O₂* alone was irreversible due to overoxidation since Gap activity could be not restored with 10 mM dithiothreitol (DTT) (Fig. 6C). To investigate whether S-bacillithiolation can protect the enzyme against irreversible overoxidation, Gap was pretreated with 10-fold molar excess of BSH before *H₂O₂* exposure. Gap activity was already 90% inhibited after oxidation with 100 μM *H₂O₂* in the presence of

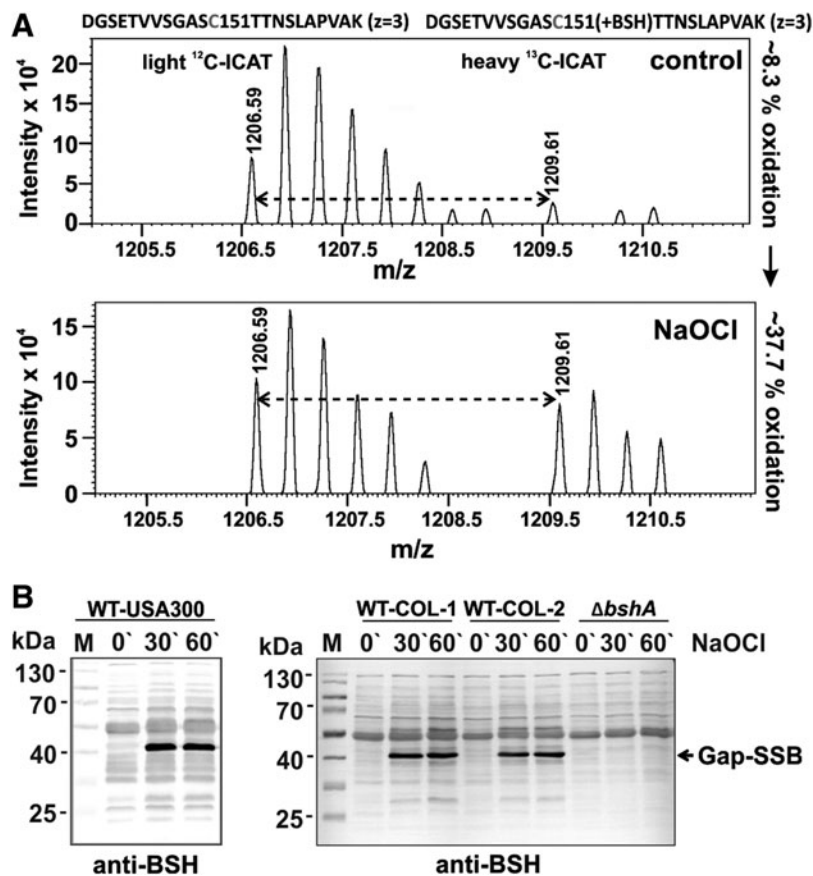


FIG. 4. OxICAT analysis revealed a 29% increased oxidation of the Gap Cys151 peptide (A) and Gap was identified as most abundant *S*-bacillithiolated protein in *S. aureus* under NaOCl stress as shown by BSH-specific Western blot analysis (B). (A) The OxICAT mass spectrometry results are shown for the Gap Cys151 peptide in *S. aureus* USA300 under control and 30 min after NaOCl stress. The reduced Gap Cys151 peptides in the cell extract are labeled with light ^{12}C -ICAT, followed by reduction of all reversible thiol oxidation, including the *S*-bacillithiolated Cys151 peptides and subsequent labeling of previously oxidized Cys151 peptide by heavy ^{13}C -ICAT reagent. According to the quantification by the MaxQuant software, the Cys151 peptide was 8.3% oxidized in the control and its oxidation level increased to 37.7% under NaOCl stress. (B) Nonreducing BSH-specific Western blot analysis identified Gap as most abundant *S*-bacillithiolated protein in *S. aureus* USA300 and COL strains under NaOCl stress. Two independent biological replicates are shown for *S. aureus* COL denoted as COL-1 and COL-2. Gap is *S*-bacillithiolated at the active site Cys151 under NaOCl stress as revealed by subsequent LC-MS/MS analysis (Supplementary Fig. S1A). BSH, bacillithiol; LC-MS/MS, liquid chromatography tandem mass spectry.

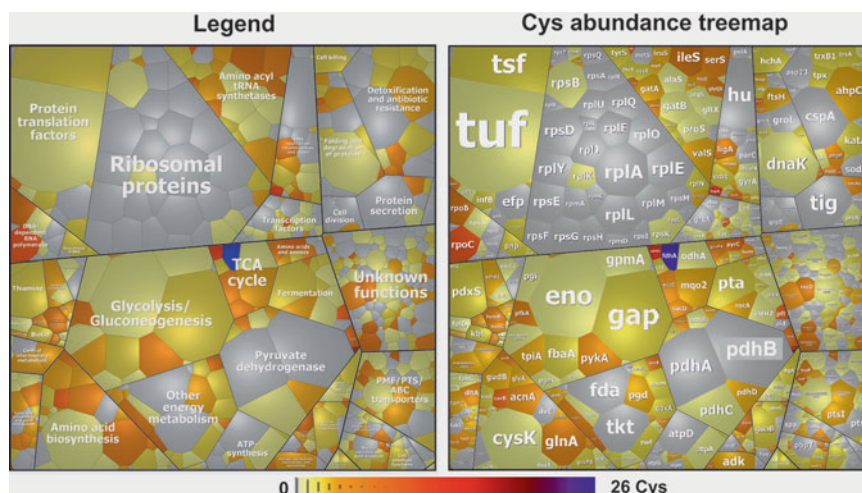


FIG. 5. Voronoi treemaps visualize Gap as the most abundant Cys protein in the total Cys proteome of *S. aureus* USA300. The treemap legend (left) indicates the classification of the *S. aureus* USA300 proteome into functional categories according to TIGRfam annotations. The cell size corresponds to the spectral counts of each protein identified in the proteome of *S. aureus* USA300 and classified according to TIGRfam. The Cys-containing proteins are color coded using a yellow–red color gradient based on their numbers of Cys residues (Supplementary Table S2). Proteins without Cys residues are displayed in gray.

BSH, while treatment with 100 μM H_2O_2 alone only led to 50% decreased activity (Fig. 6A, B). Gap inactivation with H_2O_2 and BSH was caused by reversible *S*-bacillithiolation since DTT reduction resulted in recovery of Gap activity (Fig. 6C–E; Supplementary Fig. S9). These results support that the Gap active site is highly sensitive to overoxidation, which can be prevented by *S*-bacillithiolation in the presence of H_2O_2 and BSH.

Next, we determined the time-dependent Gap inactivation by both H_2O_2 -dependent oxidation pathways (Supplementary

Fig. S4). Gap was treated with 1 mM H_2O_2 on ice with or without BSH and the remaining Gap activity was determined after different times of H_2O_2 -dependent overoxidation and *S*-bacillithiolation. The Gap activity assays revealed that both *S*-bacillithiolation and overoxidation lead to 80% enzyme inhibition after 7.5 min of H_2O_2 treatment (Supplementary Fig. S4A). In addition, we analyzed the time course for the detection of Gap-SSB or the overoxidized Cys151 under H_2O_2 treatment with or without BSH using BSH-specific Western

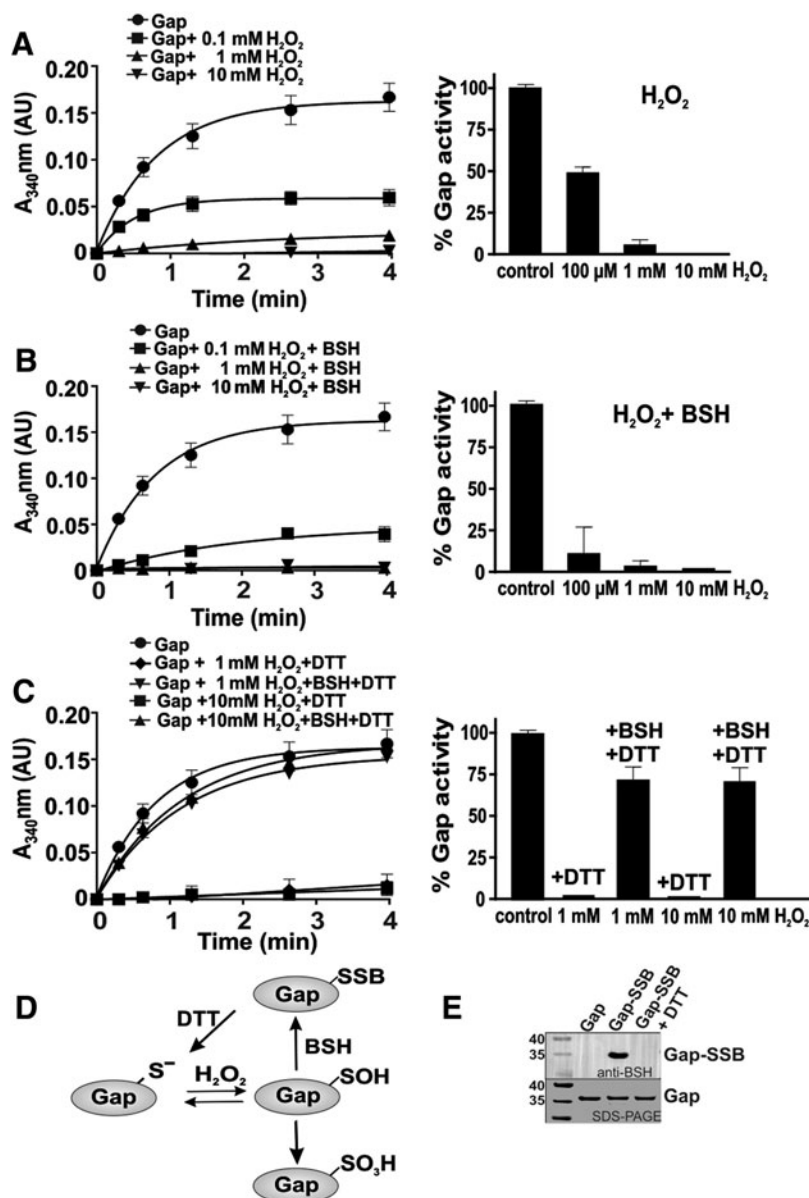


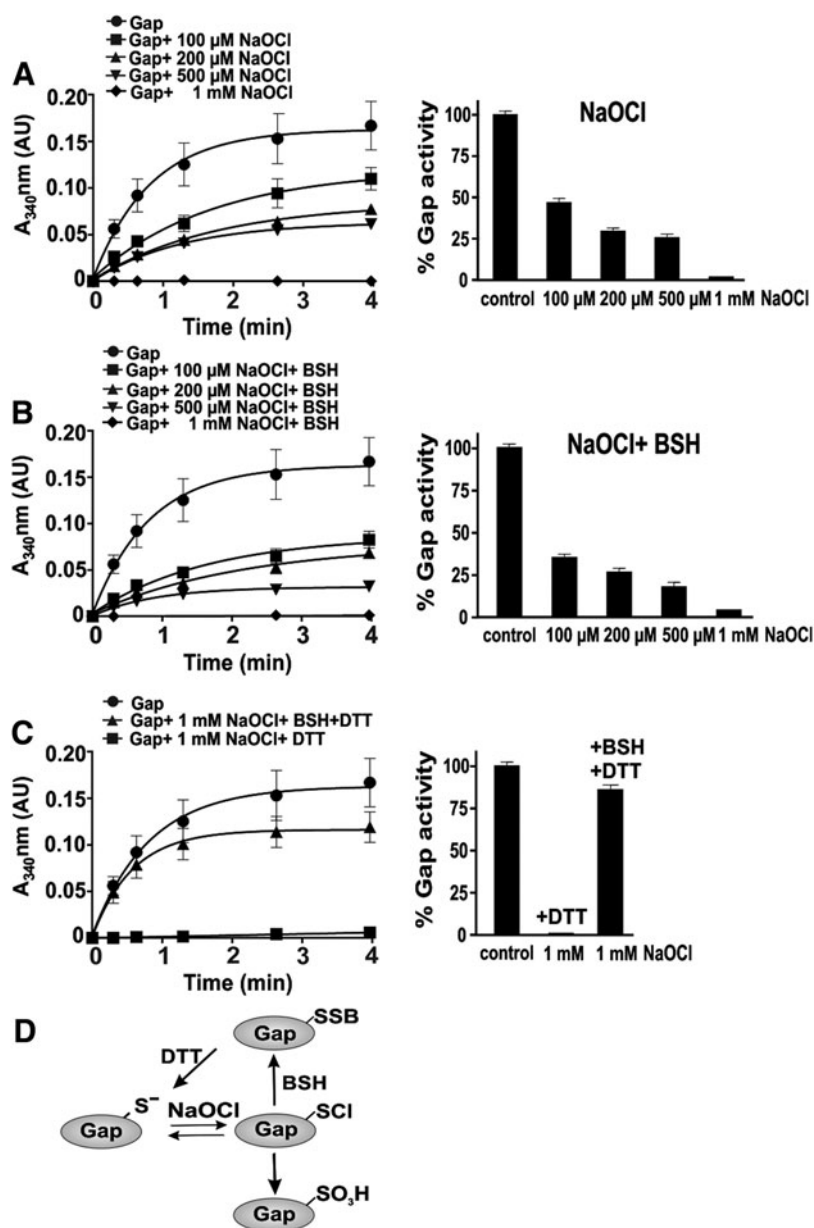
FIG. 6. Inactivation of Gap of *S. aureus* in response to H_2O_2 in vitro. (A, B) Reduced Gap (40 μM) was oxidized with 100 μM , 1, and 10 mM H_2O_2 for 5 min in the absence (A) or presence of 10-molar excess of BSH (400 μM) (B) in reaction buffer (100 mM Tris HCl, 1.35 mM EDTA, pH 8.0). The remaining Gap activity was measured in the presence of G3P and NAD^+ spectrophotometrically, following NADH production at 340 nm. The Gap activity was calculated as absorbance change from the slope of the reaction in the first 80 s, as described in the Materials and Methods section. (C) To assess the reversibility of Gap inactivation by H_2O_2 , Gap was treated with 1 and 10 mM H_2O_2 alone or with H_2O_2 and BSH, followed by reduction with 10 mM DTT. (D) Schematic showing the irreversible inhibition of Gap activity due to overoxidation of the active site Cys with H_2O_2 alone, while Gap activity was reversibly inhibited with H_2O_2 and BSH due to *S*-bacillithiolation. (E) *S*-bacillithiolation of Gap in the presence of 10 mM H_2O_2 and BSH was confirmed using a BSH-specific Western blot analysis before and after subsequent DTT reduction. DTT, dithiothreitol; EDTA, ethylenediaminetetraacetic acid; G3P, glyceraldehyde-3-phosphate; H_2O_2 , hydrogen peroxide.

blots or MS, respectively. The MS results identified the overoxidized Cys151 sulfonic acid (Cys151-SO₃H) after 1 min of H₂O₂ treatment (Supplementary Fig. S5). The S-bacillithiolated Gap could be also detected after 1 min of treatment with BSH and H₂O₂ (Supplementary Figs. S4B and S9). These results suggest that overoxidation and S-bacillithiolation occur at similar rates under H₂O₂ treatment *in vitro*. However, the Gap activity assays after treatment with different H₂O₂ concentrations indicate that Gap inhibition is faster with 100 μ M H₂O₂ in the presence of BSH compared with 100 μ M H₂O₂ alone, which only leads to 50% enzyme inhibition (Fig. 6A, B). Thus, S-bacillithiolation of Cys151 by H₂O₂ in the presence of BSH serves to protect the active site against overoxidation.

Since S-bacillithiolation of Gap was observed under NaOCl stress *in vivo*, we studied the dose-dependent Gap inactivation by NaOCl with or without prior exposure to BSH (Fig. 7). Treatment of Gap with 100–500 μ M NaOCl led to

50–75% inhibition of Gap activity. Pretreatment of Gap with BSH before exposure to 100 μ M NaOCl resulted in 70% activity decrease. Gap was fully inactivated with 1 mM NaOCl in the absence or presence of BSH. Treatment of Gap with 1 mM NaOCl alone resulted in irreversible inactivation due to overoxidation since Gap activity could be not restored using DTT. In the presence of BSH, Gap inactivation by NaOCl was caused by reversible S-bacillithiolation since 85% Gap activity could be restored by DTT reduction (Fig. 7C, D). Next, we studied the time course for NaOCl-induced overoxidation and S-bacillithiolation pathways in the presence of 1 mM NaOCl. The Gap activity assays with or without BSH showed that Gap inhibition is faster with BSH and NaOCl compared with NaOCl alone (Supplementary Fig. S6). These results indicate that S-bacillithiolation can efficiently prevent overoxidation of the Gap active site under NaOCl *in vitro*, supporting our *in vivo* finding.

FIG. 7. Inactivation of Gap of *S. aureus* in response to NaOCl *in vitro*. (A, B) Reduced Gap was treated with 0.1–1 mM NaOCl for 5 min without (A) or with 10-molar excess of BSH (B) in reaction buffer (100 mM Tris HCl, 1.35 mM EDTA, pH 8.0). The remaining Gap activity was measured spectrophotometrically, following NADH production at 340 nm. The Gap activity was calculated as absorbance change from the slope of the reaction in the first 80 s, as described in the Materials and Methods section. (C) To analyze the reversibility of Gap inactivation by NaOCl, Gap was inactivated with 1 mM NaOCl in the absence or presence of BSH, followed by DTT reduction. Gap activity was irreversibly inhibited after treatment with NaOCl due to overoxidation since Gap activity could be not restored by DTT. In the presence of NaOCl and BSH, Gap was reversibly inactivated due to S-bacillithiolation since DTT reduction resulted in 85% recovery of Gap activity. (D) Schematic showing that NaOCl leads to the transient sulphenylchloride formation as unstable intermediate that reacts further with BSH to form S-bacillithiolated Gap. In the absence of BSH, Gap-SCl is quickly overoxidized resulting in irreversible inhibition of Gap activity *in vitro*.



Regeneration of S-bacillithiolated Gap using the bacilliredoxin Brx (SAUSA300_1321) in vitro

The reversal of *S*-bacillithiolation was shown to require the glutaredoxin-like bacilliredoxins, YphP (BrxB) and YqiW (BrxB), in *B. subtilis* (24). Using a Brx-roGFP2 biosensor, we demonstrated recently that the YphP homolog of *S. aureus* (SAUSA300_1321 or Brx) is highly specific as bacilliredoxin to recognize BSSB (51). Thus, Gap activity was measured after debacillithiolation of Gap-SSB with Brx and Brx Cys mutant proteins (BrxCGA, BrxAGC) and G3P oxidation was followed by NADH production as absorbance change at 340 nm (Fig. 8A). Gap activity could be restored to 70% and 60% during debacillithiolation with Brx and the BrxCGA resolving Cys mutant *in vitro*, respectively. However, Gap activity was only 25% recovered with the BrxAGC active site mutant protein supporting the specificity of the Brx active site for the attack of BSH mixed disulfide. Debacillithiolation of

Gap-SSB by Brx and the BrxCGA mutant was verified in BSH-specific Western blots (Fig. 8B; Supplementary Fig. S9). These results indicate that *S*-bacillithiolation of Gap functions in protection and redox regulation of the active site Cys and can be reversed by the bacilliredoxin Brx *in vitro* (Fig. 8C).

Structural features of the Gap active site during overoxidation and S-bacillithiolation

We were interested in structural changes of Gap after overoxidation and *S*-bacillithiolation. The crystals of H_2O_2 -treated overoxidized Gap diffracted X-rays to 2.6 Å resolution and belonged to the $P2_12_12_1$ space group. Previously, several crystal structures of the Gap holo- and apoenzyme have been reported with the protein always crystallized in the $P2_1$ space group (57). The structure of the overoxidized Gap contains four monomers in an asymmetric unit, each consisting of the NAD^+ -binding domain (residues 1–150) and the

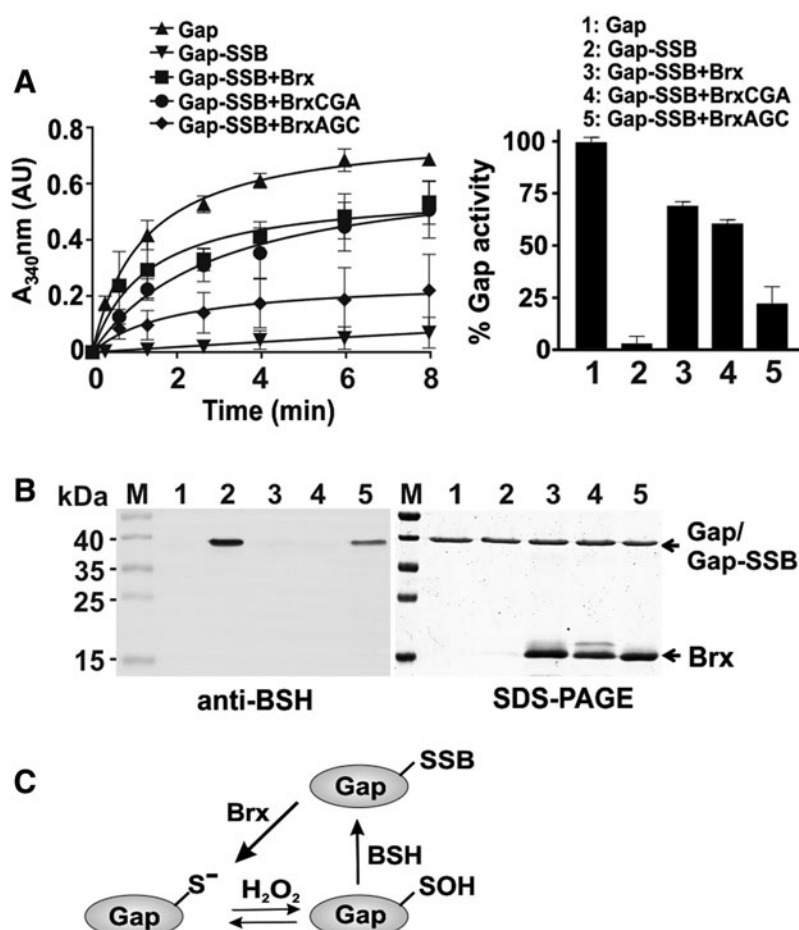


FIG. 8. Recycling of *S*-bacillithiolated Gap requires the bacilliredoxin Brx *in vitro*. (A) Gap activity is reversibly inhibited by *S*-bacillithiolation *in vitro* and can be restored by reduction using the bacilliredoxin Brx (SAUSA300_1321). Debacillithiolation required the Brx active site Cys. The BrxAGC mutant showed weak activity to reduce Gap-SSB, while the Brx resolving Cys mutant (BrxCGA) could restore Gap activity similar to the wild-type Brx protein. *S*-bacillithiolated Gap was generated *in vitro* by treatment of 25 μ M Gap with 2.5 mM H_2O_2 in the presence of 250 μ M BSH. For debacillithiolation, 2.5 μ M Gap-SSB was incubated with 12.5 μ M Brx, BrxAGC, and BrxCGA proteins for 30 min. Gap activity was measured after addition of G3P and NAD^+ by spectrophotometric monitoring of NADH generation at 340 nm. (B) The level of debacillithiolation of Gap-SSB *in vitro* by Brx and BrxCys mutant proteins was monitored using nonreducing BSH-specific Western blot analysis. The SDS-PAGE is shown as loading control (right). The numbers 1–5 shown in the BSH Western blot and in the SDS-PAGE refer to the legend shown in (A). (C) Schematic for the reduction of *S*-bacillithiolated Gap using the bacilliredoxin Brx. SDS-PAGE, sodium dodecyl sulfate–polyacrylamide gel electrophoresis.

catalytic domain (residues 151–336) (57) (Supplementary Fig. S7A). The overall fold of overoxidized Gap is almost identical to previously reported reduced Gap structures, with only slight conformational differences observed in the loop regions comprising residues 59–72, 75–90, and 111–118. The root-mean square deviation after global superposition of overoxidized Gap with the holo- (PDB code: 3LVF) or apoenzyme (PDB code: 3LC7) was 1.01 and 1.11 Å, respectively. Interestingly, during previous structural analyses, Gap always copurified with NAD^+ , which had to be removed *via* activated charcoal to obtain the apoenzyme (57). In contrast, the present Gap structure does not contain NAD^+ , thus representing an apo form of the enzyme. Thus, H_2O_2 treatment seems to have led to loss of the coenzyme.

According to our MS results and previous publications (73), the Gap sulfonic acid was identified by MS as overoxidized form. In the structure of overoxidized Gap, the sulfonic acid form could be modeled into the electron density of the active

site Cys151 in each monomer (Supplementary Fig. S7B, C). Overoxidation of Cys151 results in enzyme inhibition as supported by our activity assays. During catalysis, the sulfhydryl group of Cys151 attacks the nucleophilic carbon of the G3P substrate to form a covalent intermediate, thiohemiacetal (72). In the active enzyme, His178 forms an ion pair with Cys151, which increases the acidity and nucleophilicity of the thiol group. During G3P oxidation, His178 hydrogen bonds with the acyl carbonyl of the substrate and stabilizes the hemithioacetal intermediate (57). Apart from interfering with the function of Cys151, the sulfonyl moiety of the hyperoxidized Cys151 also interacts with the main chain carbonyl of Asn316 and the imidazole ring of His178 (Fig. 9A; Supplementary Fig. S7D). Thus, hyperoxidation of Cys151 affects the function of two key catalytic residues of Gap, Cys151, and His178, leading to irreversible inactivation of the enzyme.

To obtain insights into the structural changes upon S-bacillithiolation, BSH was modeled into the active site of the

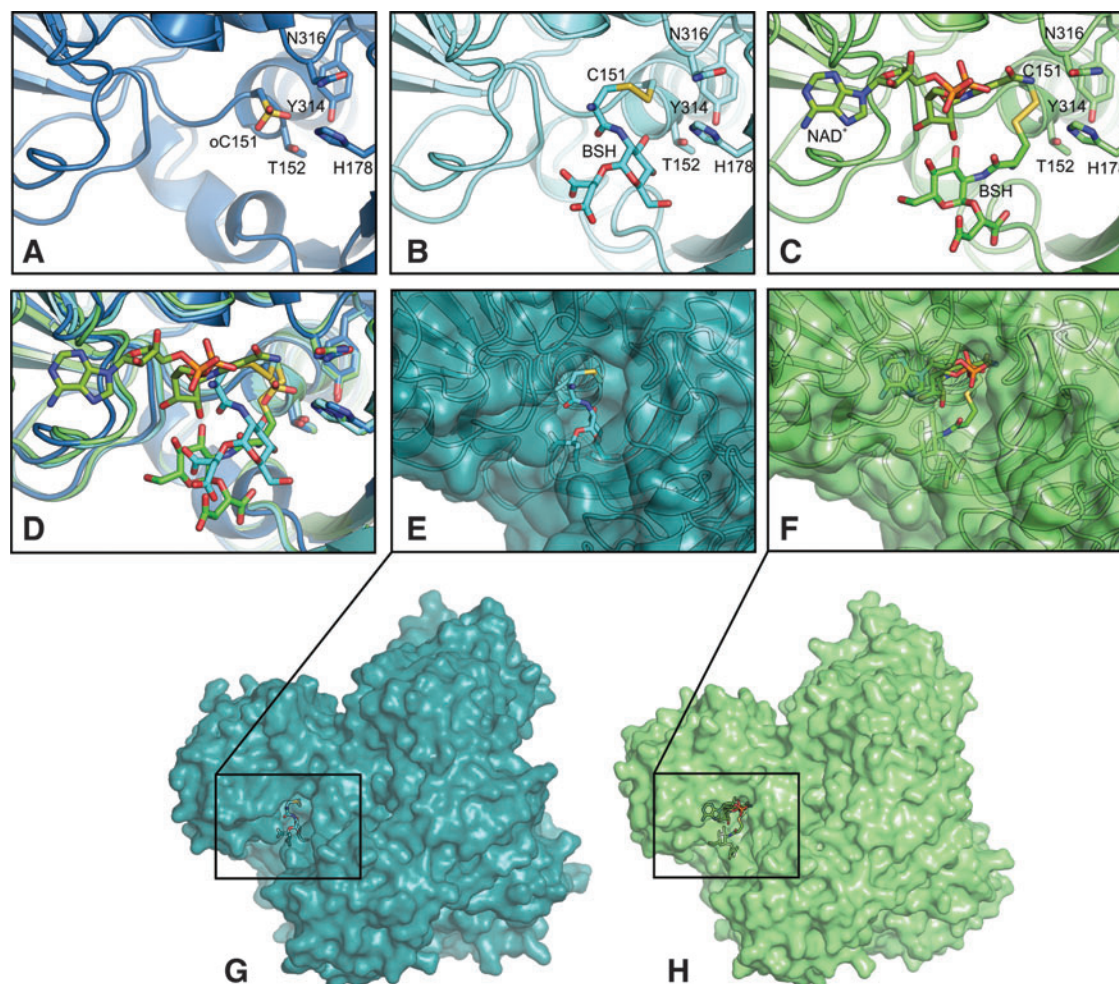


FIG. 9. Structural insights into the Gap active site after overoxidation and S-bacillithiolation. (A) Crystal structure of the overoxidized active site Cys151 (Cys-SO₃H, oC151) of Gap. (B, C) Computational model of BSH docked into the active site of the Gap apoenzyme (B) and holoenzyme with the NAD⁺ coenzyme (C) using a covalent docking algorithm that takes into account the possibility of bond formation between ligand and receptor. Shown is the best pose of 10 best poses of the S-bacillithiolated active site. (D) Superposition of Gap-SO₃H with the S-bacillithiolated apo- and holoenzyme active sites. (E, F) The S-bacillithiolated active site pocket of the apoenzyme (E) and holoenzyme (F) structures rotated by 25° over y axis in respect to (B, C). (G, H) Surface representation of apoenzyme (G) and holoenzyme (H) with docked BSH.

apo- and holoenzyme structures using molecular docking (Fig. 9B, C). We used a covalent docking algorithm that takes into account the possibility of bond formation between ligand and receptor. Docking of BSH into the apo- or holoenzyme structure resulted in a set of covalent complexes (10 best poses), in which the disulfide bond can readily form and which are structurally very similar at least in the vicinity of the disulfide bond, suggesting a high confidence in the docking pose (Supplementary Fig. S8). In the holoenzyme structure, the NAD⁺ cofactor partially occludes the binding pocket and narrows the space available for BSH binding. As a result, in the holo-Gap active site, where NAD⁺ is present, BSH takes up conformations, which differ significantly less compared with the ones in the apoenzyme. When superimposing the two best binding poses, BSH in the apoenzyme structure partially occupies the part of the pocket where NAD⁺ would be present (Fig. 9D). However, in both cases, *S*-bacillithiolation of the active site does not require major conformational changes of the protein (Fig. 9E–H). In addition, previous molecular dynamic simulations of human GAPDH (61) suggested little fluctuations of the protein. Taken together, we suggest that BSH can undergo disulfide formation with the active site at little energetic or entropic costs. This may further explain why Gap as the most abundant redox-sensitive protein in the proteome of *S. aureus* is also the most abundant *S*-bacillithiolated protein under NaOCl stress.

Discussion

Dynamic thiol redox switches are the hallmarks of oxidative stress response and the major principle of redox signaling mechanism in prokaryotes and eukaryotes (33). Quantitative redox proteomic methods such as OxICAT allow to determine the redox state of proteins thiols and to dissect redox-sensitive thiols at high resolution (9, 48). To date, global thiol redox proteomics in the major pathogen *S. aureus* identified only few targets for oxidation under H₂O₂ stress (19, 77). However, *S. aureus* shows remarkable resistance to 100 mM H₂O₂, which is attributed to the constitutive expression of the catalase KatA indicating that *S. aureus* is well adapted to peroxide stress during infections (36).

In this study, we used OxICAT to monitor the redox state of 228 Cys residues in *S. aureus* USA300 under more severe infection-like conditions as provoked by hypochlorite. In untreated cells, the majority of thiols (84.6%) are reduced with an oxidation degree <25%, which is in agreement with previous studies in *E. coli* and yeast cells (9, 48). Under NaOCl stress, 58 NaOCl-sensitive proteins showed >10% increased oxidation, indicating that 25% of all identified protein thiols are redox sensitive in *S. aureus*. To analyze whether these NaOCl-sensitive Cys residues are buried or surface exposed, we calculated their relative surface accessibilities (RSAs) using NetSurfP (www.cbs.dtu.dk/services/NetSurfP/). However, only 9 of 228 Cys residues have RSA values of >30% and are predicted as solvent exposed (Table 2 and Supplementary Table S1). The RSA calculations clearly indicate that NaOCl-sensitive Cys residues are often the active site centers that are not surface exposed and buried in the predicted secondary protein structure.

Among the NaOCl-sensitive proteins with the highest oxidation increase of 20–30%, we identified Gap, AldA, and GuaB as *S*-bacillithiolated at their conserved substrate-

binding active sites. Only a few *S*-bacillithiolated proteins were found by the shotgun proteomic approach due to the instability and low abundance of the BSH-modified peptides. Thus, we assume that many more NaOCl-sensitive proteins of our OxICAT dataset are modified by *S*-bacillithiolation, but failed to be identified using the shotgun method.

Apart from *S*-bacillithiolation, also alternative *S*-thiolations are possible in *S. aureus* under NaOCl stress such as *S*-cysteinylation or CoASH mixed disulfides since cysteine and CoASH are also present in the thiol metabolome of *S. aureus* (58, 64). Moreover, the Cdr displayed an increased oxidation level under NaOCl stress at its conserved Cys16 in our OxICAT analyses and was previously shown to function in reduction of CoASH disulfides in *S. aureus* (18, 55). However, *S*-cysteinylation and CoASH mixed disulfides were not detected by MS due to their low abundance or instability.

Many Zn-containing NaOCl-sensitive proteins were identified, such as the Fur repressor, which is oxidized in its Zn-binding site. Zn-binding sites are common redox switch motifs (37). The best-studied example is the oxidation-sensitive Hsp33 chaperone that responds to hypochlorite by a redox switch in its Zn motif and protects *E. coli* proteins against oxidative aggregation (26, 38, 46). NaOCl-sensitive Zn-containing proteins include the alcohol dehydrogenase Adh and the ribosomal proteins, RpmG3 and RpmJ. Several previously predicted redox-sensitive Cys residues are found in CxxC motifs, such as the copper chaperone, CopZ, and the antioxidant proteins, AhpC, TrxB, and ArsC (21). These results are in agreement with previous redox proteomic results in *E. coli* under NaOCl stress (48). Increased oxidation levels were detected for both MarR/OhrR family regulators MgrA and SarZ that are oxidized at their single Cys residues. Using Northern blot analyses, we confirmed that SarZ oxidation leads to derepression of transcription of the *ohrA* gene (*USA300-HOU_0835*) in *S. aureus*. Thus, the OxICAT approach identified increased oxidation of both major thiol redox regulators under NaOCl stress in *S. aureus*.

The most abundant *S*-bacillithiolated protein was the glycolytic Gap enzyme in *S. aureus* under NaOCl stress, which was *S*-bacillithiolated at the active site Cys151. Gap is the most abundant Cys-containing protein contributing 4% to the total Cys proteome. The active site Cys is used for the nucleophilic attack at the aldehyde group of the G3P substrate to catalyze the substrate-level phosphorylation of G3P to 1,3-bisphosphoglycerate with production of NADH (34). Gap homologs are common targets for oxidation in eukaryotes and prokaryotes and subject of different post-translational thiol modifications, including *S*-sulfenylation, *S*-glutathionylation, *S*-nitrosylation, and *S*-sulfhydration, resulting in reversible enzyme inactivation (10, 34). Inactivation of Gap has been shown to redirect the glycolytic flux into the pentose phosphate pathway to supply nicotinamide adenine dinucleotide phosphate (NADPH) as reducing power under oxidative stress (10, 66).

Gap of *S. aureus* was previously identified as oxidation-sensitive target for reversible thiol modification (19) and was also found to be overoxidized at its active site Cys151 under H₂O₂ stress (73). Using biochemistry, MS, and X-ray crystallography, we confirmed previous findings that the glycolytic Gap enzyme from *S. aureus* is highly sensitive to overoxidation to Cys sulfonic acid *in vitro* in the presence of H₂O₂ alone. In this work, we found that Gap is the most abundant *S*-bacillithiolated protein under NaOCl stress

in vivo. We further demonstrate that S-bacillithiolation functions in reversible inhibition of Gap activity under H₂O₂ and NaOCl treatment *in vitro* and protects the active site Cys against overoxidation to ensure fast regeneration of this essential glycolytic enzyme during recovery of cells. Our Gap activity assays suggest that both pathways, the overoxidation and S-bacillithiolation, operate at similar kinetics under H₂O₂ treatment, while inactivation due to S-bacillithiolation was faster under NaOCl stress. Together, our results confirm the preference for formation of S-thiolation in the presence of LMW thiols as observed in many eukaryotic Gap homologs (34, 43, 78).

The reactivity of the active site cysteine toward H₂O₂ and the substrate G3P was recently shown to depend on two different mechanisms (34, 61). The catalytic Cys is in close proximity with His178 in the structure of Gap of *S. aureus* that attracts the thiol proton, leading to deprotonation and increased acidity of the catalytic Cys. The acidic nature explains the reactivity of catalytic Cys toward the substrate G3P that covalently reacts with the nucleophilic thiolate during the catalytic cycle (34, 62). However, the increased acidity of Cys151 does not explain its strong reactivity toward H₂O₂. Instead, the reactivity of the active site thiolate depends on a specific H₂O₂-binding pocket, transition state stabilization, and a proton relay mechanism promoting leaving group departure (34, 61).

This proton relay mechanism also determines the preferred modification by S-bacillithiolation of Gap in *S. aureus* under H₂O₂ *in vitro*, which requires the initial formation of a sulfenic acid, followed by reaction to the BSH mixed disulfide. HOCl shows very fast reaction rates with thiols ($3 \times 10^7 \text{ M}^{-1}\text{s}^{-1}$) that are several orders of magnitude higher compared with H₂O₂ (17, 27, 30, 60, 74). HOCl first leads to chlorination of thiols resulting in an unstable sulphenylchloride intermediate that reacts further to form disulfides in the presence of another thiol. In the absence of proximal thiols, the sulphenylchloride quickly leads to irreversible oxidation stages (17, 30, 52). We have shown in *S. aureus* that S-bacillithiolation functions in protection and redox regulation of the Gap active site against overoxidation under NaOCl stress *in vitro* and *in vivo*. Molecular docking of BSH into the active site of the Gap apo- and holoenzyme was used to model the S-bacillithiolated active site at high confidence. The model of Gap-SSB structure suggests that BSH can undergo disulfide formation with Cys151 without major conformational changes. This may explain why the most abundant Cys protein Gap is the preferred and dominant target for S-bacillithiolation inside *S. aureus* cells.

S-glutathionylation of the active site Cys of Gap was found in many eukaryotic organisms, such as *Arabidopsis thaliana*, the malaria parasite *Plasmodium falciparum*, or in human endothelial cells, leading to reversible inhibition of Gap activity (3, 43, 69). Reactivation of Gap was catalyzed by glutaredoxins and thioredoxins in plants and malaria parasites (3, 43). In *B. subtilis*, the bacilliredoxins, BrxA and BrxB, were shown to catalyze the reduction of S-bacillithiolated OhrR and MetE *in vitro* (24). In this study, we showed that S-bacillithiolated Gap is also a substrate for the bacilliredoxin Brx (SAUSA300_1321) in *S. aureus*, which requires the active site Cys for debacillithiolation *in vitro*. Thus, the bacilliredoxin pathway is also involved in regeneration of Gap activity in *S. aureus*.

Materials and Methods

Bacterial strains and growth conditions

Bacterial strains used were *S. aureus* COL and USA300 and its isogenic *bshA* mutants as described previously (64). For cloning and genetic manipulation, *E. coli* DH5a and BL21 (DE3) *plysS* were cultivated in Luria Bertani (LB) medium. For NaOCl stress experiments, *S. aureus* USA300 and COL strains were cultivated in LB medium until an optical density at 540 nm (OD₅₄₀) of 2.0, transferred to Belitsky minimal medium, and treated with 150 μM NaOCl stress as described (51). NaOCl, diamide, DTT, N-ethylmaleimide (NEM), and H₂O₂ (35% w/v) were purchased from Sigma-Aldrich.

MS-based thiol redox proteomics using the OxICAT approach

S. aureus USA300 was harvested before and after exposure to 150 μM NaOCl for 30 min, respectively. The OxICAT method was performed according to the protocol of Lindemann and Leichert (49) with the modification that cells were disrupted using a ribolyzer. The ICAT-labeled peptides were dissolved in 0.1% (v/v) acetic acid and loaded onto self-packed LC columns with 10 μl of buffer A (0.1% (v/v) acetic acid) at a constant pressure of 220 bar without trapping. Peptides were eluted using a nonlinear 85-min gradient from 1% to 99% buffer B (0.1% (v/v) acetic acid in acetonitrile) with a constant flow rate of 300 nl/min and measured using Orbitrap MS as described (6). The *S. aureus* USA300 sequence database was extracted from Uniprot and used by the search engine Andromeda and the MaxQuant software (version 1.5.1.2) to quantify the ICAT-labeled Cys peptides. Two miscleavages were allowed, the parent ion mass tolerance was 10 ppm and the fragment ion mass tolerance was 1.00 Da. The average percentage of oxidation of each Cys peptide and the percentage change under NaOCl stress were calculated from 2 to 3 biological replicates using the intensity values provided by MaxQuant. Voronoi treemaps were generated using the Paver software to visualize the percentage oxidation of all identified ICAT-labeled peptide pairs. The OxICAT proteomic data have been deposited to the ProteomeXchange Consortium via the PRIDE partner repository with the dataset identifier PXD004918.

Identification of S-bacillithiolated and overoxidized Cys peptides using LTQ-Orbitrap MS

For identification of S-bacillithiolated peptides, NEM-alkylated protein extracts were prepared from *S. aureus* USA300 cells after exposure to 150 μM NaOCl for 30 min as described (15). The protein extracts were separated by 15% nonreducing sodium dodecyl sulfate–polyacrylamide gel electrophoresis (SDS-PAGE), followed by tryptic in-gel digestion and LTQ-Orbitrap-Velos MS, as described (15). Post-translational thiol modifications of proteins were identified by searching all tandem mass spectrometry (MS/MS) spectra in dta format against the *S. aureus* USA300 target–decoy protein sequence database extracted from UniprotKB release 12.7 (UniProt Consortium, Nucleic acids research 2007, 35, D193-197) using Sorcerer™-SEQUEST® (Sequest v. 2.7 rev. 11, Thermo Electron, including Scaffold 4.0; Proteome Software, Inc., Portland, OR). The SEQUEST search parameters and thiol modifications were used as described (15).

The scores and mass deviations of the *S*-bacillithiolated peptides are shown in detail in Supplementary Figure S1, including their fragmentation spectrum and ion tables.

MS of the H₂O₂-treated overoxidized Gap was performed after in-gel tryptic digestion using nLC-MS/MS by Orbitrap fusion, as described previously (45). For Cys151-SO₃H peptide identification and quantification, MS1 data were filtered to the precursor target masses applying an *m/z* window of 3 ppm. Isotopic distribution and fragmentation spectra were inspected manually in different charge states in successive MS2 scans in different overoxidized Gap samples.

Cloning, expression, and purification of the *S. aureus* Gap, Brx, and Brx Cys-Ala mutant proteins in *E. coli*

The previously constructed plasmids, pET11b-Brx-roGFP2, pET11b-BrxAGC-roGFP2, and pET11b-BrxCGA-roGFP2 (51), were used as template to amplify *S. aureus* *brx* (SAUSA300_1321), *brxAGC*, and *brxCGA* by PCR using primer pairs 1321-roGFP2-For-NheI (5'-CTAGCTAGCATGAATGCATATGATGCTTATATGAAAG-3') and roGFP2-1321-Rev-BamHI (5'-CGCGGATCCTTAGTGATGGTGATGGTGATGTTTACAA TTT TCGTCAAAGGC-3'). The reverse primer also encodes the C-terminal His₆-tag. The PCR products were digested with *NheI* and *BamHI* and inserted into plasmid pET11b (Novagen) that was digested using the same restriction enzymes to generate plasmids pET11b-*brx*, pET11b-*brxAGC*, and pET11b-*brxCGA*. The primer pairs gap-For-NdeI (5'-GGAATTCATATGGCA GTAAAAGTAGCAATTAATG-3') and gap-Rev-BamHI (5'-CGCGGATCCTTAGTGATGGTGATGGTGATGTTTAGAA AGTTCAGCTAAGTATGC-3') were used to amplify the *S. aureus* *gap* gene (SAUSA300_0756) by PCR. Chromosomal DNA of *S. aureus* USA300 was used as template. The PCR products were digested with the restriction enzymes, *NdeI* and *BamHI*, and inserted into plasmid pET11b that was digested with the same enzymes to generate plasmids pET11b-*gap*. The correct sequences of the cloned genes were confirmed by sequencing. The plasmids were transformed into *E. coli* BL21 (DE3) *plysS* (Novagen).

For protein expression, *E. coli* BL21(DE3) *plysS* strains with the plasmids, pET11b-*gap*, pET11b-*brx*, pET11b-*brxAGC*, and pET11b-*brxCGA*, were grown in 1 liter LB medium and 1 mM isopropyl- β -D-thiogalactopyranoside (IPTG) was added at the exponential phase (OD₆₀₀ of 0.8) for 3 h at 37°C. His-tagged proteins were purified using His Trap™ HP Ni-NTA columns and the ÄKTA purifier liquid chromatography system (Amersham Bioscience). The proteins were further concentrated to 2–6 mg/ml using Amicon Ultra concentrators (Millipore). Before the activity assays, Gap and Brx proteins were reduced with 10 mM DTT for 30 min, followed by DTT removal using Micro Biospin 6 columns (Biorad).

Gap activity assay

Gap activity was monitored spectrophotometrically at 340 nm and 25°C by the production of NADH. The oxidation of G3P to 1,3-bisphosphoglycerate (1,3-BPG) was measured in an assay mixture containing 1.25 mM NAD⁺ and 0.25 μ M Gap in argon-flushed 20 mM Tris-HCl, pH 8.7, with 1.25 mM ethylenediaminetetraacetic acid and 15 mM sodium arsenate. After preincubation, the reaction was started by addition of 0.25 mM D,L-G3P. Sodium arsenate was used as a cosubstrate to form unstable 1-arseno-3-phosphoglycerate, as de-

scribed previously (61). Degradation of the product allows a favorable equilibrium for measuring the rate of Gap activity in the glycolytic forward reaction. Initial rates were determined by calculation of the slope in the linear part of the curve during the first 80 seconds at the beginning of the reaction (linear regression function, GraphPad) as described previously (61). Percentage of Gap activity was calculated as (Rate_{inactivated}/Rate_{untreated} × 100%). The results are presented as mean \pm SEM from at least three separate experiments.

S-bacillithiolation of Gap in vitro and reduction by the bacilliredoxin Brx

About 25 μ M of purified Gap was *S*-bacillithiolated with 250 μ M BSH in the presence of 2.5 mM H₂O₂ for 5 min. Excess of BSH and H₂O₂ was removed with Micro Biospin 6 columns (Biorad). For the Brx debacillithiolation assay, Gap-SSB was incubated with Brx, BrxCGA, and BrxAGC at 37°C for 30 min, followed by Gap activity assays and nonreducing BSH-specific Western blot analysis, as described (16).

Western blot analysis

The *S*-bacillithiolated proteins were harvested from *S. aureus* USA300 wild-type and *bshA* mutant cells after exposure to 150 μ M NaOCl, separated by nonreducing SDS-PAGE, and subjected to BSH-specific Western blot analysis using the polyclonal rabbit anti-BSH antiserum, as described previously (16).

Northern blot experiments

Northern blot analyses were performed as described before (15) using RNA isolated from *S. aureus* USA300 wild type under control conditions and after treatment with 150 μ M NaOCl. Hybridization specific for *ohrA* (USA300HOU_0835) was performed with the digoxigenin-labeled RNA probe synthesized *in vitro* using T7 RNA polymerase from T7 promoter containing internal PCR products using the primer pairs *ohrA*-for, 5' TGGCAATACATTATGAACTAAAGC 3', and *ohrA*-T7-rev, 5' CTAATACGACTCACTATAGGGAGA TTAAATCGACATTAATATTTTCCTTGA 3'.

Crystallographic procedures

Before crystallization, H₂O₂-treated overoxidized Gap was concentrated to 11 mg/ml. Crystals of overoxidized Gap were grown at 18°C using the hanging drop vapor diffusion technique and 30% (w/v) PEG 3350, 0.1 M Tris, pH 8.5, as the reservoir solution. Crystals were cryoprotected by transfer into mother liquor mixed with 50% (v/v) PEG 400 in a 1:1 ratio and flash-cooled in liquid nitrogen. X-ray diffraction data were collected from a single crystal at 100 K on beamline 14.1 of the BESSY II storage ring (Berlin, Germany) (56) equipped with a PILATUS 6M detector (Company-REF), with a 0.1° oscillation and exposure time of 0.3 s per frame. Diffraction images were processed using XDS (41). Crystal parameters and data collection statistics are given in Supplementary Table S3. The Gap-SO₃H structure was solved by molecular replacement with Molrep (71) using the structure of the Gap apoenzyme (PDB entry 3LC7; [57]) as a model. The final model of the Gap-SO₃H was generated by iterative rounds of manual model building using Coot (20)

and automated refinement using the phenix.refine package in PHENIX (1) with the inclusion of TLS parameters generated by the TLSMD server (59). Coordinates and structure factor amplitudes have been deposited in the Protein Data Bank (4) under the accession code 5T73 and will be released upon publication.

Molecular docking of BSH into the Gap active site

To model a covalent complex between BSH and the *S. aureus* Gap active site Cys151, docking experiments were performed with the holo form containing NAD [PDB code: 3LVF chain R, (57)] as well as the apo form [PDB code: 3LC7 chain O, (57)] of the enzyme. Before molecular docking, both protein structures were prepared using the protein preparation wizard (68) in the Schrodinger software (Release 2016–1) graphical user interface Maestro. Hydrogen was added according to the protonation states at pH of 7.0 as predicted by PROPKA, bond orders were assigned, and disulfide bonds were allocated. Water with less than three hydrogen bonds to nonwater residues was removed and minimization of heavy atoms was performed using OPLS3. The BSH structure was obtained from Pubchem (ID: CID 42614123) and processed with the ligand preparation wizard. The ligand was protonated at pH of 7.0 ± 2.0 using Epik (28). Covalent molecular docking was performed using CovDock (79), which combines the two programs Glide (23) for docking and Prime (39, 40) for minimization. Cysteine 151 was set as reactive residue, and the reaction type was disulfide formation. All atom positions were fixed, except for the targeted residue and the ligand. Covalent docking was performed with default options and the poses were ranked according to the Prime energy.

Acknowledgments

This work was supported by a grant from the Deutsche Forschungsgemeinschaft (AN746/4-1) within the SPP1710 on Thiol-based Redox switches, by the DFG grants AN746/3-1 and project C1 of the Research Training Group GRK1947, and by the ERC Consolidator Grant (GA 615585) MYCOTHIOLOME to H.A. Protein crystal structure analysis was supported by an Alexander von Humboldt postdoc fellowship to A.J.P.-B. Molecular docking was supported by the Klaus Tschira Foundation to L.T., K.K., and F.G. The authors would like to thank Sandra Maaß and Dörte Becher (University of Greifswald) for MS of the ICAT-labeled peptides. MS of the over-oxidized Gap was performed at the Centre for Chemical Microscopy (ProVIS) at the Helmholtz Centre for Environmental Research, which is supported by European regional development funds (EFRE-Europe Funds Saxony) and the Helmholtz Association. The authors are grateful to Ambrose Cheung for the kind gift of *S. aureus* USA300 *bshA* mutant.

Author Disclosure Statement

No competing financial interests exist.

References

- Adams PD, Afonine PV, Bunkoczi G, Chen VB, Davis IW, Echols N, Headd JJ, Hung LW, Kapral GJ, Grosse-Kunstleve RW, McCoy AJ, Moriarty NW, Oeffner R, Read RJ, Richardson DC, Richardson JS, Terwilliger TC, and Zwart PH. PHENIX: a comprehensive Python-based system for macromolecular structure solution. *Acta Crystallogr D Biol Crystallogr* 66: 213–221, 2010.
- Archer GL. *Staphylococcus aureus*: a well-armed pathogen. *Clin Infect Dis* 26: 1179–1181, 1998.
- Bedhomme M, Adamo M, Marchand CH, Couturier J, Rouhier N, Lemaire SD, Zaffagnini M, and Trost P. Glutathionylation of cytosolic glyceraldehyde-3-phosphate dehydrogenase from the model plant *Arabidopsis thaliana* is reversed by both glutaredoxins and thioredoxins in vitro. *Biochem J* 445: 337–347, 2012.
- Berman HM, Westbrook J, Feng Z, Gilliland G, Bhat TN, Weissig H, Shindyalov IN, and Bourne PE. The Protein Data Bank. *Nucleic Acids Res* 28: 235–242, 2000.
- Blanc B, Gerez C, and Ollagnier de Choudens S. Assembly of Fe/S proteins in bacterial systems: biochemistry of the bacterial ISC system. *Biochim Biophys Acta* 1853: 1436–1447, 2015.
- Bonn F, Bartel J, Büttner K, Hecker M, Otto A, and Becher D. Picking vanished proteins from the void: how to collect and ship/share extremely dilute proteins in a reproducible and highly efficient manner. *Anal Chem* 86: 7421–7427, 2014.
- Botello-Morte L, Pellicer S, Sein-Echaluce VC, Contreras LM, Neira JL, Abian O, Velazquez-Campoy A, Peleato ML, Fillat MF, and Bes MT. Cysteine mutational studies provide insight into a thiol-based redox switch mechanism of metal and DNA binding in FurA from *Anabaena* sp. PCC 7120. *Antioxid Redox Signal* 24: 173–185, 2016.
- Boucher HW and Corey GR. Epidemiology of methicillin-resistant *Staphylococcus aureus*. *Clin Infect Dis* 46 Suppl 5: S344–S349, 2008.
- Brandes N, Reichmann D, Tiensohn H, Leichert LI, and Jakob U. Using quantitative redox proteomics to dissect the yeast redoxome. *J Biol Chem* 286: 41893–41903, 2011.
- Brandes N, Schmitt S, and Jakob U. Thiol-based redox switches in eukaryotic proteins. *Antioxid Redox Signal* 11: 997–1014, 2009.
- Chen PR, Bae T, Williams WA, Duguid EM, Rice PA, Schneewind O, and He C. An oxidation-sensing mechanism is used by the global regulator MgrA in *Staphylococcus aureus*. *Nat Chem Biol* 2: 591–595, 2006.
- Chen PR, Brugarolas P, and He C. Redox signaling in human pathogens. *Antioxid Redox Signal* 14: 1107–1118, 2011.
- Chen PR, Nishida S, Poor CB, Cheng A, Bae T, Kuechenmeister L, Dunman PM, Missiakas D, and He C. A new oxidative sensing and regulation pathway mediated by the MgrA homologue SarZ in *Staphylococcus aureus*. *Mol Microbiol* 71: 198–211, 2009.
- Chi BK, Busche T, Van Laer K, Bäsell K, Becher D, Clermont L, Seibold GM, Persicke M, Kalinowski J, Messens J, and Antelmann H. Protein S-mycothiolation functions as redox-switch and thiol protection mechanism in *Corynebacterium glutamicum* under hypochlorite stress. *Antioxid Redox Signal* 20: 589–605, 2014.
- Chi BK, Gronau K, Mäder U, Hessling B, Becher D, and Antelmann H. S-bacillithiolation protects against hypochlorite stress in *Bacillus subtilis* as revealed by transcriptomics and redox proteomics. *Mol Cell Proteomics* 10: M111.009506, 2011.
- Chi BK, Roberts AA, Huyen TT, Bäsell K, Becher D, Albrecht D, Hamilton CJ, and Antelmann H. S-bacillithiolation protects conserved and essential proteins against hypochlorite stress in firmicutes bacteria. *Antioxid Redox Signal* 18: 1273–1295, 2013.

17. Davies MJ. Myeloperoxidase-derived oxidation: mechanisms of biological damage and its prevention. *J Clin Biochem Nutr* 48: 8–19, 2011.
18. delCardayre SB, Stock KP, Newton GL, Fahey RC, and Davies JE. Coenzyme A disulfide reductase, the primary low molecular weight disulfide reductase from *Staphylococcus aureus*. Purification and characterization of the native enzyme. *J Biol Chem* 273: 5744–5751, 1998.
19. Deng X, Weerapana E, Ulanovskaya O, Sun F, Liang H, Ji Q, Ye Y, Fu Y, Zhou L, Li J, Zhang H, Wang C, Alvarez S, Hicks LM, Lan L, Wu M, Cravatt BF, and He C. Proteome-wide quantification and characterization of oxidation-sensitive cysteines in pathogenic bacteria. *Cell Host Microbe* 13: 358–370, 2013.
20. Emsley P, Lohkamp B, Scott WG, and Cowtan K. Features and development of Coot. *Acta Crystallogr D Biol Crystallogr* 66: 486–501, 2010.
21. Fomenko DE and Gladyshev VN. Comparative genomics of thiol oxidoreductases reveals widespread and essential functions of thiol-based redox control of cellular processes. *Antioxid Redox Signal* 16: 193–201, 2012.
22. Foster TJ. The *Staphylococcus aureus* “superbug”. *J Clin Invest* 114: 1693–1696, 2004.
23. Friesner RA, Murphy RB, Repasky MP, Frye LL, Greenwood JR, Halgren TA, Sanschagrin PC, and Mainz DT. Extra precision glide: docking and scoring incorporating a model of hydrophobic enclosure for protein-ligand complexes. *J Med Chem* 49: 6177–6196, 2006.
24. Gaballa A, Chi BK, Roberts AA, Becher D, Hamilton CJ, Antelmann H, and Helmann JD. Redox regulation in *Bacillus subtilis*: the bacilliredoxins BrxA(YphP) and BrxB(YqiW) function in de-bacillithiolation of S-bacillithiolated OhrR and MetE. *Antioxid Redox Signal* 21: 357–367, 2014.
25. Gaballa A, Newton GL, Antelmann H, Parsonage D, Upton H, Rawat M, Claiborne A, Fahey RC, and Helmann JD. Biosynthesis and functions of bacillithiol, a major low-molecular-weight thiol in Bacilli. *Proc Natl Acad Sci U S A* 107: 6482–6486, 2010.
26. Graumann J, Lilie H, Tang X, Tucker KA, Hoffmann JH, Vijayalakshmi J, Saper M, Bardwell JC, and Jakob U. Activation of the redox-regulated molecular chaperone Hsp33—a two-step mechanism. *Structure* 9: 377–387, 2001.
27. Gray MJ, Wholey WY, and Jakob U. Bacterial responses to reactive chlorine species. *Annu Rev Microbiol* 67: 141–160, 2013.
28. Greenwood JR, Calkins D, Sullivan AP, and Shelley JC. Towards the comprehensive, rapid, and accurate prediction of the favorable tautomeric states of drug-like molecules in aqueous solution. *J Comput Aided Mol Des* 24: 591–604, 2010.
29. Hampton MB, Kettle AJ, and Winterbourn CC. Involvement of superoxide and myeloperoxidase in oxygen-dependent killing of *Staphylococcus aureus* by neutrophils. *Infect Immun* 64: 3512–3517, 1996.
30. Hawkins CL, Pattison DI, and Davies MJ. Hypochlorite-induced oxidation of amino acids, peptides and proteins. *Amino Acids* 25: 259–274, 2003.
31. Helmann JD. Bacillithiol, a new player in bacterial redox homeostasis. *Antioxid Redox Signal* 15: 123–133, 2011.
32. Helmann JD. Specificity of metal sensing: iron and manganese homeostasis in *Bacillus subtilis*. *J Biol Chem* 289: 28112–28120, 2014.
33. Herrmann JM, Becker K, and Dick TP. Highlight: dynamics of thiol-based redox switches. *Biol Chem* 396: 385–387, 2015.
34. Hildebrandt T, Knuesting J, Berndt C, Morgan B, and Scheibe R. Cytosolic thiol switches regulating basic cellular functions: GAPDH as an information hub? *Biol Chem* 396: 523–537, 2015.
35. Hillion M and Antelmann H. Thiol-based redox switches in prokaryotes. *Biol Chem* 396: 415–444, 2015.
36. Horsburgh MJ, Clements MO, Crossley H, Ingham E, and Foster SJ. PerR controls oxidative stress resistance and iron storage proteins and is required for virulence in *Staphylococcus aureus*. *Infect Immun* 69: 3744–3754, 2001.
37. Ilbert M, Graf PC, and Jakob U. Zinc center as redox switch—new function for an old motif. *Antioxid Redox Signal* 8: 835–846, 2006.
38. Ilbert M, Horst J, Ahrens S, Winter J, Graf PC, Lilie H, and Jakob U. The redox-switch domain of Hsp33 functions as dual stress sensor. *Nat Struct Mol Biol* 14: 556–563, 2007.
39. Jacobson MP, Friesner RA, Xiang Z, and Honig B. On the role of the crystal environment in determining protein side-chain conformations. *J Mol Biol* 320: 597–608, 2002.
40. Jacobson MP, Pincus DL, Rapp CS, Day TJ, Honig B, Shaw DE, and Friesner RA. A hierarchical approach to all-atom protein loop prediction. *Proteins* 55: 351–367, 2004.
41. Kabsch W. Xds. *Acta Crystallogr D Biol Crystallogr* 66: 125–132, 2010.
42. Kay KL, Hamilton CJ, and Le Brun NE. Mass spectrometry of *B. subtilis* CopZ: Cu(i)-binding and interactions with bacillithiol. *Metallomics* 8: 709–719, 2016.
43. Kehr S, Jortzik E, Delahunty C, Yates JR, 3rd, Rahlfs S, and Becker K. Protein S-glutathionylation in malaria parasites. *Antioxid Redox Signal* 15: 2855–2865, 2011.
44. Klebanoff SJ, Kettle AJ, Rosen H, Winterbourn CC, and Nauseef WM. Myeloperoxidase: a front-line defender against phagocytosed microorganisms. *J Leukoc Biol* 93: 185–198, 2013.
45. Kublik A, Deobald D, Hartwig S, Schiffmann CL, Andrades A, von Bergen M, Sawers RG, and Adrian L. Identification of a multi-protein reductive dehalogenase complex in *Dehalococcoides mccartyi* strain CBDB1 suggests a protein-dependent respiratory electron transport chain obviating quinone involvement. *Environ Microbiol* 18: 3044–3056, 2016.
46. Kumsta C and Jakob U. Redox-regulated chaperones. *Biochemistry* 48: 4666–4676, 2009.
47. Lee JW, Soonsanga S, and Helmann JD. A complex thiolate switch regulates the *Bacillus subtilis* organic peroxide sensor OhrR. *Proc Natl Acad Sci U S A* 104: 8743–8748, 2007.
48. Leichert LI, Gehrke F, Gudiseva HV, Blackwell T, Ilbert M, Walker AK, Strahler JR, Andrews PC, and Jakob U. Quantifying changes in the thiol redox proteome upon oxidative stress in vivo. *Proc Natl Acad Sci U S A* 105: 8197–8202, 2008.
49. Lindemann C and Leichert LI. Quantitative redox proteomics: the NOxICAT method. *Methods Mol Biol* 893: 387–403, 2012.
50. Livermore DM. Antibiotic resistance in staphylococci. *Int J Antimicrob Agents* 16 Suppl 1: S3–S10, 2000.
51. Loi VV, Harms M, Müller M, Huyen NT, Hamilton CJ, Hochgräfe F, Pané-Farré J, and Antelmann H. Real-time imaging of the bacillithiol redox potential in the human pathogen *Staphylococcus aureus* using a genetically encoded

52. Loi VV, Rossius M, and Antelmann H. Redox regulation by reversible protein S-thiolation in bacteria. *Front Microbiol* 6: 187, 2015.
53. Lowy FD. *Staphylococcus aureus* infections. *N Engl J Med* 339: 520–532, 1998.
54. Makarova KS, Ponomarev VA, and Koonin EV. Two C or not two C: recurrent disruption of Zn-ribbons, gene duplication, lineage-specific gene loss, and horizontal gene transfer in evolution of bacterial ribosomal proteins. *Genome Biol* 2: 14, 2001.
55. Mallett TC, Wallen JR, Karplus PA, Sakai H, Tsukihara T, and Claiborne A. Structure of coenzyme A-disulfide reductase from *Staphylococcus aureus* at 1.54 Å resolution. *Biochemistry* 45: 11278–11289, 2006.
56. Mueller U, Forster R, Hellmig M, Huschmann FU, Kastner A, Malecki P, Puhlinger S, Rower M, Sparta K, and Steffien M. The macromolecular crystallography beamlines at BESSY II of the Helmholtz-Zentrum Berlin: current status and perspectives. *Eur Phys J Plus* 130: 141, 2015.
57. Mukherjee S, Dutta D, Saha B, and Das AK. Crystal structure of glyceraldehyde-3-phosphate dehydrogenase 1 from methicillin-resistant *Staphylococcus aureus* MRSA252 provides novel insights into substrate binding and catalytic mechanism. *J Mol Biol* 401: 949–968, 2010.
58. Newton GL, Rawat M, La Clair JJ, Jothivasan VK, Budiarto T, Hamilton CJ, Claiborne A, Helmann JD, and Fahey RC. Bacillithiol is an antioxidant thiol produced in Bacilli. *Nat Chem Biol* 5: 625–627, 2009.
59. Painter J and Merritt EA. LSMD web server for the generation of multi-group TLS models. *J Appl Crystallogr* 39: 109–111, 2006.
60. Pattison DI and Davies MJ. Absolute rate constants for the reaction of hypochlorous acid with protein side chains and peptide bonds. *Chem Res Toxicol* 14: 1453–1464, 2001.
61. Peralta D, Bronowska AK, Morgan B, Doka E, Van Laer K, Nagy P, Grater F, and Dick TP. A proton relay enhances H₂O₂ sensitivity of GAPDH to facilitate metabolic adaptation. *Nat Chem Biol* 11: 156–163, 2015.
62. Polgar L. Ion-pair formation as a source of enhanced reactivity of the essential thiol group of D-glyceraldehyde-3-phosphate dehydrogenase. *Eur J Biochem* 51: 63–71, 1975.
63. Poor CB, Chen PR, Duguid E, Rice PA, and He C. Crystal structures of the reduced, sulfenic acid, and mixed disulfide forms of SarZ, a redox active global regulator in *Staphylococcus aureus*. *J Biol Chem* 284: 23517–23524, 2009.
64. Posada AC, Kolar SL, Dusi RG, Francois P, Roberts AA, Hamilton CJ, Liu GY, and Cheung A. Importance of bacillithiol in the oxidative stress response of *Staphylococcus aureus*. *Infect Immun* 82: 316–332, 2014.
65. Pother DC, Gierok P, Harms M, Mostertz J, Hochgrafe F, Antelmann H, Hamilton CJ, Borovok I, Lalk M, Aharonowitz Y, and Hecker M. Distribution and infection-related functions of bacillithiol in *Staphylococcus aureus*. *Int J Med Microbiol* 303: 114–123, 2013.
66. Ralser M, Wamelink MM, Kowald A, Gerisch B, Heeren G, Struys EA, Klipp E, Jakobs C, Breitenbach M, Lehrach H, and Krobitsch S. Dynamic rerouting of the carbohydrate flux is key to counteracting oxidative stress. *J Biol* 6: 10, 2007.
67. Rodriguez-Granillo A and Wittung-Stafshede P. Tuning of copper-loop flexibility in *Bacillus subtilis* CopZ copper chaperone: role of conserved residues. *J Phys Chem B* 113: 1919–1932, 2009.
68. Sastry GM, Adzhigirey M, Day T, Annabhimoju R, and Sherman W. Protein and ligand preparation: parameters, protocols, and influence on virtual screening enrichments. *J Comput Aided Mol Des* 27: 221–234, 2013.
69. Schuppe-Koistinen I, Moldeus P, Bergman T, and Cotgreave IA. S-thiolation of human endothelial cell glyceraldehyde-3-phosphate dehydrogenase after hydrogen peroxide treatment. *Eur J Biochem* 221: 1033–1037, 1994.
70. Sun F, Ding Y, Ji Q, Liang Z, Deng X, Wong CC, Yi C, Zhang L, Xie S, Alvarez S, Hicks LM, Luo C, Jiang H, Lan L, and He C. Protein cysteine phosphorylation of SarA/MgrA family transcriptional regulators mediates bacterial virulence and antibiotic resistance. *Proc Natl Acad Sci U S A* 109: 15461–15466, 2012.
71. Vagin A and Teplyakov A. Molecular replacement with MOLREP. *Acta Crystallogr D Biol Crystallogr* 66: 22–25, 2010.
72. Vospelnikova ND, Safronova MI, Shuvalova ER, Baratova LA, Kniazev SP, and Nagradova NK. Identification of an arginine residue important for catalytic activity in the primary structure of D-glyceraldehyde 3-phosphate dehydrogenase. Studies with the rat skeletal-muscle enzyme. *Biochem J* 199: 757–765, 1981.
73. Weber H, Engelmann S, Becher D, and Hecker M. Oxidative stress triggers thiol oxidation in the glyceraldehyde-3-phosphate dehydrogenase of *Staphylococcus aureus*. *Mol Microbiol* 52: 133–140, 2004.
74. Winterbourn CC and Hampton MB. Thiol chemistry and specificity in redox signaling. *Free Radic Biol Med* 45: 549–561, 2008.
75. Winterbourn CC and Kettle AJ. Redox reactions and microbial killing in the neutrophil phagosome. *Antioxid Redox Signal* 18: 642–660, 2013.
76. Winterbourn CC, Kettle AJ, and Hampton MB. Reactive oxygen species and neutrophil function. *Annu Rev Biochem* 85: 765–792, 2016.
77. Wolf C, Hochgräfe F, Kusch H, Albrecht D, Hecker M, and Engelmann S. Proteomic analysis of antioxidant strategies of *Staphylococcus aureus*: diverse responses to different oxidants. *Proteomics* 8: 3139–3153, 2008.
78. Zaffagnini M, Bedhomme M, Groni H, Marchand CH, Puppo C, Gontero B, Cassier-Chauvat C, Decottignies P, and Lemaire SD. Glutathionylation in the photosynthetic model organism *Chlamydomonas reinhardtii*: a proteomic survey. *Mol Cell Proteomics* 11: M111 014142, 2012.
79. Zhu K, Borrelli KW, Greenwood JR, Day T, Abel R, Farid RS, and Harder E. Docking covalent inhibitors: a parameter free approach to pose prediction and scoring. *J Chem Inf Model* 54: 1932–1940, 2014.

Address correspondence to:

Prof. Haike Antelmann
Institute for Biology-Microbiology
Freie Universität Berlin
Berlin D-14195
Germany

E-mail: haike.antelmann@fu-berlin.de

Date of first submission to ARS Central, September 14, 2016; date of final revised submission, December 6, 2016; date of acceptance, December 7, 2016.

Abbreviations Used

1,3-BPG = 1,3-bis-phosphoglycerate
 BrxAGC = bacilliredoxin active site mutant
 BrxCGA = bacilliredoxin resolving Cys mutant
 BSH = bacillithiol
bshA = gene for BSH glycosyltransferase
 BSSB = oxidized bacillithiol disulfide
 Cdr = CoASH disulfide reductase
 CoASH = coenzymeA
 CV = coefficient of variation
 Cys = cysteine
 DTT = dithiothreitol
 EDTA = ethylenediaminetetraacetic acid
 G3P = glyceraldehyde-3-phosphate
 Gap = glyceraldehyde-3-phosphate dehydrogenase
 Gap-SO₃H = Gap sulfonic acid
 Gap-SSB = S-bacillithiolated Gap
 GlcNAc = N-acetyl glucoseamine
 H₂O₂ = hydrogen peroxide
 HOCl = hypochlorous acid
 ICAT = isotope-coded affinity tag
 IMP = inosine 5'-monophosphate
 IPTG = isopropyl- β -D-thiogalactopyranoside
 LB = Luria bertani
 LC = liquid chromatography
 LMW = low-molecular-weight
 LTQ = linear trap quadrupole
 Mal = malate

Met = methionine
 MPO = myeloperoxidase
 MRSA = methicillin-resistant *Staphylococcus aureus*
 Mrx1 = mycoredoxin1
 MS = mass spectrometry
 MS/MS = tandem mass spectrometry
 NADH = nicotinamide adenine dinucleotide
 NADPH = nicotinamide adenine dinucleotide phosphate
 NaOCl = sodium hypochlorite
 NEM = N-ethylmaleimide
 OxICAT = thiol redox proteomic methods based on the differential labeling of reduced Cys residues with light ICAT and of reversibly oxidized Cys residues with heavy ICAT after reduction using TCEP
 protein-SSB = BSH protein mixed disulfide
 RNS = reactive nitrogen species
 roGFP2 = redox-sensitive green fluorescent protein
 ROS = reactive oxygen species
 RSA = relative surface accessibility
 SDS-PAGE = sodium dodecyl sulfate-polyacrylamide gel electrophoresis
 TCEP = Tris (2-carboxyethyl) phosphine
 Trx = thioredoxin
 TrxR = thioredoxin reductase

Chapter 3

The aldehyde dehydrogenase AldA contributes to the hypochlorite defense and is redox-controlled by protein S-bacillithiolation in *Staphylococcus aureus*

Marcel Imber^{1*}, Vu Van Loi^{1*}, Sylvia Reznikov², Verena Nadin Fritsch¹, Agnieszka J. Pietrzyk-Brzezinska^{3,4}, Janek Prehn¹, Chris Hamilton⁵, Markus C. Wahl^{3,6}, Agnieszka K. Bronowska², Haike Antelmann^{1#}

¹Freie Universität Berlin, Institute for Biology-Microbiology, Königin-Luise-Strasse 12-16, D-14195 Berlin, Germany

²School of Chemistry, Bedson Building, Newcastle University, NE1 7RU Newcastle upon Tyne, UK

³Freie Universität Berlin, Laboratory of Structural Biochemistry, D-14195 Berlin, Germany

⁴Institute of Technical Biochemistry, Faculty of Biotechnology and Food Sciences, Lodz University of Technology, Lodz 90-924, Poland

⁵School of Pharmacy, University of East Anglia, Norwich Research Park, Norwich NR4 7TJ, UK

⁶Helmholtz-Zentrum Berlin für Materialien und Energie, Macromolecular Crystallography, D-12489 Berlin, Germany

Published in: *Redox Biology* 15: 557-568. (2018)

#Corresponding author: haike.antelmann@fu-berlin.de

Authors contributions:

Marcel Imber was involved in the biochemical experiments for AldA and AldAC279S protein purification, AldA enzyme activity assays and Western blot analysis for AldA S-bacillithiolation. Vu Van Loi, Verena Nadin Fritsch and Janek Prehn contributed with the *aldA* mutant constructions, Northern blot experiments, growth and survival assays *in vivo*. All authors prepared the figures for publications and contributed to writing of the manuscript.

* Shared first authorships



Research Paper

The aldehyde dehydrogenase AldA contributes to the hypochlorite defense and is redox-controlled by protein S-bacillithiolation in *Staphylococcus aureus*



Marcel Imber^{a,1}, Vu Van Loi^{a,1}, Sylvia Reznikov^b, Verena Nadin Fritsch^a,
Agnieszka J. Pietrzyk-Brzezinska^{c,d}, Janek Pehn^a, Chris Hamilton^e, Markus C. Wahl^{c,f},
Agnieszka K. Bronowska^b, Haike Antelmann^{a,*}

^a Freie Universität Berlin, Institute for Biology-Microbiology, Königin-Luise-Strasse 12-16, D-14195 Berlin, Germany

^b School of Chemistry, Bedson Building, Newcastle University, NE1 7RU Newcastle upon Tyne, UK

^c Freie Universität Berlin, Laboratory of Structural Biochemistry, D-14195 Berlin, Germany

^d Institute of Technical Biochemistry, Faculty of Biotechnology and Food Sciences, Lodz University of Technology, Lodz 90-924, Poland

^e School of Pharmacy, University of East Anglia, Norwich Research Park, Norwich NR4 7TJ, UK

^f Helmholtz-Zentrum Berlin für Materialien und Energie, Macromolecular Crystallography, D-12489 Berlin, Germany

ARTICLE INFO

Keywords:

Staphylococcus aureus

AldA

Bacillithiol

Hypochlorite stress

MD simulations

ABSTRACT

Staphylococcus aureus produces bacillithiol (BSH) as major low molecular weight (LMW) thiol which functions in thiol-protection and redox-regulation by protein S-bacillithiolation under hypochlorite stress. The aldehyde dehydrogenase AldA was identified as S-bacillithiolated at its active site Cys279 under NaOCl stress in *S. aureus*. Here, we have studied the expression, function, redox regulation and structural changes of AldA of *S. aureus*. Transcription of *aldA* was previously shown to be regulated by the alternative sigma factor SigmaB. Northern blot analysis revealed SigmaB-independent induction of *aldA* transcription under formaldehyde, methylglyoxal, diamide and NaOCl stress. Deletion of *aldA* resulted in a NaOCl-sensitive phenotype in survival assays, suggesting an important role of AldA in the NaOCl stress defense. Purified AldA showed broad substrate specificity for oxidation of several aldehydes, including formaldehyde, methylglyoxal, acetaldehyde and glycol aldehyde. Thus, AldA could be involved in detoxification of aldehyde substrates that are elevated under NaOCl stress. Kinetic activity assays revealed that AldA is irreversibly inhibited under H₂O₂ treatment *in vitro* due to over-oxidation of Cys279 in the absence of BSH. Pre-treatment of AldA with BSH prior to H₂O₂ exposure resulted in reversible AldA inactivation due to S-bacillithiolation as revealed by activity assays and BSH-specific Western blot analysis. Using molecular docking and molecular dynamic simulation, we further show that BSH occupies two different positions in the AldA active site depending on the AldA activation state. In conclusion, we show here that AldA is an important target for S-bacillithiolation in *S. aureus* that is up-regulated under NaOCl stress and functions in protection under hypochlorite stress.

1. Introduction

Staphylococcus aureus is a major human pathogen that causes local wound infections, but also life-threatening systemic and chronic

infections, such as septicemia, endocarditis, necrotizing pneumonia and osteomyelitis [1–3]. Moreover, there is an increasing prevalence of hospital- and community-acquired methicillin-resistant *S. aureus* (MRSA) isolates that are often resistant to multiple antibiotics [4]. *S.*

Abbreviations: ADH, aldehyde dehydrogenase; BSH, bacillithiol; BSSB, oxidized bacillithiol disulfide; CFU, colony-forming unit; CD, catalytic domain; Co-BD, coenzyme-binding domain; DTT, dithiothreitol; EDTA, ethylenediaminetetraacetic acid; FA, formaldehyde; H₂O₂, hydrogen peroxide; HOCl, hypochloric acid; IPTG, isopropyl-β-D-thiogalactopyranoside; LB, Luria Bertani; LMW thiol, low molecular weight thiol; MD, molecular dynamics; MG, methylglyoxal; MHQ, 2-methylhydroquinone; MPO, myeloperoxidase; MRSA, methicillin-resistant *Staphylococcus aureus*; NADH, nicotinamide adenine dinucleotide; NADPH, nicotinamide adenine dinucleotide phosphate; NaOCl, sodium hypochlorite; NEM, N-ethylmaleimide; OD₅₀₀, optical density at 500 nm; RCS, reactive chlorine species; RES, reactive electrophilic species; ROS, reactive oxygen species; SCV, small colony variant; SID, subunit interaction domain; X-gal, 5-bromo-4-chloro-3-indolyl-β-D-galactopyranoside

* Corresponding author.

E-mail address: haike.antelmann@fu-berlin.de (H. Antelmann).

¹ Both authors contributed equally to this work.

<https://doi.org/10.1016/j.redox.2018.02.001>

Received 22 November 2017; Received in revised form 1 February 2018; Accepted 2 February 2018

Available online 05 February 2018

2213-2317/ © 2018 The Authors. Published by Elsevier B.V. This is an open access article under the CC BY-NC-ND license (<http://creativecommons.org/licenses/by-nc-nd/4.0/>).

aureus quickly escapes to bactericidal action of new antibiotics and is therefore classified as ESKAPE pathogen by the “European Center of Disease Prevention and Control” [5]. The successful infection of *S. aureus* is mediated by a high diversity of virulence factors, such as toxins, proteases, lipases, superantigens, as well as efficient protection mechanisms against the host immune defense during invasion [6,7]. During infections, *S. aureus* has to cope with the oxidative burst of activated macrophages and neutrophils, including reactive oxygen and chlorine species (ROS, RCS), such as hydrogen peroxide (H_2O_2) and the strong oxidant hypochlorous acid (HOCl) [8–11]. HOCl is generated in neutrophils from H_2O_2 and chloride by the myeloperoxidase (MPO) which is the main cause of bacterial killing [12,13].

Apart from ROS and RCS, *S. aureus* is frequently exposed to reactive electrophile species (RES), such as quinones and aldehydes that originate from cellular metabolism, as secondary oxidation products from ROS and RCS as well as from external sources, such as antibiotics and host-defense components [11,14–17]. RES are α,β -unsaturated dicarbonyl compounds that have electron-deficient centers and can react with protein thiols via oxidation or thiol-S-alkylation chemistries [16,17]. Methylglyoxal is an example for a highly toxic and reactive aldehyde produced as by-product from triose-phosphate intermediates during glycolysis [14,15]. Methylglyoxal detoxification pathways and their regulatory mechanisms have been widely studied in *E. coli* and *B. subtilis*. *E. coli* utilizes a glutathione (GSH)-dependent glyoxalase pathway and a GSH-independent pathway for methylglyoxal detoxification. In the glyoxalase pathway, methylglyoxal reacts spontaneously with GSH to form hemithioacetal which is converted by glyoxalase-I to S-lactoylglutathione. S-lactoylglutathione is the substrate for glyoxalase-II leading to lactate production [14,18]. The glyoxalase *gloA* and the *nemRA* operon are induced by quinones, aldehydes and HOCl and regulated by the TetR-family NemR repressor in *E. coli* [19–22]. GloA functions as glyoxalase in methylglyoxal detoxification and NemA is an FMN-dependent oxidoreductase involved in detoxification of quinones and aldehydes. Moreover, it was shown that methylglyoxal is produced as consequence of hypochlorite stress and that NemR confers protection to methylglyoxal and HOCl via control of the *gloA-nemRA* operon [20].

Gram-positive Firmicutes, such as *Bacillus subtilis* and *S. aureus* produce bacillithiol (BSH) as GSH surrogate which functions as protection mechanism against redox-active compounds and co-factor for thiol-dependent enzymes [23,24]. Methylglyoxal detoxification in *B. subtilis* involves BSH-dependent and BSH-independent pathways [23,25]. In the BSH-dependent glyoxalase pathway, BSH reacts with methylglyoxal to form BS-hemithioacetal which is converted to S-lactoyl-BSH by Glx-I and further by Glx-II to lactate [23,25]. In addition, the thiol-dependent formaldehyde dehydrogenase AdhA confers protection under formaldehyde and methylglyoxal stress in *B. subtilis* which is controlled by the MerR/NmlR-like regulator AdhR [35]. However, the enzymatic pathways involved in detoxification of reactive aldehydes are unknown in *S. aureus*.

Recently, we identified the glycolytic glyceraldehyde-3-phosphate dehydrogenase GapDH as major S-bacillithiolated protein in *S. aureus* under NaOCl stress [26]. Apart from GapDH, the aldehyde dehydrogenase AldA was S-bacillithiolated at its active site Cys279 under NaOCl stress, which could function in detoxification of methylglyoxal or other aldehyde substrates. Here, we have studied the expression and function of AldA of *S. aureus* under formaldehyde, methylglyoxal and NaOCl stress. Transcriptional studies revealed an increased *aldA* transcription under aldehyde, NaOCl and diamide stress in *S. aureus*. In survival phenotype assays, the *aldA* mutant was more sensitive to NaOCl stress. Using biochemical activity assays, we provide evidence that S-bacillithiolation functions in redox-regulation of AldA activity. All-atom molecular dynamics (MD) simulations suggest that the location of BSH in the AldA active site depends on the Cys activation state in the apo- and holoenzyme structures. In conclusion, our results indicate that AldA plays an important role in the NaOCl stress defense and is

redox-regulated by S-bacillithiolation in *S. aureus*.

2. Materials and methods

2.1. Bacterial strains, growth and survival assays

Bacterial strains, plasmids and primers are listed in Tables S1 and S2. For cloning and genetic manipulation, *E. coli* was cultivated in Luria Bertani (LB) medium. *S. aureus* COL was cultivated either in LB or RPMI medium as described previously [26]. For survival phenotype assays, *S. aureus* COL was grown in RPMI medium until an OD_{500} of 0.5, exposed to 2 mM formaldehyde, 4 mM methylglyoxal and 3.5 mM NaOCl stress and 10 μ l of serial dilutions were spotted onto LB agar plates for 24 h to observe colonies. All complemented *aldA* deletion mutants with plasmid pRB473 were grown in the presence of 1% xylose and 10 μ g/ml chloramphenicol. Sodium hypochlorite, diamide, dithiothreitol (DTT), hydrogen peroxide (H_2O_2 , 35% w/v), formaldehyde, methylglyoxal and 2-methylhydroquinone (MHQ) were purchased from Sigma Aldrich.

2.2. RNA isolation and Northern blot analysis

For RNA isolation, *S. aureus* COL was cultivated in RPMI medium and treated with sub-lethal doses of 1 mM NaOCl, 0.75 mM formaldehyde (FA), 0.5 mM methylglyoxal (MG), 10 mM H_2O_2 and 50 μ M MHQ for different times as described previously [26]. *S. aureus* COL cells were harvested before and after stress exposure and disrupted in lysis buffer [10 mM Tris-HCl, pH 8.0; 200 mM sodium chloride (NaCl); 3 mM ethylene diamine tetra acetic acid (EDTA)] with a Precellys24 ribolyzer. RNA was isolated using acid phenol extraction as described [26] and RNA quality was assessed using the Nanodrop. Northern blot hybridizations were performed with the digoxigenin-labelled *aldA*-specific antisense RNA probe synthesized *in vitro* using T7 RNA polymerase and the primer pairs *aldA*-for and *aldA*-rev (Table S2) as described [26,27].

2.3. Cloning, expression and purification of His-tagged AldA and AldAC279S mutant proteins in *E. coli*

The *aldA* gene was amplified from chromosomal DNA of *S. aureus* COL by PCR using primers *aldA*-for-*NheI* and *aldA*-rev-*BamHI* (Table S2), digested with *NheI* and *BamHI* and inserted into plasmid pET11b (Novagen) that was digested using the same enzymes to generate plasmid pET11b-*aldA*. For construction of pET11b expressing AldAC279S mutant protein, Cys279 was replaced by serine using PCR mutagenesis. Two first-round PCR reactions were performed using primer pairs *aldA*-for-*NheI* and *aldA*-C279S-Rev as well as primer pairs *aldA*-C279S-for and *aldA*-rev-*BamHI* (Table S2). The two first round PCR products were hybridized and subsequently amplified by a second round of PCR using primers *aldA*-for-*NheI* and *aldA*-rev-*BamHI*. The second-round PCR products were digested with *NheI* and *BamHI* and inserted into plasmid pET11b digested with the same enzymes to generate plasmid pET11b-*aldAC279S*. The correct *aldA* and *aldAC279S* sequences of the plasmids were confirmed by DNA sequencing. Plasmid pET11b-*aldAC279S* was also used for construction of the *aldAC279S* mutant *in vivo* and subcloned into the *E. coli*/*S. aureus* shuttle vector pRB473 as described below.

For expression and purification of His-tagged AldA and AldAC279S mutant protein, *E. coli* BL21(DE3) *plysS* was used expressing plasmids pET11b-*aldA* and pET11b-*aldAC279S*, respectively. Cultivation was performed in 1 l LB medium until the exponential growth phase at OD_{600} of 0.8 followed by addition of 1 mM isopropyl- β -D-thiogalactopyranoside (IPTG) for 3.5 h at 37 °C. Recombinant His-AldA and His-AldAC279S mutant proteins were purified after sonication of the *E. coli* cells in binding buffer (20 mM NaH_2PO_4 , 500 mM NaCl, 20 mM imidazole, pH 7.4). Lysates were cleared from cell debris by repeated centrifugation and purification of the His-AldA and His-AldAC279S

mutant proteins was performed by application of an imidazole gradient (0–500 mM) using His Trap™ HP Ni-NTA columns (5 ml; GE Healthcare, Chalfont St. Giles, UK) and the ÄKTA purifier liquid chromatography system (GE Healthcare) according to the instructions of the manufacturer. Purified proteins were extensively dialyzed against 10 mM Tris-HCl (pH 8.0), 100 mM NaCl, and stored on ice until usage.

2.4. Construction of the *S. aureus* COL *aldA* deletion mutant and the complemented *aldA* and *aldAC279S* mutant strains

The *S. aureus* COL *ΔaldA* deletion mutant was constructed by allelic replacement via the temperature-sensitive shuttle vector pMAD as described [28]. Briefly, for construction of the plasmids pMAD-*ΔaldA*, the 500 bp up- and downstream flanking gene regions of *aldA* were amplified using the primers *aldA*-pMAD-up-for/rev and *aldA*-pMAD-down-for/rev from *S. aureus* COL genomic DNA (Table S2). The *aldA* up- and downstream flanking regions were fused by overlap extension PCR and ligated into the *Bgl*II and *Sall* sites of plasmid pMAD. The pMAD constructs were electroporated into the restriction-negative and methylation-positive intermediate *S. aureus* RN4220 strain and further transferred to *S. aureus* COL by phage transduction using phage 80 [29]. Transductants were streaked out on LB agar with 10 µg/ml erythromycin and 40 µg/ml 5-bromo-4-chloro-3-indolyl-β-D-galactopyranoside (X-gal) at 30 °C. Blue transductants with pMAD integrations were selected for plasmid excision by a heat shock as described [30]. Erythromycin-sensitive white colonies were selected on X-gal plates and screened for *aldA* deletions by PCR and DNA sequencing.

The complemented *aldA* and *aldAC279S* mutant strains were constructed using the pRB473 plasmid as described [31]. Briefly, *aldA* and *aldAC279S* sequences were amplified from plasmids pET11b-*aldA* and pET11b-*aldAC279S* using the primers *aldA*-pRB-for-*Bam*HI and *aldA*-pRB-rev-*Kpn*I. The PCR products were digested with *Bam*HI and *Kpn*I and inserted into the pRB473 plasmid that was digested using the same enzymes resulting in plasmids pRB473-*aldA* and pRB473-*aldAC279S*. The plasmids were transferred to the *ΔaldA* mutant via phage transduction as described [31].

2.5. AldA activity assays

AldA activity was monitored spectrophotometrically at 340 nm and 30 °C with the substrate and NAD⁺ as cofactor by the production of NADH using a CLARIOstar (BMG Labtech) spectrophotometer. The oxidation of different aldehyde substrates (formaldehyde, methylglyoxal, acetaldehyde and glycol aldehyde) was measured in an assay mixture containing 1.25 mM NAD⁺ and 2.5 µM AldA in reaction buffer (100 mM Tris-HCl, 1.25 mM EDTA, pH 7.5). After pre-incubation, the reaction was started by addition of the aldehyde substrates and NADH production was measured at 340 nm. The kinetic curves are presented as mean ± SEM from at least three independent experiments.

2.6. Western blot analysis

The purified His-AldA protein was separated using 12% SDS-PAGE and subjected to BSH-specific Western blot analysis using the polyclonal rabbit anti-BSH antiserum as described previously [32].

2.7. Molecular docking of the *S*-bacillithiolated AldA Cys279 active site

To model a covalent complex between BSH and the AldA Cys279 active site by molecular docking, the crystal structure of AldA from *S. aureus* was used as a receptor (PDB code 3TY7). The missing loop (residues 438–459) was modelled and fitted using MODELLER [33]. To identify the potential BSH binding site, FTMap solvent mapping calculations were performed [34] and two highest-occupancy binding sites were considered in the further calculations (Fig. 7EF). In the Q1 site, the NAD⁺ molecule has been fitted using crystal structures of the

Pseudomonas fluorescens pfAMSDH co-crystallised with NAD⁺ (PDB code 4I1W). Then, the hydrogen atoms were added, and the charges for NAD⁺ molecule were assigned using AM1-BCC method [35]. The Cys279 thiol group was considered deprotonated. The BSH molecule was built, energy minimised (5000 cycles of steepest-descent minimisation), and the partial atomic charges were generated using AM1-BCC [35].

Molecular docking was performed using the University of California, San Francisco DOCK 6.8 suite [36] with grid scoring in an implicit solvent. The grid spacing was 0.25 Å, and the grid included 12 Å beyond the NAD⁺ modelled, which was subsequently removed for the pose Q2. The energy score was the sum of electrostatic and van der Waals contributions. To check the suitability of the methodology, the NAD⁺ was removed from the binding site, its translational and rotational degrees of freedom were altered and the molecule has been redocked to the protein, in order to check whether the docking procedure was able to reproduce the native binding mode, as observed in related crystal structures. After the positive verification, the BSH molecule was docked to both Q1 (holo-enzyme with NAD⁺) and Q2 (apo-enzyme without NAD⁺) sites detected by FTMap [34].

During the docking calculations, the BSH molecule was subjected to 5000 cycles of molecular-mechanical energy minimisation at the protein-binding site. The number of maximum ligand orientations was 50,000. The constraint was the distance between sulfur atoms from the Cys279 thiol and the sulfur of BSH. The 25 best-scoring poses (BSH-protein complexes) were further analyzed by means of secondary rescoring using SeeSAR <https://www.biosolveit.de/SeeSAR/> package with more accurate HYDE scoring function [37]. The best-scoring poses in Q1 and Q2 putative binding sites were subjected to all-atom MD simulations.

2.8. Molecular dynamics (MD) simulation of *S*-bacillithiolation

All simulations for the 5 studied systems: apo-enzyme, holo-enzyme (protein-NAD⁺), BSH-holo-enzyme (Q1), BSH-apo-enzyme (Q1), and BSH-apo-enzyme (Q2) were carried out using GROMACS2016.2 code [38], with Amber99SB-ILDN [39] force field for the duplexes and the TIP3P water model. Parameters for NAD⁺ and BSH were assigned by ACPYPE [40]. Obtained partial atomic charges were derived using the RESP methodology [41] and validated with the Gaussian09 programme [42] using HF/6-31G* basis set.

The temperature was kept constant at T = 300 K by using velocity rescaling with a coupling time of 0.1 ps. The pressure was kept constant at 1 bar using an isotropic coupling to Parrinello-Rahman barostat with a coupling time of 0.1 ps [43]. A cut-off of 1 nm was used for all non-bonded interactions. Long-range electrostatic interactions were treated with the particle-mesh Ewald [44] method using a grid spacing of 0.1 nm with cubic interpolation. All bonds between hydrogens and heavy atoms were constrained using the LINCS algorithm [45]. Each of the systems were immersed in a cubic TIP3P water box containing ~ 115,000 atoms. Simulation units were maintained neutral by adding sodium and chloride counter ions (0.1 M concentration).

Prior to MD simulations, the systems undergone 50,000 steps of molecular mechanical energy minimisation. This was followed by 100 ps MD simulations, during which position constraints were used on all backbone atoms, heavy atoms of BSH and NAD⁺. After the following unrestrained equilibration phase (10 ns) the production runs were carried out for 50 ns, with an integration time step of 2 fs. The cut-off for non-bonded interactions was 0.1 nm. The atomic coordinates were saved every 100 ps. For the visual inspection of the results we used xmgrace [46] and UCSF Chimera [47] packages. Free binding energy calculations have been performed using the MMPBSA.py program from AmberTools package [48]. Binding energies have been calculated between BSH and the protein at the two different binding sites, as in Q1 and Q2, for the last 25 ns of the simulation.

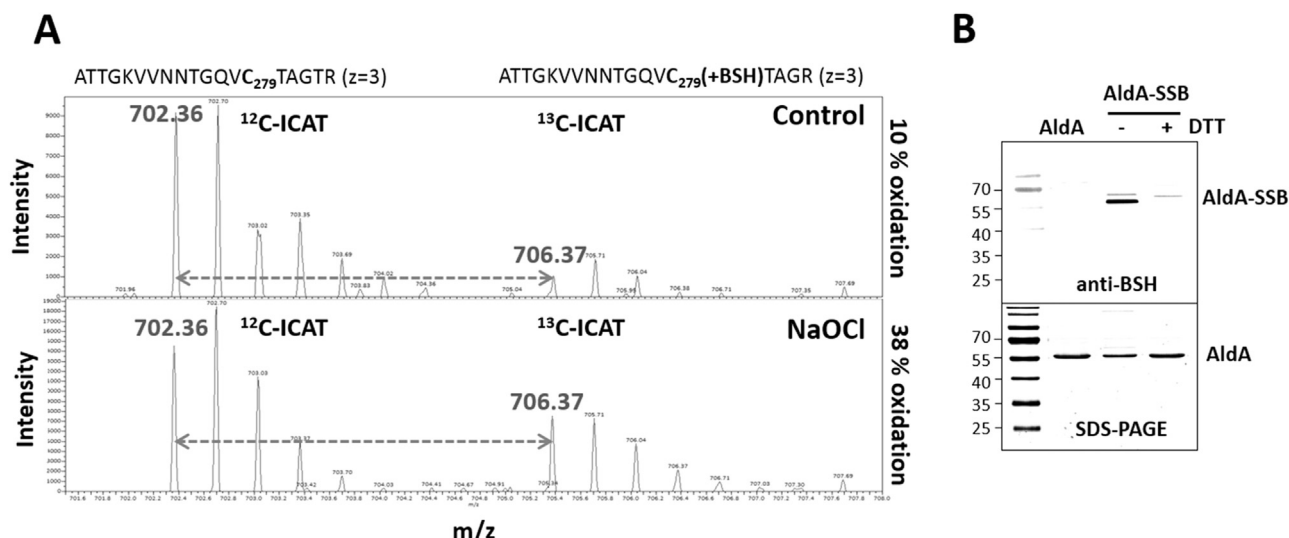


Fig. 1. OxICAT analysis revealed a 29% increased oxidation of the AldA Cys279-peptide (A) and S-bacillithiolation of the AldA protein *in vitro* is shown by BSH-specific Western blot analysis (B). (A) The OxICAT mass spectrometry results from the previous study [26] are shown for the AldA-Cys279-peptide in *S. aureus* under control and 30 min after NaOCl stress. The reduced Cys279-peptides is labelled with light ¹²C-ICAT, followed by reduction of the S-bacillithiolated Cys279-peptide and labelling with heavy ¹³C-ICAT reagent. The Cys279-peptide was 10% oxidized in the control and 38% oxidized in the NaOCl stress sample indicating a 29% oxidation increase. (B) AldA is S-bacillithiolated *in vitro* by H₂O₂ in the presence of BSH as revealed by BSH-specific Western blots. Reduced purified AldA (40 μM) is pretreated with 10-fold molar excess of BSH (400 μM) and incubated with 10 mM H₂O₂ for 5 min. The S-bacillithiolated AldA was detected using non-reducing BSH-specific Western blot analysis. The loading control of AldA and S-bacillithiolated AldA (AldA-SSB) is shown as SDS-PAGE stained with Coomassie below the anti-BSH blot.

3. Results

3.1. The aldehyde dehydrogenase AldA is strongly oxidized at its active site Cys279 due to S-bacillithiolation under NaOCl stress in *S. aureus*

The aldehyde dehydrogenase AldA was previously identified as S-bacillithiolated at its catalytic active site Cys279 in *S. aureus* and *Staphylococcus carnosus* [26,32]. In addition, both aldehyde dehydrogenases, GapDH and AldA displayed the highest oxidation increase of 29% under NaOCl stress in *S. aureus* using the thiol-redox proteomics approach OxICAT [26]. The OxICAT method is based on thiol-labelling of the reduced AldA Cys279 peptide with light ¹²C-ICAT reagent, followed by reduction of the Cys279-SSB peptide and its labelling with heavy ¹³C-ICAT reagent [49]. The percentage oxidation of the Cys279 peptide of AldA under control and NaOCl stress is reflected by the mass spectra of the ICAT-labelled peptide pair as quantified in the previous study [26] (Fig. 1A). The strong 29% oxidation increase of the active site Cys279 is shown here again which is caused by S-bacillithiolation [26]. To confirm that AldA can be S-bacillithiolated also *in vitro*, we expressed and purified His-tagged AldA from *E. coli* extracts. Purified AldA was treated with H₂O₂ after pre-exposure to 10-fold excess of BSH and the reversible S-bacillithiolation of AldA was verified using BSH-specific Western blot analyses in the absence and presence of DTT (Fig. 1B). The S-bacillithiolated AldA band is denoted with AldA-SSB. Next, we were interested to study the expression, function, redox-regulation and structural changes of AldA under NaOCl and aldehyde stress.

3.2. Transcription of *aldA* is induced SigmaB-independently under thiol-specific stress conditions by formaldehyde, NaOCl and diamide in *S. aureus* COL

We used Northern blot analysis to study *aldA* transcription in *S. aureus* COL under different thiol-specific stress conditions, including sub-lethal doses of 1 mM NaOCl, 2 mM diamide, 0.75 mM formaldehyde, 0.5 mM methylglyoxal, 50 μM methylhydroquinone (MHQ) and 10 mM H₂O₂ (Fig. 2A). The Northern blot results revealed that *aldA* transcription is strongly induced in *S. aureus* COL wild type after exposure to formaldehyde, diamide and NaOCl stress, but less strongly

under methylglyoxal stress (Fig. 2A). No significant induction of *aldA* was detected under MHQ and H₂O₂ treatment. These transcriptional results indicate that AldA could be involved in the hypochlorite stress defense or in detoxification of aldehydes. In previous microarray experiments, *aldA* was identified as member of the SigmaB general stress regulon, which responds to heat and salt stress (NaCl), MnCl₂ and alkaline stress conditions in *S. aureus* [50,51]. The *sigB*-dependent promoter sequence was mapped in the *aldA* regulatory upstream region (GTTTAT-N14-GGATAA) as promoter U1137.SigB.M2 previously (Fig. 2B) [52]. In the condition-dependent transcriptome of *S. aureus* NCTC8325-4 [53], the strongest *aldA* transcription was monitored during the stationary phase in rich LB and TSB medium as well as during plasma stress as visualized by the Aureowiki Expression data browser (http://genome.jouy.inra.fr/cgi-bin/aeb/viewdetail.py?id=NA_2184537_2185964_-1) [52].

To investigate whether the thiol-specific induction of *aldA* transcription by formaldehyde, diamide and NaOCl requires SigmaB, we performed Northern blot analysis with RNA isolated from a *sigB* deletion mutant in comparison to the wild type (Fig. 2B). The Northern blot results showed similar *aldA* transcriptional induction in the *sigB* mutant under NaOCl, diamide and formaldehyde stress compared to the wild type. Even a higher *aldA* transcription occurred under methylglyoxal stress in the *sigB* mutant. These results indicate that *aldA* transcription is subject to SigmaB-independent control mechanisms under thiol-specific stress conditions by an unknown thiol-specific transcription factor that remains to be elucidated. No additional SigA promoter was identified upstream of *aldA* previously [52], presumably because the conditions were different compared to our thiol-stress conditions. In previous studies, a refined consensus for SigA- and SigB-dependent promoter sequences was revealed based on 93% of *S. aureus* transcriptional units [52]. In the *aldA* regulatory region, a putative SigA-dependent promoter was identified upstream of the SigB promoter, which could drive the thiol-specific expression of *aldA* (Fig. 2B).

3.3. AldA plays important roles in the defense against NaOCl stress in *S. aureus* COL

Next, we analyzed the role of AldA in protection under NaOCl and aldehyde stress in *S. aureus*. It was previously shown that methylglyoxal

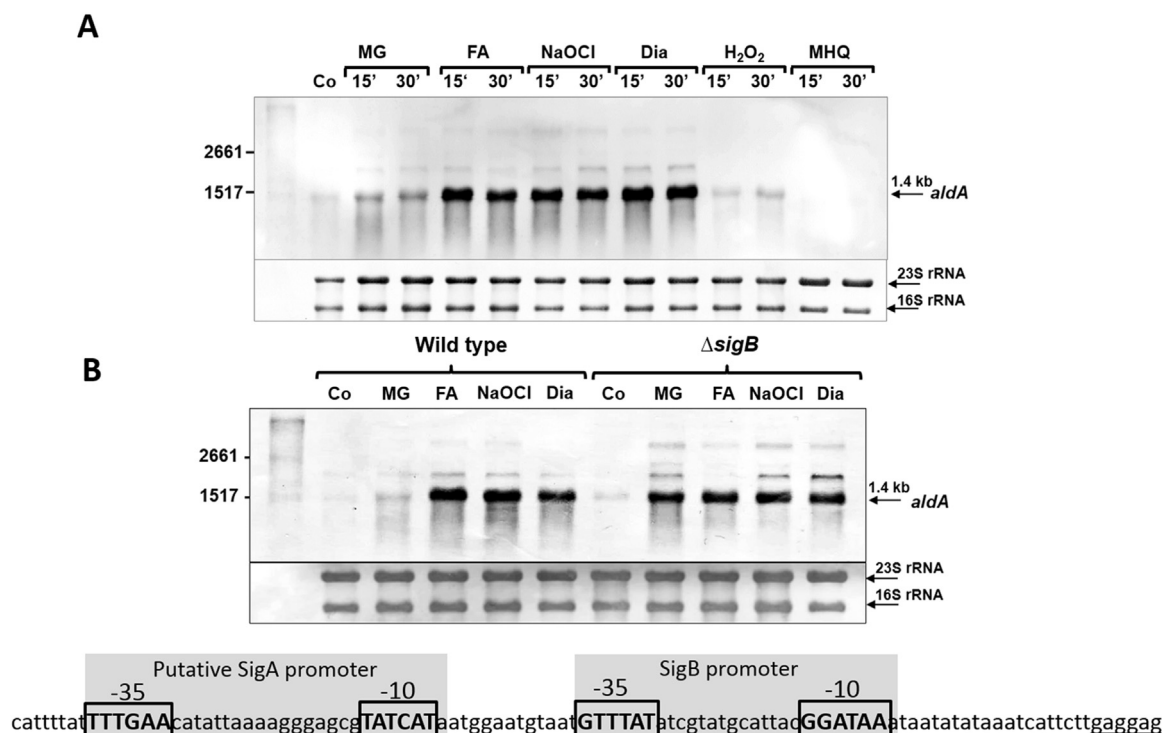


Fig. 2. Transcriptional induction of *aldA* under formaldehyde, methylglyoxal, NaOCl and diamide stress in *S. aureus* COL wild type (A) and in the *sigB* mutant (B). (A) RNA was isolated from *S. aureus* COL wild type under control conditions as well as after treatment with sub-lethal doses of 0.75 mM formaldehyde, 0.5 mM methylglyoxal, 1 mM NaOCl, 2 mM diamide, 10 mM H₂O₂ and 50 μ M methylhydroquinone (MHQ) for 15 and 30 min and subjected to Northern blot analysis for *aldA* (SACOL2114) transcription. (B) For comparison of Northern blot analysis of *aldA* transcription between the wild type and the *sigB* mutant, RNA was isolated from *S. aureus* COL wild type and the *sigB* mutant after exposure to 0.75 mM formaldehyde, 0.5 mM methylglyoxal, 1 mM NaOCl and 2 mM diamide for 15 min. Transcription of *aldA* is similarly up-regulated under formaldehyde, NaOCl and diamide stress in the wild type (A) and in the *sigB* mutant (B) indicating a SigmaB-independent thiol-stress regulatory mechanism of *aldA* transcription. The known SigmaB-dependent promoter sequence and a putative SigA-dependent promoter in the *aldA* upstream regulatory region are shown below the Northern blot in (B). The methylene blue stain is the RNA loading control showing the abundant 16S and 23S rRNAs. The experiments were performed in 3 biological replicates.

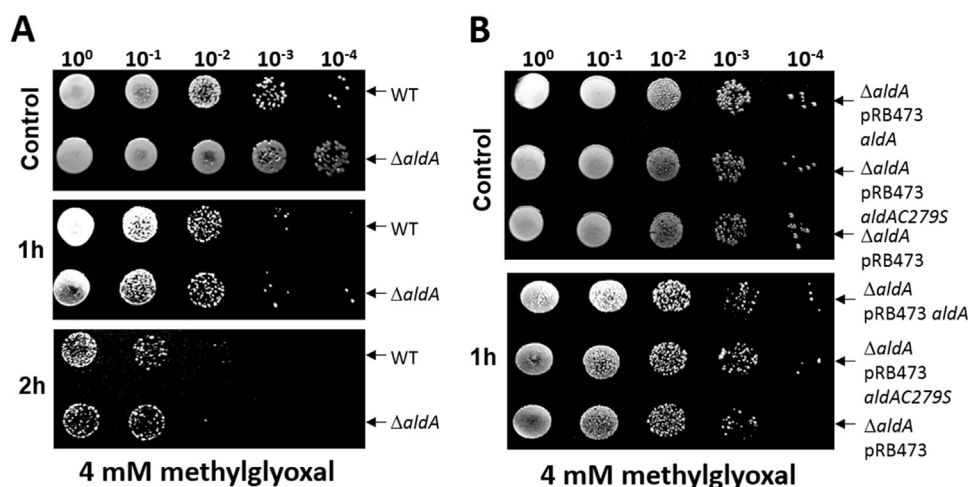


Fig. 3. AldA is not essential for the survival of *S. aureus* under methylglyoxal stress. For the survival phenotype assays, *S. aureus* COL wild-type (WT), the $\Delta aldA$ deletion mutant (A) and the *aldA* and *aldAC279S* complemented $\Delta aldA$ mutants ($\Delta aldA$ pRB473-*aldA* and $\Delta aldA$ pRB473-*aldAC279S*) (B) were grown in RPMI until an OD₅₀₀ of 0.5 and treated with 4 mM methylglyoxal. Survival assays were performed by spotting 10 μ l of serial dilutions after 1–3 h of NaOCl exposure onto LB agar plates. The experiments were performed in 3 biological replicates.

is produced in *E. coli* cells treated with HOCl [20]. Thus, AldA could function in methylglyoxal detoxification under HOCl stress also in *S. aureus*. AldA harbors a conserved active site Cys279 which is essential for its catalytic activity [54–56]. The function of AldA and the conserved Cys279 under methylglyoxal, formaldehyde and HOCl stress was analyzed in growth and survival assays of an *aldA* deletion mutant and its *aldA* and *aldAC279S* complemented strains (Figs. 3, 4, S1 and S2). The growth of the *aldA* mutant was not affected under sub-lethal formaldehyde and methylglyoxal stress in comparison to the wild type (Fig. S1). In addition, no significant phenotypes of the *aldA* mutant and the *aldA* complemented strains were detected in survival assays after exposure to 4 mM methylglyoxal (Fig. 3AB) and 2 mM formaldehyde

stress (Fig. S2). However, the *aldA* mutant was significantly impaired in growth after exposure to sub-lethal concentrations of 1.5 mM NaOCl stress (Fig. 4A). In survival assays, the *aldA* mutant showed also a strongly decreased survival after treatment with 3.5 mM NaOCl (Fig. 4C). This survival defect of the $\Delta aldA$ mutant could be restored back to wild type level in the *aldA* complemented strain, but not in the *aldAC279S* mutant (Fig. 4D). This indicates that AldA is involved in protection of *S. aureus* against NaOCl stress and that Cys279 is essential for AldA activity *in vivo*.

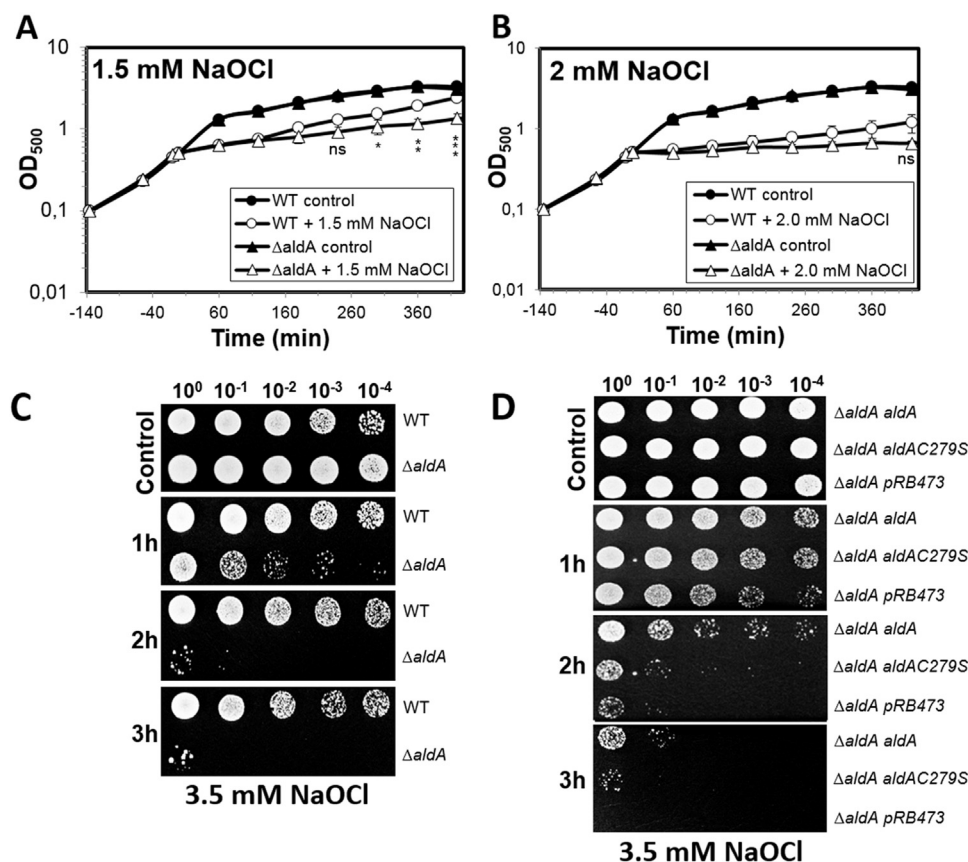


Fig. 4. AldA is required for growth and survival under NaOCl stress in *S. aureus*. (A, B) Growth curves of *S. aureus* COL wild type and the *aldA* deletion mutant in RPMI medium after exposure to sublethal concentrations of 1.5 mM and 2 mM NaOCl stress at an OD₅₄₀ of 0.5. The growth differences of the *aldA* mutant are significantly different compared to the wild type at 1.5 mM NaOCl. (C, D) For the survival phenotype assays, *S. aureus* COL wild-type (WT), the *aldA* deletion mutant (C) and the *aldA* and *aldAC279S* complemented *aldA* mutants (*aldA* pRB473-*aldA* and *aldA* pRB473-*aldAC279S*) (D) were grown in RPMI until an OD₅₀₀ of 0.5 and treated with 3.5 mM NaOCl. Survival assays were performed by spotting 10 μ l of serial dilutions after 1–3 h of NaOCl exposure onto LB agar plates. Colonies were observed after overnight incubation of the LB plates at 37 °C. The active site Cys279 of AldA is required for NaOCl stress survival. The results for the growth curves and survival assays are from 5 biological replicate experiments. For the growth curves in Fig. 4AB, error bars represent the SEM and the statistics was calculated using a Student's unpaired two-tailed *t*-test by the graph prism software. Symbols are defined as follows: ns $p > 0.05$; * $p \leq 0.05$; ** $p \leq 0.01$ and *** $p \leq 0.001$.

3.4. AldA shows broad substrate specificity for oxidation of various aldehyde substrates, including formaldehyde and methylglyoxal *in vitro*

To study the function and substrate specificity of AldA *in vitro*, the catalytic activity was measured using different aldehyde substrates, including formaldehyde, methylglyoxal, glycol aldehyde and acet-aldehyde in concentrations ranging from 0.5 to 100 mM. AldA activity was measured in a spectrophotometric assay in the presence of NAD⁺ as a cofactor with the different aldehyde substrates by monitoring the NADH production as absorbance increase at 340 nm. The AldA activity assays revealed increasing NADH production with increasing concentrations of all aldehyde substrates indicating that AldA has broad substrate specificities (Fig. 5). AldA showed the highest activities with 55 mM formaldehyde and 20 mM methylglyoxal, which could be possible substrates of AldA. Formaldehyde and methylglyoxal are oxidized to formate and lactate by AldA, resulting in NADH generation.

To further confirm that Cys279 is the active site residue and essential for AldA activity, we used the purified AldAC279S mutant protein which was analyzed for formaldehyde and methylglyoxal oxidation in the AldA activity assays. However, the AldAC279S mutant protein did not show significant activity for formaldehyde and methylglyoxal oxidation in our activity assays (Fig. S4). This indicates that the conserved Cys279 is the active site residue and required for AldA activity as shown also for other homologs previously [54,55,57].

3.5. AldA is redox-regulated and protected by protein S-bacillithiolation under H₂O₂ stress *in vitro*

We were interested whether S-bacillithiolation inhibits AldA activity and protects the active site Cys279 against overoxidation *in vitro*. Using the spectrophotometric assay, AldA activity was measured after oxidative stress with 15 mM methylglyoxal as substrate and NAD⁺ as coenzyme by monitoring NADH generation at 340 nm. Treatment of

AldA with 0.5–1 mM H₂O₂ resulted in a strong inactivation of its enzymatic activity (Fig. 6A). Inactivation of AldA with H₂O₂ alone was irreversible since AldA activity could not be restored after treatment with 10 mM DTT (Fig. 6B). These results indicate that the active site Cys279 of AldA is very sensitive to overoxidation by H₂O₂ in the absence of BSH. To assess the effect of S-bacillithiolation on AldA activity, the enzyme was pre-exposed to 0.3–0.5 mM BSH prior to oxidation with 0.3–1 mM H₂O₂ and the remaining AldA activity was measured in the spectrophotometric assay with 15 mM methylglyoxal as substrate. AldA activity was inhibited with 0.3–1 mM H₂O₂ after pre-treatment with 0.3–0.5 mM BSH (Fig. 6C). In this case, however, the activity of the oxidized AldA protein could be restored to 66% by DTT reduction indicating that AldA is subject to reversible S-bacillithiolation in the presence of BSH and H₂O₂ (Fig. 6D). S-bacillithiolation of AldA and its reversibility with DTT was further confirmed in BSH-specific Western blots (Fig. 1B). These results suggest that S-bacillithiolation protects the AldA active site Cys279 against overoxidation and functions in redox-regulation of AldA activity *in vitro*.

3.6. Structural comparison of AldA with other aldehyde dehydrogenases

We were further interested in the structure and the structural changes of AldA upon S-bacillithiolation. A crystal structure of *S. aureus* AldA (denoted as saAldA) has been determined by the Midwest Center for Structural Genomics (PDB 3TY7). For understanding the enzyme's catalytic mechanism, we performed structural homology searches for saAldA with the DALI server [58] (http://ekhidna.biocenter.helsinki.fi/dali_server/) and the PDBeFold (SSM) server (<http://www.ebi.ac.uk/msd-srv/ssm/>). SaAldA shows high homology to many other aldehyde dehydrogenases (ADHs) from bacteria, plants and humans. The root-mean-square deviations (r.m.s.d.'s) and sequence similarities of AldA's closest homologs are listed in Table S3.

In contrast to the tetrameric bacterial ADHs (*pf*AMSDH, *sa*BADH,

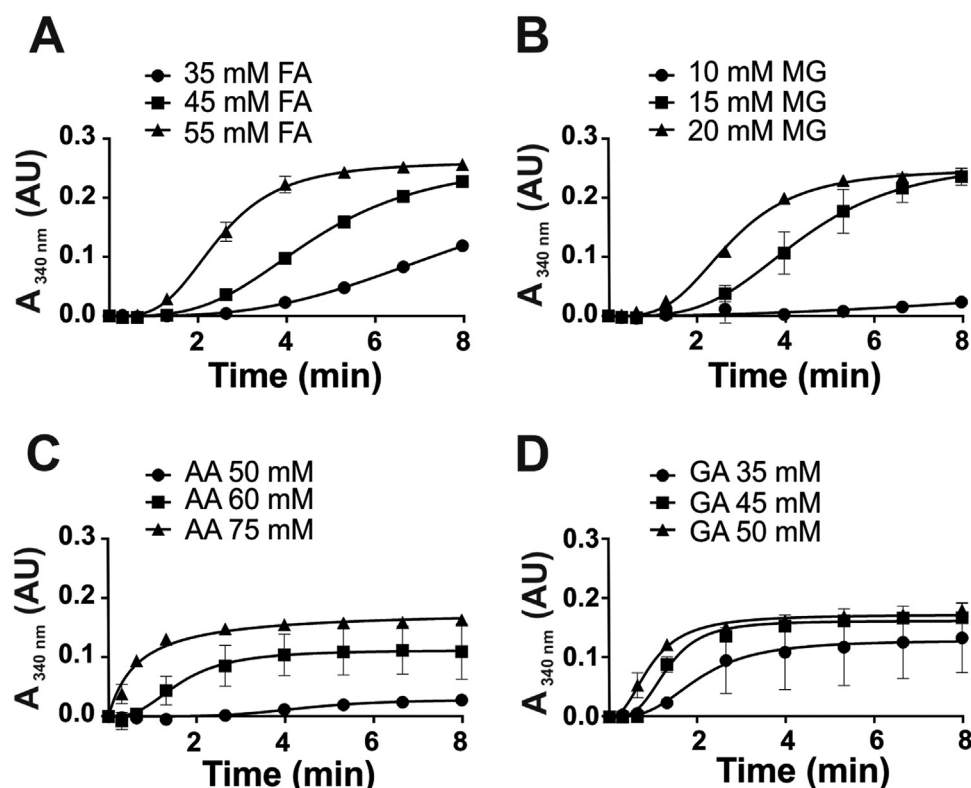


Fig. 5. Purified AldA shows broad substrate specificity towards various aldehydes *in vitro*. The catalytic activity of the aldehyde dehydrogenase AldA was analyzed with increasing concentrations of different aldehyde substrates, including (A) formaldehyde (FA), (B) methylglyoxal (MG), (C) acetaldehyde (AA) and (D) glycol aldehyde (GA). Reduced AldA (2.5 μ M) was incubated with different concentrations of aldehyde substrates ranging from 10 to 100 μ M in reaction buffer (100 mM Tris HCl, 1.25 mM EDTA, pH 7.5). The oxidation of the aldehydes was measured in the presence of NAD^+ as coenzyme and NADH generation was monitored at 340 nm using a spectrophotometer. The results are from 3 replicate experiments. Error bars represent the SEM.

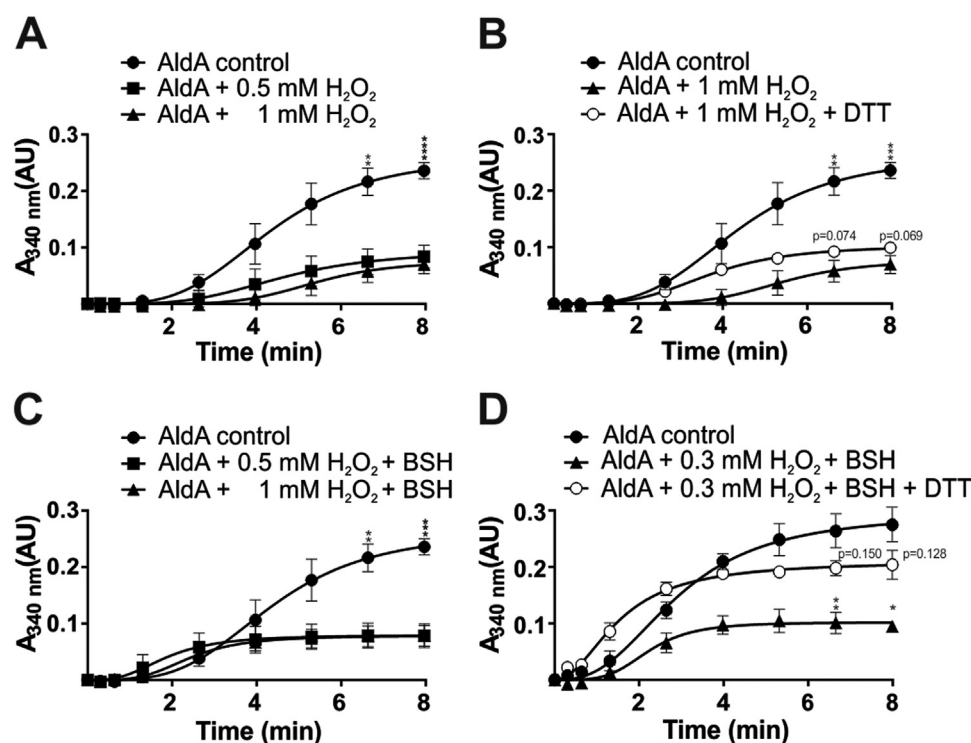


Fig. 6. Inactivation of AldA of *S. aureus* in response to H_2O_2 in the absence and presence of BSH *in vitro*. Reduced AldA (30 μ M) was oxidized with 0.3–1 mM H_2O_2 for 5 min in the absence (A, B) or presence of BSH (C, D) in reaction buffer (100 mM Tris HCl, 1.25 mM EDTA, pH 7.5). The AldA activities were measured with 15 mM methylglyoxal as substrate and NAD^+ as coenzyme by monitoring NADH production at 340 nm using a spectrophotometer. To analyze the irreversible inactivation of AldA by H_2O_2 alone, AldA was treated with 1 mM H_2O_2 without BSH followed by reduction with 10 mM DTT (C). The reversibility of AldA S-bacillithiolation with 0.3 mM H_2O_2 and 0.3 mM BSH is shown after DTT-reduction resulting in 66% of regeneration of AldA activity (D). The S-bacillithiolation of AldA and its reduction using DTT was further confirmed in BSH-specific Western blot analysis as shown in Fig. 1B. P-values were calculated as follows: $p = 0.0012$, $p = 0.0001$ for AldA control/0.5 mM H_2O_2 at 6.63 and 8 min, respectively (Fig. 6A); $p = 0.0012$, $p = 0.0002$ for AldA control/1 mM H_2O_2 at 6.63 and 8 min and $p = 0.074$, $p = 0.069$ for 1 mM H_2O_2 /1 mM H_2O_2 + DTT at 6.63 and 8 min, respectively (Fig. 6B); $p = 0.0021$, $p = 0.0008$ for AldA control/0.5 mM H_2O_2 + BSH at 6.63 and 8 min, respectively (Fig. 6C); $p = 0.003$, $p = 0.011$ for 0.3 mM H_2O_2 + BSH/0.3 mM H_2O_2 + BSH + DTT at 6.63 and 8 min; $p = 0.150$, $p = 0.128$ for AldA control/0.3 mM H_2O_2 + BSH + DTT at 6.63 and 8 min, respectively (Fig. 6D). Symbols are defined as follows: ns $p > 0.05$; * $p \leq 0.05$; ** $p \leq 0.01$; *** $p \leq 0.001$; **** $p \leq 0.0001$.

** $p \leq 0.01$; *** $p \leq 0.001$; and **** $p \leq 0.0001$. The results are from 3 replicate experiments. In all graphs, mean values are shown, error bars represent the SEM and p-values are calculated using a Student's unpaired two-tailed *t*-test by the graph prism software.

ecADH, paBADH), saAldA is a dimeric enzyme and thus more similar to plant ADHs that are also active as dimer (Fig. 7A). Regardless of the oligomerization state, the overall fold of a subunit is highly conserved among all ADH enzymes. Similarly as in other ADHs, a saAldA subunit is composed of a coenzyme (NAD^+)-binding domain (Co-BD; residues

1–122, 137–244 and 439–464), a catalytic domain (CD; residues 245–438) and a subunit interaction domain (SID; residues 123–136 and 465–475; Fig. 7A).

In all ADHs, the active site harbors conserved Cys (C279 in saAldA) and glutamate (E245 in saAldA) residues (Fig. S5). The Cys residue can

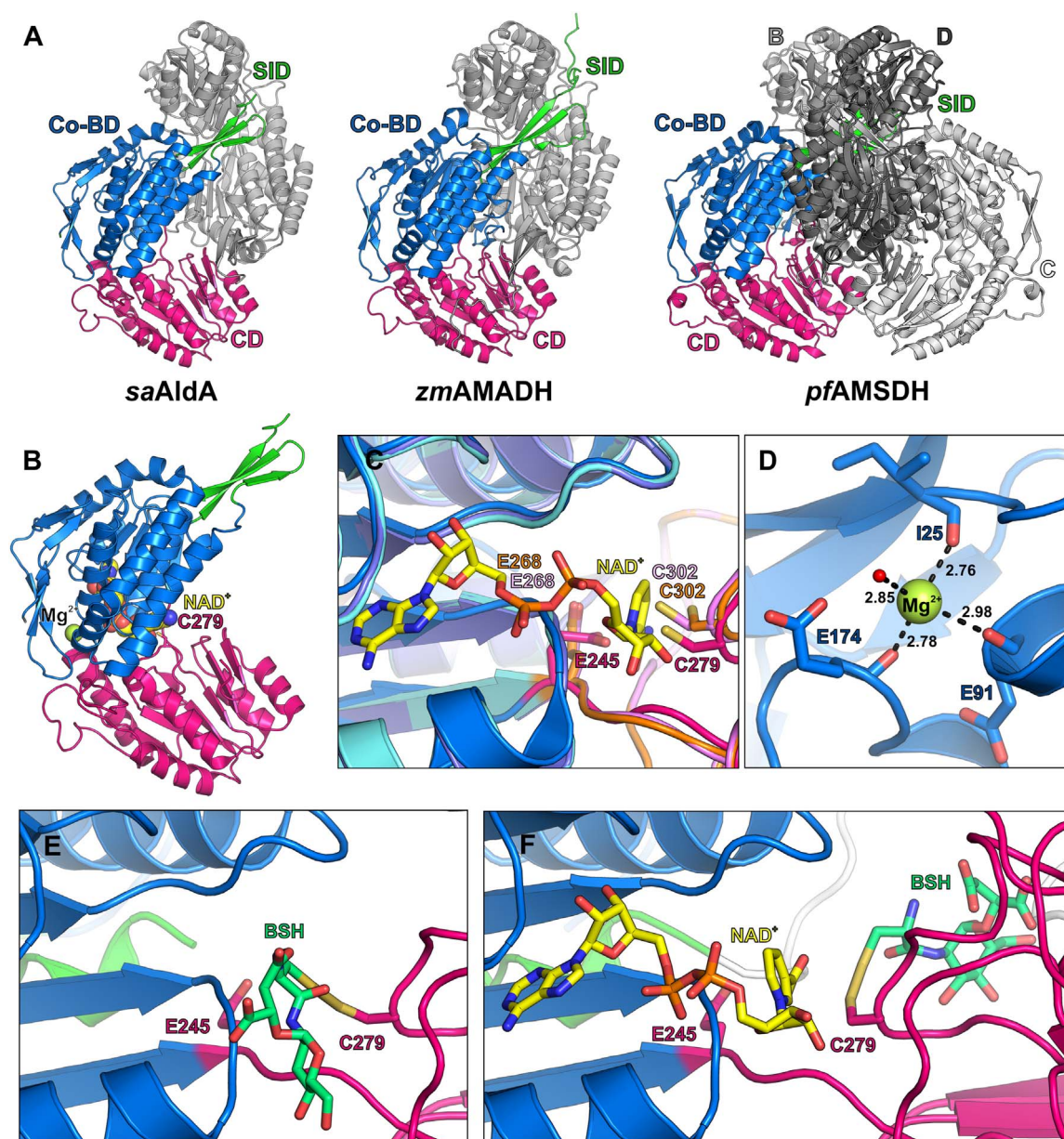


Fig. 7. Structural insights into the *S*-bacillithiolated *saAldA* active site. (A) Structural overviews of dimeric *saAldA* (PDB ID: 3TY7), dimeric *zmAMADH* (PDB ID: 4I8P) and tetrameric *pfAMSDH* (PDB ID: 4I26). Dimers formed by chains A (colored by domain; coenzyme-binding domain [Co-BD] – blue; subunit interaction domain [SID] – green; catalytic domain [CD] – magenta) and B (grey) are oriented in the same way. The other dimer of the *pfAMSDH* tetramer (chains C and D) is shown in different shades of grey. (B) Model for NAD⁺ binding by *saAldA* obtained by superimposing a subunit of NAD⁺-bound *pfAMSDH* (PDB ID: 4I1W) on apo-*saAldA*. The modelled NAD⁺ (colored by atom type; carbon – yellow; oxygen – red; nitrogen – blue; phosphorus – orange) and a bound Mg²⁺ ion (lime green) are shown as spheres, the active site cysteine (C279) is shown as sticks (carbon – magenta; sulfur – yellow). (C) Active sites and NAD⁺-binding cavities of ADHs. A subunit of *saAldA* (colored as in A) was structurally aligned with subunits of apo-*pfAMSDH* (Co-BD – violet; CD – light pink) and of NAD⁺-bound *pfAMSDH* (Co-BD – cyan; CD – orange). NAD⁺ is shown as sticks (colored by atom type as in B). The catalytic cysteine residue is in the resting state in the apo-structures and in the attacking state in NAD⁺-bound *pfAMSDH*. (D) Interactions at the cation-binding site of *saAldA*. Red sphere – water oxygen. (E, F) The *S*-bacillithiolated active site pocket of the apo-*saAldA* (E) and holo-*saAldA* (F). A subunit of *saAldA* colored as in A, view as in C, NAD⁺ and BSH are shown as sticks, NAD⁺ is colored as in B, BSH colored by atom type (carbon – aquamarine; oxygen – red; nitrogen – blue; sulfur – yellow). The loop composed of residues 438–459 that is not present in *saAldA* structure (PDB ID: 3TY7) was modelled and is shown in white.

adopt two alternative conformations, a “resting” and “attacking” (Fig. 7C), depending on the enzyme activation state. In the apo-enzyme structure, the Cys residue is in the resting conformation, whereas upon NAD⁺ binding the Cys thiol moiety rotates away from the nicotinamide part of NAD⁺ and is closer to the substrate-binding pocket [54–56]. The Cys residue serves as a nucleophile during catalysis, leading to a covalent thioester-enzyme adduct with the substrate via a nucleophilic addition [54,55,57]. The conserved glutamate residue then serves as a base to activate a water molecule for hydrolysis of the thioester-enzyme intermediate [55,59]. In addition to the Cys and glutamate residues,

there are two other conserved residues, a lysine (K156 in *saAldA*) and a glutamate (E455 in *saAldA*), that are involved in a proton relay that allows the deprotonation of E245, and, as a consequence, proton abstraction from the hydrolytic water [56].

Another common feature of the ADHs is the presence of a cation-binding site located in the Co-BD (Fig. 7B, D). Co-BD is formed by the three main chain carbonyl groups of an isoleucine/valine (I25 in *saAldA*), a glutamate/aspartate (E91 in *saAldA*) and a glutamate residue (E173 in *saAldA*) [60–62]. The cation bound at this site is usually sodium or potassium, and it was reported that the enzyme activity is

slightly higher in the presence of sodium [60]. In the *saAldA* structure, a magnesium ion is present at this site, most likely because magnesium was the only cation present in the crystallization solution. The role of the cation-binding site is to maintain the structural integrity of the protein and to stabilize a loop involved in binding of NAD^+ [60–62].

The available *saAldA* structure represents the apo-enzyme. In contrast, the structures of plant ADHs and of *paBADH* contain the coenzyme NAD^+ . In the case of *pfAMSDH*, the structures of *pfAMSDH*/ NAD^+ /intermediate complexes are also available [55]. Comparison of the apo, NAD^+ , NAD^+ /intermediate states shows that binding of the coenzyme or the formation of the intermediate does not influence the secondary structure elements within the enzyme, while rearrangements are observed in the side chains of residues involved in catalysis [54,55]. In the ADHs, the NAD^+ is bound in the hydrophobic pocket of the CoBD. Only the nicotinamide nucleotide moiety is turned towards a negatively charged pocket, in which the catalytic cysteine residue is located (Fig. 7B). NAD^+ is engaged in only few polar contacts with the enzyme [54,62].

Although the overall structure, the active site and the cation-binding site are highly conserved among the ADHs, these enzymes show broad substrate specificities and the amino acid residues involved in substrate binding are different among the ADHs. Nevertheless, even a single ADH is able to use many different aldehydes as substrates. For example, *slAMADH* can oxidize many different aminoaldehydes [62]. Thus, differences in the substrate-binding residues determine differences in the still comparatively broad substrate spectra of the enzymes.

3.7. S-bacillithiolation of the AldA active site depends on the Cys activation state as revealed by molecular dynamics simulation

Next, we analyzed the structural changes of AldA upon S-bacillithiolation and used molecular docking and molecular dynamics simulations to model BSH into the active site of the apo- and holoenzyme structures (Fig. 7EF). The structure of *saAldA* apo-enzyme (PDB 3TY7) was superimposed with the NAD^+ binding structure from *Pseudomonas fluorescens pfAMSDH* (PDB 4I1W) to model the NAD^+ cofactor into the AldA active site pocket (Fig. 7C). We further noticed that in the *saAldA* dimeric structure, the loop composed of residues 438–459 is not present which was modelled into the *saAldA* holo-enzyme structure based on the structure of *pfAMSDH* (Fig. 7F). This loop in the *saAldA* holo-enzyme structure may interfere with the location of BSH at the active site. To model the S-bacillithiolated active site Cys279 in the *saAldA* apo- and holoenzyme structures, we applied an adapted molecular docking algorithm based on Steric Clashes-Alleviated Receptor (SCAR) approaches [63], which takes into account the possibility of bond formation between ligand and receptor. Molecular docking and atomistic molecular dynamics simulation of the covalent BSH enzyme complex resulted in two best-scoring poses for BSH in the apo-enzyme (Q2) or holo-enzyme complex (Q1) (Fig. 7EF). However, no overlap between BSH and the loop (aa438–459) in the holo-enzyme structure was found and there was still room for an aldehyde substrate. Interestingly, these two different BSH positions in the AldA active site depend on the Cys279 activation state in the presence or absence of the NAD^+ cofactor (Fig. 7EF). In the apo-enzyme structure, Cys279 bound to BSH is still in "resting" position (Q2), while Cys279 is in the "attacking" position in the holo-enzyme (Q1). Thus, the location of BSH in the active site pocket depends on the Cys279 activation state in the presence or absence of NAD^+ . The Q2 pose of BSH at the apo-enzyme without NAD^+ seems to be energetically more favorable since Q2 had much better energy score (−50.2 kJ/mol), while the Q1 position of the holo-enzyme had a lower energy score (−38.1 kJ/mol). This results were quantitatively supported by our all-atom MD simulation of the complexes and the follow-up MM-PBSA calculations: the interaction energy in the apo-enzyme complex with BSH in Q2 position was -24.8 ± 15.4 kJ/mol, while the holo-enzyme complex with BSH in Q1 position had interaction energy of -19.7 ± 10.0 kJ/mol.

We have further plotted the dihedral distribution of N-CA-CB-SG dihedral (rotation around the CA-CB bond) of Cys279 and the dihedral angle at the function of simulation time (Fig. S6). The results showed that Cys279 in the apo-enzyme has very different dihedral propensity than in the holo-enzyme in complex with NAD^+ . These data support that the apo-enzyme prefers the resting state position of Cys279 with BSH while the holo-enzyme favors the BSH complex with the thiol in the attacking state position.

In agreement with our previous GapDH results [26], S-bacillithiolation of the AldA apo- and holoenzyme active site does not require major structural changes. After 50 ns of MD simulations there was very little change in the backbone flexibility of the protein between different binding positions of BSH in the apo-enzyme (Q2) or the holo-enzyme (Q1) compared to the apo-enzyme without BSH (Fig. S7). This further confirms that BSH can undergo disulfide formation with the active site Cys279 at different positions without major conformational changes.

4. Discussion

S. aureus is a major human pathogen of hospital and community-acquired infections, ranging from local skin infections to life-threatening systemic and chronic infections. During infections, *S. aureus* is exposed to ROS, RCS and RES that are produced as first line of defense by activated macrophages and neutrophils or can be also encountered as consequence of antibiotics treatment [10,11,64]. Thus, the understanding of the adaptation mechanisms of *S. aureus* to infection conditions to avoid killing by ROS, RCS and RES is important for the discovery of new drug targets to combat multi-resistant *S. aureus* infections.

In our previous work, we have identified the aldehyde dehydrogenase AldA as one of the most strongly oxidized proteins in the thiol-redox proteome in *S. aureus*, which showed a 29% oxidation increase under NaOCl stress using the OxICAT analysis [26]. AldA uses a conserved active site Cys279 that was modified by S-bacillithiolation under NaOCl stress. Apart from AldA, the glyceraldehyde-3-phosphate dehydrogenase Gap was identified as S-bacillithiolated at its active site Cys151 under NaOCl stress. Thus, it is interesting to note that two functionally related aldehyde dehydrogenases are targets for oxidation at their active site Cys residues that both function in aldehyde oxidation. In this study, we demonstrated that AldA is specifically induced under thiol-specific stress conditions, such as NaOCl, diamide and formaldehyde stress. Expression of *aldA* was previously shown to be regulated by the alternative sigma factor SigmaB in response to heat shock, salt stress caused by NaCl and Mn_2Cl as well as alkaline shock [50,51]. Here, we have shown that the thiol-specific expression of *aldA* occurs SigmaB-independently. Thus, *aldA* seems to be double-controlled by SigmaB and another thiol-stress sensing regulator to allow adaptation to general stress and starvation as well as thiol-stress conditions.

SigmaB has been previously shown to play an important role under infection conditions and controls biofilm formation and several virulence factors, such as adhesins [65,66]. The SigmaB regulon was induced after internalization of *S. aureus* by bronchial epithelial cells and required for intracellular growth as demonstrated by transcriptomics and proteomics [53,67,68]. Moreover, SigmaB has been implicated as central regulator in long-term persistence in human osteoblasts and controls the small colony variant (SCV) phenotype of persistent *S. aureus* infections [69,70]. Thus, it might be possible that adaptation of *S. aureus* from acute to chronic and persistent infections requires SigmaB and AldA to cope and adapt to the stationary phase and thiol-specific stress conditions inside macrophages and neutrophils. This adaptation to thiol-stress conditions is particularly important for *S. aureus* to survive under conditions of long-term persistent and chronic infections.

In this work, we have shown that AldA is an important member of the SigmaB regulon that provides protection under NaOCl stress

conditions as shown in survival assays. However, the thiol-specific induction of *aldA* transcription seems to be SigA-dependently since the same induction level was observed in the *sigB* mutant under thiol-stress. A putative SigA-promoter was observed upstream of the SigB-promoter indicating that *aldA* transcription might be controlled by SigB and SigA containing RNA polymerase (RNAP) from adjacent promoters. The stronger *aldA* induction in the *sigB* mutant under methylglyoxal stress could be explained by a higher affinity of SigA for the RNAP core enzyme compared to SigB and the lack of sigma factor competition in the *sigB* mutant [71]. Moreover, the thiol-stress-specific induction of *aldA* transcription might require additional transcriptional regulators that remain to be elucidated. In future studies, we also aim to investigate if AldA plays a role for the intracellular growth as well as persistence or chronic infections in *S. aureus*, which could require detoxification of toxic aldehydes to allow long-term survival.

To study the function of AldA and its redox-regulation under NaOCl stress *in vitro*, we purified the enzyme and determined its catalytic activities towards oxidation of various aldehydes. We could show that AldA has broad substrate specificities to oxidize formaldehyde, methylglyoxal, glycol aldehyde and acetaldehyde to their respective acids. The question arises about the physiological aldehyde substrate for AldA under *in vivo* conditions that are produced under infection conditions, such as under hypochlorite stress. Methylglyoxal was previously shown to be produced at higher levels under HOCl stress in *E. coli* [20]. Moreover, the *gloA-nemRA* operon was induced under methylglyoxal and HOCl stress, which functions as important HOCl and methylglyoxal defense mechanism [19–22]. The FMN-dependent oxidoreductase Nema functions in detoxification of various electrophiles, such as aldehydes, N-ethylmaleimide and quinones and its up-regulation under HOCl stress indicates the link between HOCl and aldehyde stress. In our work, we could also show that AldA responds to aldehydes, diamide and NaOCl and hence could be involved in methylglyoxal detoxification in *S. aureus* as well. However, in growth and survival assays, no phenotypes of the *aldA* mutant were detected under formaldehyde and methylglyoxal stress. Since AldA showed broad substrate specificity towards various aldehydes *in vitro*, its natural substrates could be different aldehydes that remain to be elucidated.

Of note, AldA shares strong 57% sequence similarity to betaine aldehyde dehydrogenases from *S. aureus*, *Pseudomonas aeruginosa* and *Spinacia oleracea*. These enzymes function in oxidation of the toxic betaine aldehyde to glycine betaine which is a well-known compatible solute and accumulates in bacteria under osmotic stress conditions as osmoprotectant [72,73]. Glycine betaine can be either taken up upon osmotic stress or synthesized from exogenously provided choline in a two oxidation steps via choline dehydrogenase (BetA) and betaine dehydrogenase (BetB) which are conserved in *B. subtilis* [72,73] and *S. aureus* [54]. The human tissues are rich sources of choline and betaine and thus, *S. aureus* encounters toxic aldehydes produced from choline during colonization and internalization. For some bacteria, the importance of the choline oxidation pathway for survival and virulence has been already demonstrated [73,74]. Of note, AldA is also induced under high osmolarity conditions provoked by NaCl stress in a SigmaB-dependent manner [50]. This could point to a possible function in the osmotic stress and thiol-stress response in *S. aureus* which remains to be elucidated. However, we could not detect AldA activity for oxidation of betaine aldehyde as substrate *in vitro*, indicating a different function of AldA in *S. aureus* (data not shown).

The catalytic activity of AldA depends on a highly conserved Cys279 active site which we identified as S-bacillithiolated under NaOCl stress in *S. aureus* [26]. Interestingly, this nucleophilic active site Cys residue was previously found oxidized to a mixed disulfide with beta-mercaptoethanol during protein crystallization of related betaine aldehyde dehydrogenases [54,74]. These results confirm the redox-sensitivity of the active site Cys of AldA as shown in this work. Our results have further demonstrated that S-bacillithiolation functions in redox-regulation and inactivation of AldA activity under H₂O₂ stress. In the

absence of BSH, the active site Cys279 was very sensitive to over-oxidation as shown by its irreversible inactivation. In the presence of BSH, Cys279 was protected against overoxidation by the S-bacillithiolation as shown for the glyceraldehyde-3-phosphate dehydrogenase GapDH in *S. aureus* [26]. Both enzymes use a similar catalytic mechanism for the NAD⁺-dependent oxidation of the aldehyde substrate to generate the acid product [54,55,57]. In the catalytic mechanism of aldehyde dehydrogenase, the active site Cys was shown to adopt two conformations: the “attacking” or “resting” conformation depending on the presence or absence of the NAD⁺ cofactor. We used molecular docking and molecular dynamic simulations to model the S-bacillithiolated active site in the presence and absence of NAD⁺. In the apo-enzyme structure, BSH was bound to Cys279 in the resting state (Q2) position and occupied the cofactor-binding pocket. In the presence of NAD⁺, Cys279 was modified in the attacking state position (Q1) and BSH was repositioned close to the substrate-binding site.

In our previous docking approach with BSH at the Cys151 active site of GapDH, we found similar locations of BSH in the apo-enzyme and holo-enzyme structures related to the resting and attacking state. Thus, the highly flexible active site and the redox-sensitivity of the nucleophilic Cys residues facilitate their fast oxidation to the mixed disulfides with BSH. In both structural models, S-bacillithiolation of GapDH and AldA did not require major structural changes, which further explains their preferred formation of the BSH mixed disulfides. This flexible BSH position may ensure that catalytic active and resting AldA and GapDH enzymes can both be protected against overoxidation under NaOCl stress to ensure fast regeneration and reactivation of the enzymes.

Acknowledgements

This work was supported by an ERC Consolidator Grant (GA 615585) MYCOTHIOLOME and grants from the Deutsche Forschungsgemeinschaft (AN746/4-1 and AN746/4-2) within the SPP1710 on “Thiol-based Redox switches”, by the Research Training Group GRK1947 (Project C01) and by the SFB973 Project C08 to H.A. Protein crystal structure analysis was supported by an Alexander von Humboldt Post-doc Fellowship to A.P.-B.

Author disclosure statement

No competing financial interests exist.

Appendix A. Supplementary material

Supplementary data associated with this article can be found in the online version at <http://dx.doi.org/10.1016/j.redox.2018.02.001>.

References

- [1] F.D. Lowy, *Staphylococcus aureus* infections, New Engl. J. Med. 339 (1998) 520–532.
- [2] H.W. Boucher, G.R. Corey, Epidemiology of methicillin-resistant *Staphylococcus aureus*, Clin. Infect. Dis.: Off. Publ. Infect. Dis. Soc. Am. 46 (Suppl. 5) (2008) S344–S349.
- [3] G.L. Archer, *Staphylococcus aureus*: a well-armed pathogen, Clin. Infect. Dis.: Off. Publ. Infect. Dis. Soc. Am. 26 (1998) 1179–1181.
- [4] D.M. Livermore, Antibiotic resistance in staphylococci, Intern. J. Antimicrob. Agents 16 (Suppl. 1) (2000) S3–S10.
- [5] J.N. Pendleton, S.P. Gorman, B.F. Gilmore, Clinical relevance of the ESKAPE pathogens, Expert Rev. Anti-Infect. Ther. 11 (2013) 297–308.
- [6] A.N. Spaan, J.A.G. van Strijp, V.J. Torres, Leukocidins: staphylococcal bi-component pore-forming toxins find their receptors, Nat. Rev. Microbiol. (2017).
- [7] M. Dal Peraro, F.G. van der Goot, Pore-forming toxins: ancient, but never really out of fashion, Nat. Rev. Microbiol. 14 (2016) 77–92.
- [8] C.C. Winterbourn, A.J. Kettle, Redox reactions and microbial killing in the neutrophil phagosome, Antioxid. Redox Signal. 18 (2013) 642–660.
- [9] C.C. Winterbourn, A.J. Kettle, M.B. Hampton, Reactive oxygen species and neutrophil function, Annu. Rev. Biochem. 85 (2016) 765–792.
- [10] W.N. Beavers, E.P. Skaar, Neutrophil-generated oxidative stress and protein damage in *Staphylococcus aureus*, Pathog. Dis. 74 (2016).
- [11] M. Hillion, H. Antelmann, Thiol-based redox switches in prokaryotes, Biol. Chem. 396 (2015) 415–444.

- [12] M.B. Hampton, A.J. Kettle, C.C. Winterbourn, Involvement of superoxide and myeloperoxidase in oxygen-dependent killing of *Staphylococcus aureus* by neutrophils, *Infect. Immun.* 64 (1996) 3512–3517.
- [13] S.J. Klebanoff, A.J. Kettle, H. Rosen, C.C. Winterbourn, W.M. Nauseef, Myeloperoxidase: a front-line defender against phagocytosed microorganisms, *J. Leukoc. Biol.* 93 (2013) 185–198.
- [14] I.R. Booth, G.P. Ferguson, S. Miller, C. Li, B. Gunasekera, S. Kinghorn, Bacterial production of methylglyoxal: a survival strategy or death by misadventure? *Biochem. Soc. Trans.* 31 (2003) 1406–1408.
- [15] G.P. Ferguson, S. Totemeyer, M.J. MacLean, I.R. Booth, Methylglyoxal production in bacteria: suicide or survival? *Arch. Microbiol.* 170 (1998) 209–218.
- [16] E.E. Farmer, C. Davoine, Reactive electrophile species, *Curr. Opin. Plant Biol.* 10 (2007) 380–386.
- [17] L.J. Marnett, J.N. Riggins, J.D. West, Endogenous generation of reactive oxidants and electrophiles and their reactions with DNA and protein, *J. Clin. Invest.* 111 (2003) 583–593.
- [18] G.P. Ferguson, I.R. Booth, Importance of glutathione for growth and survival of *Escherichia coli* cells: detoxification of methylglyoxal and maintenance of intracellular K⁺, *J. Bact.* 180 (1998) 4314–4318.
- [19] M.J. Gray, Y. Li, L.I. Leichert, Z. Xu, U. Jakob, Does the transcription factor NemR use a regulatory sulfenamide bond to sense bleach? *Antioxid. Redox Signal.* 23 (2015) 747–754.
- [20] M.J. Gray, W.Y. Wholey, B.W. Parker, M. Kim, U. Jakob, NemR is a bleach-sensing transcription factor, *J. Biol. Chem.* 288 (2013) 13789–13798.
- [21] C. Lee, J. Shin, C. Park, Novel regulatory system *nemRA-gloA* for electrophile reduction in *Escherichia coli* K-12, *Mol. Microbiol.* 88 (2013) 395–412.
- [22] E. Ozyamak, C. de Almeida, A.P. de Moura, S. Miller, I.R. Booth, Integrated stress response of *Escherichia coli* to methylglyoxal: transcriptional readthrough from the *nemRA* operon enhances protection through increased expression of glyoxalase I, *Mol. Microbiol.* 88 (2013) 936–950.
- [23] P. Chandrangu, V.V. Loi, H. Antelmann, J.D. Helmann, The role of bacillithiol in gram-positive *Firmicutes*, *Antioxid. Redox Signal.* (2017).
- [24] G.L. Newton, M. Rawat, J.J. La Clair, V.K. Jothivasan, T. Budiarto, C.J. Hamilton, A. Claiborne, J.D. Helmann, R.C. Fahey, Bacillithiol is an antioxidant thiol produced in *Bacilli*, *Nat. Chem. Biol.* 5 (2009) 625–627.
- [25] P. Chandrangu, R. Dusi, C.J. Hamilton, J.D. Helmann, Methylglyoxal resistance in *Bacillus subtilis*: contributions of bacillithiol-dependent and independent pathways, *Mol. Microbiol.* 91 (2014) 706–715.
- [26] M. Imber, N.T.T. Huyen, A.J. Pietrzyk-Brzezinska, V.V. Loi, M. Hillion, J. Bernhardt, T. Thärichen, K. Kolkse, M. Saleh, C.J. Hamilton, L. Adrian, F. Gräter, M.C. Wahl, H. Antelmann, Protein S-Bacillithiolation functions in thiol protection and redox regulation of the glyceraldehyde-3-phosphate dehydrogenase gap in *Staphylococcus aureus* under hypochlorite stress, *Antioxid. Redox Signal.* (2017).
- [27] M. Wetstein, U. Völker, J. Dedio, S. Lobau, U. Zuber, M. Schieswohl, C. Herget, M. Hecker, W. Schumann, Cloning, sequencing, and molecular analysis of the *dnkA* locus from *Bacillus subtilis*, *J. Bact.* 174 (1992) 3300–3310.
- [28] M. Arnaud, A. Chastanet, M. Debarbouille, New vector for efficient allelic replacement in naturally nontransformable, low-GC-content, gram-positive bacteria, *Appl. Environ. Microbiol.* 70 (2004) 6887–6891.
- [29] E.D. Rosenblum, S. Tyrone, Serology, density, and morphology of *Staphylococcal* phages, *J. Bact.* 88 (1964) 1737–1742.
- [30] M. Müller, S. Reiss, R. Schlüter, U. Mäder, A. Beyer, W. Reiss, J. Marles-Wright, R.J. Lewis, H. Pfortner, U. Völker, K. Riedel, M. Hecker, S. Engelmann, J. Pane-Farre, Deletion of membrane-associated Asp23 leads to upregulation of cell wall stress genes in *Staphylococcus aureus*, *Mol. Microbiol.* 93 (2014) 1259–1268.
- [31] V.V. Loi, M. Müller, N.T.T. Huyen, C.J. Hamilton, F. Hochgräfe, J. Pane-Farre, H. Antelmann, Real-time imaging of the bacillithiol redox potential in the human pathogen *Staphylococcus aureus* using a genetically encoded bacilliredoxin-fused redox biosensor, *Antioxid. Redox Signal.* 26 (2017) 835–848.
- [32] B.K. Chi, A.A. Roberts, T.T. Huyen, K. Baisel, D. Becher, D. Albrecht, C.J. Hamilton, H. Antelmann, S-bacillithiolation protects conserved and essential proteins against hypochlorite stress in firmicutes bacteria, *Antioxid. Redox Signal.* 18 (2013) 1273–1295.
- [33] B. Webb, A. Sali, Protein structure modeling with MODELLER, *Methods Mol. Biol.* 1654 (2017) 39–54.
- [34] D. Kozakov, L.E. Grove, D.R. Hall, T. Bohnuud, S.E. Mottarella, L. Luo, B. Xia, D. Beglov, S. Vajda, The FTMap family of web servers for determining and characterizing ligand-binding hot spots of proteins, *Nat. Prot.* 10 (2015) 733–755.
- [35] G.S. Couch, D.K. Hendrix, T.E. Ferrin, Nucleic acid visualization with UCSF Chimera, *Nucleic Acids Res.* 34 (2006) e29.
- [36] W.J. Allen, T.E. Balus, S. Mukherjee, S.R. Brozell, D.T. Moustakas, P.T. Lang, D.A. Case, I.D. Kuntz, R.C. Rizzo, DOCK 6: impact of new features and current docking performance, *J. Comput. Chem.* 36 (2015) 1132–1156.
- [37] N. Schneider, G. Lange, S. Hindle, R. Klein, M. Rarey, A consistent description of H-bond and D-hydrogen energies in protein-ligand complexes: methods behind the HYDE scoring function, *J. Comput. Mol. Des.* 27 (2013) 15–29.
- [38] D. Van Der Spoel, E. Lindahl, B. Hess, G. Groenhof, A.E. Mark, H.J. Berendsen, GROMACS: fast, flexible, and free, *J. Comput. Chem.* 26 (2005) 1701–1718.
- [39] K. Lindorff-Larsen, S. Piana, C. Palmo, P. Maragakis, J.L. Klepeis, R.O. Dror, D.E. Shaw, Improved side-chain torsion potentials for the Amber ff99SB protein force field, *Proteins* 78 (2010) 1950–1958.
- [40] A.W. Sousa da Silva, W.F. Vranken, ACPYPE – AnteChamber PYthon Parser interface, *BMC Res. Notes* 5 (2012) 367.
- [41] F.Y. Dupradeau, A. Pigache, T. Zaffran, C. Savineau, R. Lelong, N. Grivel, D. Lelong, W. Rosanski, P. Cieplak, The R.E.D. tools: advances in RESP and ESP charge derivation and force field library building, *Phys. Chem. Chem. Phys.* 12 (2010) 7821–7839.
- [42] M.J. Frisch, G. T. H.B. Schlegel, G.E. Scuseria, M.A. Robb, J.R. Cheeseman, et al., Gaussian 09, Revision A.02, 34 Gaussian Inc., Wallingford, CT, 2009.
- [43] M. Parrinello, A. Rahman, Polymorphic transitions in single crystals: a new molecular dynamics method, *J. Appl. Phys.* 52 (1981) 7182–7190.
- [44] T. Darden, D. York, L., J. Pedersen, Particle mesh Ewald: an N-log(N) method for Ewald sums in large systems, *J. Chem. Phys.* 98 (1993) 10089–10092.
- [45] B. Hess, H. Bekker, H.J.C. Berendsen, J.G.E.M. Fraaije, LINC: a linear constraint solver for molecular simulations, *J. Comput. Chem.* 18 (1997) 1463–1472.
- [46] C.C. Huang, E.C. Meng, J.H. Morris, E.F. Pettersen, T.E. Ferrin, Enhancing UCSF Chimera through web services, *Nucleic Acids Res.* 42 (2014) W478–484.
- [47] E.F. Pettersen, T.D. Goddard, C.C. Huang, G.S. Couch, D.M. Greenblatt, E.C. Meng, T.E. Ferrin, UCSF Chimera—a visualization system for exploratory research and analysis, *J. Comput. Chem.* 25 (2004) 1605–1612.
- [48] B.R. Miller 3rd, T.D. McGee Jr., J.M. Swails, N. Homeyer, H. Gohlke, A.E. Roitberg, MMPBSA.py: an efficient program for end-state free energy calculations, *J. Chem. Theory Comput.* 8 (2012) 3314–3321.
- [49] L.I. Leichert, F. Gehrke, H.V. Gudiseva, T. Blackwell, M. Ilbert, A.K. Walker, J.R. Strahler, P.C. Andrews, U. Jakob, Quantifying changes in the thiol redox proteome upon oxidative stress in vivo, *Proc. Natl. Acad. Sci. USA* 105 (2008) 8197–8202.
- [50] J. Pane-Farre, B. Jonas, K. Förstner, S. Engelmann, M. Hecker, The sigmaB regulon in *Staphylococcus aureus* and its regulation, *Int. J. Med. Microbiol.* 296 (2006) 237–258.
- [51] M. Bischoff, P. Dunman, J. Kormanec, D. Macapagal, E. Murphy, W. Mounts, B. Berger-Bachi, S. Projan, Microarray-based analysis of the *Staphylococcus aureus* sigmaB regulon, *J. Bact.* 186 (2004) 4085–4099.
- [52] S. Fuchs, H. Mehlan, J. Bernhardt, A. Hennig, S. Michalik, K. Surmann, J. Pane-Farre, A. Giese, S. Weiss, L. Backert, A. Herbig, K. Nieselt, M. Hecker, U. Völker, U. Mäder, AureoWiki the repository of the *Staphylococcus aureus* research and annotation community, *Int. J. Med. Microbiol.* (2017).
- [53] U. Mäder, P. Nicolas, M. Depke, J. Pane-Farre, M. Debarbouille, M.M. van der Kooi-Pol, C. Guerin, S. Derozier, A. Hiron, H. Jarmer, A. Leduc, S. Michalik, E. Reilman, M. Schaffer, F. Schmidt, P. Bessieres, P. Noirot, M. Hecker, T. Msadek, U. Völker, J.M. van Dijk, *Staphylococcus aureus* transcriptome architecture: from laboratory to infection-mimicking conditions, *PLoS Genet.* 12 (2016) e1005962.
- [54] A.S. Halavaty, R.L. Rich, C. Chen, J.C. Joo, G. Minasov, I. Dubrovskaya, J.R. Winsor, D.G. Myszkla, M. Duban, L. Shuvalova, A.F. Yakunin, W.F. Anderson, Structural and functional analysis of betaine aldehyde dehydrogenase from *Staphylococcus aureus*, *Act. Cryst. Sect. D. Biol. Cryst.* 71 (2015) 1159–1175.
- [55] L. Huo, I. Davis, F. Liu, B. Andi, S. Esaki, H. Iwaki, Y. Hasegawa, A.M. Orville, A. Liu, Crystallographic and spectroscopic snapshots reveal a dehydrogenase in action, *Nat. Commun.* 6 (2015) 5935.
- [56] L. Gonzalez-Segura, E. Rudino-Pinera, R.A. Munoz-Clares, E. Horjales, The crystal structure of a ternary complex of betaine aldehyde dehydrogenase from *Pseudomonas aeruginosa* provides new insight into the reaction mechanism and shows a novel binding mode of the 2-phosphate of NADP⁺ and a novel cation binding site, *J. Mol. Biol.* 385 (2009) 542–557.
- [57] D.P. Abriola, R. Fields, S. Stein, A.D. MacKerell Jr, R. Pietruszko, Active site of human liver aldehyde dehydrogenase, *Biochemistry* 26 (1987) 5679–5684.
- [58] L. Holm, P. Rosenstrom, Dali server: conservation mapping in 3D, *Nucleic Acids Res.* 38 (2010) W545–549.
- [59] K. D'Ambrosio, A. Pailot, F. Talfournier, C. Didierjean, E. Benedetti, A. Aubry, G. Branlant, C. Corbier, The first crystal structure of a thioacylzyme intermediate in the ALDH family: new coenzyme conformation and relevance to catalysis, *Biochemistry* 45 (2006) 2978–2986.
- [60] A. Gruet, V. Roig-Zamboni, S. Grisel, A. Salomoni, C. Valencia, V. Campanacci, M. Tegoni, C. Cambillau, Crystal structure and kinetics identify *Escherichia coli* ydcW gene product as a medium-chain aldehyde dehydrogenase, *J. Mol. Biol.* 343 (2004) 29–41.
- [61] T.D. Hurley, S. Perez-Miller, H. Breen, Order and disorder in mitochondrial aldehyde dehydrogenase, *Chem.-Biol. Interact.* 130–132 (2001) 3–14.
- [62] D. Kopecky, R. Koncitikova, M. Tylichova, A. Vigouroux, H. Moskalikova, M. Soural, M. Sebela, S. Morera, Plant ALDH10 family: identifying critical residues for substrate specificity and trapping a thiohemiacetal intermediate, *J. Biol. Chem.* 288 (2013) 9491–9507.
- [63] Y. Ai, L. Yu, X. Tan, X. Chai, S. Liu, Discovery of covalent ligands via noncovalent docking by dissecting covalent docking based on a "Steric-Clashes Alleviating Receptor (SCAR)" strategy, *J. Chem. Inform. Model.* 56 (2016) 1563–1575.
- [64] A.L. Cheung, K.A. Nishina, M.P. Trotton, S. Tamber, The SarA protein family of *Staphylococcus aureus*, *Int. J. Biochem. Cell Biol.* 40 (2008) 355–361.
- [65] G. Mitchell, E. Brouillette, D.L. Seguin, A.E. Asselin, C.L. Jacob, F. Malouin, A role for sigma factor B in the emergence of *Staphylococcus aureus* small-colony variants and elevated biofilm production resulting from an exposure to aminoglycosides, *Microb. Pathog.* 48 (2010) 18–27.
- [66] G. Mitchell, D.L. Seguin, A.E. Asselin, E. Deziel, A.M. Cantin, E.H. Frost, S. Michaud, F. Malouin, *Staphylococcus aureus* sigma B-dependent emergence of small-colony variants and biofilm production following exposure to *Pseudomonas aeruginosa* 4-hydroxy-2-heptylquinoline-N-oxide, *BMC Microbiol.* 10 (2010) 33.
- [67] H. Pfortner, J. Wagner, K. Surmann, P. Hildebrandt, S. Ernst, J. Bernhardt, C. Schurmann, M. Gutjahr, M. Depke, U. Jehmlich, V. Dhople, E. Hammer, L. Steil, U. Völker, F. Schmidt, A proteomics workflow for quantitative and time-resolved analysis of adaptation reactions of internalized bacteria, *Methods* 61 (2013) 244–250.
- [68] S. Michalik, M. Depke, A. Murr, M. Gesell Salazar, U. Kusebauch, Z. Sun, T.C. Meyer, K. Surmann, H. Pfortner, P. Hildebrandt, S. Weiss, L.M. Palma Medina,

- M. Gutjahr, E. Hammer, D. Becher, T. Pribyl, S. Hammerschmidt, E.W. Deutsch, S.L. Bader, M. Hecker, R.L. Moritz, U. Mäder, U. Völker, F. Schmidt, A global *Staphylococcus aureus* proteome resource applied to the *in vivo* characterization of host-pathogen interactions, *Sci. Rep.* 7 (2017) 9718.
- [69] L. Tuchscher, M. Bischoff, S.M. Lattar, M. Noto Llana, H. Pfortner, S. Niemann, J. Geraci, H. Van de Vyver, M.J. Fraunholz, A.L. Cheung, M. Herrmann, U. Völker, D.O. Sordelli, G. Peters, B. Löffler, Sigma factor SigB is crucial to mediate *Staphylococcus aureus* adaptation during chronic infections, *PLoS Pathog.* 11 (2015) e1004870.
- [70] L. Tuchscher, B. Löffler, *Staphylococcus aureus* dynamically adapts global regulators and virulence factor expression in the course from acute to chronic infection, *Curr. Genet.* 62 (2016) 15–17.
- [71] C. Rollenhagen, H. Antelmann, J. Kirstein, O. Delumeau, M. Hecker, M.D. Yudkin, Binding of sigma(A) and sigma(B) to core RNA polymerase after environmental stress in *Bacillus subtilis*, *J. Bact.* 185 (2003) 35–40.
- [72] J. Boch, B. Kempf, E. Bremer, Osmoregulation in *Bacillus subtilis*: synthesis of the osmoprotectant glycine betaine from exogenously provided choline, *J. Bact.* 176 (1994) 5364–5371.
- [73] J. Boch, G. Nau-Wagner, S. Kneip, E. Bremer, Glycine betaine aldehyde dehydrogenase from *Bacillus subtilis*: characterization of an enzyme required for the synthesis of the osmoprotectant glycine betaine, *Arch. Microbiol.* 168 (1997) 282–289.
- [74] J.J. Lee, J.H. Kim, D.G. Kim, D.H. Kim, H.L. Simborio, W.G. Min, M.H. Rhee, J.H. Lim, H.H. Chang, S. Kim, Characterization of betaine aldehyde dehydrogenase (BetB) as an essential virulence factor of *Brucella abortus*, *Vet. Microbiol.* 168 (2014) 131–140.

Chapter 4

Redox regulation by reversible protein S-thiolation in Gram-positive bacteria

Marcel Imber¹, Agnieszka J. Pietrzyk-Brzezinska^{2,3}, Haike Antelmann^{1,#}

¹*Institute for Biology-Microbiology, Freie Universität Berlin, D-14195 Berlin, Germany*

²*Laboratory of Structural Biochemistry, Freie Universität Berlin, D-14195 Berlin, Germany*

³*Institute of Technical Biochemistry, Faculty of Biotechnology and Food Sciences, Lodz University of Technology, Lodz 90-924, Poland*

Published in: *Redox Biology* 20: 130-145. (2018)

#Corresponding author: haike.antelmann@fu-berlin.de

Authors contributions:

Marcel Imber contributed with writing of the review and prepared some figures of the manuscript.



Redox regulation by reversible protein S-thiolation in Gram-positive bacteria

Marcel Imber^a, Agnieszka J. Pietrzyk-Brzezinska^{b,c}, Haike Antelmann^{a,*}

^a Freie Universität Berlin, Institute for Biology-Microbiology, Königin-Luise-Strasse 12-16, D-14195 Berlin, Germany

^b Freie Universität Berlin, Laboratory of Structural Biochemistry, D-14195 Berlin, Germany

^c Institute of Technical Biochemistry, Faculty of Biotechnology and Food Sciences, Lodz University of Technology, Lodz 90-924, Poland

ARTICLE INFO

Keywords:

Protein S-thiolation
Bacillithiol
Mycothiol
Gram-positive bacteria

ABSTRACT

Low molecular weight (LMW) thiols play an important role as thiol-cofactors for many enzymes and are crucial to maintain the reduced state of the cytoplasm. Most Gram-negative bacteria utilize glutathione (GSH) as major LMW thiol. However, in Gram-positive *Actinomycetes* and *Firmicutes* alternative LMW thiols, such as mycothiol (MSH) and bacillithiol (BSH) play related roles as GSH surrogates, respectively. Under conditions of hypochlorite stress, MSH and BSH are known to form mixed disulfides with protein thiols, termed as S-mycothiolation or S-bacillithiolation that function in thiol-protection and redox regulation. Protein S-thiolations are widespread redox-modifications discovered in different Gram-positive bacteria, such as *Bacillus* and *Staphylococcus* species, *Mycobacterium smegmatis*, *Corynebacterium glutamicum* and *Corynebacterium diphtheriae*. S-thiolated proteins are mainly involved in cellular metabolism, protein translation, redox regulation and antioxidant functions with some conserved targets across bacteria. The reduction of protein S-mycothiolations and S-bacillithiolations requires glutaredoxin-related mycoredoxin and bacilliredoxin pathways to regenerate protein functions.

In this review, we present an overview of the functions of mycothiol and bacillithiol and their physiological roles in protein S-bacillithiolations and S-mycothiolations in Gram-positive bacteria. Significant progress has been made to characterize the role of protein S-thiolation in redox-regulation and thiol protection of main metabolic and antioxidant enzymes. However, the physiological roles of the pathways for regeneration are only beginning to emerge as well as their interactions with other cellular redox systems. Future studies should be also directed to explore the roles of protein S-thiolations and their redox pathways in pathogenic bacteria under infection conditions to discover new drug targets and treatment options against multiple antibiotic resistant bacteria.

Abbreviations: Ac, acetyl; AcCys, acetyl cysteine; AhpE, membrane-associated peroxidase; AldA, aldehyde dehydrogenase A; Bca, BSH S-conjugate amidase; Brx, bacilliredoxin; BSH, bacillithiol; BshA, glycosyltransferase for GlcNAc-Mal biosynthesis; BshB, deacetylase producing GlcN-Mal; BshC, cysteine ligase for BSH biosynthesis; BSSB, oxidized bacillithiol disulfide; Bst, BSH-S-transferases; CA-MRSA, community acquired MRSA; CHP, cumene hydroperoxide; CoASH, coenzymeA; CoASSH, CoASH persulfide; Cys, cysteine; DHAP, dihydroxyacetone phosphate; DTT, dithiothreitol; EGT, ergothioneine; FA, formaldehyde; FeS, iron-sulfur; GapDH, glycolytic glyceraldehyde 3-phosphate dehydrogenase; GuaB, inosine-5-monophosphate dehydrogenases; GlcN, glucoseamine; GlcNAc, N-acetyl glucoseamine; GlxA/B, glyoxalases A and B; Grx, glutaredoxin; GSH, glutathione; GSSG, oxidized glutathione disulfide; Gst, GSH-S-transferases; H₂O₂, hydrogen peroxide; HED, hydroxyethyl disulfide; HTA, hemithioacetal; INH, isoniazid; Ins, myoinositol; LC-MS/MS, liquid chromatography tandem mass spectrometry; LMW, low molecular weight; Mal, malate; Mca, mycothiol-S-conjugate amidase; Met, methionine; MetE, methionine synthase; MetSO, methionine sulfoxide; MG, methylglyoxal; MgsA, methylglyoxal synthase; MRSA, methicillin-resistant *Staphylococcus aureus*; Mrx1, mycoredoxin1; MSH, mycothiol; MSONH₂, MSH sulfonamide; MSNO, S-nitrosomycothiol; MsrA/B, methionine sulfoxide reductase A/B; MST, mycothiol-S-transferase; MT, metallothionein; Mtb, *Mycobacterium tuberculosis*; NADH, nicotinamide adenine dinucleotide; NADPH, nicotinamide adenine dinucleotide phosphate; HOCl, sodium hypochlorite; NFC, nitrofuranylcalanolide; OHP, organic hydroperoxide; OhrR, organic hydroperoxide repressor; PDB, Protein Data Bank; PpaC, inorganic pyrophosphatase; pKa, negative base-10 logarithm of the acid dissociation constant; PPP, pentose phosphate pathway; protein-SSB, BSH protein mixed disulfide; RES, reactive electrophilic species; RNS, reactive nitrogen species; RSS, reactive sulfur species; roGFP2, redox-sensitive green fluorescent protein; ROS, reactive oxygen species; SarZ, redox-sensing virulence regulator; STRING, Search Tool for the Retrieval of Interacting Genes/Proteins; Trx, thioredoxin; TrxR, thioredoxin reductase; YpdA, NADPH-dependent flavin oxidoreductase

* Corresponding author.

E-mail address: haike.antelmann@fu-berlin.de (H. Antelmann).

<https://doi.org/10.1016/j.redox.2018.08.017>

Received 6 July 2018; Received in revised form 9 August 2018; Accepted 23 August 2018

Available online 24 August 2018

2213-2317/ © 2018 The Authors. Published by Elsevier B.V. This is an open access article under the CC BY-NC-ND license (<http://creativecommons.org/licenses/by-nc-nd/4.0/>).

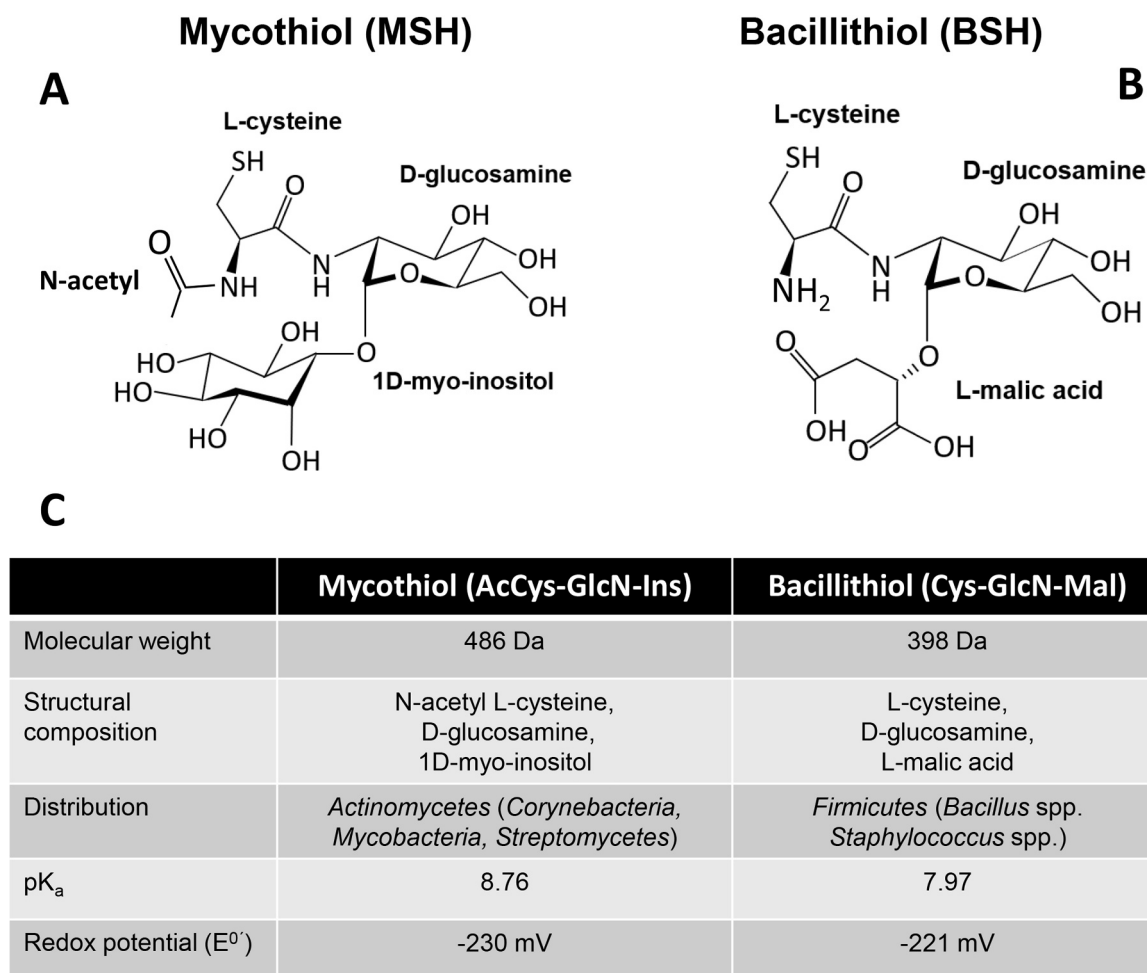


Fig. 1. Structures, distributions and chemical properties of mycithiol and bacillithiol. (A, C) Mycithiol (MSH, AcCys-GlcN-Ins) is composed of acetyl cysteine, glucosamine and myoinositol and has a molecular weight (MW) of 486 Da. MSH has a standard thiol redox potential of -230 mV and the pK_a of the mycithiolate anion was determined as 8.76. MSH is the major low molecular weight (LMW) thiol in high-GC Gram-positive *Actinomycetes*, including *Corynebacteria*, *Mycobacteria* and *Streptomyces*. (B, C) Bacillithiol (BSH, Cys-GlcN-Ins) consists of cysteine, glucosamine and malate. BSH has an MW of 398 Da and a standard thiol redox potential of -221 mV. The pK_a of the bacillithiolate anion was determined as 7.96. BSH is utilized as the major LMW thiol in low-GC content Gram-positive *Firmicutes*, such as *Bacillus* and *Staphylococcus* species. This figure is adapted from [7].

1. Introduction

Low molecular weight (LMW) thiols play an important role in many cellular processes in all organisms. They are crucial to maintain the reduced state of the cytoplasm and function as thiol-cofactors of enzymes involved in detoxification of reactive oxygen, electrophilic, chlorine, nitrogen and sulfur species (ROS, RES, RCS, RNS, RSS), toxins and antibiotics, in metal storage, buffering and transport, and sulfide homeostasis [1–3]. The well-studied LMW thiol glutathione (GSH) is produced in most eukaryotes, Gram-negative bacteria, and some Gram-positive bacteria, such as *Streptococci*, *Listeria*, *Lactobacilli* and *Clostridia* [2,4]. Most Gram-positive bacteria do not produce GSH and utilize instead alternative LMW thiols to cope with oxidative stress and redox regulation of metabolic enzymes. *Actinomycetes* utilize mycithiol (MSH) as their major LMW thiol (Fig. 1A) [5,6]. In *Firmicutes*, such as *Bacillus* and *Staphylococcus* species, bacillithiol (BSH) plays a related role like GSH to control cellular redox homeostasis under oxidative stress and infection conditions (Fig. 1B) [3,7]. There is also evidence that coenzyme A (CoASH) may substitute for the absence of BSH in some *Firmicutes*, such as *S. aureus* or *Bacillus megaterium* [2,8]. In addition, *S. aureus* and *Borrelia burgdorferi* both encode a CoAS disulfide reductase, further indicating that CoASH plays a role to cope with oxidative stress [8,9].

The question arises why different bacteria utilize different LMW thiols? Phylogenetic analyses revealed that the γ -glutamylcysteine synthase GshA, which catalyzes the first step of GSH biosynthesis, likely evolved in cyanobacteria and was distributed then to other bacteria and eukaryotes by lateral gene transfer [10,11]. Since the major function of GSH is the protection against oxygen toxicity, GSH biosynthesis was acquired with the evolution of oxygen by cyanobacteria. However, there was significant microbial diversity before the evolution of cyanobacteria, resulting in the evolution of alternative LMW thiols as protection mechanisms against increasing oxygen toxicity. Thus, it is not surprising that various prokaryotes utilize different LMW thiols [10].

LMW thiols are usually present in millimolar concentrations in the cytosol and are kept reduced by NADPH-dependent thiol-disulfide reductases [2,12]. Under oxidative and hypochlorite stress, redox-sensitive protein thiols are susceptible to various forms of thiol-oxidations, including reversible *S*-thiolations with LMW thiols as well as intra- or intermolecular protein disulfides (Fig. 2). In the absence of adjacent thiols, protein thiols can be also overoxidized to irreversible Cys sulfinic or sulfonic acids. Protein *S*-thiolations can have protective functions and control the activity of metabolic enzymes or transcription factors (Fig. 2). This review summarizes the current knowledge about the role of protein *S*-thiolations in cellular physiology and under oxidative stress

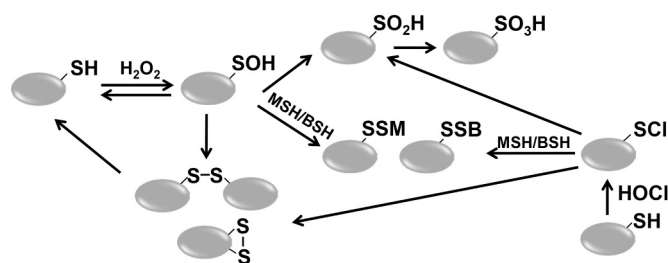


Fig. 2. Thiol-chemistry in response to H_2O_2 and $HOCl$ stress. Thiol-oxidation of Cys residues by H_2O_2 generates an unstable Cys sulfenic acid intermediate (Cys-SOH) that can rapidly react with LMW thiols, such as mycothiol (MSH) and bacillithiol (BSH), resulting in S-mycothiolations (Cys-SSM) and S-bacillithiolations (Cys-SSB) respectively. Alternatively, Cys oxidation can lead to the formation of intermolecular or intramolecular disulfides in proteins. In the absence of LMW thiols, protein thiols can be overoxidized to irreversible Cys sulfinic acid (Cys-SO₂H) and sulfonic acid (Cys-SO₃H). $HOCl$ reacts with protein thiols via chlorination, generating an unstable sulfenylchloride intermediate (Cys-SCI) that reacts further with MSH, BSH or protein-thiols to reversible S-mycothiolations, S-bacillithiolations or protein disulfides. In the absence of adjacent thiols, sulfenylchloride rapidly leads to overoxidation generating Cys sulfinic and sulfonic acids.

in Gram-positive bacteria, such as *Bacillus subtilis*, *Staphylococcus aureus*, *Corynebacterium diphtheriae* and *Mycobacterium smegmatis*. Molecular dynamics simulations have provided further insights into the structural protein changes upon S-thiolation, which are discussed for conserved S-bacillithiolated proteins at the molecular and mechanistic level.

2. Biosynthesis and functions of mycothiol and bacillithiol in Gram-positive bacteria

2.1. The biosynthetic pathway and functions of mycothiol in *Actinomycetes*

The cysteinyl pseudo-disaccharide mycothiol (MSH; AcCys-GlcN-Ins) is composed of acetyl cysteine (AcCys), glucosamine (GlcN) and myo-inositol (Ins) and has a molecular weight of 486 Da. MSH is the major LMW thiol in all *Actinomycetes*, including *Corynebacteria*, *Mycobacteria* and *Streptomyces* (Fig. 1AC) [6,7,13]. The biosynthesis of MSH is catalyzed in five enzymatic steps, which involve MshA, MshA2, MshB, MshC and MshD (Fig. 3). The first step of the MSH biosynthesis is catalyzed by the glycosyltransferase MshA, which conjugates myo-inositol-1-phosphate (Ins-P) to UDP-N-acetyl glucosamine (UDP-GlcNAc) leading to the formation of N-acetyl glucosamine myo-inositol-1-phosphate (GlcNAc-Ins-P). In the second step, the phosphatase MshA2 catalyzes dephosphorylation of GlcNAc-Ins-P to N-acetyl glucosamine myo-inositol (GlcNAc-Ins). The third step involves the metal-dependent deacetylase MshB for deacetylation of GlcNAc-Ins leading to GlcN-Ins [6,14]. The MshB enzyme is a homolog of the MSH-conjugate amidase (Mca) that catalyzes the hydrolysis of MS-conjugates. In the fourth step of the MSH biosynthesis, the ATP-dependent ligase MshC ligates cysteine to GlcN-Ins leading to Cys-GlcN-Ins. The Cys ligase MshC is a homolog of the Cys-tRNA synthetase. The acetyltransferase MshD catalyzes the acetylation of the Cys amino group by acetyl-CoA as final step of MSH biosynthesis [6,13,15]. Under oxidative stress, MSH is oxidized to mycothiol disulfide (MSSM) which requires the NADPH-dependent mycothiol disulfide reductase (Mtr) for NADPH-dependent reduction of MSSM to maintain a high MSH: MSSM redox ratio [13,16]. The levels of MSH vary strongly between different members of *Actinomycetes* with the highest levels of ~1–20 $\mu\text{mol/g}$ raw dry weight (rdw) in *Mycobacteria* and much lower levels of 0.3 $\mu\text{mol/g}$ rdw in *C. diphtheriae* [17,18].

The thiol pK_a for MSH was determined as 8.76, which is only slightly more acidic (0.17 pH units) compared to the thiol pK_a of GSH, and 0.4 pH units less acidic compared to the first microscopic thiol pK_a value of free Cys (Fig. 1C) [19]. Since MSH is present at much higher

levels compared to Cys in *Actinomycetes*, the mycothiolate anion is the most abundant LMW thiolate anion that reacts with oxidants and electrophiles *in vivo*. The thiol-redox potential of MSH is in the range of GSH and was calculated as $E^0(\text{MSSM}/\text{MSH})$ of -230 mV (Fig. 1C). However, the thiol-redox potential of MSH calculated with biophysical methods showed discrepancies compared to previously measured E_{MSH} values determined as -300 mV using the Mrx1-roGFP2 biosensor [19,20]. This indicates technical challenges to measure the exact MSH/MSSM ratio inside bacterial cells.

MSH plays an important role as thiol-cofactor for many enzymes that are involved in the detoxification of antibiotics, xenobiotics, ROS, RES, RNS, and other reactive species (Fig. 4) [2,6,7]. For a comprehensive overview of the detailed functions of MSH in different *Actinomycetes* the reader is referred to recent reviews which will be briefly outlined here and updated based on novel results [6,7,13].

MSH conjugates xenobiotics and antibiotics either spontaneously or enzyme-catalyzed by MSH S-transferases (MST), which belong to the DinB superfamily (Figs. 3 and 4) [21]. These MSH-S-conjugates are hydrolyzed by the mycothiol-S-conjugate amidase (Mca), releasing mercapturic acid derivatives (AcCys-R) and GlcN-Ins. The GlcN-Ins is recycled to MSH and the toxic mercapturic acid derivatives are exported from the cell. Mca was shown to be involved in detoxification of MSH-S-conjugates with the antibiotics cerulenin and rifamycin in *Mycobacteria* [13]. MSH and ergothioneine (EGT) were also shown to function as sulfur donors through S-glycosylation reactions to mediate amino sugar transfer, activation and modification during the biosynthesis of the lincosamide antibiotic lincomycin in *Streptomyces lincolnensis* [22,23]. This indicates a direct function of the LMW thiols MSH and EGT in the biosynthesis and molecular assembly of sulfur-containing natural products [22,23].

MSH functions as thiol-cofactor for detoxification of formaldehyde, RNS, maleylpyruvate, methylglyoxal and arsenate and is required for activation of anti-mycobacterial prodrugs (Fig. 4). The MSH-dependent detoxification enzyme MscR is a dual function enzyme with S-nitrosomycothiol (MSNO) reductase and formaldehyde dehydrogenase activities [6,13]. Formaldehyde is conjugated to MSH leading to S-hydroxymethyl-MSH, which is further oxidized to an S-formyl thioester and formate. MSNO is converted by MscR to MSH sulfinamide (MSONH₂). The maleylpyruvate isomerase of *C. glutamicum* uses MSH as a cofactor for the enzymatic isomerization of maleylpyruvate to fumarylpyruvate [24]. MSH was shown as cofactor of the MSH-dependent arsenate reductases ArsC1/C2 in the detoxification of arsenate [25,26].

MSH further contributes to antibiotic resistance in *Mycobacterium tuberculosis* (Mtb). MSH is required for activation of the pro-drugs isoniazid (INH) and nitrofuranylcalanolides (NFCs) which are potent anti-mycobacterial drugs [27,28]. INH is activated by the catalase KatG and MSH, leading to NAD-INH adduct formation and inhibition of the *enoyl*-ACP reductase (InhA) of the mycolic acid biosynthesis pathway [29]. INH resistant Mtb isolates often carry spontaneous mutations in *katG* or *mshA* [14]. Novel antimycobacterial drugs, such as the nitrofurantoin derivatives NFC or the thienopyrimidine compound TP053 are activated by the MSH-dependent oxidoreductase Rv2466c, which was recently revealed as MSH-dependent nitroreductase to reduce nitro groups to amines [28,30]. Importantly, NFC-resistant mutants were selected which had mutations in the gene encoding Rv2466c. This indicates that the MSH-dependent nitroreductase activity of Rv2466c is crucial for pro-drug activation [28]. Rv2466c has a DsbA-like structure and can also function as mycoredoxin-2 in demycothiolation with electrons from the MSH/Mtr pathway [30]. Rv2466c uses a monothiol-disulfide mechanism for reduction of S-mycothiolated proteins or intramolecular disulfides and a dithiol mechanism for prodrug activation (TP053) *in vitro*.

MSH further functions as reservoir of cysteine and is much less susceptible to auto-oxidation compared to cysteine [13]. In addition, MSH has important functions in the virulence and survival of the pathogen Mtb under infection conditions [31]. An essential function of

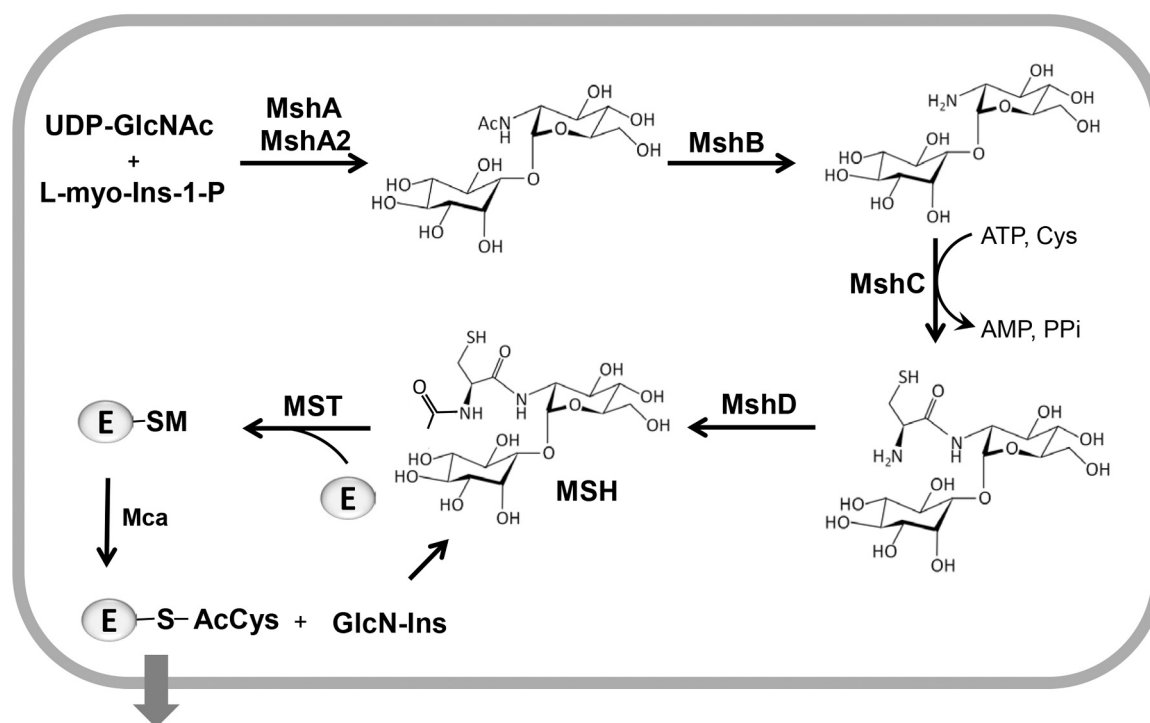


Fig. 3. The biosynthesis pathway of MSH and detoxification of electrophiles in *Actinomycetes*. The MSH glycosyltransferase MshA conjugates *myo*-inositol-1-phosphate (Ins-P) to UDP-*N*-acetyl glucosamine (UDP-GlcNAc) leading to *N*-acetyl glucosamine *myo*-inositol-1-phosphate (GlcNAc-Ins-P). Dephosphorylation and deacetylation of GlcNAc-Ins-P is catalyzed by the phosphatase MshA2 and the deacetylase MshB, respectively. MshC ligates cysteine to GlcN-Ins in an ATP-dependent reaction. MshD acetylates the Cys moiety of Cys-GlcN-Ins to produce MSH. The mycothiol-S-transferase (MST) catalyzes the MSH-dependent detoxification of toxic electrophiles (E), xenobiotics and antibiotics. The mycothiol-S-conjugate amidase (Mca) cleaves the amide bond to produce mercapturic acids (AcCys-R) and GlcN-Ins. Mercapturic acids are exported and GlcN-Ins is recycled to MSH. This figure is adapted from [93].

MSH for growth and viability was found in *Mtb* since the *mshC* mutant could be only generated in the presence of a second copy of *mshC* [31].

2.2. Shotgun proteomics identified widespread protein S-mycothiolations in *Actinomycetes*

Under HOCl stress, MSH was shown to form mixed disulfides with protein thiols, termed as protein S-mycothiolations. Protein S-mycothiolations are widespread redox-modifications and were identified in many *Actinomycetes*, such as *C. glutamicum*, *C. diphtheriae* and *M. smegmatis* [18,25,32]. However, the extent of protein S-mycothiolation under HOCl stress differs with 58, 25 and 26 proteins identified in *M. smegmatis*, *C. glutamicum* and *C. diphtheriae*, respectively (Table S1). This higher level of S-mycothiolated proteins in *Mycobacteria* might be correlated with the 20-fold higher MSH level compared to *Corynebacteria* [17]. Overall, S-mycothiolated proteins were shown to be involved in many metabolic pathways, including glycolysis, gluconeogenesis, glycogen and maltodextrin degradation, as well as in the biosynthetic pathways for fatty acids, amino acids and nucleotides, co-factors, and protein translation. Several conserved S-mycothiolated proteins have antioxidant functions, such as peroxiredoxins (Tpx, Mpx, AhpE, AhpC) and the methionine sulfoxide reductase MsrA [18,25,32,33].

In *C. glutamicum*, 25 proteins with S-mycothiolations were identified under HOCl stress and their level of oxidation was quantified using fluorescence-based thiol-redox proteomics [25] (Table S1). These S-mycothiolation targets function in glycolysis (Fba, Pta, XylB), glycogen and maltodextrin degradation (MalP), in the amino acid biosynthesis pathways for serine, cysteine, methionine (MetE, SerA, Hom), nucleotides and thiamine cofactors (GuaB, PurL, ThiD1, ThiD2), antioxidant functions (Tpx, Mpx), methionine sulfoxide reduction (MsrA), heme degradation (HmuO), and protein translation (RpsF, RpsC, RpsM, Tuf).

Among these, Tuf, GuaB1, GuaB2, SerA and MetE are also conserved targets for S-thiolations across Gram-positive bacteria [25]. The most interesting S-mycothiolated metabolic enzyme in *C. glutamicum* was the maltodextrin phosphorylase (MalP), which is involved in glycogen degradation during the stationary phase [34]. The *malP* mutant was very sensitive under HOCl stress indicating an essential function of MalP under oxidative stress [25]. Furthermore, the glycogen content was not decreased in *C. glutamicum* wild type under HOCl stress despite drastically reduced glucose uptake rates. Thus, S-mycothiolation of MalP is suggested to inhibit its function in glycogen degradation to save the source of energy under oxidative stress [25].

Many antioxidant enzymes were S-mycothiolated at their active site Cys residues and it was further investigated if S-mycothiolation functions in redox-regulation of peroxiredoxins (Tpx, Mpx, AhpE) and methionine sulfoxide reductases (MsrA, MsrB) [25,33,35–38]. The thiol peroxidase (Tpx), an atypical 2-Cys peroxiredoxin was S-mycothiolated at its active and resolving Cys60 and Cys94 residues [25]. S-mycothiolation of Tpx *in vitro* inhibited its peroxidase activity. The MSH peroxidase (Mpx) was also S-mycothiolated at its peroxidatic Cys36 residue. The methionine sulfoxide reductase MsrA is involved in the repair of methionine sulfoxides and was S-mycothiolated at its conserved Cys91 residue. The cobalamin-independent methionine synthase (MetE) was S-mycothiolated at its Zn-binding active site Cys713 under HOCl stress and S-mycothiolation of MetE was shown to function in thiol-protection under acid stress [25,39]. The inosine-5-monophosphate (IMP) dehydrogenases GuaB1 and GuaB2 are conserved S-thiolated proteins across bacteria. GuaB1 and GuaB2 were S-mycothiolated at their active site Cys302 and Cys317 respectively, forming the thioimide intermediate [25].

In the pathogen *C. diphtheriae*, 26 S-mycothiolated proteins were identified under HOCl stress using shotgun liquid chromatography tandem mass spectrometry (LC-MS/MS) analysis [18] (Table S1). These

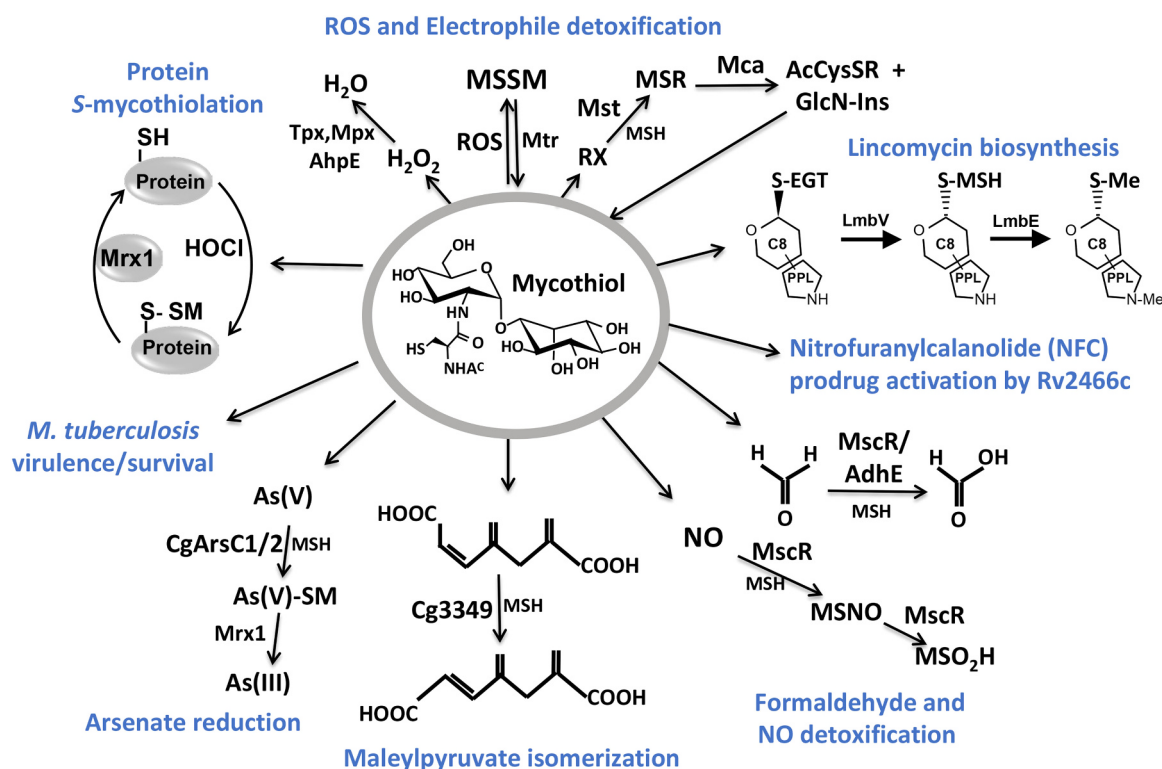


Fig. 4. The functions of mycothiol (MSH) in *Actinomycetes*. Mycothiol (MSH) is oxidized by ROS to mycothiol disulfide (MSSM) and regenerated by the mycothiol disulfide reductase (Mtr). The antioxidant enzymes Mpx, Tpx and AhpE were shown to function in H_2O_2 detoxification. Electrophiles (RX) are detoxified by the MSH S-transferase (MST) leading to MS-electrophiles (MSR) that are cleaved by the MSH S-conjugate amidase (Mca) to mercapturic acids (AcCyS-R) that are exported. MSH and ergothioneine (EGT) are involved in natural product biosynthesis of the lincosamide antibiotic lincomycin in *Streptomyces lincolnensis*. MSH functions as cofactor for the nitroreductase Rv2466c which activates the new mycobactericidal prodrug Nitrofuranylcalanolide (NFC) for reduction of the nitro group to amines. MSH is also a thiol-cofactor for detoxification of formaldehyde, S-nitrosomycothiol (MSNO) and arsenate. MscR is involved in MSNO detoxification generating MSH sulfinamide (MSONH₂). MscR and AdhE both catalyze oxidation of formaldehyde to formate. In *C. glutamicum*, MSH is a cofactor for maleylpyruvate isomerase involved in isomerization of maleylpyruvate to fumarate. The arsenate reductases ArsC1/C2 catalyze conjugation of MSH to arsenate [Ars(V)] which is further reduced by Mrx1 to arsenite [Ars(III)]. MSH is also important for growth, survival and virulence in *M. tuberculosis*. Under HOCl stress, MSH functions in post-translational modification of proteins, termed as S-mycothiolations. This figure is adapted from [2].

include five conserved targets for S-thiolations across Gram-positive bacteria, such as AhpC, the ribosomal proteins RplC and RpsM, the glycolytic enzyme glyceraldehyde-3-phosphate dehydrogenase (GapDH), and GuaB [18]. Other S-mycothiolated proteins are involved in energy metabolism, including the ribose 5-phosphate isomerase DIP1796 and the NADH dehydrogenases Ndh, GlpD and DIP1726. Further targets for S-mycothiolation function in the biosynthesis of amino acids (LeuB, DapA, GlnA), purine (PurA), iron sulfur-clusters (DIP1631) and cell wall metabolites (GlmS). The S-mycothiolated proteins contributed with 0.2–0.75% Cys abundance to the total Cys proteome of *C. diphtheriae* as revealed by shotgun proteomics [18]. Further biochemical studies of GapDH confirmed that protein S-mycothiolations function in redox-regulation and thiol-protection against overoxidation as referred in the following section.

In *M. smegmatis*, we identified 58 S-mycothiolated proteins under HOCl stress [32] (Table S1). The conserved peroxiredoxins Tpx, AhpC and OsmC are S-mycothiolated at their active and/or resolving Cys residues, which are involved in redox-regulation and detoxification processes in *M. smegmatis*. The global transcriptional regulator for iron uptake of the DtxR-family (IdeR) was S-mycothiolated at Cys102 in its primary iron-binding site [32]. Many abundant enzymes of the energy metabolism were further identified as S-mycothiolated in *M. smegmatis*. These are involved in the glycerol catabolism, glycolysis, the glyoxalate shunt and gluconeogenesis. The glycerol kinase GlpK3 and the glycerol dehydrogenase Adh2 are abundant S-mycothiolated proteins since glycerol is used as sole source of carbon and energy in *M. smegmatis*. The generation of dihydroxyacetone phosphate (DHAP) involves GlpK3

and Adh2. Thus, S-mycothiolation could prevent glycerol degradation under HOCl stress to save the carbon and energy source. The isocitrate lyase AceA and the myo-inositol-1-phosphate synthase Ino1 were further identified as abundant S-mycothiolated proteins in *M. smegmatis*. AceA is the key enzyme of the glyoxylate bypass of the TCA cycle in *M. tuberculosis*, which enables the use of carbon for biomass production via gluconeogenesis during growth on fatty acids as sole source of carbon and energy [40]. Thus, S-mycothiolation could inhibit AceA under oxidative stress to stop gluconeogenesis [32]. Furthermore, abundant enzymes involved in the biosynthesis of fatty acids as precursors for mycolic acids were S-mycothiolated in *M. smegmatis*, including acetyl-CoA carboxylases (AccD5 and AccD6), the enoyl-CoA hydratase (EchA6), the methoxy mycolic acid synthase (UmaA), the acyl-CoA dehydrogenase (MSMEG_0531), and the acyl-CoA-thioesterase (MSMEG_6208). Other S-mycothiolated proteins of *M. smegmatis* are involved in the nucleotide biosynthesis, including GuaB and GuaB2, and biosynthesis enzymes for thiamine (ThiG, MSMEG_4827), cobalamin (CobN), iron sulfur-cluster assembly (YfhF2) as well as ribosomal proteins (RplC, RpsM, RpsR2) and amino acyl tRNA synthetases (GatC, PheT) for protein translation [32]. Overall, many detailed future studies are required to elucidate the physiological role of the widespread protein S-mycothiolations in redox regulation and/or thiol-protection in *Mycobacteria*. In particular, it would be interesting if mycothiolation functions in redox regulation of transcriptional regulators under infection conditions in *M. tuberculosis*. Recent biochemical studies revealed the formation of S-mycothiolated NsrR, a FeS-cluster-based Rrf2-family regulator and NO-sensor in many Gram-positive bacteria [41].

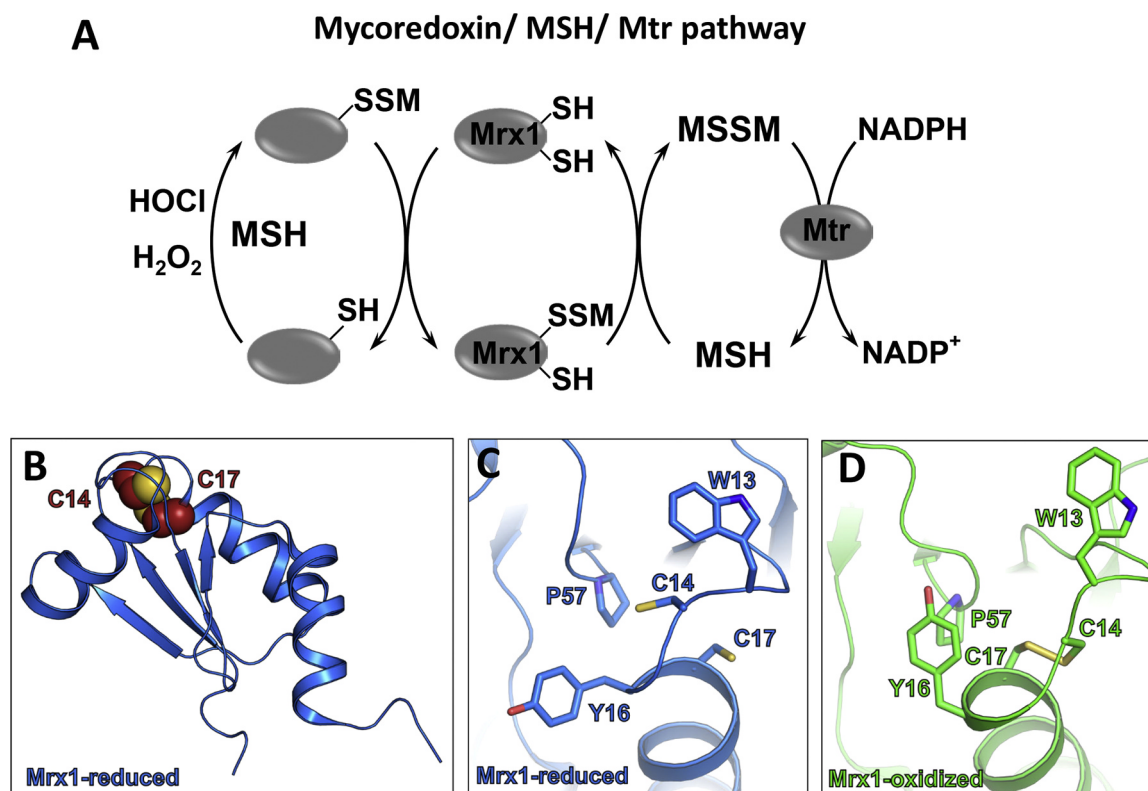


Fig. 5. Reversal of protein S-mycothiolation by the mycoredoxin-1 pathway. (A) In MSH-producing *Actinomycetes*, S-mycothiolated proteins are reduced by mycoredoxin-1 (Mrx1), resulting in an Mrx1-SSM intermediate that is reduced by MSH leading to MSSM. The NADPH-dependent mycothiol disulfide reductase Mtr recycles MSSM back to MSH. (B) The crystal structure of the reduced Mrx1 (PDB ID: 2LQO) and (C) its active site. (D) The oxidized Mrx1 active site in its intramolecular disulfide form (PDB ID: 2LQQ). The active and resolving Cys residues of Mrx1 are shown as spheres in (B) and as sticks in (C, D).

Using mass spectrometry, the formation of several iron nitrosyl species and S-thiolated forms of the Cys residues coordinating the FeS cluster have been reported for NsrR [41]. Thus, related S-nitrosylation and S-thiolation mechanisms could be relevant for redox-sensing of NsrR under *in vivo* conditions. In support of this notion, the NsrR-controlled *hmp* gene is also induced under HOCl stress in the RNAseq transcriptome of *C. glutamicum* and *S. aureus* [32,42]. This might indicate that NsrR could sense HOCl stress via protein S-thiolation which remains to be investigated.

2.3. Protein S-mycothiolation is redox-controlled by the mycoredoxin-1 (Mrx1) and thioredoxin pathways

The redox regulation of protein S-mycothiolations requires specific thiol-disulfide reducing pathways to restore the protein activity. The Mrx1/MSH/Mtr system is specific for the de-mycothiolation of MSH-mixed protein disulfides (Fig. 5). Mycoredoxin-1 (Mrx1) was characterized as a glutaredoxin-homolog in *Actinomycetes* [43]. Mrx1 has a typical Trx-like fold with a CGYC catalytic active site, composed of a four-stranded antiparallel β -sheet and surrounded by three α -helices. The CGYC motif is located at the N-terminus of the first α -helix. The conserved proline residue (Pro57) is located in *cis*-conformation opposite to the active site. The active site Cys14 is solvent exposed in both oxidized and reduced forms of Mrx1, while the C-terminal resolving Cys17 is buried inside the protein [43]. Mrx1 has a negative redox potential of -218 mV that is in the same range as for glutaredoxins. Thus, Mrx1 can function as effective thiol disulfide reducing enzyme in *Actinomycetes* [44]. Mrx1 catalyzes the de-mycothiolation of MSH-mixed protein disulfides in a bimolecular nucleophilic substitution reaction analogous to the monothiol reaction mechanisms of glutaredoxins. During de-mycothiolation of the substrates, Mrx1 is S-mycothiolated at its active site Cys14. Oxidized Mrx1 is regenerated by

MSH leading to formation of MSSM, which is reduced by Mtr with NADPH as electron donor. The electron transfer from the Mrx1/MSH/Mtr electron pathway to the MSH mixed disulfide substrate was shown in a hydroxyethyl disulfide (HED) assay [43].

The peroxiredoxin Tpx of *C. glutamicum* was identified as first substrate for Mrx1 *in vitro*. S-mycothiolation of the peroxidatic Cys60 inhibited the peroxidase activity of Tpx, which could be restored by the Mrx1/MSH/Mtr electron pathway. Mass spectrometry confirmed the complete reduction of Tpx-SSM and MSH transfer to Mrx1, resulting in the formation of a transient Mrx1-SSM intermediate [25]. Another mycothiol peroxidase, Mpx of *C. glutamicum* controls intracellular ROS levels and was shown to be recycled by both, the Mrx1 and the thioredoxin/ thioredoxin reductase (Trx/TrxR) pathways [35,38]. Reduction of the S-mycothiolated peroxidatic Cys36 of Mpx by Mrx1 proceeds via a monothiol mechanism as demonstrated by kinetic assays and MSH-specific Western blots [35]. Arsenate [Ars(V)] detoxification by the arsenate reductases ArsC1 and ArsC2 in *C. glutamicum* requires MSH and the Mrx1/MSH/Mtr pathway. ArsC1/C2 catalyze conjugation of MSH to As(V) resulting in an arseno-MSH conjugate (As(V)-SM). Mrx1 reduces the As(V)-SM conjugate to arsenite [As(III)] via a monothiol mechanism (Fig. 4) [26].

In *C. diphtheriae*, the glycolytic GapDH was the most abundant S-mycothiolated protein contributing with 0.75% to the total Cys proteome [18]. GapDH uses the active site Cys for the nucleophilic attack at the aldehyde group of glyceraldehyde-3-phosphate (G3P) to catalyze its phosphorylation to 1,3-bisphosphoglycerate and thereby generating NADH [45]. GapDH is S-mycothiolated at the conserved catalytic active site Cys153 resulting in reversible inhibition of GapDH activity under HOCl stress [18]. It was previously shown that H₂O₂-stress leads to an inactivation of GapDH upon S-thiolation, resulting in a metabolic re-configuration of central carbon metabolism [46,47]. The lack of glycolysis is compensated by an increased glycolytic flux through the

pentose-phosphate pathway (PPP) to provide increased levels of NADPH as cofactor for thiol-disulfide oxidoreductases. The active site Cys of GapDH is highly reactive and susceptible for various post-translational thiol-modifications in response to ROS and RNS, including S-glutathionylation, S-nitrosylation and sulfenic acid formation in many eukaryotes [48,49]. It was shown that the relatively high reactivity of the active site thiolate towards H_2O_2 depends on the stabilization of the transition state and a dedicated proton relay mechanism that promotes leaving group departure [50].

We demonstrated that S-mycothiolation protects the active site Cys of GapDH in *C. diphtheriae* against irreversible overoxidation under both H_2O_2 and HOCl treatments [18]. In our GapDH assays without MSH, increasing doses of H_2O_2 and HOCl resulted in an irreversible overoxidation of Cys153 to the sulfonic acid and partially Cys153-SS-Cys157 intramolecular disulfide bond formation [18]. In the presence of MSH, S-mycothiolation of the catalytic active site Cys153 could be verified by mass spectrometry and non-reducing MSH-specific Western blot analysis. Time course experiments indicated that inactivation of GapDH by S-mycothiolation was faster compared to its inactivation in the overoxidation pathway under HOCl and H_2O_2 stress [18]. In addition, intramolecular disulfides were detected under both, H_2O_2 and HOCl treatment in the presence and absence of MSH as an additional redox-regulatory mechanism of GapDH [18]. We also studied the redox-regulation of protein S-mycothiolation by the Mrx1 and Trx pathway. Reduction of S-mycothiolated GapDH occurred much faster by the Mrx1 pathway compared to Trx *in vitro*. Thus, Mrx1 plays probably the major role in demycothiolation of GapDH *in vivo* while Trx has only a minor role. These data are in agreement with the kinetics obtained for demycothiolation of Mpx by Mrx1, which was also faster compared to reduction by the Trx pathway [35].

MsrA and MsrB are further important redox enzymes which catalyze the reduction of two stereotypes of methionine sulfoxides (MetSO) to L-methionine [51]. While MsrA is specific for reduction of methionine-S-sulfoxide, MsrB shows activity for reduction of methionine-R-sulfoxides [52]. The Mrx1 and Trx pathway were shown to be involved in the recycling of the methionine sulfoxide reductase Cd-MsrA and Cg-MsrA during reduction of methionine sulfoxides in *C. diphtheriae* and *C. glutamicum* [36,37,53]. Two different redox relays operate in recycling of Cd-MsrA by the Trx and Mrx1 pathway upon MetSO reduction. Cd-MsrA has three Cys residues in positions 52, 206 and 215 with Cys52 as the active site. The disulfide relay which couples MetSO reduction by Cd-MsrA to the Trx pathway starts with formation of the Cys52-SOH upon attack of the MetSO substrate releasing reduced L-Met. Next, Cys52 is attacked by Cys206 or Cys216 resulting in intramolecular disulfides between Cys52 and either Cys206 or Cys215. This disulfide is reshuffled to a Cys206-Cys215 disulfide which is a substrate of Trx. In the MSH redox relay, Cys52-SOH forms an MSH mixed disulfide, followed by the subsequent transfer of MSH to Cys215 and Cys206. Cys206-SSM is finally the substrate that is recycled by the Mrx1 pathway. Thus, two different redox relays were discovered for Cd-MsrA upon MetSO reduction that require the Trx or Mrx1 pathway for regeneration [36]. Another study of Cg-MsrA's catalytic mechanism in *C. glutamicum* revealed that Mrx1 reduces Cys56-SSM while Trx reduces the intramolecular disulfide between both C-terminal resolving Cys residues [53]. In addition, the Trx and Mrx1 pathways were required for reduction of Cg-MsrA under stress and the Trx pathway was found to be involved in Cg-MsrA regeneration under non-stress conditions. Apart from MsrA, the redox cycle of the methionine sulfoxide reductase MsrB of *C. glutamicum* was recently studied [37]. MsrB is specific for reduction of methionine-R-sulfoxides which requires the Trx pathway for recycling and was not important under oxidative stress *in vivo* [37].

The membrane-associated one-Cys peroxidase AhpE of *M. tuberculosis* was identified as S-mycothiolated at its active site Cys45 and was shown to be reduced by Mrx1 *in vitro* [33]. AhpE is S-mycothiolated during H_2O_2 detoxification. The reduction of AhpE-SSM was demonstrated in the presence of wild type Mrx1, indicating a dithiol

mechanism. The peroxiredoxin AhpE comprises a molecular link between the peroxidase system and the Mrx1 redox pathway in *Mycobacteria*. Using NMR spectroscopy, the AhpE structures were resolved in the reduced, sulfenic acid, and sulfenic acid forms giving insights into the MSH-dependent reduction mechanism of AhpE [54].

In conclusion, recent studies on several identified S-mycothiolated antioxidant and metabolic enzymes (Tpx, Mpx, MsrA, and GapDH) revealed that both, the Mrx1 and Trx pathway are coupled to regeneration of their enzymatic activities under oxidative stress. However, Mrx1 was faster in demycothiolation of GapDH and Mpx compared to Trx indicating that Mrx1 is the primary de-mycothiolating enzyme under oxidative stress. In concert with MSH and Mtr, Mrx1 can undergo mono- and dithiol mechanisms to reduce protein MSH-mixed disulfides. It remains to be further investigated whether mycoredoxin-2 (Rv2466c) plays a related or alternative role in reduction of S-mycothiolated proteins.

2.4. The biosynthetic pathway and functions of bacillithiol in Firmicutes

Bacillithiol (BSH, Cys-GlcN-malate) is the α -anomeric glycoside of L-cysteinyl-D-glucosamine with L-malic acid and has an MW of 398 Da (Fig. 1BC). BSH functions as the major LMW thiol in many Firmicutes bacteria, including *Bacillus* and *Staphylococcus* species [5]. The biosynthesis of BSH occurs in three steps by the enzymes BshA, BshB and BshC. The glycosyltransferase BshA catalyzes the conjugation of UDP-N-acetylglucosamine (UDP-GlcNAc) to L-malate leading to GlcNAc-Mal (Fig. 6). GlcNAc-Mal is further deacetylated by the deacetylase BshB to GlcN-Mal. The cysteine ligase BshC adds cysteine to GlcN-Mal as final step in the BSH biosynthesis [3,55]. BSH is oxidized to BSSB under oxidative stress and high BSH/BSSB ratios were calculated as 100:1–400:1 in *B. subtilis* cells [56]. The putative BSSB reductase was suggested to function as NADPH-dependent flavin oxidoreductase YpdA which co-occurs with the BSH biosynthesis enzymes in BSH-producing bacteria [55]. However, experimental evidence is lacking to demonstrate a role of YpdA as BSSB reductase [3]. The standard thiol redox potential of BSH was calculated as $E^0(\text{BSSB}/\text{BSH})$ of -221 mV which is more positive compared to GSH ($E^0(\text{GSSG}/\text{GSH})$ is -240 mV) (Fig. 1C) [56]. However, microscopic pK_a values of $\text{pK}_{\text{aSH}} = 7.97$ and $\text{pK}_{\text{aSH}} = 9.55$ were determined for the bacillithiolate anion (with protonated and deprotonated Cys amino group, respectively), suggesting a more acidic BSH thiolate anion with enhanced reactivity (Fig. 1C) [56].

BSH functions in the detoxification of many thiol-reactive compounds, electrophiles, alkylating agents, toxic metals and antibiotics (Fig. 7) [3,55]. BSH-deficient mutants in *B. subtilis* showed increased sensitivities toward hypochlorite, diamide, methylglyoxal, ROS, osmotic and acidic stress, alkylating agents, and fosfomycin. For a comprehensive overview of the many functions of BSH, the reader is referred to a recent review, which will be summarized and updated here only briefly [3].

The BSH-dependent thiol-S-transferase FosB is involved in the detoxification of the antibiotic fosfomycin and cleaves the ring structure of the BS-fosfomycin-conjugate [57]. The *fosB* and *bsh* mutants showed equal sensitivities towards fosfomycin treatment in *B. subtilis* and *S. aureus* indicating that FosB is a BSH-dependent S-transferase for fosfomycin detoxification. Co-crystallization of *S. aureus* FosB with BSH resulted in the formation of a BSH-mixed disulfide at the active site Cys9 of FosB of *S. aureus in vitro* [55,58]. However, the electron density for the whole molecule of BSH was not complete in the FosB structure. The BSH S-transferase BstA catalyzes the conjugation of BSH to reactive electrophiles, such as chlorinated hydrocarbons and monobromobimane *in vitro* [21]. The resulting BS-electrophiles (BSR) are cleaved by the BSH S-conjugate amidases Bca or BshB2 into GlcNAc-Mal and mercapturic acids (CysSR). CysSR are exported from the cell by the potential efflux pumps encoded by the *yfiS* and *yfiU* genes [21].

BSH functions in detoxification of methylglyoxal as cofactor for the BSH-dependent glyoxalases GlxAB in *B. subtilis* [59]. Methylglyoxal

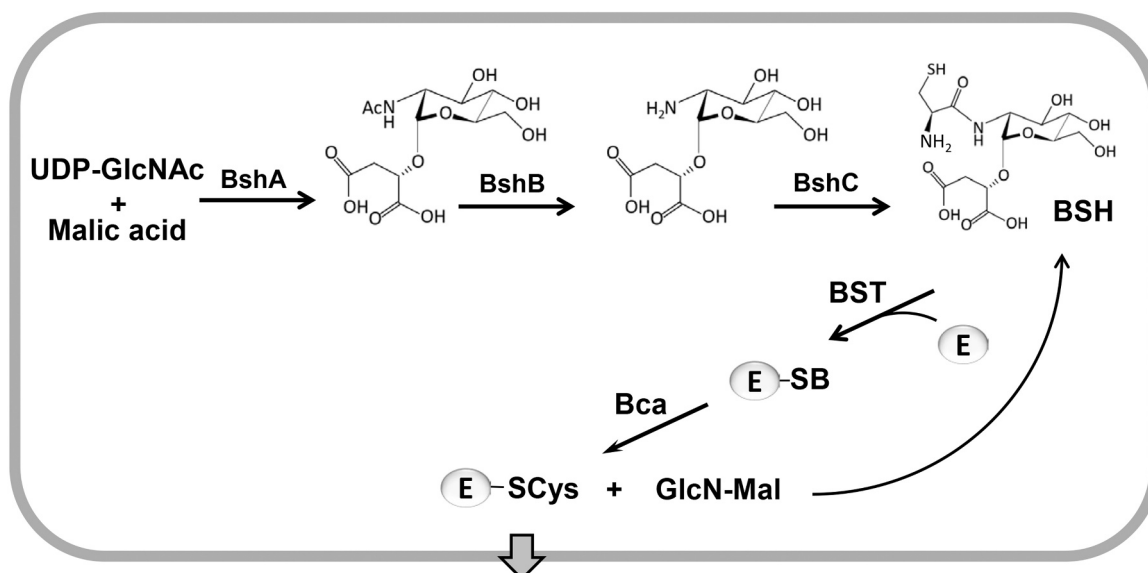


Fig. 6. The biosynthesis pathway of bacillithiol in *Firmicutes*. The glycosyltransferase BshA catalyzes the conjugation of UDP-*N*-acetylglucosamine (UDP-GlcNAc) to L-malate leading to *N*-acetylglucosamine malate (GlcNAc-Mal). GlcNAc-Mal is deacetylated by the deacetylase BshB to GlcN-Mal. The cysteine ligase BshC ligates cysteine to GlcN-Mal. The detoxification of toxic electrophiles (E) requires conjugation by the bacillithiol-S-transferase (BST) leading to BSH-S-conjugates which are cleaved by the BSH-S-conjugate amidase (Bca). Mercapturic acids are exported and GlcN-Mal is recycled to BSH. This figure is adapted from [93].

reacts spontaneously with BSH to form BSH-hemithioacetal that is converted to *S*-lactoyl-BSH by GlxA. GlxB catalyzes the hydrolysis of *S*-lactoyl-BSH to lactate which is secreted. BSH is involved in detoxification of the toxic electrophile formaldehyde in the facultative

methylotrophic bacterium *Bacillus methanolicus* which uses methanol as sole source of energy and carbon [60]. An unknown formaldehyde dehydrogenase is involved in oxidation of *S*-formyl-BSH in *Bacillus methanolicus* cells during growth on methanol, which is required for

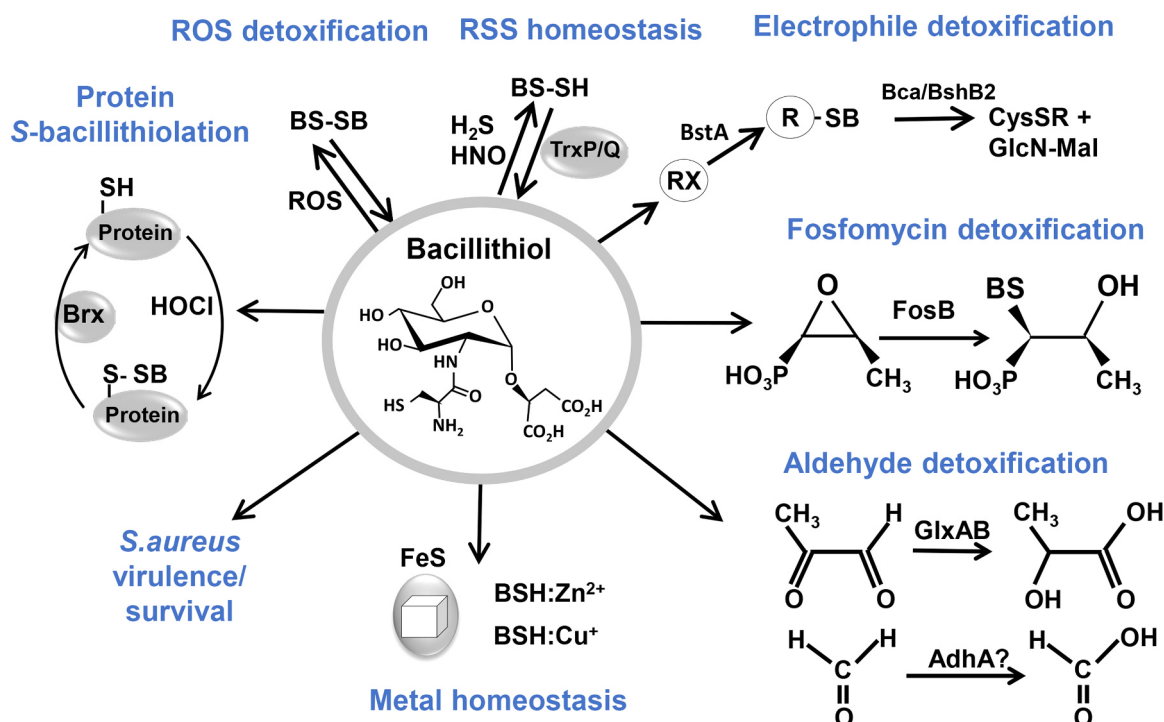


Fig. 7. The many functions of bacillithiol in *Firmicutes*. BSH is involved in detoxification of ROS, RES, HOCl, RSS and antibiotics (fosfomycin, rifampicin) in *B. subtilis* and *S. aureus*. ROS lead to oxidation of BSH producing bacillithiol disulfide (BSSB). Under sulfide stress, BSH persulfides (BSSH) were determined, which can be reduced by thioredoxins (TrxP and TrxQ). Electrophiles (RX) are conjugated to BSH by the BSH *S*-transferase BstA to form BS-electrophiles (BSR). The BSH *S*-conjugate amidases Bca or BshB2 cleave BSR into GlcNAc-Mal and mercapturic acids (CysSR) that are exported. BSH is used as cofactor for the epoxide hydrolase FosB in fosfomycin detoxification and functions as a cofactor for the glyoxalases GlxA and GlxB in *B. subtilis* in methylglyoxal detoxification. GlxA converts BSH-hemithioacetal to *S*-lactoyl-BSH that is a substrate for GlxB producing D-lactate. BSH-dependent detoxification of formaldehyde might be catalyzed by the formaldehyde dehydrogenase (AdhA) in *B. subtilis*. BSH functions in metal homeostasis as Zn^{2+} buffer and in FeS cluster assembly. In *S. aureus*, BSH is important for the virulence of *S. aureus* in macrophage infection assays. Under HOCl stress, proteins are *S*-bacillithiolated, which can be reversed by bacilliredoxins (Brx). This figure is adapted from [2].

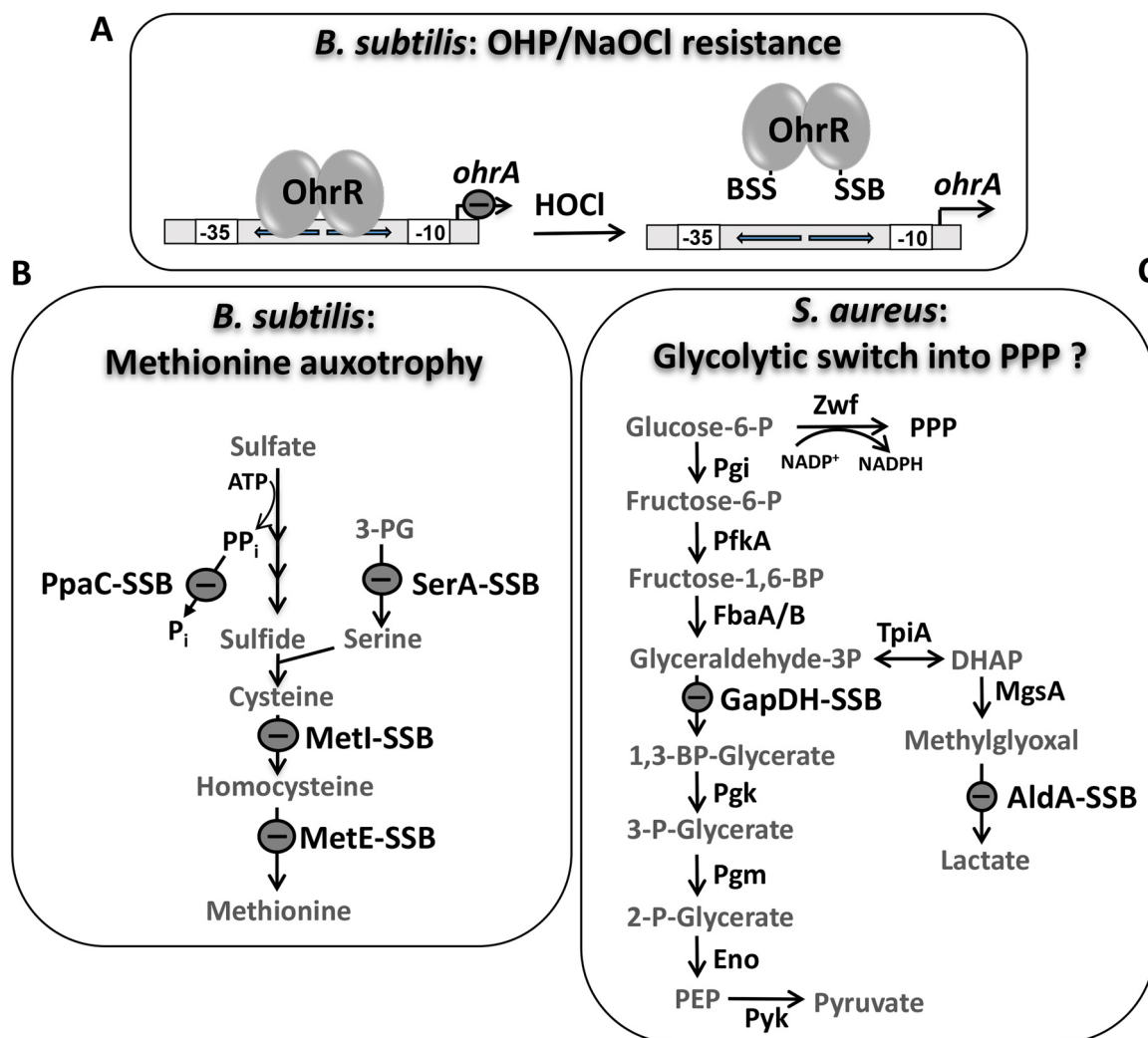


Fig. 8. Physiological roles of S-bacillithiolations of OhrR, MetE, GapDH and AldA under HOCl stress. (A, B) HOCl stress leads to S-bacillithiolation of OhrR and MetE in *B. subtilis*. (A) The repressor activity of the OhrR repressor is inhibited by S-bacillithiolation under HOCl and organic hydroperoxide (OHP) stress resulting in up-regulation of the OhrA peroxiredoxin that confers resistance. (B) S-bacillithiolation of the methionine synthase MetE and of other enzymes of the Cys and Met biosynthesis pathway (YxjG, PpaC, SerA, MetI) leads to methionine auxotrophy. (C) In *S. aureus*, the glycolytic GapDH and the aldehyde dehydrogenase AldA are the main targets for S-bacillithiolation under HOCl stress. S-bacillithiolation of their active site Cys residues leads to reversible inactivation. The physiological role of GapDH and AldA S-bacillithiolation under HOCl stress might be to redirect the glycolytic flux into the pentose phosphate pathway (PPP) for NADPH regeneration and perhaps to detoxify methylglyoxal by AldA and other glyoxalases. This figure is adapted from [3].

energy production [60].

BSH is further involved in detoxification of toxic heavy metals, such as tellurite and selenite and functions in metal homeostasis [61]. BSH can bind and store Zn^{2+} and functions as intracellular Zn^{2+} buffer in metal ion homeostasis [62]. The thiolate, amine, and carboxylate groups of BSH serve as ligands for metal coordination and can bind Zn^{2+} as $(\text{BSH})_2\text{Zn}^{2+}$ complex under Zn^{2+} stress. Treatment of the BSH-deficient mutant with Zn^{2+} resulted in a decreased accumulation of Zn^{2+} due to an increased expression of the CadA and CzcD efflux systems. BSH also protects against Zn^{2+} toxicity in cells lacking Zn^{2+} efflux pumps [62].

BSH is further implicated in Fe^{2+} homeostasis and is suggested to play a role in FeS cluster assembly and transport in *S. aureus* and *B. subtilis* [63,64]. Mutants with defects in BSH biosynthesis showed a delayed growth upon depletion of Fe^{2+} or branched chain amino acids in the growth medium. The activities of several FeS-cluster enzymes (e.g. LeuCD, IlvD) were also decreased in the BSH-deficient mutant. These phenotypes suggest a potential role of BSH in FeS cluster biogenesis [64,65]. Further growth analyses with *nfu* and *sufA* mutants indicate that BSH may participate in the biogenesis of FeS cluster

proteins independently of the SufA and Nfu carriers [64,65]. Finally, BSH has been shown to play a role in transport of copper to the Cu^+ chaperone CopZ and Cu^+ buffering to avoid Cu^+ toxicity [66]. During Cu^+ transport by BSH, CopZ was identified as S-bacillithiolated *in vitro*.

BSH was recently shown to control sulfide homeostasis under H_2S and nitroxyl (HNO) stress in *S. aureus* [67,68]. Strongly increased endogenous levels of BSH persulfide (BSSH), CoASH persulfide (CoASSH) and cysteine persulfide (CysSSH) were measured under Na_2S and HNO treatment. Using a proteomics approach, several S-sulfhydrated proteins were identified by RSS stress including the glycolytic GapDH and the OhrR-type regulator MgrA. Biochemical experiments provided evidence that S-sulfhydration leads to inhibition of GapDH activity and functions in redox-regulation of the MgrA repressor to induce virulence factor expression. The thioredoxins (TrxP and TrxQ) enabled the specific reduction of protein S-sulfhydrations. The predicted CoASH disulfide reductases (Cdr) was suggested to function as CoASSH reductase [67].

BSH is also involved in virulence and survival of *S. aureus* under macrophage infection conditions as revealed by phenotype analysis of *bshA* mutants in clinical methicillin-resistant *S. aureus* (MRSA) isolates

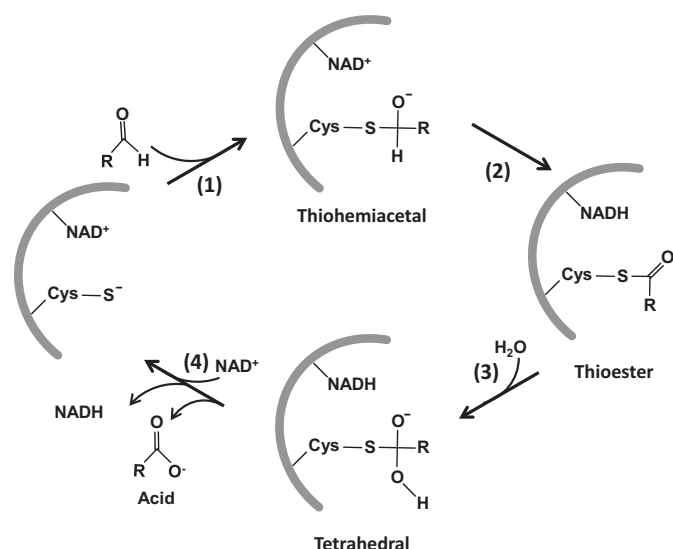


Fig. 9. Catalytic mechanism of NAD⁺-dependent aldehyde dehydrogenases. NAD⁺ binds tightly to the enzymes active site, resulting in a conformational change and activation of the catalytic Cys thiol. Nucleophilic attack on the carbonyl carbon of the aldehyde substrate leads to the formation of a covalently bound tetrahedral thiohemiacetal intermediate (1). Hydride transfer from the tetrahedral thiohemiacetal intermediate to NAD⁺ generates a thioester intermediate (2). Deacylation of the thioester intermediate by nucleophilic attack of a water molecule produces a second tetrahedral intermediate (3). The acid product and NADH are released from the enzymes active site and a new NAD⁺ molecule binds (4). This figure is adapted from [94].

COL, USA300 and SH1000 [69–71]. *S. aureus* COL represents a hospital-acquired (HA) MRSA strain while USA300 was isolated as community-acquired (CA)-MRSA strain with strongly increased virulence due to many toxins encoded on prophages and other mobile genetic elements [72]. SH1000 is a natural *bshC* mutant belonging to the NCTC8325-4 lineage [73]. NCTC8325-4 is a laboratory model strain that was obtained from a sepsis isolate after removal of three resident prophages by UV. The survival of *S. aureus* COL and USA300 *bshA* mutants as well as of the natural *bshC* mutant of strain SH1000 were decreased in phagocytosis infections assays using murine macrophages and human whole-blood assays as compared to the wild type [69,71]. These results suggest a role of BSH in the defense against the host-immune system and in the survival of *S. aureus* under infection conditions [69–71]. However, it remains to be shown if BSH is required for protection of *S. aureus* inside neutrophils against the antimicrobial activity of the myeloperoxidase (MPO) which is involved in HOCl production.

2.5. Physiological role of protein S-bacillithiolations in Firmicutes

BSH plays an important role in post-translational modifications of proteins under oxidative stress in Gram-positive bacteria. In response to HOCl stress, protein thiols are oxidized to mixed disulfides with BSH, termed as protein S-bacillithiolation [74–76]. In total, we identified eight common and 29 unique S-bacillithiolated proteins using shotgun proteomics in *B. subtilis*, *B. amyloliquefaciens*, *Bacillus pumilus*, *Bacillus megaterium* and *Staphylococcus carnosus* (Table S2) [75,76]. Many of the identified S-bacillithiolated proteins are involved in important cellular processes, such as the biosynthesis of amino acids, cofactors and nucleotides, protein translation, and redox-signalling of ROS. In *B. subtilis*, the MarR-type repressor OhrR was S-bacillithiolated under HOCl and organic hydroperoxide (OHP) stress at its redox-sensing Cys15. S-bacillithiolation of OhrR at its lone Cys residue leads to inactivation of its repressor function and derepression of transcription of the *ohrA* gene encoding the OhrA peroxiredoxin which confers resistance under HOCl and OHP stress (Fig. 8A) [74,75]. MetE was identified as the most

abundant S-bacillithiolated protein in *B. subtilis*, which was S-bacillithiolated at the active site Cys730 and at the non-conserved Cys719 [75]. S-bacillithiolation of MetE under HOCl stress resulted in a methionine auxotrophy phenotype perhaps to stop translation during recovery from oxidative stress (Fig. 8B). In addition, other enzymes involved in the Cys and Met biosynthesis pathways were identified as targets for S-bacillithiolation, including SerA, PpaC, MetI and YxjG. The translation elongation factor EF-Tu (TufA) and GuaB were also identified as abundant and essential S-bacillithiolated proteins under HOCl stress [25,75,76]. The bacilliredoxins BrxA, BrxB and BrxC were identified as S-bacillithiolated in *B. subtilis* and *S. carnosus*, which could be intermediates of the bacilliredoxin redox pathway [76].

In *S. aureus* we determined the redox state of 228 Cys residues using OxICAT. We identified 58 HOCl-sensitive Cys residues that showed > 10% increased oxidation levels under HOCl stress. Among these HOCl-sensitive thiol-switches, 19 showed 20–30% increased oxidation that included the S-bacillithiolated proteins GapDH, AldA, GuaB and RpmJ. GapDH is S-bacillithiolated at the active site Cys151 and represents the most abundant S-bacillithiolated protein contributing with 4% to the total Cys proteome of *S. aureus* (Fig. 8C) [42]. In kinetic assays, GapDH of *S. aureus* was faster inactivated by H₂O₂ and HOCl stress in the presence of BSH due to S-bacillithiolation compared to overoxidation with the oxidants alone *in vitro* [42]. These experiments provide evidence that S-bacillithiolation is involved in redox regulation and thiol-protection of Cys151 of GapDH against overoxidation in *S. aureus* [42]. The oxidative inactivation of GapDH in *S. aureus* may induce metabolic re-configuration of carbon metabolism and redirection into the PPP as shown in eukaryotic organisms [47,49].

The aldehyde dehydrogenase AldA was identified as another target for S-bacillithiolation under HOCl stress in *S. aureus* (Fig. 8C) [77]. Aldehyde dehydrogenases (ALDHs) catalyze the NAD⁺-dependent oxidation of aldehydes to their carboxylic acids in four steps (Fig. 9) [78]. In the first step, a tetrahedral hemithioacetal-enzyme complex is formed. NAD⁺ binding repositions the catalytic cysteine, allowing the nucleophilic attack on the carbonyl carbon of an aldehyde substrate. The nucleophilicity of the catalytic cysteine is achieved by deprotonation through an adjacent conserved glutamate residue. In the second step, hydride transfer from the hemithioacetal intermediate to NAD⁺ generates a covalent thioester intermediate. In the third step, NADH is released from the enzyme allowing hydrolysis of the thioester intermediate. Therefore, nucleophilic water attacks the thioester intermediate to generate a second tetrahedral intermediate. In the final step, hydrolysis of the thioacyl-enzyme complex releases a carboxylic acid product [78].

GapDH and AldA displayed both 29% increased oxidation under HOCl stress as revealed by the OxICAT approach *in vivo* [18,77]. Treatment of AldA with H₂O₂ in the presence of BSH resulted in reversible S-bacillithiolation and loss of activity, which could be restored upon DTT reduction [77]. The purified AldA enzyme showed a broad substrate spectrum, catalyzing the oxidation of various aldehydes, including formaldehyde, methylglyoxal, acetaldehyde and glycolaldehyde. Thus, the question of the natural substrate for AldA remains unresolved. Transcriptional analysis further revealed an increased *aldA* transcription under formaldehyde, methylglyoxal and HOCl stress in a SigB-independent manner. Thus, our results point to an unknown redox-sensing regulator controlling expression of *aldA* under thiol-stress conditions. However, in survival phenotype assays, the *aldA* mutant was more sensitive to HOCl stress, but not to aldehydes. This suggests that unknown aldehyde substrates might be generated under HOCl stress as potential substrate for AldA [77].

2.6. Structural insights into the active sites of targets for S-bacillithiolations

We were further interested in the structural changes of redox-sensitive proteins after S-bacillithiolation of their active sites. Molecular docking and molecular dynamic simulations were used to model the

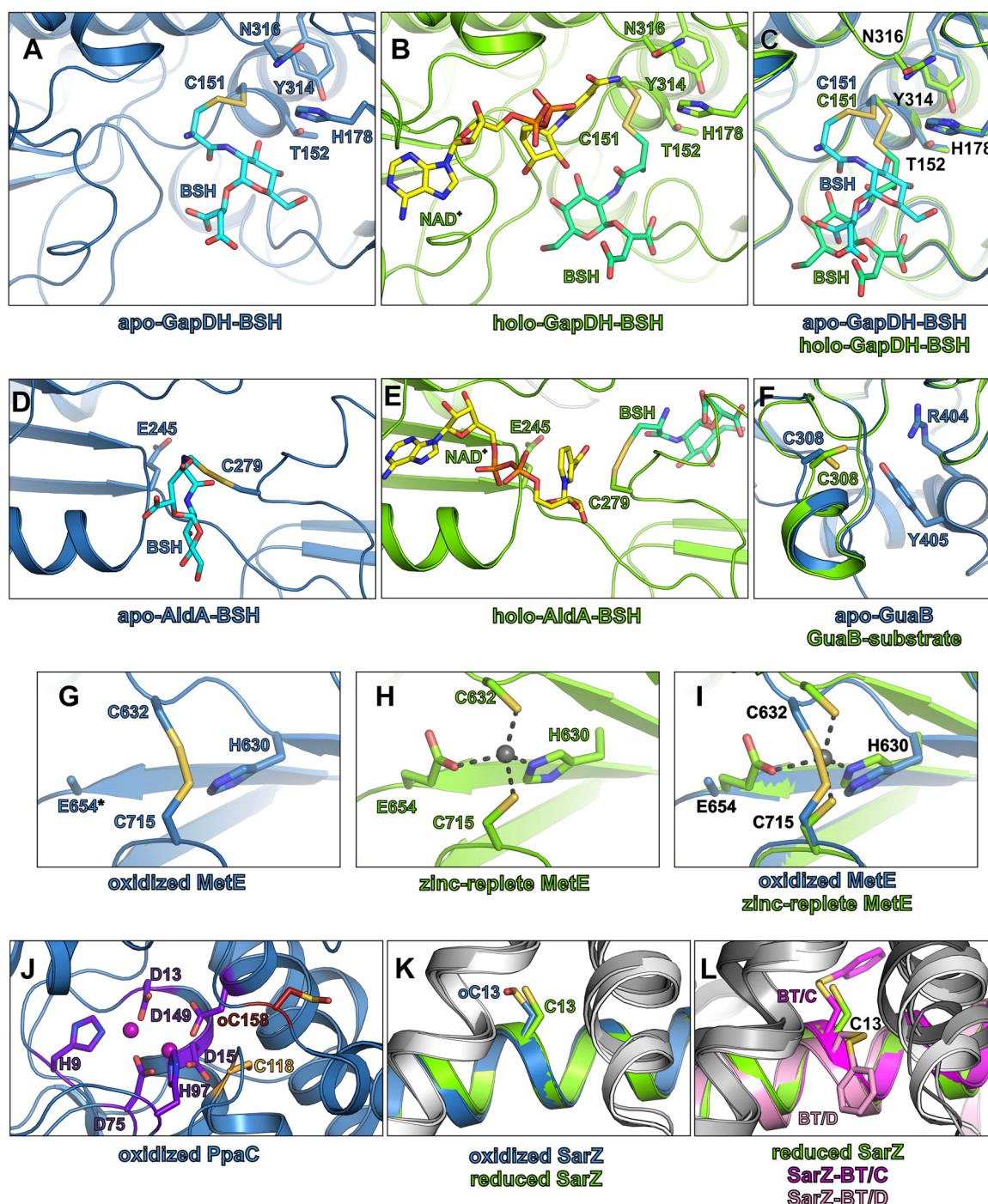


Fig. 10. Structural insights into conserved targets for S-bacillithiolation. (A, B) The S-bacillithiolated active site pocket of *S. aureus* GapDH in the apo- (A) and holo-enzyme (B). (C) The superposition of the GapDH active site of the apo- (blue) and holo-enzyme (green). The molecular docking of BSH was performed on the GapDH apo- (PDB ID: 3LC7) and holo-enzyme structures (PDB ID: 3LVF) (D, E) The S-bacillithiolated active site pocket of *S. aureus* AldA in the apo- (blue) (D) and holo-enzyme (green) (E). Molecular docking of BSH was performed on the AldA structure (PDB ID: 3TY7). (F) The active site of the *B. anthracis* GuaB in the apo-enzyme (blue) (PDB ID: 3TSB) and substrate-bound structure (green) (PDB ID: 3USB), the substrate is not shown. (G, H) The active site of the *S. mutans* MetE in the oxidized (PDB ID: 3L7R) (G) and in the zinc-replete structure (PDB ID: 3TOC) (H). In the oxidized structure, C632 and C715 form an intramolecular disulfide bond. The asterisk indicates a glutamate residue that was modelled as alanine due to the lack of the electron density at this position. (I) The superposition of the active site of the MetE oxidized (blue) and zinc-replete (green) structures. The zinc cation is shown as gray sphere. (J) The active site of the *S. aureus* PpaC (PDB ID: 4RPA). The active site residues and the neighboring cysteine residues are shown as sticks and coloured by atom type. The colour of the carbon atoms allows to distinguish between active site residues (purple) and neighboring cysteine residues that were found S-bacillithiolated (dark red) or were not S-bacillithiolated (light orange). The manganese cations are shown as pink spheres. (K, L) The redox-active cysteine residue of *S. aureus* SarZ. (K) Superposition of the reduced (blue) (PDB ID: 3HSE) and oxidized form (green) (PDB ID: 3HRM) of SarZ. (L) Superposition of the reduced (blue) and benzene thiol-bound SarZ in chain C (magenta) and in chain D (light pink) (PDB ID: 3HSR). One monomer of the SarZ dimer is shown in blue (reduced SarZ), green (oxidized SarZ), magenta (benzene thiol-bound SarZ chain C) or light pink (benzene thiol-bound SarZ chain D), whereas the other monomer is shown in shades of gray. All the important residues in all panels are shown as sticks and coloured by atom types (oxygen-red, nitrogen-blue, sulfur-yellow, phosphor-orange, carbon-variable) (For interpretation of the references to color in this figure legend, the reader is referred to the web version of this article).

S-bacillithiolated active sites C151 of GapDH (PDB ID: 3LC7, 3LVF) [79] and C279 of AldA (PDB ID: 3TY7) of *S. aureus* in the apo- and holo-enzyme structures, respectively (Fig. 10A–E) [42,77]. Both Cys residues act as a nucleophile in catalysis, leading to the formation of a covalent intermediate [79,80]. Interestingly, in aldehyde dehydrogenases, the Cys residue adopts a “resting” conformation in the apo-enzyme and an “attacking” conformation in the holo-enzyme [80]. The molecular docking of BSH into the AldA active site resulted in two different positions of the BSH depending on C279 activation state (Fig. 10D, E). While C279 is in “resting” position in the absence of the NAD⁺ cofactor, BSH partially occupies the cofactor-binding cavity. However, in the presence of NAD⁺, BSH is located closer to the substrate-binding pocket [77]. Although the conformation of C151 of GapDH is very similar in both apo- and holo-enzyme structures, molecular docking also resulted in two different positions of the BSH (Fig. 10A–C). The position of BSH in the apo- and holo-GapDH does not differ so significantly as in AldA. However, in the holo-GapDH BSH is still shifted towards the substrate-binding pocket, whereas in the apo-enzyme the BSH position partially overlaps with the NAD⁺-binding site [42]. However, in both models of S-bacillithiolated GapDH and AldA active sites, docking of the BSH did neither require major conformational changes in the overall structure of both proteins, nor in the conformation of the neighboring secondary structure elements.

We further compared these models of GapDH-SSB and AldA-SSB with other structures of conserved S-bacillithiolated proteins that were identified under HOCl stress previously. Among the targets for S-bacillithiolations, GuaB, MetE, the inorganic pyrophosphatase (PpaC), and the redox-sensing virulence regulator SarZ are conserved in *Staphylococcus* and *Bacillus* species [75–77]. Thus, we focused on the crystal structure analysis of *S. aureus* PpaC [81] and SarZ [82], GuaB of *Bacillus anthracis* [83], and MetE of *Streptococcus mutans* [84], which were available in the PDB database (Table 1).

GuaB is another enzyme that uses NAD⁺ as a cofactor and contains C308 at the active site. The Cys acts as a nucleophile and forms a covalent adduct with the substrate [83,85], similarly as discussed for GapDH and AldA. The conformation of the C308 in the substrate IMP-bound enzyme (PDB ID: 3USB) is different from the conformation adopted in the presence of the product (PDB ID: 3TSD) or in the apo-enzyme (PDB ID: 3TSB) (Fig. 10F). Although the two conformations were not termed “resting/attacking” as in AldA, it seems that the active site C308 of GuaB acts similarly to the C279 of AldA. Therefore, we would expect that GuaB might also bind BSH in two alternative positions depending on the C308 activation state. Interestingly, GuaB

contains a flexible loop involving the residues 380–430, commonly termed the active site flap, that changes the conformation upon binding to a cofactor or substrate. The residues R404 and Y405 play an important role in the catalytic dyad that activates the water molecule through proton abstraction and allows the release of the product [83,85]. The active site flap is well-resolved in the apo-enzyme structure, but in the IMP-GuaB the large part of the flap is missing due to the disorder of this part in the structure (Fig. 10F) [83]. We speculate that this structural element might also influence BSH binding and depending on its conformation, BSH could occupy different cavities in GuaB.

In contrast to GapDH, AldA and GuaB, the two active site Cys residues C632 and C715 of MetE play a different role in catalysis. The main function of these two Cys together with H630 and E654 is coordination of the zinc atom. Zinc acts as a Lewis acid and activates the thiol of a homocysteine which is one of the substrates of the MetE [84,86]. In MetE of *B. subtilis*, only one active site C730 was S-bacillithiolated under HOCl stress (corresponding to C715 of *S. aureus* and *S. mutans*) [75]. The analysis of the crystal structures of *S. mutans* MetE (PDB ID: 3L7R, 3T0C) [84] suggests an explanation. The binding of the BSH to both Cys residues at the active site would not be possible due to the close location of C632 and C715 (Fig. 10G–I) and space limitation that do not allow for accommodation of two molecules of BSH.

Another conserved target for S-bacillithiolation is the manganese-dependent inorganic pyrophosphatase PpaC which degrades pyrophosphate to inorganic phosphate. The active site of PpaC is composed of H9, D13, D15, D75, H97, D149 and two manganese atoms, but does not contain Cys (Fig. 10J) [81]. However, three conserved Cys residues C110, C118 and C158 are present in PpaC. C110 and C158 were identified as S-bacillithiolated in *B. subtilis* and *S. aureus* under HOCl stress [42,75]. This observation is in a good agreement with the crystal structure of *S. aureus* PpaC (PDB ID: 4RPA) [81], where both, C110 and C158 are oxidized to sulfonic acids, indicating their susceptibilities to redox changes. C110 is buried in a cavity at the interface of the two monomers forming the PpaC dimer, whereas C158 is located at the protein surface (Fig. 11A). Thus, C110 and C158 are easily accessible for S-bacillithiolation or overoxidation. In contrast, C118 is buried in the N-terminal domain (Fig. 11A). Although C118 is close to the PpaC active site, it is difficult to access and was also not oxidized in the PpaC structure. Nevertheless, it remains intriguing whether S-bacillithiolation of the non-catalytic Cys residues in PpaC protects the enzyme against overoxidation or functions in redox-regulation which remains to be elucidated.

Similar to PpaC, GapDH and GuaB also contain non-catalytic and

Table 1
The conserved targets for S-bacillithiolation and their available crystal structures.

Protein	Organism	Related structures (PDB ID)	Cysteine residues	Function of the cysteine residue	Confirmed post-translational modification ^a
AldA	<i>Staphylococcus aureus</i>	3TY7	C279	active site residue	S-bacillithiolation
GapDH	<i>Staphylococcus aureus</i>	3LC7	C96	-	-
		3LVF	C151	active site residue	S-bacillithiolation, overoxidation
		5T73			
GuaB	<i>Staphylococcus aureus</i>	-	C307	active site	S-bacillithiolation
GuaB	<i>Bacillus anthracis</i>	3TSB 3USB 3TSD	C326	-	S-bacillithiolation
			C308	active site	S-bacillithiolation
			C327	-	S-bacillithiolation
MetE	<i>Staphylococcus aureus</i>	-	C632	zinc-binding site	-
MetE	<i>Streptococcus mutans</i>	3L7R 3T0C	C715	zinc-binding site	S-bacillithiolation
			C632	zinc-binding site	-
			C715	zinc-binding site	S-bacillithiolation
PpaC	<i>Staphylococcus aureus</i>	4RPA	C110	-	overoxidation
			C118	-	-
			C158	-	S-bacillithiolation, overoxidation
			C13	redox-active	S-bacillithiolation
SarZ	<i>Staphylococcus aureus</i>	3HRM			
		3HSE			
		3HSR			

^a Also if confirmed in other species.

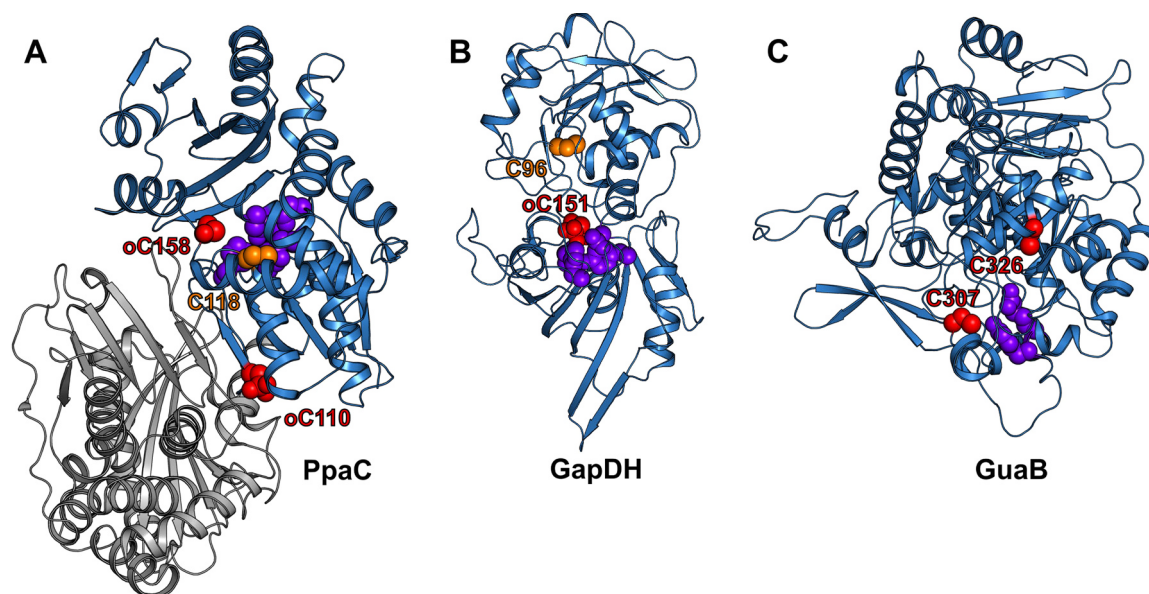


Fig. 11. The distribution of the cysteine residues in *S*-bacillithiolation targets. All active site and cysteine residues of *S. aureus* PpaC (PDB ID: 4RPA) (A), *S. aureus* GapDH (PDB ID: 5T73) (B) and *B. anthracis* GuaB (PDB ID: 3TSB) (C) are shown as spheres. The cysteine residues for which the *S*-bacillithiolation was confirmed are highlighted in red, whereas the other cysteine residues are coloured orange. The active sites residues that are not cysteine are shown in purple. The overoxidized Cys residues are marked as oC. The chain B is shown in gray (For interpretation of the references to color in this figure legend, the reader is referred to the web version of this article).

non-conserved Cys residues, such as C96 of *S. aureus* GapDH that was neither *S*-bacillithiolated nor overoxidized and is buried in the structure like C118 in PpaC (Fig. 11B) [42]. In contrast, in GuaB of *B. anthracis*, the non-conserved C326 close to the active site was identified as *S*-bacillithiolated because it is accessible for BSH (Fig. 11C) [77].

The most interesting targets for *S*-bacillithiolation are redox-sensing regulators, such as the thiol-based OhrR repressor which was *S*-bacillithiolated at the conserved C15 under HOCl and CHP stress [74,75]. In *S. aureus*, the OhrR-homolog SarZ was identified as redox-sensitive repressor and the structural changes were investigated during thiol-oxidation of the single C13, including *S*-thiolation with the synthetic benzene thiol [75,82,87,88]. The crystal structures of SarZ in reduced (PDB ID: 3HSE), sulfenic acid (PDB ID: 3HRM), and mixed disulfide form (PDB ID: 3HSR) [82] provide the explanation for inhibition of SarZ repressor activity. Upon C13 oxidation, several α -helices of the DNA-binding helix-turn-helix motif change their conformations leading to dissociation of SarZ from the promoter DNA. Inhibition of SarZ repressor activity results in derepression of transcription of a large SarZ regulon, including the *ohr* peroxiredoxin gene and genes involved in cellular metabolism, virulence, and antibiotic resistance [87]. Interestingly, oxidation of SarZ to the C13 sulfenic acid does not lead to inactivation and structural changes of SarZ (Fig. 10K). Only further overoxidations of C13 to sulfonic acid or *S*-thiolation causes SarZ inactivation [82]. The structure of the *S*-thiolated C13-benzene thiol complex provides insights into possible binding sites for LMW thiols. Benzene thiol occupies different positions in different SarZ monomers present in the asymmetric unit of the *S*-thiolated SarZ structure. In monomer B and C, benzene thiol is oriented toward the surface of the protein, whereas in monomer D, it is buried in a hydrophobic cavity in the dimer interface (Fig. 10L). Benzene thiol might enter the cavity with C13 and the formation of the disulfide bond occurs at a position seen in monomer B, C. Afterwards, C13 changes the conformation yielding another orientation of benzene thiol, as in monomer D [82]. In the case of the BSH binding, the location of BSH in the hydrophobic pocket is less probable because BSH contains several charged groups.

In general, all discussed potential BSH-binding site are composed of positively or negatively charged residues that can interact with the amine, hydroxyl and carboxyl groups of the BSH. Our structural

analysis shows that the *S*-bacillithiolated Cys residues in different proteins are easily accessible for BSH due to their location either in the active sites of proteins or at the protein surface. The Cys residues buried in protein structure, e.g. C96 of GapDH and C118 of GuaB, do not undergo *S*-bacillithiolation. In the majority of targets, *S*-bacillithiolation occurs at the catalytic active sites (C151 of GapDH, C279 of AldA, C308 of GuaB, C715 of MetE) or redox-sensing Cys residues of thiol-based redox sensors, such as C13 of SarZ or C15 of OhrR. *S*-thiolation of SarZ leads to conformational changes, which is the mechanism of derepression of SarZ controlled target genes [82]. The models of *S*-bacillithiolated GapDH and AldA do not support structural changes. This is in agreement with the catalytic reactions of substrate conversion in GapDH and AldA that are not accompanied by significant structural alterations. In contrast, the inactivation of SarZ requires structural changes in the DNA binding domains as redox-regulatory mechanism. Therefore, it is tempting to speculate that *S*-thiolation of enzymes in most cases does not lead to structural changes, although exceptions are possible.

2.7. Protein *S*-bacillithiolation is redox controlled by bacilliredoxins (Brx)

The reduction of *S*-bacillithiolated proteins in *Firmicutes* is catalyzed by the bacilliredoxin redox pathway (Fig. 12). The bacilliredoxins BrxA and BrxB were identified as paralogs of the DUF1094 family in *B. subtilis*, which shared 53% sequence identity [89,90]. Phylogenomic profiling identified BrxA and BrxB as Trx-like proteins with unusual CGC active sites. The crystal structure of BrxA revealed overall structural similarities to thioredoxins. However, the redox potential was determined as -130 mV, which is much more positive compared to that of thioredoxin proteins [91]. Furthermore, BrxC was identified as candidate for a monothiol Brx which has a TCPIS active motif and is similar to monothiol Grx. However, the function of BrxC in de-bacillithiolation remains to be elucidated [92]. The flavin disulfide reductase YpdA was suggested as putative BSSB reductase in the STRING search due to its phylogenetic co-occurrence together with the BSH biosynthesis enzymes [55]. However, the catalytic activity of YpdA in BSSB reduction could not be demonstrated yet.

Bacilliredoxins function analogous to glutaredoxins by the attack of

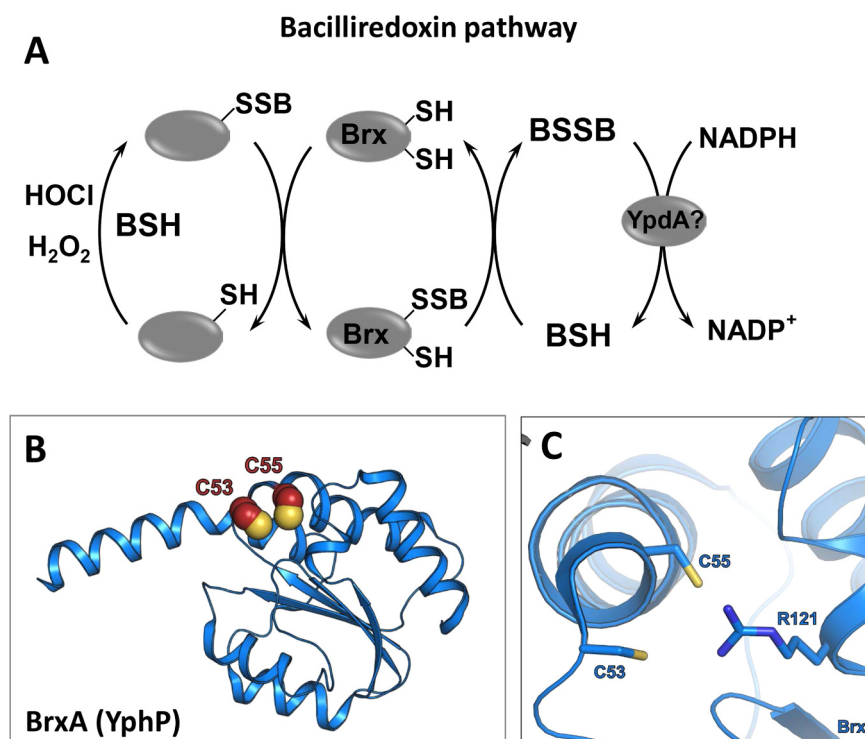


Fig. 12. Reversal of protein S-bacillithiolation by the bacilliredoxin pathway. (A) In BSH-producing *Firmicutes*, such as *B. subtilis* and *S. aureus*, a bacilliredoxin (Brx) redox pathway is proposed for reduction of S-bacillithiolated proteins. During the reduction of S-bacillithiolated proteins, a Brx-SSB intermediate is generated that could be reduced by BSH leading to oxidized BSSH. The reduction of BSSH may require the NADPH-dependent bacillithiol disulfide reductase YpdA which remains to be elucidated. (B) The crystal structure of BrxA (YphP) (PDB ID: 3FHK) and (C) its active site. The active and resolving Cys residues of Brx are displayed as spheres (B) and sticks (C).

This figure is adapted from [2].

the active site Cys on BSH-mixed protein disulfides, resulting in the transfer of BSH to the active site Cys of Brx (Fig. 12) [89]. In *B. subtilis*, the S-bacillithiolated OhrR repressor and MetE were identified as natural substrates for BrxA and BrxB *in vitro*. The DNA-binding activity of the OhrR repressor could be recovered after de-bacillithiolation by the BrxBC54A mutant protein. The de-bacillithiolation of MetE-SSB was demonstrated by BSH-specific Western blot analysis and mass spectrometry, but MetE reactivation could not be shown *in vitro*. While de-bacillithiolation of OhrR-SSB is catalyzed mainly by BrxB, reduction of MetE-SSB can be catalyzed by both BrxA and BrxB [89].

In *S. aureus*, the glycolytic GapDH was demonstrated as specific substrate for de-bacillithiolation by BrxA (SAUSA300_1321) during recovery from oxidative stress [42]. Using *in vitro* activity assays, the glycolytic GapDH activity could be restored after de-bacillithiolation by BrxA and the BrxCGA-resolving Cys mutant, but not by the BrxAGC-active site Cys mutant. BSH-specific Western blot analysis supported the reduction of GapDH-SSB *in vitro* [42]. However, *in vivo* evidence for the functions of Brx and YpdA in the oxidative stress response is still missing in *Firmicutes*.

3. Outlook for future research

In this review, we report an update in the research of the functions and properties of the LMW thiols mycothiol and bacillithiol, which are dominant scavengers of ROS and other reactive species in *Actinomycetes* and *Firmicutes*. MSH and BSH were also shown to contribute to the pathogenicity and antibiotic resistance mechanisms of major human pathogens, such as *M. tuberculosis* and *S. aureus* indicating the importance of LMW thiols in the defense against the host innate immune system during infections. Significant progress has been made in the structural and mechanistic characterization of many MSH and BSH-dependent detoxification enzymes, as well as MSH and BSH biosynthesis enzymes. However, the catalytic mechanism of the putative BshC ligase and the NADPH-dependent flavin disulfide reductase YpdA are still unknown. Similarly, other unknown MSH- or BSH-dependent formaldehyde dehydrogenases, quinone reductases, and peroxidases might play important roles in detoxification of reactive compounds. There is

also significant progress for the role of BSH in FeS cluster assembly, Zn²⁺ and Cu⁺ homeostasis, but related roles of MSH have not been investigated and may be important to maintain metal homeostasis under infection conditions. Recent work also showed an involvement of BSH in sulfide homeostasis and sulphydrations that are implicated in redox regulation of metabolic enzymes and virulence regulators. Finally, over the last years many targets for protein S-mycothiolation and S-bacillithiolation have been discovered through shotgun proteomics and quantitative thiol-redox proteomics. For some antioxidant enzymes (AhpE, Mpx, MsrA) and metabolic enzymes (GapDH), the roles of MSH and BSH in thiol-protection and redox-regulation under oxidative stress have been clearly shown. Molecular docking of BSH into the active sites of GapDH and AldA of *S. aureus* provided first insights that S-bacillithiolation does not require structural changes. Moreover, BSH can occupy two different positions in the active sites with the active site Cys in the attacking or resting state, depending on the presence of the NAD⁺ cofactor. Our structural comparison here revealed that these mechanisms could be relevant also for many other conserved targets for S-thiolations, such as GuaB. However, the physiological roles of these protein S-thiolations in cellular physiology in *Actinomycetes* and *Firmicutes* requires much more detailed future work. In addition, the functions of bacilliredoxins under oxidative stress remain to be elucidated. Thus, future research should be directed to elucidate the physiological roles of the LMW thiols BSH and MSH and the many targets for protein S-bacillithiolation and S-mycothiolation in bacterial physiology under stress and infection conditions.

Acknowledgements

This work was supported by an European Research Council (ERC) Consolidator grant (GA 615585) MYCOTHILOME (EU) and grants from the Deutsche Forschungsgemeinschaft, Germany (AN746/4-1 and AN746/4-2) within the SPP1710 on “Thiol-based Redox switches”, by the Research Training Group GRK1947 (project C01) and by the SFB973 project C08 to H.A. Protein crystal structure analysis was supported by an Alexander von Humboldt post-doc fellowship to A.P.-B.

Author disclosure statement

No competing financial interests exist.

Appendix A. Supplementary material

Supplementary data associated with this article can be found in the online version at <https://doi.org/10.1016/j.redox.2018.08.017>.

References

- [1] K. Van Laer, C.J. Hamilton, J. Messens, Low-molecular-weight thiols in thiol-disulfide exchange, *Antioxid. Redox Signal* 18 (13) (2013) 1642–1653.
- [2] V.V. Loi, M. Rossius, H. Antelmann, Redox regulation by reversible protein S-thiolation in bacteria, *Front. Microbiol.* 6 (2015) 187.
- [3] P. Chandrangu, V.V. Loi, H. Antelmann, J.D. Helmann, The role of bacillithiol in Gram-positive *Firmicutes*, *Antioxid. Redox Signal* 28 (6) (2018) 445–462.
- [4] A.J. Potter, C. Trappetti, J.C. Paton, *Streptococcus pneumoniae* uses glutathione to defend against oxidative stress and metal ion toxicity, *J. Bacteriol.* 194 (22) (2012) 6248–6254.
- [5] G.L. Newton, M. Rawat, J.J. La Clair, V.K. Jothivasan, T. Budiarto, C.J. Hamilton, A. Claiborne, J.D. Helmann, R.C. Fahey, Bacillithiol is an antioxidant thiol produced in *Bacilli*, *Nat. Chem. Biol.* 5 (9) (2009) 625–627.
- [6] G.L. Newton, N. Buchmeier, R.C. Fahey, Biosynthesis and functions of mycothiol, the unique protective thiol of Actinobacteria, *Microbiol. Mol. Biol. Rev.* 72 (3) (2008) 471–494.
- [7] A.M. Reyes, B. Pedre, M.I. De Armas, M.A. Tossounian, R. Radi, J. Messens, M. Trujillo, Chemistry and redox biology of mycothiol, *Antioxid. Redox Signal* 28 (6) (2018) 487–504.
- [8] S.B. d. elCardayre, J.E. Davies, *Staphylococcus aureus* coenzyme A disulfide reductase, a new subfamily of pyridine nucleotide-disulfide oxidoreductase. Sequence, expression, and analysis of *cdr*, *J. Biol. Chem.* 273 (10) (1998) 5752–5757.
- [9] J.A. Boylan, C.S. Hummel, S. Benoit, J. Garcia-Lara, J. Treglown-Downey, E.J. Crane 3rd, F.C. Gherardini, *Borrelia burgdorferi* bb0728 encodes a coenzyme A disulfide reductase whose function suggests a role in intracellular redox and the oxidative stress response, *Mol. Microbiol.* 59 (2) (2006) 475–486.
- [10] R.C. Fahey, Glutathione analogs in prokaryotes, *Biochim. Biophys. Acta* 1830 (5) (2013) 3182–3198.
- [11] S.D. Copley, J.K. Dhillon, Lateral gene transfer and parallel evolution in the history of glutathione biosynthesis genes, *Genome Biol.* 3 (5) (2002) (research0025).
- [12] D. Ritz, J. Beckwith, Roles of thiol-redox pathways in bacteria, *Annu. Rev. Microbiol.* 55 (2001) 21–48.
- [13] V.K. Jothivasan, C.J. Hamilton, Mycothiol: synthesis, biosynthesis and biological functions of the major low molecular weight thiol in actinomycetes, *Nat. Prod. Rep.* 25 (6) (2008) 1091–1117.
- [14] N.A. Buchmeier, G.L. Newton, T. Koledin, R.C. Fahey, Association of mycothiol with protection of *Mycobacterium tuberculosis* from toxic oxidants and antibiotics, *Mol. Microbiol.* 47 (6) (2003) 1723–1732.
- [15] G.L. Newton, Y. Av-Gay, R.C. Fahey, A novel mycothiol-dependent detoxification pathway in mycobacteria involving mycothiol S-conjugate amidase, *Biochemistry* 39 (35) (2000) 10739–10746.
- [16] A. Kumar, W. Nartey, J. Shin, M.S.S. Manimekalai, G. Gruber, Structural and mechanistic insights into mycothiol disulfide reductase and the mycoredoxin-1-alkylhydroperoxide reductase E assembly of *Mycobacterium tuberculosis*, *Biochim. Biophys. Acta* 1861 (9) (2017) 2354–2366.
- [17] G.L. Newton, K. Arnold, M.S. Price, C. Sherrill, S.B. Delcardayre, Y. Aharonowitz, G. Cohen, J. Davies, R.C. Fahey, C. Davis, Distribution of thiols in microorganisms: mycothiol is a major thiol in most actinomycetes, *J. Bacteriol.* 178 (7) (1996) 1990–1995.
- [18] M. Hillion, M. Imber, B. Pedre, J. Bernhardt, M. Saleh, V.V. Loi, S. Maass, D. Becher, L. Astolfi Rosado, L. Adrian, C. Weise, R. Hell, M. Wirtz, J. Messens, H. Antelmann, The glyceraldehyde-3-phosphate dehydrogenase GapDH of *Corynebacterium diphtheriae* is redox-controlled by protein S-mycothiolation under oxidative stress, *Sci. Rep.* 7 (1) (2017) 5020.
- [19] S.V. Sharma, K. Van Laer, J. Messens, C.J. Hamilton, Thiol redox and pKa properties of mycothiol, the predominant low-molecular-weight thiol cofactor in the actinomycetes, *ChemBiochem* 17 (18) (2016) 1689–1692.
- [20] A. Bhaskar, M. Chawla, M. Mehta, P. Parikh, P. Chandra, D. Bhave, D. Kumar, K.S. Carroll, A. Singh, Reengineering redox sensitive GFP to measure mycothiol redox potential of *Mycobacterium tuberculosis* during infection, *PLoS Pathog.* 10 (1) (2014) e1003902.
- [21] G.L. Newton, S.S. Leung, J.I. Wakabayashi, M. Rawat, R.C. Fahey, The DinB superfamily includes novel mycothiol, bacillithiol, and glutathione S-transferases, *Biochemistry* 50 (49) (2011) 10751–10760.
- [22] Q. Zhao, M. Wang, D. Xu, Q. Zhang, W. Liu, Metabolic coupling of two small-molecule thiols programs the biosynthesis of lincomycin A, *Nature* 518 (7537) (2015) 115–119.
- [23] D. Zhang, Z. Tang, W. Liu, Biosynthesis of lincosamide antibiotics: reactions associated with degradation and detoxification pathways play a constructive role, *Acc. Chem. Res.* 51 (6) (2018) 1496–1506.
- [24] J. Feng, Y. Che, J. Milse, Y.J. Yin, L. Liu, C. Ruckert, X.H. Shen, S.W. Qi, J. Kalinowski, S.J. Liu, The gene *ncgl2918* encodes a novel maleylpyruvate isomerase that needs mycothiol as cofactor and links mycothiol biosynthesis and gentisate assimilation in *Corynebacterium glutamicum*, *J. Biol. Chem.* 281 (16) (2006) 10778–10785.
- [25] B.K. Chi, T. Busche, K. Van Laer, K. Bäsle, D. Becher, L. Clermont, G.M. Seibold, M. Persicke, J. Kalinowski, J. Messens, H. Antelmann, Protein S-mycothiolation functions as redox-switch and thiol protection mechanism in *Corynebacterium glutamicum* under hypochlorite stress, *Antioxid. Redox Signal* 20 (4) (2014) 589–605.
- [26] E. Ordóñez, K. Van Belle, G. Roos, S. De Galan, M. Letek, J.A. Gil, L. Wyns, L.M. Mateos, J. Messens, Arsenate reductase, mycothiol, and mycoredoxin concert thiol/disulfide exchange, *J. Biol. Chem.* 284 (22) (2009) 15107–15116.
- [27] M.H. Hazbon, M. Brimacombe, M. Bobadilla del Valle, M. Cavatore, M.I. Guerrero, M. Varma-Basil, H. Billman-Jacobe, C. Lavender, J. Fyfe, L. Garcia-Garcia, C.I. Leon, M. Bose, F. Chaves, M. Murray, K.D. Eisenach, J. Sifuentes-Osorio, M.D. Cave, A. Ponce de Leon, D. Alland, Population genetics study of isoniazid resistance mutations and evolution of multidrug-resistant *Mycobacterium tuberculosis*, *Antimicrob. Agents Chemother.* 50 (8) (2006) 2640–2649.
- [28] A. Negri, P. Javidnia, R. Mu, X. Zhang, J. Vendome, B. Gold, J. Roberts, D. Barman, T. Ioerger, J.C. Sacchettini, X. Jiang, K. Burns-Huang, T. Warrier, Y. Ling, J.D. Warren, D.A. Oren, T. Beumung, H. Wang, J. Wu, H. Li, K.Y. Rhee, C.F. Nathan, G. Liu, S. Somersan-Karakaya, Identification of a mycothiol-dependent nitroreductase from *Mycobacterium tuberculosis*, *ACS Infect. Dis.* 4 (5) (2018) 771–787.
- [29] J. Padiadpu, P. Baloni, K. Anand, M. Munshi, C. Thakur, A. Mohan, A. Singh, N. Chandra, Identifying and tackling emergent vulnerability in drug-resistant *Mycobacteria*, *ACS Infect. Dis.* 2 (9) (2016) 592–607.
- [30] L.A. Rosado, K. Wahn, G. Degiacomi, B. Pedre, D. Young, A.G. de la Rubia, F. Boldrin, E. Martens, L. Marcos-Pascual, E. Sancho-Vaello, D. Albesa-Jove, R. Provvedi, C. Martin, V. Makarov, W. Versees, G. Verniest, M.E. Guerin, L.M. Mateos, R. Manganelli, J. Messens, The antibacterial prodrug activator Rv2466c is a mycothiol-dependent reductase in the oxidative stress response of *Mycobacterium tuberculosis*, *J. Biol. Chem.* 292 (32) (2017) 13097–13110.
- [31] D. Sareen, G.L. Newton, R.C. Fahey, N.A. Buchmeier, Mycothiol is essential for growth of *Mycobacterium tuberculosis* Erdman, *J. Bacteriol.* 185 (22) (2003) 6736–6740.
- [32] M. Hillion, J. Bernhardt, T. Busche, M. Rossius, S. Maass, D. Becher, M. Rawat, M. Wirtz, R. Hell, C. Ruckert, J. Kalinowski, H. Antelmann, Monitoring global protein thiol-oxidation and protein S-mycothiolation in *Mycobacterium smegmatis* under hypochlorite stress, *Sci. Rep.* 7 (1) (2017) 1195.
- [33] M. Hugo, K. Van Laer, A.M. Reyes, D. Vertommen, J. Messens, R. Radi, M. Trujillo, Mycothiol/mycoredoxin 1-dependent reduction of the peroxiredoxin AhpE from *Mycobacterium tuberculosis*, *J. Biol. Chem.* 289 (8) (2014) 5228–5239.
- [34] G.M. Seibold, B.J. Eikmanns, The *glgX* gene product of *Corynebacterium glutamicum* is required for glycogen degradation and for fast adaptation to hyperosmotic stress, *Microbiology* 153 (Pt 7) (2007) 2212–2220.
- [35] B. Pedre, I. Van Molle, A.F. Villadangos, K. Wahn, D. Vertommen, L. Turell, H. Erdogan, L.M. Mateos, J. Messens, The *Corynebacterium glutamicum* mycothiol peroxidase is a reactive oxygen species-scavenging enzyme that shows promiscuity in thiol redox control, *Mol. Microbiol.* 96 (6) (2015) 1176–1191.
- [36] M.A. Tossounian, B. Pedre, K. Wahn, H. Erdogan, D. Vertommen, I. Van Molle, J. Messens, *Corynebacterium diphtheriae* methionine sulfoxide reductase exploits a unique mycothiol redox relay mechanism, *J. Biol. Chem.* 290 (18) (2015) 11365–11375.
- [37] M. Si, Y. Feng, K. Chen, Y. Kang, C. Chen, Y. Wang, X. Shen, Functional comparison of methionine sulphoxide reductase A and B in *Corynebacterium glutamicum*, *J. Gen. Appl. Microbiol.* 63 (5) (2017) 280–286.
- [38] M. Si, Y. Xu, T. Wang, M. Long, W. Ding, C. Chen, X. Guan, Y. Liu, Y. Wang, X. Shen, S.J. Liu, Functional characterization of a mycothiol peroxidase in *Corynebacterium glutamicum* that uses both mycoredoxin and thioredoxin reducing systems in the response to oxidative stress, *Biochem. J.* 469 (1) (2015) 45–57.
- [39] Y. Liu, X. Yang, Y. Yin, J. Lin, C. Chen, J. Pan, M. Si, X. Shen, Mycothiol protects *Corynebacterium glutamicum* against acid stress via maintaining intracellular pH homeostasis, scavenging ROS, and S-mycothiolating MetE, *J. Gen. Appl. Microbiol.* 62 (3) (2016) 144–153.
- [40] E.J. Munoz-Elias, J.D. McKinney, *Mycobacterium tuberculosis* isocitrate lyases 1 and 2 are jointly required for in vivo growth and virulence, *Nat. Med.* 11 (6) (2005) 638–644.
- [41] J.C. Crack, C.J. Hamilton, N.E. Le Brun, Mass spectrometric detection of iron nitrosyls, sulfide oxidation and mycothiolation during nitrosylation of the NO sensor [4Fe-4S] NsrR, *Chem. Commun.* 54 (47) (2018) 5992–5995.
- [42] M. Imber, N.T.T. Huyen, A.J. Pietrzyk-Brzezinska, V.V. Loi, M. Hillion, J. Bernhardt, L. Thärichen, K. Kolsek, M. Saleh, C.J. Hamilton, L. Adrian, F. Gräter, M.C. Wahl, H. Antelmann, Protein S-bacillithiolation functions in thiol protection and redox regulation of the glyceraldehyde-3-phosphate dehydrogenase Gap in *Staphylococcus aureus* under hypochlorite stress, *Antioxid. Redox Signal* 28 (6) (2018) 410–430.
- [43] K. Van Laer, L. Buts, N. Foloppe, D. Vertommen, K. Van Belle, K. Wahn, G. Roos, L. Nilsson, L.M. Mateos, M. Rawat, N.A. Van Nuland, J. Messens, Mycoredoxin-1 is one of the missing links in the oxidative stress defence mechanism of *Mycobacteria*, *Mol. Microbiol.* 86 (4) (2012) 787–804.
- [44] F. Aslund, K.D. Berndt, A. Holmgren, Redox potentials of glutaredoxins and other thiol-disulfide oxidoreductases of the thioredoxin superfamily determined by direct protein-protein redox equilibria, *J. Biol. Chem.* 272 (49) (1997) 30780–30786.
- [45] M. Reis, C.N. Alves, J. Lameira, I. Tunon, S. Marti, V. Moliner, The catalytic mechanism of glyceraldehyde 3-phosphate dehydrogenase from *Trypanosoma cruzi* elucidated via the QM/MM approach, *Phys. Chem. Chem. Phys.* 15 (11) (2013) 3772–3785.
- [46] D. Shenton, C.M. Grant, Protein S-thiolation targets glycolysis and protein synthesis

- in response to oxidative stress in the yeast *Saccharomyces cerevisiae*, *Biochem. J.* 374 (Pt 2) (2003) 513–519.
- [47] M. Ralser, M.M. Wamelink, A. Kowald, B. Gerisch, G. Heeren, E.A. Struys, E. Klipp, C. Jakobs, M. Breitenbach, H. Lehrach, S. Krobitsch, Dynamic rerouting of the carbohydrate flux is key to counteracting oxidative stress, *J. Biol.* 6 (4) (2007) 10.
- [48] T. Hildebrandt, J. Knuesting, C. Berndt, B. Morgan, R. Scheibe, Cytosolic thiol switches regulating basic cellular functions: gapdh as an information hub? *Biol. Chem.* 396 (5) (2015) 523–537.
- [49] N. Brandes, S. Schmitt, U. Jakob, Thiol-based redox switches in eukaryotic proteins, *Antioxid. Redox Signal* 11 (5) (2009) 997–1014.
- [50] D. Peralta, A.K. Bronowska, B. Morgan, E. Doka, K. Van Laer, P. Nagy, F. Grater, T.P. Dick, A proton relay enhances H₂O₂ sensitivity of GAPDH to facilitate metabolic adaptation, *Nat. Chem. Biol.* 11 (2) (2015) 156–163.
- [51] A. Drazic, J. Winter, The physiological role of reversible methionine oxidation, *Biochim. Biophys. Acta* 1844 (8) (2014) 1367–1382.
- [52] V.S. Sharov, D.A. Ferrington, T.C. Squier, C. Schoneich, Diastereoselective reduction of protein-bound methionine sulfoxide by methionine sulfoxide reductase, *FEBS Lett.* 455 (3) (1999) 247–250.
- [53] M. Si, L. Zhang, M.T. Chaudhry, W. Ding, Y. Xu, C. Chen, A. Akbar, X. Shen, S.J. Liu, *Corynebacterium glutamicum* methionine sulfoxide reductase A uses both myco-redoxin and thioredoxin for regeneration and oxidative stress resistance, *Appl. Environ. Microbiol.* 81 (8) (2015) 2781–2796.
- [54] A. Kumar, A.M. Balakrishna, W. Nartey, M.S.S. Manimekalai, G. Gruber, Redox chemistry of *Mycobacterium tuberculosis* alkylhydroperoxide reductase E (AhpE): structural and mechanistic insight into a myco-reodoxin-1 independent reductive pathway of AhpE via mycothiol, *Free Radic. Biol. Med.* 97 (2016) 588–601.
- [55] A. Gaballa, G.L. Newton, H. Antelmann, D. Parsonage, H. Upton, M. Rawat, A. Claiborne, R.C. Fahey, J.D. Helmann, Biosynthesis and functions of bacillithiol, a major low-molecular-weight thiol in *Bacilli*, *Proc. Natl. Acad. Sci. USA* 107 (14) (2010) 6482–6486.
- [56] S.V. Sharma, M. Arbach, A.A. Roberts, C.J. Macdonald, M. Groom, C.J. Hamilton, Biophysical features of bacillithiol, the glutathione surrogate of *Bacillus subtilis* and other firmicutes, *Chembiochem* 14 (16) (2013) 2160–2168.
- [57] A.A. Roberts, S.V. Sharma, A.W. Strankman, S.R. Duran, M. Rawat, C.J. Hamilton, Mechanistic studies of FosB: a divalent-metal-dependent bacillithiol-S-transferase that mediates fosfomycin resistance in *Staphylococcus aureus*, *Biochem. J.* 451 (1) (2013) 69–79.
- [58] M.K. Thompson, M.E. Keithly, M.C. Goodman, N.D. Hammer, P.D. Cook, K.L. Jagessar, J. Harp, E.P. Skaar, R.N. Armstrong, Structure and function of the genomically encoded fosfomycin resistance enzyme, FosB, from *Staphylococcus aureus*, *Biochemistry* 53 (4) (2014) 755–765.
- [59] P. Chandrangu, R. Dusi, C.J. Hamilton, J.D. Helmann, Methylglyoxal resistance in *Bacillus subtilis*: contributions of bacillithiol-dependent and independent pathways, *Mol. Microbiol.* 91 (4) (2014) 706–715.
- [60] J.E. Müller, F. Meyer, B. Litsanov, P. Kiefer, J.A. Vorholt, Core pathways operating during methylotrophy of *Bacillus methanolicus* MGA3 and induction of a bacillithiol-dependent detoxification pathway upon formaldehyde stress, *Mol. Microbiol.* 98 (6) (2015) 1089–1100.
- [61] J.D. Helmann, Bacillithiol, a new player in bacterial redox homeostasis, *Antioxid. Redox Signal* 15 (1) (2011) 123–133.
- [62] Z. Ma, P. Chandrangu, T.C. Helmann, A. Romsang, A. Gaballa, J.D. Helmann, Bacillithiol is a major buffer of the labile zinc pool in *Bacillus subtilis*, *Mol. Microbiol.* 94 (4) (2014) 756–770.
- [63] Z. Fang, P.C. Dos Santos, Protective role of bacillithiol in superoxide stress and Fe-S metabolism in *Bacillus subtilis*, *Microbiol. Open* 4 (4) (2015) 616–631.
- [64] Z. Rosario-Cruz, H.K. Chahal, L.A. Mike, E.P. Skaar, J.M. Boyd, Bacillithiol has a role in Fe-S cluster biogenesis in *Staphylococcus aureus*, *Mol. Microbiol.* 98 (2) (2015) 218–242.
- [65] Z. Rosario-Cruz, J.M. Boyd, Physiological roles of bacillithiol in intracellular metal processing, *Curr. Genet.* 62 (1) (2016) 59–65.
- [66] K.L. Kay, C.J. Hamilton, N.E. Le Brun, Mass spectrometry of *B. subtilis* CopZ: Cu(i)-binding and interactions with bacillithiol, *Metallomics* 8 (7) (2016) 709–719.
- [67] H. Peng, Y. Zhang, L.D. Palmer, T.E. Kehl-Fie, E.P. Skaar, J.C. Trinidad, D.P. Giedroc, Hydrogen sulfide and reactive sulfur species impact proteome S-sulfhydration and global virulence regulation in *Staphylococcus aureus*, *ACS Infect. Dis.* 3 (10) (2017) 744–755.
- [68] H. Peng, J. Shen, K.A. Edmonds, J.L. Luebke, A.K. Hickey, L.D. Palmer, F.J. Chang, K.A. Bruce, T.E. Kehl-Fie, E.P. Skaar, D.P. Giedroc, Sulfide homeostasis and nitroxyl intersect via formation of reactive sulfur species in *Staphylococcus aureus*, *mSphere* 2 (3) (2017).
- [69] D.C. Pöther, P. Gierok, M. Harms, J. Mostertz, F. Hochgräfe, H. Antelmann, C.J. Hamilton, I. Borovok, M. Lalk, Y. Aharonowitz, M. Hecker, Distribution and infection-related functions of bacillithiol in *Staphylococcus aureus*, *Int. J. Med. Microbiol.* 303 (3) (2013) 114–123.
- [70] A. Rajkarnikar, A. Strankman, S. Duran, D. Vargas, A.A. Roberts, K. Barretto, H. Upton, C.J. Hamilton, M. Rawat, Analysis of mutants disrupted in bacillithiol metabolism in *Staphylococcus aureus*, *Biochem. Biophys. Res. Commun.* 436 (2) (2013) 128–133.
- [71] A.C. Posada, S.L. Kolar, R.G. Dusi, P. Francois, A.A. Roberts, C.J. Hamilton, G.Y. Liu, A. Cheung, Importance of bacillithiol in the oxidative stress response of *Staphylococcus aureus*, *Infect. Immun.* 82 (1) (2014) 316–332.
- [72] M. Otto, Community-associated MRSA: what makes them special? *Int. J. Med. Microbiol.* 303 (6–7) (2013) 324–330.
- [73] R. Novick, Properties of a cryptic high-frequency transducing phage in *Staphylococcus aureus*, *Virology* 33 (1) (1967) 155–166.
- [74] J.W. Lee, S. Soonsanga, J.D. Helmann, A complex thiolate switch regulates the *Bacillus subtilis* organic peroxide sensor OhrR, *Proc. Natl. Acad. Sci. USA* 104 (21) (2007) 8743–8748.
- [75] B.K. Chi, K. Gronau, U. Mäder, B. Hessling, D. Becher, H. Antelmann, S-bacillithiolation protects against hypochlorite stress in *Bacillus subtilis* as revealed by transcriptomics and redox proteomics, *Mol. Cell Proteom.* 10 (11) (2011) (M111 009506).
- [76] B.K. Chi, A.A. Roberts, T.T. Huyen, K. Bäsell, D. Becher, D. Albrecht, C.J. Hamilton, H. Antelmann, S-bacillithiolation protects conserved and essential proteins against hypochlorite stress in firmicutes bacteria, *Antioxid. Redox Signal.* 18 (11) (2013) 1273–1295.
- [77] M. Imber, V.V. Loi, S. Reznikov, V.N. Fritsch, A.J. Pietrzyk-Brzezinska, J. Prehn, C. Hamilton, M.C. Wahl, A.K. Bronowska, H. Antelmann, The aldehyde dehydrogenase AldA contributes to the hypochlorite defense and is redox-controlled by protein S-bacillithiolation in *Staphylococcus aureus*, *Redox Biol.* 15 (2018) 557–568.
- [78] A.S. Halavaty, R.L. Rich, C. Chen, J.C. Joo, G. Minasov, I. Dubrovskaya, J.R. Winsor, D.G. Myszk, M. Duban, L. Shuvalova, A.F. Yakunin, W.F. Anderson, Structural and functional analysis of betaine aldehyde dehydrogenase from *Staphylococcus aureus*, *Acta Crystallogr. D. Biol. Crystallogr.* 71 (Pt 5) (2015) 1159–1175.
- [79] S. Mukherjee, D. Dutta, B. Saha, A.K. Das, Crystal structure of glyceraldehyde-3-phosphate dehydrogenase 1 from methicillin-resistant *Staphylococcus aureus* MRSA252 provides novel insights into substrate binding and catalytic mechanism, *J. Mol. Biol.* 401 (5) (2010) 949–968.
- [80] L. Huo, I. Davis, F. Liu, B. Andi, S. Esaki, H. Iwaki, Y. Hasegawa, A.M. Orville, A. Liu, Crystallographic and spectroscopic snapshots reveal a dehydrogenase in action, *Nat. Commun.* 6 (2015) 5935.
- [81] C.S. Gajadeera, X. Zhang, Y. Wei, O.V. Tsodikov, Structure of inorganic pyrophosphatase from *Staphylococcus aureus* reveals conformational flexibility of the active site, *J. Struct. Biol.* 189 (2) (2015) 81–86.
- [82] C.B. Poor, P.R. Chen, E. Duguid, P.A. Rice, C. He, Crystal structures of the reduced, sulfenic acid, and mixed disulfide forms of SarZ, a redox active global regulator in *Staphylococcus aureus*, *J. Biol. Chem.* 284 (35) (2009) 23517–23524.
- [83] M. Makowska-Grzyska, Y. Kim, R. Wu, R. Wilton, D.R. Gollapalli, X.K. Wang, R. Zhang, R. Jedrzejczak, J.C. Mack, N. Maltseva, R. Mulligan, T.A. Binkowski, P. Gornicki, M.L. Kuhn, W.F. Anderson, L. Hedstrom, A. Joachimiak, Bacillus anthracis inosine 5'-monophosphate dehydrogenase in action: the first bacterial series of structures of phosphate ion-, substrate-, and product-bound complexes, *Biochemistry* 51 (31) (2012) 6148–6163.
- [84] T.M. Fu, J. Almqvist, Y.H. Liang, L. Li, Y. Huang, X.D. Su, Crystal structures of cobalamin-independent methionine synthase (MetE) from *Streptococcus mutans*: a dynamic zinc-inversion model, *J. Mol. Biol.* 412 (4) (2011) 688–697.
- [85] L. Hedstrom, IMP dehydrogenase: structure, mechanism, and inhibition, *Chem. Rev.* 109 (7) (2009) 2903–2928.
- [86] K. Peariso, C.W. Goulding, S. Huang, R.G. Matthews, J.E. Penner-Hahn, Characterization of the zinc binding site in methionine synthase enzymes of *Escherichia coli*: the role of zinc in the methylation of homocysteine, *J. Am. Chem. Soc.* 120 (1998) 8410–8416.
- [87] P.R. Chen, S. Nishida, C.B. Poor, A. Cheng, T. Bae, L. Kuechenmeister, P.M. Dunman, D. Missiakas, C. He, A new oxidative sensing and regulation pathway mediated by the MgrA homologue SarZ in *Staphylococcus aureus*, *Mol. Microbiol.* 71 (1) (2009) 198–211.
- [88] M. Hillion, H. Antelmann, Thiol-based redox switches in prokaryotes, *Biol. Chem.* 396 (5) (2015) 415–444.
- [89] A. Gaballa, B.K. Chi, A.A. Roberts, D. Becher, C.J. Hamilton, H. Antelmann, J.D. Helmann, Redox regulation in *Bacillus subtilis*: the bacilliredoxins BrxA(YphP) and BrxB(YqiW) function in de-bacillithiolation of S-bacillithiolated OhrR and MetE, *Antioxid. Redox Signal.* 21 (3) (2014) 357–367.
- [90] F. Hochgräfe, J. Mostertz, D. Albrecht, M. Hecker, Fluorescence thiol modification assay: oxidatively modified proteins in *Bacillus subtilis*, *Mol. Microbiol.* 58 (2) (2005) 409–425.
- [91] U. Derewenda, T. Boczek, K.L. Gorres, M. Yu, L.W. Hung, D. Cooper, A. Joachimiak, R.T. Raines, Z.S. Derewenda, Structure and function of *Bacillus subtilis* YphP, a prokaryotic disulfide isomerase with a CXC catalytic motif, *Biochemistry* 48 (36) (2009) 8664–8671.
- [92] A. Petersohn, M. Brigulla, S. Haas, J.D. Hoheisel, U. Völker, M. Hecker, Global analysis of the general stress response of *Bacillus subtilis*, *J. Bacteriol.* 183 (19) (2001) 5617–5631.
- [93] S. Viars, J. Valentine, M. Hernick, Structure and function of the LmbE-like superfamily, *Biomolecules* 4 (2) (2014) 527–545.
- [94] R.A. Munoz-Clares, L. Gonzalez-Segura, A.G. Diaz-Sanchez, Crystallographic evidence for active-site dynamics in the hydrolytic aldehyde dehydrogenases. Implications for the deacylation step of the catalyzed reaction, *Chem. Biol. Interact.* 191 (1–3) (2011) 137–146.

Curriculum vitae

Allgemeine Informationen

Name: Imber, Marcel
Akademischer Titel: Diplom-Biochemiker
Geburtstag: 25.02.1988
Geburtsort: Ribnitz-Damgarten
Geschlecht: Männlich
Familienstand: Ledig
Nationalität: Deutsch
Adresse des Instituts: Freie Universität Berlin
Institut für Biologie-Mikrobiologie
Königin-Luise-Straße 12-16
14195 Berlin, Germany
Tel.-Nummer: 0152/38956460
E-Mail Adresse: marcel.imber@gmail.com

Akademischer Werdegang und Qualifikationen

2004-2008 Erwerb der Allgemeinen Hochschulreife, Fachgymnasium für Ernährungslehre und Hauswirtschaft, Velgast, Deutschland

10/2008-10/2013 Studium der Biochemie, Ernst-Moritz-Arndt Universität Greifswald, Deutschland

2012-2013 Erwerb des akademischen Grades Diplom-Biochemiker, Institut für Medizinische Biochemie und Molekularbiologie, Universitätsmedizin, Ernst-Moritz-Arndt Universität Greifswald, Deutschland
Thema der Diplomarbeit: "Charakterisierung des Säugetiers Nucleoredoxins"

10/2014-09/2015 Doktorand im DFG Graduiertenkollegs RTG 1947 BiOx, Betreuer: Prof. Dr. Haike Antelmann, Institut für Mikrobiologie, Ernst-Moritz-Arndt-Universität Greifswald, Deutschland; Prof. Dr. Michael Lalk, Institut für Biochemie, Ernst-Moritz-Arndt-Universität Greifswald, Deutschland

10/2015-07/2018 Doktorand im DFG Graduiertenkolleg RTG 1947 BiOx, Betreuer: Prof. Dr. Haike Antelmann, Institut für Biologie-Mikrobiologie, Freie Universität Berlin, Deutschland; Prof. Dr. Michael Lalk, Institut für Biochemie, Ernst-Moritz-Arndt-Universität Greifswald, Deutschland
Thema der Doktorarbeit: "Thiol-redox proteomics in *Mycobacterium smegmatis* in response to ROS, RNS and antibiotics"

Liste veröffentlichter Publikationen innerhalb der Doktorarbeit

- Hillion M*, **Imber M***, Pedre B, Bernhardt J, Saleh M, Loi VV, Maaß S, Becher D, Astolfi Rosado L, Adrian L, Weise C, Hell R, Wirtz M, Messens J, Antelmann H. The glyceraldehyde-3-phosphate dehydrogenase GapDH of *Corynebacterium diphtheriae* is redox-controlled by protein S-mycothiolation under oxidative stress. *Sci Rep* 7: 5020. (2017)
- **Imber M***, Huyen NT*, Pietrzyk-Brzezinska AJ*, Loi VV*, Hillion M, Bernhardt J, Thärichen L, Kolšek K, Saleh M, Hamilton CJ, Adrian L, Gräter F, Wahl MC, Antelmann H. Protein S-bacillithiolation functions in thiol protection and redox regulation of the glyceraldehyde-3-phosphate dehydrogenase Gap in *Staphylococcus aureus* under hypochlorite stress. *Antioxid Redox Signal* 28: 410-430. (2018)
- **Imber M***, Loi VV*, Reznikov S, Fritsch VN, Pietrzyk-Brzezinska AJ, Prehn J, Hamilton CJ, Wahl MC, Bronowska AK, Antelmann H. The aldehyde dehydrogenase AldA contributes to the hypochlorite defense and is redox-controlled by protein S-bacillithiolation in *Staphylococcus aureus*. *Redox Biol.* 15: 557-568. (2018).
- **Imber, M**, Pietrzyk-Brzezinska AJ, Antelmann H. Redox regulation by reversible protein S-thiolation in Gram-positive bacteria. *Redox Biol.* 20: 130-145. (2018).

*Shared first authorships

Teilnahme an nationalen Konferenzen

- **01-04th March 2015**: Annual Conference of the Association for General and Applied Microbiology (VAAM), Marburg, Germany.
- **20-21st March 2015**: 3rd Symposium on Dynamics of Thiol-based Redox Switches in Cellular Physiology of the SPP1710, Rauischholzhausen, Germany
- **13-16th March 2016**: VAAM conference, Jena, Germany.
Poster presentation "Protein S-mycothiolation functions in redox regulation of the Glyceraldehyde 3-phosphate dehydrogenase GapDH in the pathogen *Corynebacterium diphtheriae*".
- **27-28th June 2016**: ZIBI Summer Symposium on Therapeutic Resistances in Infectious Disease - Status Quo and Future Challenges, Berlin, Germany.
- **11-15th June 2017**: 19th international conference on Bacilli & Gram-positive bacteria.
Poster presentation "The glyceraldehyde-3-phosphate dehydrogenase GapDH of *Corynebacterium diphtheriae* is redox-controlled by protein S-mycothiolation under oxidative stress".
- **15-18th April 2018**: VAAM conference, Wolfsburg, Germany. Poster presentation "The aldehyde dehydrogenase AldA contributes to the hypochlorite defense and is redox-controlled by protein S-bacillithiolation in *Staphylococcus aureus*".

Acknowledgements

Firstly, I would like to express my sincere gratitude to my advisor Prof. Dr. Haike Antelmann for the continuous support of my Ph.D study and related research, for her patience, motivation, and immense knowledge. His guidance helped me in all the time of research and writing of this thesis.

Besides my advisor, I would like to thank the GRK RTG 1947 BiOx and all its members, especially Prof. Dr. Christiane Helm and PD Dr. Christopher Horst Lillig for letting me be a part of it and Anett Stolte for the continuous help in all organizational matters.

My sincere thanks also go to Dr. Gottfried Palm, who shared his knowledge and time for enlightening me the first glance of research in the field of enzyme kinetics.

I would like to thank Prof. Dr. Markus C. Wahl and Dr. Agnieszka J. Pietrzyk-Brzezinska for the protein crystal structure analysis.

My special thanks also go to:

Prof. Dr. Frauke Gräter, Dr. Katra Kolsěk, Lena Thärichen and Dr. Agnieszka K. Bronowska for molecular docking and molecular dynamics simulations to model BSH into the active site of GapDH and AldA.

Prof. Dr. Dörte Becher and Dr. Sandra Maaß for MS of the ICAT-labeled peptides, and Prof. Dr. Lorenz Adrian and Dr. Christoph Weise for MS of the overoxidized and S-bacillithiolated GapDH.

Dr. Jörg Bernhardt and Dr. Melanie Hillion for performing the bioinformatics analysis and treemap constructions.

Prof. Dr. Rüdiger Hell and Dr. Markus Wirtz for the metabolomics of monobromobimane-labelled thiols.

Further, I would like to thank all our collaboration partners, especially Prof. Dr. Chris J. Hamilton and Prof. Dr. Jöris Messens for providing BSH and MSH, respectively.

And finally, I would also like to thank the DFG and also the ERC Consolidator grant (GA 615585) MYCOTHILOME for all the financial support.

I thank my fellow lab mates for the stimulating discussions, long days we were working together before deadlines, and for all the fun we have had in the last 3.5 years.

Last but not the least, my deep gratitude goes to my family: my parents and to my sister and brother-in-law who have given me so much support, encouragement and strength. I am very thankful to know that they will always stand behind me.

Eigenständigkeitserklärung

Hiermit erkläre ich, dass diese Arbeit bisher von mir weder an der Mathematisch-Naturwissenschaftlichen Fakultät der Ernst-Moritz-Arndt-Universität Greifswald noch einer anderen wissenschaftlichen Einrichtung zum Zwecke der Promotion eingereicht wurde.

Ferner erkläre ich, dass ich diese Arbeit selbstständig verfasst und keine anderen als die darin angegebenen Hilfsmittel und Hilfen benutzt und keine Textabschnitte eines Dritten ohne Kennzeichnung übernommen habe.

Unterschrift des Promovenden